Non-linear stability of a liquid propelled rocket engine in closed loop regulation

Jules Gibart

université PARIS-SACLAY

Non-linear stability of a liquid propelled rocket engine in closed loop regulation

Stabilité non-linéaire d'un moteur fusée régulé en boucle fermée

Thèse de doctorat de l'université Paris-Saclay

École doctorale n°580, Sciences et Technologies de l'Information et de la Communication (STIC)
Spécialité de doctorat : Automatique
Graduate School : Sciences de l'ingénierie et des systèmes. Référent : Faculté des sciences d'Orsay

Thèse préparée dans l'unité de recherche **DTIS** (Université Paris-Saclay,ONERA), sous la direction de **Hélène PIET-LAHANIER**, directeur de recherche (ONERA), le co-encadrement de **François FARAGO**, docteur (CNES).

Thèse soutenue à Paris-Saclay, le 09 octobre 2024, par

Jules GIBART

Composition du jury

Membres du jury avec voix délibérative

Sihem TEBBANI Professeur des Universités, L2S, Université Paris-Saclay	Présidente
Bernhard MASCHKE Professeur des Universités, LAGEPP UMR CNRS	Rapporteur & Examinateur
Günther WAXENEGGER-WILFING Professeur des Universités, Université Würzbug	Rapporteur & Examinateur
Denis MATIGNON Professeur des Universités, ISAE-SUPAERO	Examinateur

THESE DE DOCTORAT

NNT : 2024UPAST110

université PARIS-SACLAY
ÉCOLE DOCTORALE
Sciences et technologies de l'information et de la communication (STIC)

Titre : Stabilité non-linéaire d'un moteur fusée régulé en boucle fermée
Mots clés : Lanceurs réutilisables, Systèmes non-linéaires, Stabilité, Commande non-linéaire, Systèmes Hamiltoniens à Ports

Résumé : Dans le cadre du développement de moteurs de fusée réutilisables, les exigences de fonctionnement des différents éléments composant un moteur ont connu de grandes évolutions. Alors qu'un moteur classique était conçu pour un nombre restreint de points de fonctionnement, un moteur réutilisable doit répondre à des exigences sur une large plage de points, afin d'effectuer des manœuvres plus complexes. En conséquence, les lois de commande des moteurs fusées ont subi une évolution similaire, rendant nécessaire la loi de commande en boucle fermée. Bien que de nombreuses études aient été réalisées sur des lois de commande, peu de travaux portent sur la stabilité du moteur en boucle fermée. Dans cette optique, l'objectif de ces travaux est de proposer une démonstration de stabilité d'un modèle de moteur fusée, ainsi qu'un contrôleur permettant d'obtenir des garanties de stabilité du modèle.
En premier lieu, un modèle typique de moteur de fusée à ergols liquide est développé, sous forme d'espace d'états. Ce type de modèle, bien que plus courant, se révèle peu adapté à l'étude de la stabilité, de par sa formulation hautement non-linéaire. Dans ce cadre, l'utilisation d'une fonction de Lyapunov se révèle complexe, et une reformulation du modèle est envisagée, sous forme d'un modèle Hamiltonien à ports.
Un second chapitre permet d'introduire la notion de modèle Hamiltonien à ports. Ce type de modèle met en valeur les transferts énergétiques qui ont lieu entre les différents éléments d'un système, et sont construits avec une structure géométrique fixe. Ces différentes caractéristiques permettent une étude directe de la passivité d'un système, un outil d'analyse de la stabilité d'un système. La reformulation permet de trouver une fonction caractéristique d'un système Hamiltonien à ports, l'Hamiltonien, qui prouve la passivité d'un système et peut être formulé comme une fonction de Lyapunov. Cette démonstration donne des conditions de stabilité sur la modélisation du système, ainsi que sur le contrôleur appliqué en boucle fermée. Dans le cas où la démonstration directe de passivité n'est pas réalisable, un contrôleur peut être construit pour assurer la passivité de la boucle fermée.
Pour conférer les propriétés de la passivité au modèle de moteur utilisé, la théorie du contrôle par passivité est présentée. Le principe d'un tel contrôleur est d'assurer la stabilité d'un système en rendant la boucle fermée passive. Avec la théorie des systèmes Hamiltonien à ports cependant, ce contrôleur permet aussi de modifier la structure géométrique hamiltonienne, afin de reformuler un système sous forme Hamiltonienne à ports. Ce contrôleur permet de rendre le système passif autour d'un point de fonctionnement désiré par l'utilisateur, qui peut être changé au cours du temps. Ainsi, ce contrôleur permet un suivi de trajectoire avec des garanties de passivité du système au cours du temps. Le quatrième chapitre propose une approche différente pour établir un contrôleur stabilisant, à l'aide de la théorie de la contraction. La propriété de contraction d'un système dénote sa capacité à converger rapidement vers une trajectoire de référence. Cette propriété constitue une forme de stabilité exponentielle, plus puissante que la stabilité par passivation. Le contrôleur peut de plus être réalisé aisément, en résolvant des inégalités linéaires matricielles.
Enfin, les résultats de ces travaux sont présentés à l'aide de simulations sur MATLAB Simulink, et permettent de conclure sur les différents contrôleurs présentés. Un contrôleur simple proportionnel intégral dérivé (PID) est construit pour permettre une comparaison. Les résultats montrent que les contrôleurs réalisés proposent des propriétés stabilisantes, alors que le contrôleur PID est instable dans certaines zones de fonctionnement. Le contrôleur par passivité étend le domaine de stabilité du système, et le contrôleur par contraction empêche le système de quitter le domaine de stabilité du système original.

Title : Non-linear stability of a liquid propelled rocket engine in closed loop regulation
Keywords : Reusable launchers, Non-linear systems, Stability, Non-linear control, Port-Hamiltonian systems

Abstract : With the development of reusable rocket engines, the operating requirements of the various components in an engine have significantly increased. While a non-reusable engine was designed for a limited number of operating points, a reusable engine must meet requirements over a wide range of points to perform complex maneuvers. Consequently, rocket engine control laws have evolved similarly, with the introduction of closed-loop control laws. Although many studies have been conducted on control laws, few works focus on the stability of the engine in closed-loop control. In this context, the objective of this work is to propose a demonstration of the stability of a rocket engine model, as well as a controller that guarantees the stability of the model.

First, a model of a liquid propelled rocket engine is proposed under a state-space form. Although more common, this type of modeling does not allow for an easy stability analysis due to its highly nonlinear terms. In this context, the use of a Lyapunov function proves to be cumbersome, and a reformulation of the model is considered, in the form of a Port-Hamiltonian model, more suited for stability analysis of the system.

A second chapter introduces the concept of the Port-Hamiltonian model. This type of model highlights the energy transfers that occur between the various components of a system and is built with a fixed geometric structure. These characteristics allow for a direct study of the passivity of a system, a tool for stability analysis the stability. The reformulation allows for the identification of a characteristic function of a Port-Hamiltonian system, the Hamiltonian function, which can be used to prove the passivity of a system and can be formulated as a Lyapunov function. This demonstration provides stability conditions for the system as well as the controller applied in the closed-loop system. In cases where a direct demonstration of passivity is not possible, a controller can be constructed to ensure the passivity of the closed-loop system.

To endow the rocket engine model with passivity properties, the third chapter presents passivity-based control (PBC) theory. The principle of such a controller is to ensure the stability of a system by making the closed-loop system passive. Coupled with Port-Hamiltonian systems theory, however, this controller also allows for modification of the Hamiltonian geometric structure to reformulate a system into Port-Hamiltonian form. This controller makes the system passive around a desired operating point, which can be changed over time. Thus, this controller enables trajectory tracking with passivity guarantees over time.

The fourth chapter proposes a different approach to establish a stabilizing controller using contraction theory. The contraction property of a system indicates its ability to rapidly converge towards a reference trajectory. This property represents a form of exponential stability, which is more robust than stability through passivation. Moreover, the controller can be easily implemented by solving linear matrix inequalities.

Finally, the results of this work are presented through simulations on MATLAB Simulink, allowing for conclusions on the various controllers presented. A simple proportional-integral-derivative (PID) controller is constructed for comparison. The results show that the designed controllers offer stabilizing properties, while the PID controller is unstable in certain operating regions. The passivity-based controller extends the stability domain of the system, and the contraction-based controller prevents the system from leaving the stability domain of the original system.

À Pierre, à Patrice

Remerciements

Cette thèse n'aurait pu aboutir sans le soutien et la collaboration des nombreuses personnes que j'ai eu la chance de croiser durant ces trois années.
Je voudrais d'abord remercier mes rapporteurs, Bernhard Maschke et Günther Waxenegger-Wilfing, pour leurs rapports et les corrections proposées. Je voudrais aussi remercier les autres membres du jury Sihem Tebbani qui a assisté à mes deux soutenances à ce jour et Denis Matignon qui a pu suivre la thèse depuis la seconde année et voir son évolution.
J'aimerais remercier aussi François Farago qui a été d'une aide précieuse sur cette thèse, ainsi que Marco Galeotta , qui après avoir participé au lancement, a pu revenir pour la conclusion. J'aimerais en particulier remercier Hélène Piet-Lahanier , qui a été une directrice de thèse présente, attentive, avec de bons conseils et qui n'a pas hésité à me dire quand les écrits n'étaient pas bons, mais qui surtout sait féliciter et encourager quand j'en ai eu le plus besoin. Pendant ma troisième année, j'aimerais aussi remercier Xavier Cauvin et Brice Matuszczak, qui ont montré un intérêt certain pour mes travaux, ce qui est toujours motivant. Merci aussi à Camille Sarotte, qui m'a beaucoup aidé quand j'ai eu du mal avec la modélisation. J'adresse aussi un remerciement particulier à Florence Marie et Caroline Grippon-Lamotte, assistantes du département à l'ONERA, et qui font fonctionner toute les interactions des doctorants avec le monde administratif.
Pour une partie plus personnelle, je garderai toujours en tête l'équipe de doctorants qui s'est constituée en première année, et qui n'a pas arrêté de se soutenir, s'aider, stresser et fêter ensemble tous les moments qui font de la thèse une drôle d'aventure. Pelin, Périclès, Romain, Renato, merci à vous d'avoir été là. Périclès qui a partagé mon bureau pendant trois ans, je me souviendrais de ce fameux message de 3h du matin, disant que l'on se refaisait un café. Pelin qui a toujours arboré le sourire, à croire que c'était facile la thèse pour elle. Renato qui m'a montré ce qu'était des bons joueurs de volley-ball, j'ai eu des courbatures une semaine entière après l'avoir suivi. Romain qui a toujours suivi tous les sports du monde, je ne l'ai d'ailleurs jamais vu perdre un match à un sport de raquette. Un merci particulier à Lucas et Shon, qui m'ont traîné au sport et qui m'ont montré ce qu'était un bon rythme de vie, avec une séance de sport, un sauna et une bière. Merci aussi à ceux qui m'ont précédé, Julius, Etienne, Mathieu, Clara, Juliette, Hanae et à ceux qui ont commencé après moi, Lucas (aussi), Amina, Matthieu pour avoir formé un superbe groupe de doctorants avec des traditions intéressantes (manger à 11h30 par exemple).
J'aimerais aussi remercier ma famille et mes amis. Papa, Maman, Manon et Roméo, qui ont su m'encourager et qui sont toujours restés proches de moi (quitte à venir aussi travailler à l'ONERA). Merci Flora, la meilleure marraine, Isabelle, Matie et Pierre pour vos conseils sur la thèse. Merci à mes amis de lycée Eliot, Hugues, Narindo, Procha, Vincent, Vi qui seront toujours les premiers à être là que ce soit dans les bons et les mauvais moments (et Tristan, maintenant, on est content). Merci enfin à Alexiane qui a été mon roc tout au long de la thèse, qui a suivi du premier papier au dernier caractère du manuscrit, qui m'a accompagné au bout du monde pour que je présente mes travaux, qui m'a encouragé, félicité et supporté pendant ces trois années. Merci à tous ceux que j'ai croisé et que je n'ai pas mentionné, c'est aussi grâce à vous que j'en suis là.

Résumé en français

Dans le cadre du développement de moteurs de fusée réutilisables, les exigences de fonctionnement des différents éléments composant un moteur ont connu de grandes évolutions. Alors qu'un moteur classique était conçu pour un nombre restreint de points de fonctionnement, un moteur réutilisable doit répondre à des exigences sur une large plage de points, afin d'effectuer des manœuvres plus complexes. En conséquence, les lois de commande des moteurs fusées ont subi une évolution similaire, rendant nécessaire la loi de commande en boucle fermée. Bien que de nombreuses études aient été réalisées sur des lois de commande, peu de travaux portent sur la stabilité du moteur en boucle fermée. Dans cette optique, l'objectif de ces travaux est de proposer une démonstration de stabilité d'un modèle de moteur fusée, ainsi qu'un contrôleur permettant d'obtenir des garanties de stabilité du modèle.

En premier lieu, un modèle typique de moteur de fusée à ergols liquides est développé, en présentant les différents composants du moteur et les équations de la physique associées. Ces équations permettent d'écrire une première approche pour la modélisation, sous forme d'espace d'états. Ce type de modèle, bien que plus courant, se révèle peu adapté à l'étude de la stabilité, de par sa formulation hautement non-linéaire. En effet, pour démontrer la stabilité par l'utilisation de méthodes classiques comme une fonction de Lyapunov, la complexité du modèle constitue un nouvel obstacle. Dans ce cadre, cette thèse propose une reformulation du modèle moteur, sous forme d'un modèle Hamiltonien à ports, afin d'obtenir une forme plus adaptée à l'étude de stabilité.

Un second chapitre permet d'introduire la notion de modèle Hamiltonien à ports. Ce type de modèle met en valeur les transferts énergétiques qui ont lieu entre les différents éléments d'un système, et est construit avec une structure géométrique fixe. Ces différentes caractéristiques permettent une étude directe de la passivité d'un système, un outil d'analyse de la stabilité d'un système. La reformulation permet de trouver une fonction caractéristique d'un système Hamiltonien à ports, l'Hamiltonien, qui prouve la passivité d'un système et peut être formulé comme une fonction de Lyapunov. L'avantage de cette approche est une simplification de l'analyse de stabilité mais aussi une meilleure compréhension des obstacles à la stabilité du système et des éléments problématiques. Cette démonstration permet aussi d'identifier des conditions de stabilité sur la modélisation du système, ainsi que sur le contrôleur appliqué en boucle fermée. Dans le cas où la démonstration directe de passivité n'est pas réalisable, un contrôleur peut être construit pour assurer la passivité de la boucle fermée.

Pour conférer les propriétés de la passivité au modèle de moteur utilisé, la théorie du contrôle par passivité est présentée dans cette thèse. Le principe d'un tel contrôleur est d'assurer la stabilité d'un système en rendant la boucle fermée passive. Avec la théorie des systèmes Hamiltonien à ports cependant, ce contrôleur permet aussi de modifier la structure géométrique hamiltonienne, afin de reformuler un système sous forme Hamiltonienne à ports. Dans le cas du moteur fusée, cette propriété s'avère cruciale car certains composants, de par leur modélisation approchée, ne permettent pas d'écrire le système dans son entiereté sous cette forme. Ce contrôleur permet alors de rendre le système passif autour d'un point de fonctionnement désiré par l'utilisateur, qui peut être changé au cours du temps. Ainsi, ce contrôleur permet un suivi de trajectoire avec des garanties de passivité du système. Cette première solution stabilisante a permis de développer un contrôleur et une méthode

d'analyse de système de type moteur de fusée, répondant à une des exigences de la problématique initiale. Cependant, la construction du contrôleur n'étant pas orientée pour le suivi de trajectoire, une seconde approche est proposée pour répondre à cette exigence. Le quatrième chapitre propose une approche différente pour établir un contrôleur stabilisant, à l'aide de la théorie de la contraction. La propriété de contraction d'un système dénote sa capacité à converger rapidement vers une trajectoire de référence. Cette propriété constitue une forme de stabilité exponentielle, plus puissante que la stabilité par passivation. Par ailleurs, cette théorie est axée sur la convergences de trajectoires, plutôt que par rapport à un point de fonctionnement. En ce sens, cette méthode est plus adaptée au suivi de trajectoire. Le contrôleur peut de plus être intégré aisément, en résolvant des inégalités linéaires matricielles et avec un retour d'état.
Les résultats de ces travaux sont présentés à l'aide de simulations sur MATLAB Simulink, et permettent de conclure sur les différents contrôleurs présentés. Un contrôleur simple proportionnel intégral dérivé (PID) est construit pour permettre une comparaison. Les résultats montrent que les contrôleurs réalisés proposent des propriétés stabilisantes, alors que le contrôleur PID est instable dans certaines zones de fonctionnement. Le contrôleur par passivité étend le domaine de stabilité du système, et le contrôleur par contraction empêche le système de quitter le domaine de stabilité du système original, en plus d'être plus performant que les autres contrôleurs pour le suivi de trajectoire. Ce travail permet d'ouvrir la voie à de nouvelles méthodes de modélisation et d'analyse de stabilité pour des systèmes multi-physiques complexes.

Table des matières

Nomenclature

General symbols	
f	vector function
g	input vector function
x	state vector
y	output vector
u	input vector
v	positive function
t	time (s)
I_d	unit matrix
$H(x)$	Hamiltonian function
$J(x)$	Hamiltonian structure matrix
$R(x)$	Hamiltonian dissipation matrix
G	input matrix
x_r	reference state vector
x_0	equilibrium state vector
$V(x)$	Lyapunov function
W, K, N, Z	contraction matrices
$\mathcal{P}$	contraction metric
$\mathcal{D}$	domain
Variables and constants	
γ	specific heat ratio [-]
ω	rotational speed [$rad.s^{-1}$]
π	ratio [-]
ρ	density [$kq.m^{-3}$]
Θ	temperature [K]
A_v	surface [m^2]
C	velocity [$m.s^{-1}$]
d	diameter [m]
h	enthalpy [$J.kq^{-1}$]
I	hydraulic inertia [m^{-1}]
J	angular inertia [$kg.m^2$]
m	mass [kg]
MR	mixture ratio [-]
N_R	reduced rotational speed [-]

p	pressure [Pa]
q	mass flow [$kg.s^{-1}$]
R_g	gas constant [$J.kg^{-1}.K^{-1}$]
ST	specific torque [-]
T	torque [$N.m$]
V_c	volume [m^3]
W	work [J]
Z_{res}	equivalent resistive coefficient [$kg^{-1}m^{-1}$]

Suffixes

$\bullet_{cc}$	main combustion chamber
$\bullet_{gg}$	gas generator
$\bullet_{tu}$	turbine intake
$\bullet_{ep}$	pump input
$\bullet_{ip}$	pump output
$\bullet_{H}$	hydrogen line
$\bullet_{O}$	oxygen line
$\bullet_{out}$	flow exiting the system (turbine or main combustion chamber)
$\bullet_{in}$	flow entering the element

1 - Introduction

The stability and automatic control of liquid-propelled rocket engines (LPREs) is a dense field that aims to regulate a complex non-linear system that is often simplified to a finite set of operating points. For a non-throttlable engine, stability is asserted for a small number of operating points, and the control action is devoted to maintaining stability around a single operating point. The replacement of hydraulic actuators with electrical ones enabled the closed-loop control of such engines and encouraged the industry to shift towards developing throttlable engines. The notion of throttle denotes the ability of the engine to function for several operating points, allowing a wide range of variation of the thrust produced. A throttlable engine enables a rocket stage to perform a safe power landing in good operating condition, such that it can be re-purposed for future launches. This capability defines the notion of reusability of a rocket stage.

The powered landing process of the first stage implies a strict following of the planned trajectory of the stage, to ensure a safe landing and mitigation of the damages caused to the engine. Such requirements facing the simplicity of a single operating point lead inevitably to the complexification of control laws [1]. With the addition of modeling errors and perturbations in the functioning, the control laws must ensure robustness and stability during the operation. The requirements of the landing maneuver imply variations of the thrust produced by the engine, that are performed using the electrical actuators. In an LPRE, the control variables mainly consist of the thrust of the engine which defines the acceleration of the body, and the mixture ratio of the propellants in the chamber, which defines the efficiency of the combustion. In addition, accurate control of the mixture ratio is critical for a parallel consumption of species in both storage tanks, and reduce unburned species resulting from the combustion.

In this introductory chapter, a global context of reusable and non-reusable engines is given in section 1.1. The state-of-the-art of control laws developed for LPREs is given in section 1.2. The notion of stability for an LPRE system is described in section 1.3. A summary concludes this introduction.

1.1 . Reusable launchers, context and problematic

Space launchers constitute a competitive environment, as the number of objects launched into space has highly increased since the beginning of the space race. Following *Space X* [2], *Blue Origin* [3], the main actors of the space scene have grasped the benefits of rocket stage reusability due to the high demand for launches. In [4], the main factors contributing to this race to a reusable launcher are described as cost reduction, return capability enhancement, and environmental impact. While Space X and Blue Origin already developed reusable technology with *Falcon 9*, *Falcon Heavy* or even *New Shepherd*, other agencies such as *JAXA* [5] and ESA [6] are developing reusable stages.

1.1.1 . Rocket engine generalities

A rocket engine is a complex combustion that system, that aims at providing a high thrust to launch a rocket body. The general rocket engine is composed of 5 main elements,

- Tanks that store the propellants used
- Lines that direct the propellants during the functioning
- A main combustion chamber, that builds up the pressure with the combustion of the propellant species
- A nozzle, a component whose specific geometry provokes expansion of high-pressured gases, and ejects them at high speeds resulting in the generation of thrust for the rocket
- Valves that are placed on the lines of the propellants and serve multiple purposes, such as regulation, safety, or even shutdown.

To attain higher pressures and thrust, turbo-pumps can be added to the engine, to increase the pressure of the propellants after exiting the tanks. Higher pressure in the propellants leads to higher pressure in the combustion chamber. This addition adds high complexity to the engine, as the addition of the turbopumps requires a component to provide the torque needed by the pumps to function. In the vast majority of the literature, this component is a gas-generator (GG), which is a smaller combustion chamber aimed at redirecting the burned gases to propel the pumps. Other cycles are available in the industry, such as staged combustion, which requires pre-burners that heat the propellants before the main combustion chamber, and increase efficiency. Similarly, expander cycles have been developed, where the turbines are propelled using the expansion of the cold fuel in the regenerative circuit. The main difference between the two cycles presented and the GG cycle resides in the possible thrust output. With the addition of the gas-generator, higher torques are attainable in the pumps, leading to higher maximum thrust outputs. This difference is of interest in the case of a first-stage engine (which is the case in reusable launchers), which requires higher thrusts than other stages. Therefore in this work, we will limit ourselves to a GG cycle of an LPRE.

1.1.2 . Reusable launchers

As described in [7], classical LPRE designs consider constant thrust of the engine, with small variations around the operating point. However, for a diverse class of missions (rendez-vous, landing, orbital maneuver), it is necessary to provide throttling capabilities to a rocket engine. In [7], the author describes a range of solution designs to provide a wider range of variation to the thrust of an engine. Nonetheless, mass flow regulation proves to be the more efficient and reliable solution for a wide range of variations of the engine thrust. It is however no simple task to control such an engine, as the range of variation is greatly dependent on the internal structure of the engine. While rocket engines are considered stable around the main operating point, the requirements for down-throttling introduce new hazards, as the combustion instabilities and sub-optimal performance of the other components such as the biphasic mass flow in the regenerative circuit in very low thrust outputs. ([7]).

Development of rocket engines with throttling capabilities has nonetheless risen in the space industry. For example, *Blue Origin*'s *BE-3* throttles down to 18% of its operating value [7] and *Space X*'s *Merlin 1-D Vacuum* engine is estimated to 39% of the nominal value.

These capabilities add complexity to the engine design while the modeling and control of such characteristics have to mirror the design complexity. This modeling complexity is often reflected in the validity range of the model. As the system evolves in the considered domain of variation, it is necessary to qualify the stability of the system, approached by the modeling, especially when the operating point is near the edges of the validity domain of the model. This requirement for stability when dealing with variations of the thrust is the motivation of this thesis.

In the literature, while control laws have been developed for the permanent regime of an LPRE, few references concerning the stability of an engine are available. Mainly due to the high confidentiality of this growing industrial sector, the requirements for stability are seldom of interest and authors focus on the robustness of the control designed. In most cases, the stability of the engine is asserted by simulations, or post-proved by bench-testing of the engine. This thesis aims to provide tools and methods to analyze the stability of an LPRE and derive relevant conditions for controllers' proof of stability.

1.1.3 . Mission design

Stage recovery has been an important aspect of launches, and since the early days of space conquest has proven to be a challenge. Early attempts to recover some stage of a rocket mainly concerned the booster elements. These methods for booster recovery have been designed around the gliding of the considered stage back to the launch site. The first stage recovery performed concerned the space shuttle solid boosters [8], however, the re-purposing of such boosters proved to be of very high cost and maintenance. Other booster recoveries have been performed, mainly for expertise, such as Ariane 5 [9], using chutes to slow down the fall of the engine. However, such recovery does not allow the engine to be re-used, due to the damages caused by the launch.

The development of reusable technology using re-ignition and throttling of the main engine has led to more optimized recovery missions. The design of the recovery process has shifted from simple gliding or parachutes to active engine propulsion to slow down the recovered stage. In the several mission designs proposed in [9] and illustrated in figure 1.1, scenarios A and B are of interest in this work, and the technological solution adapted to the engine presented later in this thesis. Scenario A features the toss-back strategy which consists of a first boost to re-orient the recovered stage of the rocket, and using active propulsion of the main engine to slow down the body for the landing at the launch site. Scenario B illustrates the recovery of the engine on a barge prepared upfront to the launch, which follows the same idea as scenario A with a notable difference in the re-orienting initial boost. Both scenarios have already been used by Space X to recover the first stage of the Falcon 9, and have proven efficient mission design.

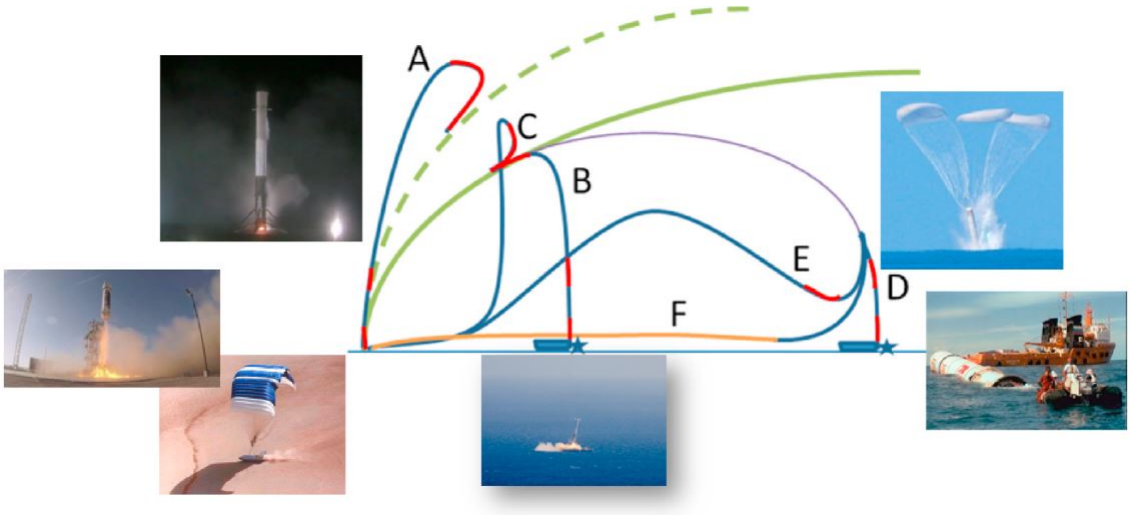

Figure 1.1 – Some of the possible recovery scenarios for reusable engines by Baiocco & al. [9]

1.2 . Overview of modeling and control of liquid-propelled rocket engines

1.2.1 . Review of modeling techniques

An LPRE is a complex physical system whose exact dynamics are still being studied. The numerous components that define the overall system lead to increasing complexity and uncertainties on the variables considered. In the literature, the modeling of LPREs takes numerous forms, depending on the objective of the model and the methods employed to obtain the evolution equations.

Models built using linear identification of terms are obtained via simulations or bench testing of the engine [10], most of the time, such models aim to identify non-linearities and dynamics of a pre-existing engine, or during the design of the engine.

Linearized models in general constitute the most common approach when aiming for the control of an engine. A control law is constructed for A linear model around an operating point of the system and is then validated for a wider range of thrust values. In [11], the modeling of the engine simplifies the combustion dynamics to focus the study on the fluid evolution, allowing for precise control of the mass flows involved. In [12], an engine capable of down-throttling is linearized around the operating point of the system, and a non-linear closed-loop controller is designed for the model. The controller proved relevant for large variations of thrust, validating the linear approach for a variation of thrust between 133 and $432N$.

Non-linear models serve multiple purposes, ranging from model validation to control design. While non-linear models were previously rarely used for control design, the past 10 years have shown a new interest in non-linear models for control. The work of Sergio Pérez-Roca [13], one of the main references in this thesis, has led to the development of a non-linear model for a gas-generator LPRE. The objective of this model was to derive robust controllers for the transient control of the LPRE. This model, which inspired the one presented later in this thesis, is comprised of 13 states with non-linear evolution to encapsulate the behavior of the engine. More recently, non-linear models trained for AI-generated controllers have risen. In [14], the author modeled an LPRE as a feed-forward neural network for engine monitoring and control. In [15, 16], the author has modeled heat conduction in regenerative circuits using neural networks. Such modeling techniques make use of neural networks which are mathematical entities that can be trained to reproduce the behavior of a real system. In use, such models are able to efficiently reconstruct the state of a system from measurements, and, therefore, provide powerful tools for the control design with non-measurable states.

1.2.2 . Review of control methods

Control of a liquid-propelled rocket engine recalls from the early stages of the rocket industry. Initial designs for controllers have no throttling requirements to fulfill and often consist of single operating points, where the controller is designed for a linearized state-space [17] about the considered point. An extensive review of control methods in rocket engine control and modeling is available in [18], and is summarized here.

LPREs present a stable behavior in general, leading to open-loop control techniques with high performance. In [19, 20], the author introduces an optimal policy to control an engine during throttling transients. The optimization is performed off-line to take into account several parameters. While this approach proposes an optimal controller, the stability of the system must be asserted previous to the

operation of the engine. A second off-line optimal control strategy for thrust control is developed in [21]. This approach takes into account the whole body of the rocket rather than the sole engine. This adds complexity to the optimization problem as the whole mass of the rocket is taken into account, englobing fuel consumption and acceleration of the body (dependent on the varying mass of the rocket). The control is developed on a simplified engine, with an algebraic relation between the mass flow injected and the thrust produced.

While open-loop controllers are stable due to the LPRE stability, their performance is not sufficient in most cases. First, the design of the open-loop controller requires a method, which is to be conducted again for each operating point. When facing very low thrust levels or mixture ratio regulation, an open-loop control method is insufficient. In addition, open-loop controllers are unable to deal with faults that can occur in the engine. Therefore for precision and reference tracking, control methods have been oriented towards closed-loop controllers. Such controllers enable to perform complex maneuvers for throttlable engines, however may introduce unstable behavior in the system. And while robustness is required in most designs, there is a lack in formal stability analysis in the approaches proposed.

Intelligent control systems, which consist of a superposition of control and diagnostics methods. Here the mission control is integrated to the design, defining the requirements for thrust level and mixture ratio online. A second layer of the controller performs the control action on the actuators. This type of control makes use of multivariable control loops, to monitor and control multiple life-extending parameters of an engine. In [22], model-based fault detection has been successfully integrated on a representation of the space shuttle main engine. The controller proves to be efficient in facing several failure scenarios, validating the approach for life-extending control. In [23],[24], a cluster of three engines is controlled. The control policy is to distribute the thrust requirements due to the health of all three monitored engines.

Control strategies developed are considered for valve actuators. The main tendency is oriented towards the control of the fuel mass flow to determine the main chamber pressure and the control of the oxidizer mass flow to control the mixture ratio in the main chamber. In [17], the regulation loop is built using PI controllers, where the oxidizer line has a faster controller than the fuel line. As the oxidizer line is dedicated to mixture ratio control, it is designed to follow the fuel line and therefore requires a smaller time response to avoid spikes in the mixture ratio caused by delays.

Another approach to life-extending control has been presented in [25], which is accomplished by introducing a structural stability to prevent damages at the cost of performance. One of the main drawbacks of intelligent control systems or life-extending policies, in general, resides in the computational requirements of the optimal policy. Indeed according to [26], nonlinear optimization is key to minimizing the damage to an engine.

Model predictive control approaches, developed in [27], [13] for the transient control of a reusable engine, prove to be a powerful tool for optimal control policies. The approach relies on the determination of an optimal time frame for the prediction of the model behavior, and the cost function of the

optimization which determines the objectives of the controller. In this sense, this optimization problem offers more flexibility to the user, with the tuning of the cost function to determine the control policies.

In parallel to this work, control strategies have been developed in an ongoing thesis, which aims to design a robust controller for the transient regime of an LPRE using neural networks-based controllers [28, 29]. The reinforcement learning approach is developed for the control of the transient regime of an LPRE. The control is computed after training a neural network on a proposed model and allows for a controller with good performance. The author furthermore emphasizes the benefits of a reinforced learning-based controller :

- Diversification of the objectives of the controller (the reward function used to define the objective can be tuned by the user).
- Multiplicity of the considered variables of the physical system (provided the reinforced learning is able to find a solution to the optimization problem defined by the variables).
- Robust to operating conditions.

Following from these conclusions, the reinforcement learning approach is a suitable technology for the aerospace domain, as it allows for an accurate modeling of nonlinear dynamics, notably for fault detection [30]. However, this approach does not provide a proof of stability of the LPRE system.

1.3 . Stability of an LPRE state-of-the-art

While efficient and robust control laws have been designed for an LPRE system, validation of the stability lacks mathematical demonstration. In [31, 32], the author proposes stable region computation for the combustion chamber of an LPRE and frequency couplings between the different components of an LPRE. This method requires frequency plots of the system and proves to be complex. Although rocket engines are often considered stable systems, hence the multiplicity of open-loop controllers, the need for a proper demonstration validating future control laws is required. In this section, the stability requirements for an LPRE are presented. The definition of stability is briefly recalled in a first place, and the objectives facing the problem statement are defined in a second time.

1.3.1 . Stability requirements

The notion of stability of the closed-loop controlled LPRE in a permanent regime is seldom evoked in the literature. Indeed in a classical engine, the notion of stability is often associated with the coupling of oscillations between the different phenomena (chugging, chamber instabilities). In this work, the notion of stability concerns the coupling of the closed-loop controller with the engine. In the literature, proof of the stability of the controller is often not required as the thrust requirement evolves in a narrow space around the desired nominal thrust. In throttling engines, the engine is required to perform transitions between operating points, leaving room for uncertainties and unstable behavior to disturb the functioning of the engine. The validity domain of the evolution models for LPREs adds complexity to the study, as the edges of the validity domain often prove to lose some representativeness of the states. To account for this, stability requirements are introduced for a rocket engine.

In control theory, the stability of a system characterizes the ability of a system to remain within a

bounded domain of the state-space. This is often associated with the notion of convergence of the states to a single point, and stability can characterize an operating point of the state-space.

Let an autonomous system, of state $x \in \mathbb{R}^n$ and non-linear vector function $f : \mathbb{R}^n \to \mathbb{R}^n$ and let f be locally Lipschitz over a domain $\mathbb{D} \subset \mathbb{R}$,

$$\dot{x} = f(x). \tag{1.1}$$

An equilibrium point x_0 of the system (1.1) is defined such that

$$f(x_0) = 0. \tag{1.2}$$

Definition 1. An equilibrium point [33] is **stable** if for each $\epsilon > 0$, there exists $\delta > 0$ such that

$$||x(0) - x_0|| < \delta \Rightarrow ||x(t) - x_0|| < \epsilon, \forall t > 0. \tag{1.3}$$

Conversely, an equilibrium is said to be **unstable** if property (1.3) does not stand. This definition of stability characterizes a region of the domain $\mathbb{D}$, where an autonomous system remains at all times. Such characterization of stability is insufficient for the study, as oscillations of the system are not considered unstable behavior according to this definition. The stability definition aimed for the LPRE study is asymptotic stability.

Definition 2. An equilibrium point is **asymptotically stable** [33] if it is stable and

$$\exists \delta > 0, ||x(0) - x_0|| < \delta \Rightarrow \lim_{t \to \infty} x(t) = x_0. \tag{1.4}$$

In this case, the solution $x(t)$ is said to converge asymptotically to x_0.

This definition of stability is more suitable for a non-linear system, as it contains the requirements of the study : the convergence of the solution to the equilibrium of the system, and the stability of the system.

Definition 3. The region of asymptotic stability [33] (also called region of attraction) is the set of all points $\hat{x}$ in $\mathbb{D}$ such that the solution of $\dot{x} = f(x)$ for initial condition $x(0) = \hat{x}$ is defined for all time $t > 0$ and converges to the equilibrium x_0 when t tends to ∞.

The equilibrium x_0 is globally asymptotically stable if the region of asymptotic stability is the whole space $\mathbb{R}^n$.

More powerful definitions of the stability of an equilibrium are available in the literature, such as the exponential stability of an equilibrium.

Definition 4. An equilibrium point x_0 is exponentially stable [33] if

$$||x(t) - x_0|| \leq k||x(0) - x_0||e^{-\lambda t}, \forall t > 0 \tag{1.5}$$

with $k \geq 1$, $\lambda > 0$, for all $||x(0)|| < c$.

where c is a constant that defines the radius of the region of exponential stability.

Stability analysis of a system often relies on the Lyapunov theorem [33],

Theorem 1. Lyapunov If there exists a continuously differentiable positive definite function $V(x)$ such that $\dot{V}(x)$ is negative semidefinite, then the origin of the system is stable. If $\dot{V}(x)$ is negative definite, then the origin is asymptotically stable.

The definition of the Lyapunov function characterizes the equilibrium corresponding to the origin of the system. For a different equilibrium, the definition holds, if the minimum of the Lyapunov function is $V(x_0)$. Finding a Lyapunov function for a system is a sufficient condition to assert the stability of the system. Since there is no general method that yields a Lyapunov function, failure to retrieve such a function does not imply instability.

For a non-autonomous system,

$$\dot{x} = f(x, u) \tag{1.6}$$

where $u \in \mathbb{R}^p$ is the controller and $f : \mathbb{R}^n \times \mathbb{R}^p \to \mathbb{R}^n$. The notion of stability for a controlled system requires taking into account the controller action. The equilibrium of a system is expressed for a couple (x_0, u_0). In order to introduce the controller action in the stability equation, the notion of passivity of a system is introduced.

Definition 5. A system

$$\begin{aligned} \dot{x} &= f(x, u) \\ y &= h(x, u), \end{aligned} \tag{1.7}$$

is *dissipative* with supply rate $w(u, y)$ if there exists a storage function $S(x)$, $S(0) = 0$, such that for all x,

$$S(x) \geq 0 \text{ and } S(x(T)) - S(x(0)) \leq \int_0^T w(u(t), y(t)). \tag{1.8}$$

Definition 6. A system is *passive* if it is dissipative with supply rate $w(u, y) = u^\top y$. If the storage function S is differentiable, then the equation (1.8) for a passive system can be written,

$$\dot{S}(x) \leq u^\top y. \tag{1.9}$$

If the system (1.7) is passive with a positive storage function $S(x)$, then the equilibrium $\dot{x} = f(x, 0)$ is stable. A strictly passive system is defined by the following storage function

$$\dot{S}(x) + \psi(x) \leq u^\top y. \tag{1.10}$$

where ψ is a positive definite function. If the system (1.7) is strictly passive, then the equilibrium $\dot{x} = f(x, 0)$ is asymptotically stable.

In this thesis, proof of asymptotic stability of an equilibrium x_0 of a closed-loop controlled LPRE model is sought.

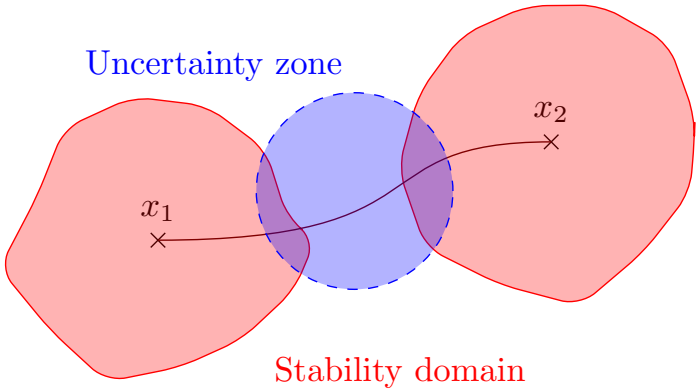

Figure 1.2 – Stability during a transition between operating points

1.3.2 . Point-based stability

Stability analysis of a system, according to the previous definitions, is driven relative to an equilibrium point of the system. Such analysis studies the convergence of the solutions for initial conditions of x. In the case of an LPRE, asymptotic convergence of the system to different equilibria defined by the controller is enough to ensure stable transitions between operating points. This can be performed by analysis of an increasing number of operating points so that the attraction regions overlap. A stable transition from one operating point to another can be performed when the initial condition is situated in both attractors (the initial and the target attraction regions). Such a method is applicable for discrete inputs, with a succession of operating points that the system must follow. In this case, to ensure the stability of the system, the initial condition $x[n]$ must be in both the attraction region of the $n+1$ target point and the one of n the point of the reference. For a time-continuous reference, it is therefore necessary to discretize the input in order to study the evolution of the attraction region of the system. This can be performed by choosing a sufficient number of operating points such that attractors can be defined and fulfill the conditions. In figure 1.2, the transition between two operating points x_1 and x_2 is illustrated. If the attractors defined around the operating points have no intersection, then an uncertain region appears, where no stability proof is available.

An alternative to this is to introduce the notion of convergence of a trajectory and consider the flow of trajectories of a system. Such analysis is performed in chapter 5.

1.3.3 . Review of stability analysis methods in rocket engines

Previous to this work, Sergio Pérez-Roca [13] developed an analysis and control on the transient behavior of the state-space of an LPRE. The author developed an MPC-based control for robust control of the transient behavior of a rocket engine, paired with an analysis of the stability of the engine. The analysis has emphasized the difficulties of obtaining a Lyapunov function for the complex nonlinear behavior of the system.

The stability analysis and design of a stabilizing controller is seldom performed, and the stable behavior is proven by simulations of the system. Analysis of the stability is seldom proposed in the literature, in [34], the author derives the state space responses for a variable thrust engine, with a pressure-fed actuator. However, no formal stability guarantees are derived. In [35], the author proposes a stabilizing

control design for combustion processes in LPREs, with validation of the stable behavior through simulations.

In linear modeling of an LPRE, stability analysis can be derived from the poles of the transfer function [13]. However, extension of the results to a non-linear model proves to be difficult, as few references are available. A common approach for non-linear systems relies on the definition of a Lyapunov function, which proves the stability of the system around an equilibrium. As stated in [13], derivation of a Lyapunov function for such complex non-linear systems proves to be very difficult in a direct approach, due to the lack of methodology to find a Lyapunov function. An alternative that relies on the physical interpretation of the system is the passivity of a system. Formal stabilizing designs have been proposed, mainly through the use of a passivity-based controller [36, 37]. As the rocket engine constitutes a combustion system, which consumes propellants to produce a thrust, the notion of passivity of the system is a suitable approach for stability analysis. Although the latter has been proven for several subsystems used in a rocket engine, the formal proof of the passivity of an engine is lacking in the literature. Passivity analysis of systems that present similar properties to that of an engine has been driven, for example in [38] for a class of chemical reactors. The passivity of the system is proven by an entropy production approach, resulting from the chemical reaction that occurs. In [39], a Lyapunov function-based controller is derived for a turbocharged diesel engine, which in design resembles a simplified and less powerful rocket engine. A passivity analysis of a full re-entry body, using a gliding strategy is provided in [40]. The author shows that while passivity conditions are not met in the whole considered domain, a simple feed-forward controller allows it to fulfill the passivity requirements. In the field of LPREs, the mass flow regulation for an LPRE has been studied in [41], where the regulation of the flows in the feeding lines of an LPRE is performed using a passive controller. While these approaches lack validation on a rocket engine, they provide useful insights on the method to be carried on a rocket engine to analyze the passivity of the system.

1.3.4 . Review of classical perturbations and instabilities

When studying the stability of a system, it is necessary to derive the main perturbations and instabilities dealt with in the considered system. Although many phenomena are neglected in the approach chosen, due to the high frequencies of said phenomena, robustness requirements are derived from the perturbations mentioned in the literature. A thorough study of combustion instabilities is proposed in [42]. According to this source, the main combustion instabilities rely on oscillations of thermo-acoustic modes in the combustion. For smooth combustion, such oscillations should not exceed 5% of the chamber pressure value. Such oscillations can lead to mass flow perturbation, and reflect on the rest of the system. Similarly in [43], the author derives simulations for the modeling of combustion instabilities and the results show a variation of 6% of the pressure value. As combustion instabilities depend on the geometry of the nozzle, the propellants used and the injector properties, several relevant pieces of the literature can be mentioned.

A second source of instability of an engine is engine failures, which are not considered in this thesis.

When dealing with down-throttling, another source of instability relies on the different elements, operating lower than for their nominal design. A comprehensive review by [7] describes the loss of performance in certain components and changes in behavior. The loss of efficiency of certain components can hardly be illustrated in a steady-state, but can be a source of instability under a certain threshold. For example, the author in [7] describes injector components that suffer a high drop in performance

under 20% of the nominal value, leading to a sharp decrease in combustion efficiency.

Most of the perturbations in this work will be illustrated with the addition of noise to the chamber equations. In 2, a closer insight into the modeling hypothesis and phenomena taken into account is given.

1.4 . Summary and answers provided

In the wake of reusable rockets, the design of rocket engines and technological requirements have shifted to the ability to perform efficiently for a wide range of thrust variations. The control laws built to satisfy the mission requirements have consequently increased in complexity, and the need for optimal control has led to several new technologies being introduced. However, the down-throttling of an engine introduces new perturbations and uncertainties in the engine's functioning, leading to the need for robust and stable control. While robust control laws have been designed to face perturbations, the analysis lacks formal proof of the stability of the engine, and stability is often proved in simulations, or assumed around the functioning points considered. The proof of the stability of an engine is a powerful tool that enables new control laws to emerge, under the guarantees provided by the stability of the engine. Validation of a controller can be performed using the initial properties of the engine, and understanding the limits of the modeling are all important consequences of the initial stability analysis.

In this thesis, we aim to provide a better understanding of the stability of the engine. While stability proof is often performed by the derivation of a Lyapunov function, it is shown that the complexity of the state-space model makes it no easy task [13]. In chapter 2, the state-space modeling of an LPRE is presented. This state-space is designed using non-linear equations for the behavior of the components in a GG cycle of an LPRE. The limitations of the state-space analysis render the direct approach to stability cumbersome (for example finding a Lyapunov function) and therefore this work proposes a new formulation of the dynamics of the engine, more adapted to the stability analysis under Port-Hamiltonian form [44], in 3. This reformulation provides insights into a formal proof of the passivity of the LPRE system, and the design of a passivity-based controller following the new reformulation is proposed. Such proof provides the asymptotic stability of the system, but faces the issue mentioned in 1.3.2, to assert stability over a trajectory. To address this, a second analysis using contraction theory [45] focuses on the stability of the LPRE facing a reference trajectory in chapter 5. In chapter 6, the comparison between the modeling approaches is provided, and simulations of the controllers show the stabilizing properties of the different approaches.

1.5 . List of publications

The following list summarizes the publications in the scope of this thesis.
Peer-Reviewed International Conference papers :

1. Gibart J., Piet-Lahanier H., Farago F., Galeotta M., *Regulation of a liquid-propelled rocket engine using contraction theory*, in 12th IFAC symposium on Nonlinear Control Systems (NOLCOS), (Camberra, Australia), pp. 307-312, January 2023. [46].
2. Gibart J., Piet-Lahanier H., Farago F., *Port-Hamiltonian Modelling of Complex Non-Linear Systems, Application to a liquid-propelled Rocket Engine*, in 8th IFAC Workshop on Lagrangian and Hamiltonian Methods for Non Linear Control - LHMNC 2024, (Besançon, FRANCE), June 2024. [47].

3. Murata, Renato and Gibart, Jules and Marzat, Julien and Piet-Lahanier, Hélene and Boujnah, Sandra and Farago, François, *Structural analysis of a rocket's multi-engine propulsion cluster for fault detection and isolation*, in 12th IFAC symposium on Fault Detection, Supervision and Safety for Technical Processes (SAFEPROCESS), (Ferrarra, Italy), June 2024. [48].
4. Gibart J., Piet-Lahanier H., Farago F., *Mass flow control design for a reusable liquid-propelled rocket engine using contraction theory*, in American Control Conference (ACC), (Toronto, Canada), July 2024. [49].

Abstract-selection International Conference papers :

5. Gibart J., Piet-Lahanier H., Farago F., *Stabilizing control design for liquid-propelled rocket engines*, in 9th Edition of the Space Propulsion Conference 3af, (Glasgow, Scotland), May 2024. [50].

2 - State-space model of an LPRE

This chapter describes the state-space model of an LPRE. This model will be used for the simulations described in the next chapters. A model for the transient behavior of an LPRE was developed in Sergio Perèz-Roca Ph-D Thesis [13]. It is used as a basis for the current model which aims at representing the permanent regime. The set of physical equations is thus unchanged but some simplifications are made.

The description of the considered engine is given in Section 2.1, where the hypotheses formulated are listed, and the main differences with a transient modeling are emphasized. In Section 2.2, the physical equations for each component are detailed. A simplified and a complete model are described in Section 2.3. An analysis of the limitations of the description in state-space form is provided in Section 2.4.

2.1 . Modeling of a reusable LPRE in permanent regime

The engine used for a reusable launcher must be able to achieve the variations of thrust required during the powered landing of the rocket's first stage. The engine considered in this thesis consists in a liquid-propelled rocket engine with a gas-generator cycle, regulated using electrical actuators. The actuators consist of valves whose openings modify the mass flows in the feeding lines. The valves respond to an electrical stimulation from the on-board control devices. During the landing phase of the stage, the combustion is already established in the different chambers, and the engine is in a permanent regime.

This section describes the cycle of a gas generator LPRE, and details the hypotheses and differences with a transient modeling.

2.1.1 . Description of the gas-generator cycle

The engine considered in this thesis is inspired by [13]. A rocket engine propels the body of the rocket by providing a high thrust. The thrust action results from the ejection of matter through the nozzle at hyper-sonic speeds. The conservation of the quantity of movement allows the body of the rocket to be propelled by the counteraction of the ejected gas. To this end, the rocket engine features a main combustion chamber, whose aim is to create high-pressure gases with the combustion of both fuel and oxidizer in the chamber. The ejected gases are composed of the products of the chemical reaction and unburned species. In the following, the components allowing to obtain a high pressure in the combustion chamber are described.

First, the fuel and oxidizer chosen for this study are liquid hydrogen (LH) and liquid oxygen (LO). The two propellants are fed to the system using two distinct tanks, that provide an initial storage pressure to the propellants. Contrary to simple cycles that rely on the pressure provided by the tanks, the gas-generator cycle aims to increase the tank pressure with the use of turbopumps. To this end, two turbopumps are placed at the outputs of the tanks in the cycle providing an increase of pressure in the feeding line of the cycle. To power the turbopumps, the cycle makes use of a gas-generator, which consists of a secondary combustion chamber that aims to propel the turbopumps. A portion of the propellants in the feeding line is redirected to the gas-generator, to be burned. The hot gases hereby produced are redirected in both turbines and provide the necessary torque for the functioning of the turbopumps. The hot gases are then ejected in the turbine exhaust directly into the ambient atmosphere.

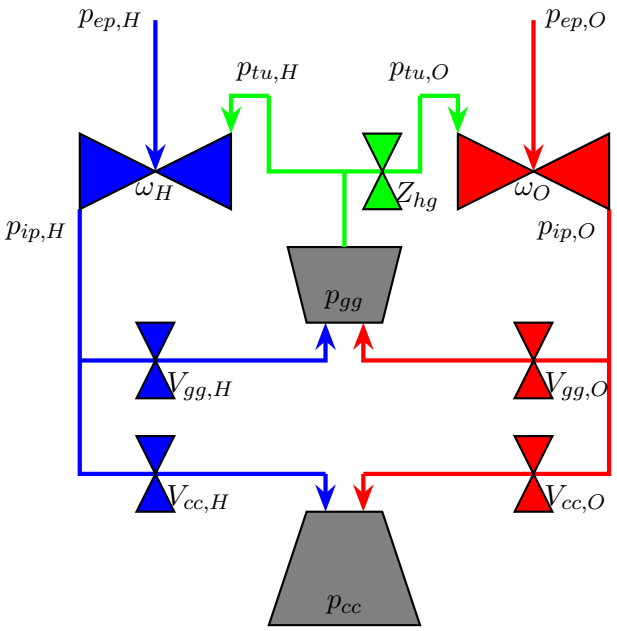

Figure 2.1 – Representation of the gas generator cycle

The main combustion chamber is the receptacle of the combustion, expansion, and temperature increase of the species in the reacting chamber. The propellants are fed to the reacting chamber through injectors, which aim to the scattering of the propellants, to obtain a homogeneous mixture of fuel and oxidizer and optimize the chemical efficiency. Moreover, the injection results in a pressure drop in the line, that prevents the mass flows from reversing as the injection pressure is lower than the turbopump outlet pressure. The high temperature in the main combustion chamber requires the addition of a regenerative circuit. It consists of the hydrogen line circulating around the chamber's walls to transfer heat and prevent damage to the engine.

Six propellant lines are considered in the modeling, summarized in table 2.1. The mass flows with the subscript H consist in liquid hydrogen, while the subscript O denotes liquid hydrogen. Note that for the turbine mass flows $q_{tu,\bullet}$, the composition of the mass flow is burned gas.

To describe the evolution of the combustion that takes place in the main combustion chamber, it is necessary to obtain the ratios between the different reactive species in the chemical process. To this end, the mixture ratio MR is introduced for both chambers (MR_{cc} and MR_{gg}), defined by $MR = \frac{q_O}{q_H}$ for both chambers, where q_O, q_H are the oxygen and hydrogen mass flows entering the chamber.

Each propellant line mass flow is powered by the difference between the upstream and downstream flow pressures. To model the evolution of the mass flows over time, the following pressures are considered, represented in figure 2.1 : the main chamber pressure (p_{cc}), the gas generator pressure (p_{gg}) and the turbine input pressures ($p_{tu,H}$,$p_{tu,O}$). Additionally, the tank pressures ($p_{ep,H}$,$p_{ep,O}$) and the pressure at the outlet of the turbopumps are considered ($p_{ip,H}$,$p_{ip,O}$) in the modeling. Note that the pressure outlet is different from the pressure increase $\Delta p_{ip,\bullet}$ with the relation $p_{ip,\bullet} = \Delta p_{ip,\bullet} + p_{ep,\bullet}$.

The system is controlled using five distinct valves,

- $V_{gg,H}$,$V_{gg,O}$ regulate the mass flows inputs of the gas generator $q_{gg,H}$, $q_{gg,O}$, by changing the equi-

Massflow	Function	Upstream pressure	Downstream pressure	Valve associated
$q_{cc,H}$	Feed the main combustion chamber	$p_{ip,H}$	p_{cc}	$V_{cc,H}$
$q_{cc,O}$	Feed the main combustion chamber	$p_{ip,O}$	p_{cc}	$V_{cc,O}$
$q_{gg,H}$	Feed the gas-generator	$p_{ip,H}$	p_{gg}	$V_{gg,H}$
$q_{gg,O}$	Feed the gas-generator	$p_{ip,O}$	p_{gg}	$V_{gg,O}$
$q_{tu,H}$	Feed the Hydrogen turbine	p_{gg}	$p_{tu,H}$	None
$q_{tu,O}$	Feed the Oxygen turbine	p_{gg}	$p_{tu,O}$	V_{hg}

Table 2.1 – Description of the different considered mass flows $q_\bullet$

valent resistance $Z_{valve} = \frac{1}{2\rho A_{valve}^2}$ where A_{valve} is the opening surface of the valve. This equivalent resistance denotes the friction induced by the valve in the mass flow equation detailed later in (2.19).

- $V_{cc,H}$,$V_{cc,O}$ regulate the mass flows input of the main combustion chamber $q_{cc,H}, q_{cc,O}$, similarly to the gas generator valves.
- V_{hg} aims to regulate the flows of hot gases between the different turbines $q_{tu,H}, q_{tu,O}$, distributing the power to both turbopumps.

The control action of the valves in the LPRE aims to regulate the thrust of the engine. While not used in the state-space model, the thrust of the engine is directly computed from the main chamber pressure,

$$F = q_{out} I_{sp} g_0 \tag{2.1}$$

where I_{sp} is the specific impulse of the engine in a vacuum, g_0 is the standard gravity acceleration and q_{out} is the output mass flow of the engine (ejected matter), that is computed in the component formulation in (2.22). The ejected matter flow q_{out} is computed using the chamber pressure, leading to the reformulation,

$$F = C_F p_{cc} A_{th} \tag{2.2}$$

where C_F is the thrust coefficient, A_{th} is the throat area. In the following of this work, the goal of the controllers established will be to regulate the main chamber pressure p_{cc} which is analog to the thrust as shown in (2.2).

In order to give an insight on the orders of magnitude of the different variables described, table 2.2 represents the operating data of a liquid-propelled rocket engine taken from [13] are presented. This data will be mentioned in this work as a reference for the orders of magnitude between variables. Typically, the conditioning of matrices derived from the state space provided in 2.3 will be described through this data.

2.1.2 . Physical considerations and hypotheses

Differences with a transient model

In this thesis, the focus of the stability analysis is on the permanent regime of the rocket engine. In this sense, it differs from the model in [13] as new simplifications and hypotheses can be formulated. In a

Variable	Value
Chamber mixture ratio MR_{cc}	6
Gas generator mixture ratio MR_{gg}	1
Thrust F (ground)	815kN
Chamber pressure p_{cc}	100bar
Gas generator pressure p_{gg}	87bar
Chamber temperature Θ_{cc}	3500K
Gas generator temperature Θ_{gg}	1000K
Hydrogen turbopump rotational impulse ω_H	$[28500, 36000]$rpm
Oxygen turbopump rotational impulse ω_O	$[11000, 14800]$rpm

Table 2.2 – Example of steady-state operating data [13]

start-up transient, an additional mass flow starts the ignition in the gas generator which is not featured in this work. Indeed, during the start-up, it is necessary to initiate the rotation of the turbopumps and flow the fuels to the combustion chamber to pursue the chemical reaction. During the permanent regime, however, this input in the gas generator is not used, as the combustion is already set and running.

The valves controlling the mass flows in the main combustion chamber lines do not change position during a permanent regime as their purpose is to redirect the propellants in the gas generator during the system ignition. Both valves $V_{cc,H}, V_{cc,O}$ are therefore considered of constant value.

The temperature mainly depends on the mixture ratio of the considered combustion chamber, in a permanent regime, and for a good regulation of the mixture ratio (i.e. the mixture ratio has a very small range of variation), the temperature variations can be neglected in the main combustion chamber.

The domain of the study is greatly affected by the validity of the approximations used for the different components (see 2.2.1). The components provided are not valid for low thrusts and therefore it is necessary to adapt the considered range of variation. In this thesis, we consider a domain of functioning between 100% and 150% of the states' nominal values, corresponding to the steady-state of the engine.

Simplifications and hypotheses

The functioning of the main combustion chamber is simplified by considering that the design has been performed to drastically reduce the instabilities in the combustion. Combustion instabilities mainly originate from the thermo-acoustic shock waves produced during the combustion. These waves manifest in the combustion pressure by introducing oscillations that can range to $5-7\%$ of the pressure value p_{cc} depending on the design of the chamber ([42, 43]). Higher frequency phenomena originate from the injectors, with the scattering and mixing of the species in the chamber. The components are supposed well designed so that such phenomena do not occur. Chugging, cavitation, and water hammer surges are in this model neglected as in other simulations [13, 51, 52] and the system is considered well mechanically designed to avoid such phenomena in the lines. In general, high-frequency phenomena (when compared to the actuators $> 10Hz$) are considered out of the scope of this work, and the thermo-acoustic oscillations are represented with the addition of noise on the chamber temperature in 6.

One of the main hypotheses of the system is the simplification of the thermodynamic parameters

such as the specific heat ratio γ or the heat capacity at constant volume C_v. The chemical reaction is also simplified by considering the efficiency of the reaction constant and equal to 1. This implies that all reactive species are consumed (until the stoichiometric ratio). Additionally, the fractions of species created in the chemical reaction are supposed constant, neglecting combustion instabilities. Finally, the effect of the cooling circuit on the combustion temperature is neglected, from the chamber perspective only. This simplification has been compared with a more complex state-space in [13], and illustrated a difference of behavior in the transient phase of the engine, mainly on the mass-flow behavior (which varies around 5% of the real value). However, the effects on the permanent regime are negligible as the author in [13] registered a less than 1% difference in the final value of the transient simulation.

All fluids are presumed to follow the perfect gas law (2.9). Additionally, the liquid propellants in the feeding lines (q_{cc}, q_{gg}) are considered of constant density ρ. Note that this hypothesis only concerns the feeding lines and not the hot gas line, where the density varies with the pressure in the gas generator. The regenerative circuit is simplified and is represented with an increase in the temperature of the fuel LH_2, and a resistive term in the mass flow equation. Indeed in [53], a RANS-based numerical simulation of a combustion chamber is proposed, to model the heat flux circulation in the regenerative circuit of an LPRE. The main result shows that the heat flow have a strong impact near the cooling walls, with a low impact on the overall flow.

The fluid tanks in the LPRE are considered ideal in the state-space equations. Such a hypothesis implies that the pressure delivered by the tanks does not vary over time (in practice, this pressure varies due to the acceleration of the stage, however is measurable, which allows to mitigate the impact on the system), and is considered constant. The tanks are therefore considered an infinite pressure reservoir, with the pressure p_{ep}. In practice, the fluid tanks' pressure $p_{ep,\bullet}$ is maintained by pressurized Helium [52]. The small variations of the tank pressure [54] has a very low impact on the system, as shown in 6.1.5, where a variation of 10% in the tank pressure $p_{ep,\bullet}$ results in a variation of 0.2% for the chamber pressure p_{cc}.

2.2 . Components modeling

The different equations considered in the model are regrouped around the corresponding component. This allows to encapsulate the different physical domains covered by the individual components of the engine. Additionally, the model is simplified in a first approach, by considering only a certain amount of physical components. In this section, the physical equations that dictate the component's behavior are described. The modeling of the components follows the equations described in [13], and are recalled here.

The conservation equations used in the determination of the system state-space are the following

- The conservation of mass, written in (2.3).
- The conservation of momentum, in (2.5).
- The conservation of energy, in (2.6).
- The conservation of kinetic momentum, in (2.8).

The general form of the conservation of mass equation in a flow is,

$$\frac{\partial}{\partial t}\int_V \rho dV + \int_A \rho.(\vec{n}.\vec{v})dA = 0, \tag{2.3}$$

where V is a control volume, A is a control area, for instance, the area of the pipe in which the considered flow circulates, $\vec{n}, \vec{v}$ are respectively the normal vector to the area and the flow velocity and ρ is the density of the fluid. Equation (2.3) is applied to constant-volume cavities, for a pipe with a constant area and is rewritten,

$$V\frac{d\rho}{dt} = q_{in} - q_{out} \tag{2.4}$$

where q_{in}, q_{out} are the input and output flows of the cavity. In particular, this expression is used at the intersection between the GG and CC lines. Indeed to describe the relation between the flow through the pump and both flows in the GG and CC line, the conservation of mass is used (2.4). As the density ρ of the fluids is considered constant in the lines, the input and output flows are equal. The mass flow circulating in the turbopump is then the sum of both mass flows in the split, $q_{cc} + q_{gg}$.

The general form of the conservation of momentum is expressed

$$\frac{\partial}{\partial t}\int_V \vec{v}\rho dV + \int_A \vec{v}\rho.(\vec{n}.\vec{v})dA = 0. \tag{2.5}$$

The conservation of energy is written,

$$\frac{\partial}{\partial t}\int_V e\rho dV + \int_A e\rho.(\vec{n}.\vec{v})dA = \psi. \tag{2.6}$$

where ψ is the heat transferred to the closed system under consideration, e is the energy per unit of volume. To apply this equation to the combustion chambers, the following formulation is used in [55],

$$\frac{d}{dt}\left(\frac{pV}{\gamma - 1}\right) = h_{in}q_{in} - h_{out}q_{out} + \psi, \tag{2.7}$$

where h is the enthalpy per unit of mass of the considered flow. In the scope of this thesis, the heat transfers through the walls are neglected in combustion chambers, therefore the heat term ψ is neglected in this approach. Note that for the expander cycle, for example, such a term is not negligible as it is responsible for fluid expansion and therefore propels the turbines.

Finally, the conservation of the momentum is written,

$$\frac{d\omega}{dt} = \frac{1}{J}\sum_i T_i, \tag{2.8}$$

where J is the kinetic inertia of the pump, and T_i are the different torques applied to the considered system (see 2.2.1,2.2.1).

Additionally, consider the perfect gas equation

$$p = \rho RT \tag{2.9}$$

In the following, the description and equations of the different components are provided, deriving from the physical equations presented.

2.2.1 . Pumps modeling

Motopumps modeling

A motopump is an ideal component that provides a pressure increase from an energetic input from the exterior of the system. Here the considered motopump delivers a pressure increase in the fuel lines from an input in the form of a torque (T_m) or a power (P_m). The behavior of such a system is complex to model as it implies both the mass flow of the fluid in the line and the rotational speed of the pump. The component behavior is described using two equations, the formulation of the pressure increase in the line Δp_{ip} and the resistive torque T_r resulting from the energy transfer from the pump to the fluid. Each equation corresponds to a polynomial description of the considered term (Δp_{ip} or T_r) provided by the manufacturer [13], and is recalled here. The equation of the resistive torque from the pumped fluid is,

$$T_r = |\frac{a_c}{\rho} q_{cc}^2 + b_c q_{cc} \omega + c_c \rho \omega^2|, \tag{2.10}$$

where the coefficients a_c, b_c, c_c are given by the constructor. With the considered range of variations of the parameters ($100\% - 150\%$ of nominal value), the torque equation (2.10) does not become negative, and for simplification, the absolute value is suppressed in the following equations. Similarly, a second polynomial function is given for the pressure increase $\Delta p_i p$,

$$\Delta p_{ip} = \frac{a_p}{\rho} q_{cc}^2 + b_p q_{cc} \omega + c_p \rho \omega^2. \tag{2.11}$$

The polynomial function denoted in (2.10) paired with the conservation of the kinetic momentum (2.8) leads to the evolution of the rotational speed of the pump,

$$\dot{\omega} = \frac{1}{J} \left(T_m - T_r \right), \tag{2.12}$$

where the motor torque is given as the input.

Remark 1. The motopump component requires an input torque or power, originating from another component on board the rocket. In practice, the component supplying the required torque (resp. power) is the turbine (with some exceptions such as in [56], which considers electro-pumps), which is propelled with the exhaust gases of the GG. In this case, as the torque generation (resp. power) is decided by the user, it supposes the existence of a perfect storage of torque (resp. power). In fact, one could see the motopump as the ideal gas-generator. Such an ideal gas-generator would provide the exact torque desired by the user, yielding an energetic input for regulation purposes.

Turbines and turbopumps

The turbine's main function is to provide a motor torque for the pump, T_m. The equation of T_m is constructed using constructor data. First define a reduced rotational speed N_R,

$$N_R = \frac{\omega d_t u}{\sqrt{\gamma R \Theta_{gg}}}. \tag{2.13}$$

where d_tu is the diameter of the turbine. The reduced rotational speed is used to build a polynomial approximation of the data provided by the manufacturer [13], corresponding to a regression using 8 coefficients that approximate the specific torque of the turbine,

$$ST = (a_1 + N_R(a_2 + N_R a_3) + \pi_{tu}(a4 + \pi_{tu} a_5) + a_6 \pi_{tu} N_R + a_7 \ln \pi_{tu} + a_8 \ln N_R).Corr \tag{2.14}$$

where the $a_1, ...a_8$ are constant coefficients determined by subsystem tests, and π_{tu} is the pressure ratio between the inlet and outlet of the turbine. As both pressures are computed using the choked equation (2.22), this ratio can be computed with the ratio between both the turbine inlet and outlet areas $\pi_T = \frac{A_{tu}}{A_{tu,outlet}}$, leading to a constant value. The approximation here concerns the validity of the choked equation for the turbine intake. As described in [13], the design of hot lines in a gas generator features small areas, to maximize the expansion of the hot gases in the turbine, justifying the use of the choked equation.

The work of the mass flow on the turbine is given by

$$W = q_{out} \frac{\sqrt{\gamma R \Theta_{gg}}}{\gamma - 1} (1 - \pi_{tu}^{\frac{1-\gamma}{\gamma}}) d_{tu} \tag{2.15}$$

where the mass flow q_{out} is computed with the choked equation (2.22),

$$q_{out} = \frac{p_{tu} A_{tu}}{\gamma} \sqrt{\frac{R\Theta_{gg}}{\gamma} (\frac{2}{\gamma + 1})^{-\frac{\gamma+1}{\gamma-1}}}. \tag{2.16}$$

This equation can be used in the case of supersonic turbines, which is the case here. Again, a different cycle will lead to a different equation and considerations. Finally, the motor torque equation is given by,

$$T_m = ST.W \tag{2.17}$$

In the following, the fact that the equation for the leaving mass flow q_{out} is linear in the pressure is used, and the expression for the motor torque is denoted by

$$T_m = p_{tu} ST(\omega) w_{tu} \tag{2.18}$$

where $w_{tu} = \frac{A_{tu}}{\gamma} \sqrt{\frac{R\Theta}{\gamma} (\frac{2}{\gamma+1})^{-\frac{\gamma+1}{\gamma-1}}}$.

2.2.2 . Lines modeling

The modeling of the behavior of the fluid in the lines is expressed through the evolution of the flow through the pipe. The flow originates from the pressure difference between the pressure upstream and downstream in the line. Additionally, elements along the pipe that compose the line induce a resistive term in the momentum conservation equation. Equation (2.5) is used in the lines' expression as in [90,96], since the area and length of the pipe are constant,

$$\dot{q} = \frac{A}{L} \left(p_{in} - p_{out} - Z_{res} q|q| \right), \tag{2.19}$$

where L is the length of the line, and Z_{res} is the equivalent resistive coefficient of the line. The term $\frac{L}{A}$ is the inertia of the line and will be noted I_{line}. The resistive terms are expressed under a single term Z_{res}

in the momentum conservation (2.19). The different resistive elements originate from the resistance of the pipe itself Z_{pipe} (considered given by the manufacturer), the resistance of the injector of the combustion chamber at the end of the pipe Z_{inj} and the valve equivalent resistance Z_{valve} (see 2.2.6). As resistive terms are expressed under the same form $Z_{res}|q|q$, the different resistive terms are regrouped in the evolution equation $Z_{res} = Z_{pipe} + Z_{inj} + Z_{valve}$. For the main chamber hydrogen mass flow only, the regenerative circuit introduces an additional resistive term Z_{regen}. The inertia of the line $I_{line} = \frac{L}{A}$ depends on the opening area of the valve (detailed in 2.2.6). By notation abuse, the resistive term will be written $Z_{res}q^2$ since the considered domain solely contains positive mass flows. As an example, the evolution of the main chamber hydrogen mass flow $q_{cc,H}$ is expressed

$$\dot{q}_{cc,H} = \frac{1}{I}\left(p_{ip,H} - p_{cc} - (Z_{pipe} + Z_{inj} + Z_{valve} + Z_{regen})q_{cc}^2\right). \tag{2.20}$$

2.2.3 . Main combustion chamber modeling

The pressure evolution in the main combustion chamber is due to two main physical phenomena : the contribution in terms of kinetic energy from the entering mass flows in the chamber and the pressure increase to the combustion and creation of new species in the chamber. On the other hand, the dissipation of the energy is due to the matter leaving the chamber with the ejection of the hot gases through the nozzle, and the heating of the species entering the chamber, before their ignition. The evolution model of the pressure is taken as in [13].

First introduce the pressure variations due to the kinetic energy variations,

$$\frac{(\gamma_{out}-1)}{V_g}\left(\frac{\gamma_{in}p_{cc}}{(\gamma-1)\rho_{in}} + \frac{C_{v,in}p_{cc}(\gamma_{in}-\gamma_{out})}{C_{v,out}\rho_{cc}(\gamma_{out}-1)^2}\right)q_{in} - \frac{p_{cc}\gamma_{out}}{V_g\rho_c}q_{out} \tag{2.21}$$

where C_v denotes the heat capacity at constant volume of the mixture. q_{out} designates the output flow of the chamber, and is computed in permanent regime using the choked equation [57],

$$q_{out} = \frac{p_c A_{th}}{\sqrt{\frac{R\Theta_{cc}}{\gamma_{out}}\left(\frac{2}{\gamma_{out}+1}\right)^{-\frac{\gamma_{out}+1}{\gamma_{out}-1}}}} \tag{2.22}$$

The variation due to the creation and consumption of species follows,

$$(\gamma_{out}-1)\sum_{mixture}(\upsilon h_{f,i} - \frac{\gamma_{out}p_{cc}}{(\gamma_{out}-1)\rho_c}\sum_{mixture}\left(\frac{C_{p,i}}{C_{p,out}} - \frac{C_{v,i}}{C_{v,out}}\right)\upsilon_i), \tag{2.23}$$

where $h_{f,i}$ is the formation enthalpy of the associated specie and C_v denotes the heat capacity at constant pressure. υ designs the variation rate of each species per unit of volume denoted in [13]. Such variation rate solely depends on the mass flow and the mixture ratio. The subscript i is used in sums to denote one of the species considered (fuels H_2, O_2 or product H_2O). The term mixture denotes all the different species contained at a time t in the chamber, injected species are H_2 and O_2, and created species contain all combustion products. The subscript "in" therefore denotes only injected species, while the subscript "out" denotes created species and unburned fuel.

Finally, the variation originating from the heating of the injected species is expressed as,

$$\frac{(\gamma_{out}-1)}{V_g}\sum_{injected}(C_{p,out}\Theta_{vap,i} - (L_{v,j} + C_{p,i}(\Theta_{vap,i} - \Theta_{in,i})))\,q_{in}, \tag{2.24}$$

where Θ_{vap} denotes the vaporization temperature of a specie, $L_{v,j}$ is the vaporisation heat of a specie.

Equations (2.21), (2.23) and (2.24) are summed to obtain the total evolution of the chamber pressure p_{cc}. The three equations can be simplified when taking into account the constant nature of the thermodynamical terms and the permanent regime character of the chemical reaction. The different terms can be regrouped by first-order Taylor expansion [13] of the expression into,

$$\dot{p}_{cc} = (k_{4cc} + k_{5cc} + (k_{2cc} - k_{1cc})\Theta_{cc})(q_{cc,H} + q_{cc,O}) - k_{3cc}\sqrt{\Theta_{cc}}p_{cc}. \tag{2.25}$$

Remark 2. Noticing that both mass flows $q_{cc,H}, q_{cc,O}$ are multiplied by the same term in (2.25), it is possible to substitute $MR_{cc}q_{cc,H} = q_{cc,O}$ in the pressure p_{cc} equation. Thus p_{cc} only depends on $q_{cc,H}$ provided the value of the mixture ratio MR_{cc} is known. This substitution is used in the following chapters by supposing $MR_{cc} = 6$, to consider only the hydrogen line and simplify the system.

2.2.4 . Gas generator chamber modeling

The model of the gas generator chamber pressure p_{gg} is based on the same equations as the combustion chamber pressure p_{cc},

$$\dot{p}_{cc} = (k_{4cc} + k_{5cc} + (k_{2cc} - k_{1cc})\Theta_{cc})(q_{cc,H} + q_{cc,O}) - k_{3cc}\sqrt{\Theta_{cc}}p_{cc}.$$

The modeling of the gas generator follows the same equations as the main combustion chamber in 2.2.2, with the additional consideration that the mass flow leaving the cavity is modeled using the sum of both hot gas mass flows $q_{out,gg} = q_{tu,H} + q_{tu,O}$,

$$\dot{p}_{gg} = (k_{4gg} + k_{5gg} + (k_{2gg} - k_{1gg})\Theta_{gg})(q_{gg,H} + q_{gg,O}) - k_{3gg}\sqrt{\Theta_{gg}}(q_{tu,H} + q_{tu,O}). \tag{2.26}$$

Note that the pressure p_{gg} does not directly appear in the evolution equation. It is also necessary to modify the expected value for the mixture ratio. Indeed, the temperature tolerated in the gas-generator is lower than the temperature in the main combustion chamber. The desired mass flow is therefore chosen as $MR_{gg} = 1$.

2.2.5 . Turbine pressures modeling

The evolution of the turbine pressure is also based on the combustion chamber equations. Indeed, the turbine intake represents a cavity in which the pressured hot gases leaving the gas generator chamber expand and propel the turbine. In this sense, since this expansion involves no combustion, the pressure evolution only follows the kinetic contribution of the hot gases,

$$\frac{\gamma_{out}RT_{GG}}{V_{turbine}}q_{in} - \frac{p_{tu}\gamma_{out}}{V_g\rho_c}q_{out}$$

where $V_{turbine}$ is the equivalent volume of the turbine intake. The formulation of the turbine pressure evolution then follows,

$$\dot{p}_{tu,H} = k_{2tu,H}\Theta_{gg}q_{tu,H} - k_{3tu,H}\sqrt{\Theta_{gg}}p_{tu,H} \tag{2.27}$$

2.2.6 . Valves modeling

Valve components act as control surfaces for the mass flow regulation. We first describe the behavior of the valves situated in the lines $V_{gg,H}$, $V_{gg,O}$, $V_{cc,H}$, $V_{cc,O}$. The last valve V_{hg}'s conception differs from the line valves since it is designed to redirect hot gases in the turbines. Although the resistive equation defined by both valve types ((2.28), (2.29)) are similar, the hot gas needs additional computation to include the varying density of the hot gases.

The main effect of a line valve is to modify the value of the resistive term associated Z_{valve}. Let the area of a valve A_v, then the equivalent valve resistance is expressed as

$$Z_{valve} = \frac{1}{2\rho A_v^2}. \tag{2.28}$$

Additionally, the valve component dictates the inertia of a line under the form $I_{line} = \frac{A_v}{L}$.

The alternative valve used in the hot gas line is modeled using the same resistive effect, with $Z_{valve,hg} = \frac{1}{2\rho_{hg} A_{v,hg}^2}$. However, while the density can be reasonably considered constant in the feeding lines of the engine, the hot gases do not verify such a hypothesis. To represent the variations of the hot gas density ρ_{hg}, the perfect gas equation is used. The density is then a function of the pressure, leading to the resistive term

$$Z_{valve,hg} = \frac{RT_{gg}}{2p_{gg} A_{v,hg}^2}. \tag{2.29}$$

This dependency in p_{gg} is valid only for strictly positive GG pressure, which is the case in the scenarios accounted for in this thesis. In the case of the transient behavior in [13], the additional mass flow used to start the gas generator allows to set a positive minimum for p_{gg}.

Note that the dynamic evolution of the valve itself is not modeled, and the variation of A_v is considered instantaneous, as this is a control parameter for the regulation of the engine. The same considerations apply to the equivalent resistive coefficient Z_{valve}. To model the valve actuator more realistically, an introduction of their dynamics is proposed in 3 with a second-order model,

$$\ddot{A_v} = -2\xi w_0 \dot{A_v} - w_0^2 A_v, \tag{2.30}$$

for $\xi = 0.7$ and the pulsation $w_0 = 25 rad.s^{-1}$.

2.3 . State-space models

In this section, the state-space models that will be considered in this thesis are presented. Two separate space-state models have been developed in the scope of this thesis. A first, simplified model that does not feature the gas-generator part has been built to propose a first design for the control methods applied in the next chapters 3, 5. The method can then be generalized to a complex model, that takes into account the gas-generator elements of the LPRE. The extension of the method often requires additional considerations and conditions, highlighting the impact of the gas generator on the difficulties of analyzing the stability.

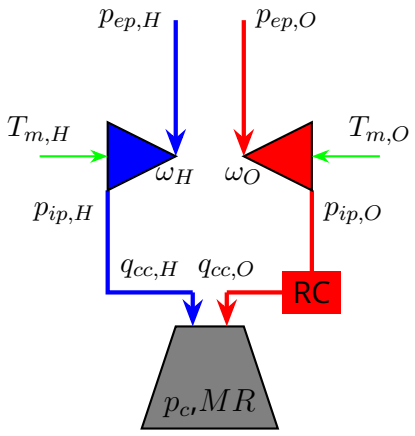

Figure 2.2 – Simplified state-space cycle under study

2.3.1 . Simplified model

The first model considered contains 5 states, as it only takes into account one hydrogen line and one oxygen line. It uses both mass flows for the combustion chamber $q_{cc,H}, q_{cc,O}$, the main combustion chamber pressure p_{cc} and the rotational speed for both motopumps ω_H, ω_O. The gas-generator part of the model is supposed ideal and the motor torques $T_{m,H}, T_{m,O}$ in the rotational speed equations (2.12) are the inputs of the system. The simplified model cycle is recalled in figure 2.2.

$$
\begin{aligned}
\dot{\omega}_H =& \frac{1}{J_H}\left(T_{m,H} - \left|\frac{a_{c,H}}{\rho_H} q_{cc,H}^2 + b_{c,H}\omega_H q_{cc,H} + c_{c,H}\rho_H \omega_H^2\right|\right) \\
\dot{q}_{cc,H} =& \frac{1}{I_{cc,H}}\left(p_{ep,H} - p_{cc} + (\frac{a_{p,H}}{\rho_H} - Z_{res,H}) q_{cc,H}^2 + b_{p,H}\omega_H q_{cc,H}\right. \\
& \left. + c_{p,H}\rho_H \omega_H^2\right) \\
\dot{\omega}_O =& \frac{1}{J_O}\left(T_{m,O} - \left|\frac{a_{c,O}}{\rho_O} q_{cc,O}^2 + b_{c,O}\omega_O q_{cc,O} + c_{c,O}\rho_O \omega_O^2\right|\right) \\
\dot{q}_{cc,O} =& \frac{1}{I_{cc,O}}\left(p_{ep,O} - p_{cc} + (\frac{a_{p,O}}{\rho_O} - Z_{res,O}) q_{cc,O}^2 + b_{p,O}\omega_O q_{cc,O}\right. \\
& \left. + c_{p,O}\rho_O \omega_O^2\right) \\
\dot{p}_{cc} =& (k_{4cc} + k_{5cc} + (k_{2cc} - k_{1cc})\Theta_{cc})(q_{cc,H} + q_{cc,O}) - k_{3cc}\sqrt{\Theta_{cc}} p_{cc}
\end{aligned}
\tag{2.31}
$$

For a power input P_m, the rotational speed ω equation (2.12) expresses

$$
\dot{\omega} = \frac{1}{J}\left(\frac{P_m}{\omega} - T_r\right). \tag{2.32}
$$

The fraction $\frac{1}{\omega}$, leads to an unstable term at the origin. Therefore by noticing that $\frac{d}{dt}(\omega^2) = 2 * \dot{\omega}\omega$, and multiplying both right and left terms in (2.32) by ω, it is more convenient to use the change of variables $\Omega = \omega^2$. which leads to the system expression,

$$
\begin{aligned}
\dot{\Omega}_H =& \frac{2}{J_H}\left(P_{m,H} - \left|\frac{a_{c,H}}{\rho_H} q_{cc,H}^2 \Omega_H^{\frac{1}{2}} + b_{c,H}\Omega_H q_{cc,H} + c_{c,H}\rho_H \Omega_H^{\frac{3}{2}}\right|\right) \\
\dot{q}_{cc,H} =& \frac{1}{I_{cc,H}}\Bigg(p_{ep,H} - p_{cc} + (\frac{a_{p,H}}{\rho_H} - Z_{rescc,H}) q_{cc,H}^2 + b_{p,H}\Omega_H^{\frac{1}{2}} q_{cc,H} \\
& + c_{p,H}\rho_H \Omega_H\Bigg) \\
\dot{\Omega}_O =& \frac{2}{J_O}\left(P_{m,O} - \left|\frac{a_{c,O}}{\rho_O} q_{cc,O}^2 \Omega_O^{\frac{1}{2}} + b_{c,O}\Omega_O q_{cc,O} + c_{c,O}\rho_O \Omega_O^{\frac{3}{2}}\right|\right) \\
\dot{q}_{cc,O} =& \frac{1}{I_{cc,O}}\Bigg(p_{ep,O} - p_{cc} + (\frac{a_{p,O}}{\rho_O} - Z_{rescc,O}) q_{cc,O}^2 + b_{p,O}\Omega_O^{\frac{1}{2}} q_{cc,O} \\
& + c_{p,O}\rho_O \Omega_O\Bigg) \\
\dot{p}_{cc} =& (k_{4cc} + k_{5cc} + (k_{2cc} - k_{1cc})\Theta_{cc})(q_{cc,H} + q_{cc,O}) - k_{3cc}\sqrt{\Theta_{cc}} p_{cc}
\end{aligned}
\tag{2.33}
$$

2.3.2 . Complex model

Providing tools to analyze the stability of the controlled model and designing control laws to stabilize it are two of the major goals of this thesis. Stability analysis of the complex model of the LPRE is the goal of this thesis. In the following, the state equations that describe the evolution of the variables considered are presented. The complex model follows the behavior described in 2.1.1 and comprises 12 states to describe the LPRE. 6 states represent the mass flows in each considered line (CC, GG and turbine exhaust), 4 pressures are featured (CC, GG, and the 2 turbine pressures) and 2 rotational speeds describe the functioning of the pumps. The structure of the cycle is reminded in figure 2.3.

$$
\text{The state vector is } x = \begin{bmatrix} \omega_H \\ \omega_O \\ q_{cc,H} \\ q_{cc,O} \\ q_{gg,H} \\ q_{gg,O} \\ q_{tu,H} \\ q_{tu,O} \\ p_{cc} \\ p_{gg} \\ p_{tu,H} \\ p_{tu,O} \end{bmatrix} \quad \text{the control vector is } u = \begin{bmatrix} A_{vcc,H} \\ A_{vcc,O} \\ A_{vgg,H} \\ A_{vgg,O} \\ A_{vhg} \end{bmatrix} \tag{2.34}
$$

$$
\dot{\omega_H} = \frac{1}{J_H}(p_{tu,H} S T_H(\omega_H) w_{tu,H} - \left|\frac{a_{c,H}}{\rho_H}(q_{cc,H} + q_{gg,H})^2 + b_{c,H}\omega_H(q_{cc,H} + q_{gg,H}) + c_{c,H}\rho_H \omega_H^2\right|)
$$

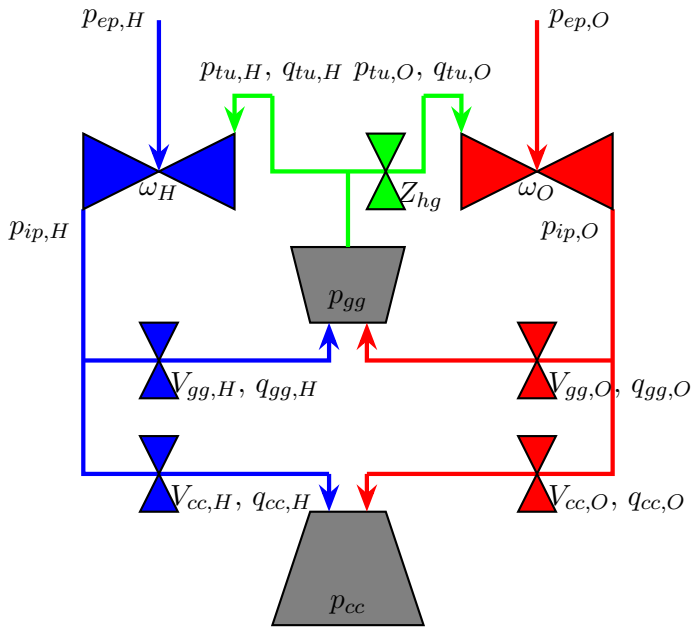

Figure 2.3 – Complex state-space cycle under study

$$\dot{\omega_O} = \frac{1}{J_O}(p_{tu,O} ST_O(\omega_O) w_{tu,O} - |\frac{a_{c,O}}{\rho_O}(q_{cc,O} + q_{gg,O})^2 + b_{c,O}\omega_O(q_{cc,O} + q_{gg,O}) + c_{c,O}\rho_O\omega_O^2|)$$

$$\dot{q}_{cc,H} = \frac{1}{I_{cc,H}}(p_{ep,H} + |\frac{a_{c,H}}{\rho_H}(q_{cc,H} + q_{gg,H})^2 + b_{c,H}\omega_H(q_{cc,H} + q_{gg,H}) + c_{c,H}\rho_H\omega_H^2|$$
$$- p_{cc} - (\frac{1}{2\rho A_{cc,H}^2} + Z_{rescc,H})q_{cc,H}^2)$$

$$\dot{q}_{cc,O} = \frac{1}{I_{cc,O}}(p_{ep,O} + |\frac{a_{c,O}}{\rho_O}(q_{cc,O} + q_{gg,O})^2 + b_{c,O}\omega_O(q_{cc,O} + q_{gg,O}) + c_{c,O}\rho_O\omega_O^2|$$
$$- p_{cc} - (\frac{1}{2\rho A_{cc,O}^2} + Z_{rescc,O})q_{cc,O}^2)$$

$$\dot{q}_{gg,H} = \frac{1}{I_{gg,H}}(p_{ep,H} + |\frac{a_{c,H}}{\rho_H}(q_{cc,H} + q_{gg,H})^2 + b_{c,H}\omega_H(q_{cc,H} + q_{gg,H}) + c_{c,H}\rho_H\omega_H^2|$$
$$- p_{gg} - (\frac{1}{2\rho A_{gg,H}^2} + Z_{resgg,H})q_{gg,H}^2)$$

$$\dot{q}_{gg,O} = \frac{1}{I_{gg,O}}(p_{ep,O} + \left|\frac{a_{c,O}}{\rho_O}(q_{cc,O} + q_{gg,O})^2 + b_{c,O}\omega_O(q_{cc,O} + q_{gg,O}) + c_{c,O}\rho_O\omega_O^2\right| - p_{gg} - (\frac{1}{2\rho A_{gg,O}^2} + Z_{resgg,O})q_{gg,O}^2)$$

$$\dot{q}_{tu,H} = \frac{1}{I_{tu,H}}(p_{gg} - p_{tu,H} - \frac{Z_{restu,H}R_{gg}\Theta_{gg}}{p_{gg}}q_{tu,H}^2)$$

$$\dot{q}_{tu,O} = \frac{1}{I_{tu,O}}(p_{gg} - p_{tu,O} - \frac{Z_{valve,hg}R_{gg}\Theta_{gg}}{p_{gg}}q_{tu,O}^2)$$

$$\dot{p}_{cc} = (k_{4cc} + k_{5cc} + (k_{2cc} - k_{1cc})\Theta_{cc})(q_{cc,H} + q_{cc,O}) - k_{3cc}\sqrt{\Theta_{cc}}p_{cc}$$

$$\dot{p}_{gg} = (k_{4gg} + k_{5gg} + (k_{2gg} - k_{1gg})\Theta_{gg})(q_{gg,H} + q_{gg,O}) - k_{3gg}\sqrt{\Theta_{gg}}(q_{tu,H} + q_{tu,O})$$

$$\dot{p}_{tu,H} = k_{2tu,H}\Theta_{gg}q_{tu,H} - k_{3tu,H}\sqrt{\Theta_{gg}}p_{tu,H}$$

$$\dot{p}_{tu,O} = k_{2tu,O}\Theta_{gg}q_{tu,O} - k_{3tu,O}\sqrt{\Theta_{gg}}p_{tu,O}. \tag{2.35}$$

2.4 . Limitations of a state-space representation

State-space representation of a system is the most common representation for a system's equations. Such representation is easily derived from physical equations and requires no additional computation. Indeed, the derivation of a state-space representation from the equation is complexified due to the number of equations. Additionally, state-space representation yields high freedom in the choice of the state variables, compared to Port-Hamiltonian systems, described in chapter 3, where the choice of variables is limited to coupled quantities [44]. This flexibility is also reflected in the addition of new dynamics. Indeed, the changes from the simplified model where the GG is not modeled, to the complex non-linear model only required the equations associated with the non-modeled dynamics. However, the state-space representation while prevalent for linear systems suffers limitations when it is used for describing complex non-linear systems. In this section, the practical aspect of the state-space representation to describe loops and retro-actions is discussed. In a second paragraph, the numerical issues of the simulations with the model are presented. In a third paragraph, the stability aspect of the model is discussed.

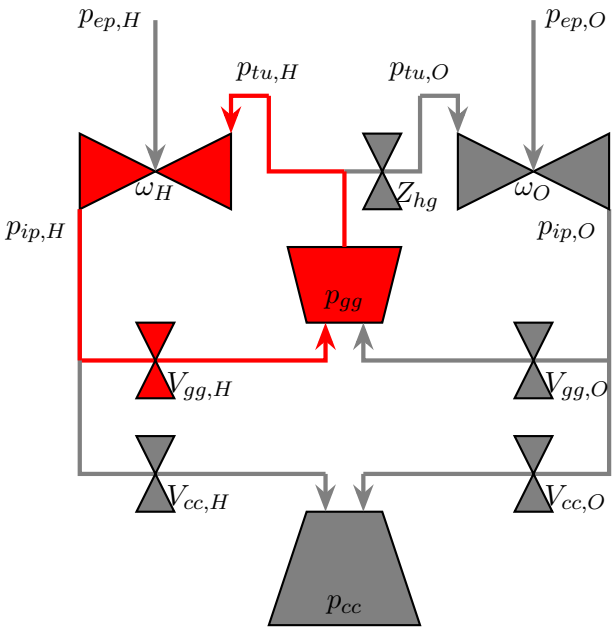

Figure 2.4 – Hydrogen feedback loop in the LPRE

Feedback loops

Equations of the complex system, although simplified by the hypothesis made in 2.1.2, illustrate a complex behavior for a non-linear system. At first glance, it is hard to grasp the feedback loop due to the introduction of a gas-generator in the complex system (2.35). A feedback loop consists of a structure of the system that leads to one or more states having an influence on themselves in the evolution. Namely, in [58], a feedback loop for a nonlinear system $\dot{x} = f(x)$ with jacobian $\frac{\partial f}{\partial x} = f_{i,j}$, If there exists an ordered set

$$I_k = i_1, ..., i_k \text{ and a permutation } J_k = j_1, ...j_k \tag{2.36}$$

such that the product $f_{i_1,j_1}...f_{i_k,j_k}$ is nonzero, there is a composite k-dimensional loop in the system. in figure 2.4, the Hydrogen feedback is illustrated, where the hydrogen turbopump is fed via the gas generator burned gases, which are themselves fed by the pump.

$$\omega_H \rightarrow q_{gg,H} \rightarrow p_{gg} \rightarrow q_{tu,H} \rightarrow p_{tu,H} \rightarrow \omega_H$$

Similarly to the stability of a feedback controller, a feedback loop must present stability properties [58]. Namely the influence of a state x on itself must be negative. In a more practical sense, the friction generated in the loop with the valve or the lines' resistive inertia must counteract the increase in energy originating from the gas generator equation. Since this loop is comprised of polynomial functions in the equations, a direct derivation of dissipativity conditions of feedback proves difficult.

Numerical issues and simulation

In multi-physical systems, the different physical domains covered are prone to face a high heterogeneity in the different variables composing the state vector. As depicted in the table 2.2, the operating

values of an LPRE suffer from a large disparity in orders of magnitude. For example, while the mass flows considered vary around $10^2 kg.s^{-1}$, the chamber pressure fluctuates around $10^7 Pa$. This high disparity affects the state-space equations, taking as an example, the chamber pressure equation,

$$\dot{p}_{cc} = (k_{4cc} + k_{5cc} + (k_{2cc} - k_{1cc})\Theta_{cc})(q_{cc,H} + q_{cc,O}) - k_{3cc}\sqrt{\Theta_{cc}}p_{cc} \tag{2.37}$$

The high disparity is illustrated in the equations by the different multiplying terms. Here in order to obtain an equilibrium $(k_{4cc} + k_{5cc} + (k_{2cc} - k_{1cc})\Theta_{cc})$ requires to be 10^5 times greater than k_{3cc}. Such consideration paired with the highly non-linear character of certain equations creates a highly sensitive system to perturbations, as a difference of and difficulties to simulate the behavior. As an example, using *SIMULINK* and the equations presented for the system, a time step of 10^{-6} seconds is required to compute the system.

As the disparity in the order of magnitude reflects on the non-variables term of the equations, the analysis of the linearized behavior of the system deals with bad conditioning on the matrices, as it is difficult to distinguish computation artifacts from small terms directly derived from the equations. A linearized matrix A for the pressure equation and the hydrodynamical equation 2.19 leads to

$$A = \begin{bmatrix} -\frac{1}{I_{cc,H}}(\frac{1}{2\rho A_{cc,H}^2} + Z_{rescc,H})q_{cc,H} & -\frac{1}{I_{cc,H}} \\ (k_{4cc} + k_{5cc} + (k_{2cc} - k_{1cc})\Theta_{cc}) & -k_{3cc}\sqrt{\Theta_{cc}}p_{cc} \end{bmatrix} \tag{2.38}$$

where the two terms in the right column of A are less than 10^5 times the terms in the left column. In Chapter 5, an LMI method is derived to obtain a stabilizing controller and suffers from the conditioning of such matrices. Numerical methods and tools such as *YALMIP* [59] do not cope well with bad-conditioned matrices and will run into numerical issues.

Definition of an equilibrium

In the following, the stability of the system is discussed regarding an equilibrium point. The equilibrium point is defined by a state vector X_0 for which the state derivatives are all equal to 0. The equilibrium is defined by the valve opening areas $A_{vgg,\bullet}$. The equilibrium is computed from the state-equations (2.35). Although a unique solution can be found for most of the equations, the polynomial functions to express the pressure increase (2.11) and the resistive torque (2.10) require additional considerations. Both polynomial functions are indeed of degree 2 and therefore provide two distinct solutions for the pair (ω, q_{tot}) with a difference of tenfold in the orders of magnitude. However, with additional information on the polynomial functions, it is possible to deduce that there is no intersection between the two solutions, leading to a unique solution defined by the initial conditions of the system. It is then possible to compute an equilibrium when initial conditions are properly defined.

Lyapunov stability of the state-space representation

The main aspect of this thesis is the stability analysis of the system represented in this chapter. Due to the complexity of the above equations, attempts to directly derive a Lyapunov function in [13] have proven unsuccessful. The author achieved the derivation of numerical approaches for a Lyapunov function with a time-dependent positive factor $P(x)$. The difficulties to properly obtain a Lyapunov function

arise from the non-linearities and the several polynomial approximations ((2.10), (2.11)) which add both negative and positive terms to the state-space representation. The lack of prior information renders the derivation of a Lyapunov function, as the polynomial functions used to represent the turbo-pumps do not represent the physical behavior of the component. For example, the polynomial terms in the outlet pressure of the pump equation (2.11), are not associated with distinct physical phenomena. This absence of information renders the computation of a presumed Lyapunov function's derivative difficult since compensation of the positive terms requires additional information.
An approach based on the search for a storage function suffers the same limitations, as the notion of energy provided to the system and dissipated is hindered by the lack of physical representation of the polynomial approximations. An energy-based approach also highlights the other main obstacle to stability analysis, which resides in the lack of homogeneity of the variables' dimensions. Indeed, while the mechanical equation of the pumps is expressed with torque and rotational speed, the hydrodynamical equation makes use of mass flows and pressure. This results in the computation of an energy (a torque multiplied by a rotational speed equation) and an energy multiplied by a density (with a mass flow instead of a volume flow). A direct determination of a storage function then requires taking into account this lack of a common dimension for the different elements in the system. Overall, the upper remarks underline the lack of a proper structure of the system to apply classical stability theorems.

Similarly a Popov criterion [60] approach to prove the stability of the system is to consider, however, the complexity of the state space renders the approach difficult. While the Popov criterion can be applied to a linearized model around the functioning point, its generalization to the non-linear system is not an easy task.

2.5 . Summary

In this chapter, the description of the considered LPRE cycle using a gas generator and turbopumps has been provided. With considerations on the mechanical design of the system and on the simplification of phenomena, the description of the components and their physical equations that drive the evolution of an LPRE is given. Two different non-linear state-space representations can be derived from the equations. A first simplified model, where the GG loop is not represented, will be used to build simplified controllers. A complex model including the GG loop is then proposed, which better represents the difficulties when studying the stability of an LPRE. Indeed, the state-space representation of the LPRE lacks clarity in the feedback loops and renders the stability approach more cumbersome. Additionally, numerical issues occur from the high heterogeneity of the multi-physical state vector and hinder the computation of the simulations. All in all, the direct stability of the state-space is a complex approach, and a second approach is considered. With the limitations of the state-space representation, a reformulation of the system under a form that is more adapted to stability analysis is proposed in the following chapter 3. To this end, Port-Hamiltonian systems theory [44] is introduced and a Port-Hamiltonian model of the LPRE is derived.

3 - Port-Hamiltonian Systems, modeling and control

While the state-space modeling of the LPRE system proves efficient in building simulations of the process, analysis of its stability using this framework proves rather difficult. In the previous work of Perez Roca [13], the search for a suitable Lyapunov function was not achieved, and proving the passivity of the system appears untractable. The recent results on stability analysis of nonlinear systems described by Port-Hamiltonian models have driven this work to determine whether this modeling applied to an LPRE.

Port-Hamiltonian models are based on an energetic representation of a system. As will be seen in this chapter, this framework provides Lyapunov functions of the dynamics derived from the Hamiltonian associated with the energy exchanges. Moreover, passivity properties that are fundamental to stability study can be easily derived from Port-Hamiltonian structures.

This chapter briefly introduces the notion of a Port-Hamiltonian system in section 3.1. In section 3.2, the reformulation of the LPRE is described while in 3.3, the stability conditions yielded by the reformulation are presented.

3.1 . Introduction to Port-Hamiltonian systems

Port-Hamiltonian systems framework, described in [61] and [44], derived from bond graphs theory [62], makes use of physical invariants of a system, such as the total energy, to highlight the energy transfers between the different elements composing a system. Port-based modeling can be recalled to the 1950s, when the spread of new complex engineering systems required a tool to unify the modeling of the different physical domains. The common thread between any physical domain being energy, port-based modeling represents a powerful tool to combine several distinct physical domains into a single model. The addition leading to Port-Hamiltonian systems has been the introduction of a geometric structure to the bond-graph theory. Through its development, the diverse applications of the Port-Hamiltonian framework have been extended to various systems such as hydrodynamics in [63] or even thermodynamic processes in [64, 65, 66].

3.1.1 . From Bond-graphs to Hamiltonian function

Modeling under Port-Hamiltonian framework uses Dirac structures [44] which are defined in the following, as a generalization of 0- and 1- junctions in bond graphs [62]. To provide a brief explanation of bond graphs, let the introduction of the notion of flow f and effort e, which represent coupled quantities (e.g. volume flow and pressure). Per convention, the flow is taken as the rate of change of a quantity ($\dot{x}$) and the effort is the coupled quantity that receives or sends energy to the flow. The notion of coupled quantities denotes the fact that the product ef is a power. A 0- junction relating two pairs of effort and flow (e_1, f_1) and (e_2, f_2) follows,

$$e_1 = e_2,\ f_1 + f_2 = 0. \tag{3.1}$$

Similarly, the 1- junction is defined by

$$f_1 = f_2,\ e_1 + e_2 = 0. \tag{3.2}$$

The objective of such junctions is to build power-conserving structures, where $e_1 f_1 + e_2 f_2 = 0$. A Dirac structure consists in the generalization of the 0- and 1-junctions, and is defined by a structure where $\sum_i e_i f_i = 0$ and by a relation $f_i = f_1,\ i \in [1, n]$. To build the Dirac structures, the coupled quantities also denoted as the nodes of the structure can be classified into three distinct functions :

- Energy-storing, denoted by e_s, f_s, defines elements representing energy storage (kinetic, potential, ...).
- Energy-dissipating, denoted by e_r, f_r defines elements that dissipates energy (friction, loss, ...).
- Energy-routing, denoted by e_t, f_t defines energy transfers, with no storage nor loss. These elements are by construction perfect transformers and are often paired with a resistive element to represent real systems.
- Interactions with the exterior environment are denoted by e_p, f_p

The construction of a Port-Hamiltonian model consists in assembling the different elements by equating the nodes (for example the 0- and 1-junction structures). Therefore the function of each element and the definition of the nodes is a crucial preliminary in Port-Hamiltonian modeling. Let for example a hydrodynamical equation,

$$I\dot{q} = p_{ep} - p_{cc} - Z_{res} q^2. \tag{3.3}$$

The elements can be classified into storage for $I\dot{q}$, resistive with $-Z_{res}q^2$, routing with $-p_{cc}$ and exterior interaction with p_{ep}. The sum of all the elements following 1- junctions yields the original equation.

Remark 3. The notion of a Dirac structure implies that the sum of the powers in the system is equal to zero. When building a Port-Hamiltonian system from a state-space system, this property originates from the equations of the system, take for example the conservation of the kinetic energy,

$$J\dot{\omega} = T_m - T_r \tag{3.4}$$

The power stored by the system can be computed with $J\dot{\omega}\omega$, which corresponds to a couple $(e_s = \omega, f_s = -J\dot{\omega})$. Through the same process, the motor torque T_m and the resistive torque T_r yield the provided and dissipated power when multiplied by ω, with couples ($e_p = \omega$, $f_p = T_m$) and ($e_r = \omega$, $f_r = T_r$). Under this form, the sum of the powers in the system is equal to 0, and the equation defines a Dirac structure $\mathcal{D} = \{(J\dot{\omega}, \omega) | \sum T\omega - J\dot{\omega}\omega = 0\}$. Note that the storage element is the rate of change $f_s = -\dot{x}$, to respect the signs in the original state-space.

The energy transfers highlighted by Port-Hamiltonian framework are due to the definition of the product $e^\top f$. In particular, the power fed to the system $e_p^\top f_p$ and the consumed power $e_r \top f_r$ are used in the stability analysis of Port-Hamiltonian systems.

Let the introduction of the Hamiltonian function, which is equal to the total energy of the system. The power-balance equation is defined from the Hamiltonian,

$$\frac{dH}{dt} = \frac{\partial H}{\partial x}\dot{x}, \tag{3.5}$$

which in other terms illustrates the fact that the rate of change of the energy in the system is equal to the rate of change of the states multiplied by the co-energy variables, $\frac{\partial H}{\partial x}$. The ports of the energy-storing elements are then assigned to $f_s = -\dot{x}$ and $e_s = \frac{\partial H}{\partial x}$.

From the Dirac structure the following equation is obtained,

$$e_s^\top f_s + e_r^\top f_r + e_p^\top f_p = 0. \tag{3.6}$$

By definition, the dissipative elements yield $e_r^\top f_r <= 0$, as they dissipate energy, therefore equation (3.6) can be written,

$$-e_s^\top f_s \leq e_p^\top f_p. \tag{3.7}$$

Equation (3.7) is a classical equation for the passivity of a system (see 1.9) where the system energetic input is e_p and the output y is f_p.

From these definitions, the system is then expressed under the form

$$\begin{aligned} \dot{x} &= (J(x) - R(x))\frac{\partial H}{\partial x} + G(x)u \\ y &= G(x)^\top \frac{\partial H}{\partial x} \end{aligned} \tag{3.8}$$

where the matrix $J(x)$ expresses the energy storage terms, $J = -J^\top$ and $R(x)$ expresses the energy dissipation $R(x) \geq 0$. $G(x)$ is the control matrix defined in a state-space system. The output y is however the passive output, defined by the matrix $G^\top(x)$. Note that the passive output and the state-space output often differ one from another.

3.1.2 . Port-Hamiltonian Systems, properties and passivity

Passivity and Port-Hamiltonian systems

From the power-balance equation (3.5) and th equation (3.7) the Hamiltonian H verifies,

$$\frac{dH}{dt} \leq e_p^\top f_p, \tag{3.9}$$

where e_p and f_p are the passive input u and output y of the system. Here the passivity equation in definition 6 is retrieved, where the user searches for a function V such that,

$$\dot{V} \leq u^\top y \tag{3.10}$$

Therefore, if $H(x) > 0$ for all x, H is a candidate storage function for the passivity of a system. The Hamiltonian function $H(x)$ of a system characterizes the stability regarding the minimum of the Hamiltonian function. Indeed by fixing the energetic input to 0, the Hamiltonian function acts as a Lyapunov function in theorem 1, with

$$\dot{V} \leq 0, \tag{3.11}$$

and the definition of a Lyapunov function is retrieved.

Interconnection of Port-Hamiltonian systems

Let two Port-Hamiltonian subsystems

$$\begin{aligned} \dot{x}_1 &= (J_1 - R_1)\frac{\partial H_1}{\partial x_1} + G_1(x_1)x_2 \\ \dot{x}_2 &= (J_2 - R_2)\frac{\partial H_2}{\partial x_2} + G_2(x_2)x_1, \end{aligned} \tag{3.12}$$

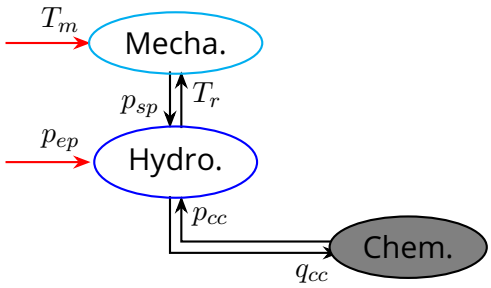

Figure 3.1 – Example of the interconnection of the physical domains for the simplified model

where $J_1, R_1, H_1, J_2, R_2, H_2$ are respectively the storage, dissipation matrices, and Hamiltonian function of the considered systems and G_1, G_2 are the control matrices, that design the interactions between the two subsystems. The following interconnection of the subsystems in (3.12) is considered,

$$\begin{bmatrix} \dot{x}_1 \\ \dot{x}_2 \end{bmatrix} = \left(\begin{bmatrix} J' \end{bmatrix} - \begin{bmatrix} R' \end{bmatrix} \right) \begin{bmatrix} \frac{\partial H_1}{\partial x_1} \\ \frac{\partial H_2}{\partial x_2} \end{bmatrix}. \tag{3.13}$$

Port-Hamiltonian systems share interconnection properties [67, 44], that allow to create complex multi-physical systems from subsystems. To conserve the equations (3.12), it is necessary to find J' and R' in (3.13). The method presented in [67] proposes to use a shared space of variables, namely a common quantity to the two subsystems. Let two Dirac structures $\mathcal{D}_A, \mathcal{D}_B$ on product spaces respectively $\mathcal{F}_1 \times \mathcal{F}_3, \mathcal{F}_2 \times \mathcal{F}_3$. $\mathcal{F}_3$ is the space of shared variables (here as both evolution equations depend on x_1, x_2, the shared space of variables is defined by x_1, x_2). For example, in figure 3.1, the interconnection between the hydrodynamical and chemical domains presents a shared space of variables (pressures and mass flows) while the interconnection between hydrodynamical and mechanical does not.

The interconnection is then realized by equating the efforts (or flows) on the shared space (see figure 3.2. In this figure, the flows and efforts are taken as $f_A = -\dot{x_1}, e_A = x_2$ and $f_B = -\dot{x_2}, e_B = x_1$, and the shared space of variables is (x_1, x_2). In [67], the author proves that the Dirac structure is conserved by the composition operation on Dirac structures. Therefore the Hamiltonian structure is conserved by the composition operation. Additionally, the total Hamiltonian H resulting from the interconnection (3.13) is obtained directly from the two subsystems' Hamiltonian functions,

$$H'(x) = H_1(x_1) + H_2(x_2). \tag{3.14}$$

This property is key to the creation of multi-physical systems and is used in 3.2.2 to build the LPRE under Port-Hamiltonian formulation.

3.1.3 . Control of Port-Hamiltonian systems

The control of a Port-Hamiltonian system often aims to regulate the energy balance of the model, and the conservation of the physical Hamiltonian structure in a closed-loop. The energy-balance of a system is represented by the passivity equation 3.7. As Port-Hamiltonian systems already provide powerful properties to a system, simple controllers can provide stability to a system. Let the definition of zero-state detectability,

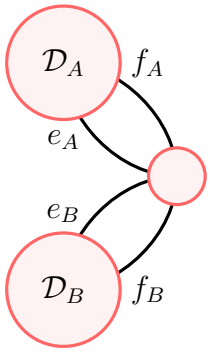

Figure 3.2 – Composition of two Dirac structures

Definition 7. A system is said to be zero-state detectable system if it admits one and only one solution for the input $u = 0$, which is defined by $x = 0$.

From this definition, the lemma in [68], is applicable,

Lemma 1. Let a Port-Hamiltonian system defined by (3.8), with $H(x)$ positive definite, $\frac{\partial H}{\partial x} \leq 0$ and suppose that the system is zero-state detectable. The feedback controller $u = -v(x)y$ with $v(x) > 0, \forall x \in \mathbb{R}$ defines the origin $x = 0$ as globally asymptotically stable.

Such properties have led to a wide development of controllers using Port-Hamiltonian properties. In [69, 70], an adaptive controller is designed for complex systems under Por-Hamiltonian formulation. A survey [71] shows that the Port-Hamiltonian framework can be used to design learning-based controllers. However, these approaches originate from two main control techniques, energy-shaping and passivity-based control.

Energy-shaping of a system [72] is mainly used for a dissipative controller. In [73], a dissipative device is controlled using the energy-shaping of the system. Energy-shaping shifts the minimal value of a Hamiltonian function to stabilize the system at the desired equilibrium.

Passivity-based control (PBC) is a strong tool to achieve stabilization by passivation of a system. Although similar to energy-shaping, PBC also makes use of a new structure for the system and enables the user to formulate a non-Port-Hamiltonian system under a closed-loop controlled Port-Hamiltonian system. In the scope of this thesis, the PBC approach is preferred, to achieve closed-loop stabilization with a desired damping matrix R. PBC is often coupled with interconnection and damping assignment [74], and the system is regulated by interconnection with a second Port-Hamiltonian system.

3.2 . Port-Hamiltonian modeling of an LPRE, subsystems and interconnection

In this section, the reformulation of the state-space models presented in 2 is depicted. First, the modeling of the different physical domains covered by the LPRE is described. In a second time, the total model is built by interconnection of the various subsystems.

3.2.1 . Port-Hamiltonian modeling of the LPRE elements

The different physical domains covered by the modeling of an LPRE lead to a complex expression of the interactions among the individual domains. Previous work in the Port-Hamiltonian framework depicts the formulation of different physical equations under the Port-Hamiltonian structure. Moreover, Port-Hamiltonian framework has been proven to suit the formulation of multi-physical systems in [76].

In the following formulations, the equations are written with scaling terms on the left-hand side of the evolution equations, along with the derivative. This is a choice of modeling that will allow better conditioning of the matrices $J(x), R(x)$ in the final formulation of the Port-Hamiltonian system in 3.2.3.

The formulation of hydrodynamics has been thoroughly studied in [44],[63] or see the example in [77]. The formulation is constructed around the analogy between hydrodynamics and electronics, replacing the current with the volume flow and the voltage with the pressure. The couple effort/flow is composed of $(\dot{V}, p)$ the volume flow/pressure couple. Here the mass flow q is preferred to the volume flow as the state-space equations of the engine have been expressed using a mass flow q in 2. The conservation of the quantity of movement is then written

$$\begin{bmatrix} I_q \dot{q} \\ k_p \dot{p} \end{bmatrix} = \begin{bmatrix} -R_q & -1 \\ 1 & -R_p \end{bmatrix} \begin{bmatrix} q \\ p \end{bmatrix}, \tag{3.15}$$

for a mass flow q and a pressure p in a line. The resistive terms R_q, R_p are composed of the friction terms in the line. The matrix $J(x)$ is taken as the canonical symplectic, leading to the scaling term k_p.

The expression of the conservation of the momentum for the mechanical subsystem is written in Port-Hamiltonian form directly using the same analogy [44]. Here the couple (ω, T) (rotational speed/couple) is used.

$$\left[J\dot{\omega}\right] = \left[-1\right]\left[T_r\right] + T_m, \tag{3.16}$$

where T_r and T_m are respectively the resistive and motor torques. For this subsystem on its own, the motor torque is the energetic input of the subsystem while the resistive torque consists in energy dissipation.

Finally, the conservation of energy applied to the combustion chambers can be derived in Port-Hamiltonian form using the couple mass quantity/enthalpy. However, as stated in 2.1.2, the thermodynamic properties of the fluids in the chamber are considered constant over time. As the enthalpy per quantity of matter and the chamber volume are constant, the couple (q, p) is taken. The conservation of energy expressed for a chamber reads,

$$\left[\dot{p}V\right] = \left[-(\gamma - 1)h_{out}\right]\left[q_{out}\right] + (\gamma - 1)q_{in}h_{in} \tag{3.17}$$

where the entering and exiting flow q_in and q_{out} depend on the chamber considered.

In the case of the main combustion chamber, the entering flows are q_{ccH}, q_{ccO} and the output flow is $q_{pcc,out}$ which has been computed previously 2.22. The conservation of energy for the main combustion chamber is written

$$\left[k_{pcc}\dot{p}_{cc}\right] = \left[-R_{pcc}\right]\left[pcc\right] + (q_{ccH} + q_{ccO}). \tag{3.18}$$

The gas generator pressure is expressed using the computed turbine mass flows for output flows (q_{tuH}, q_{tuO}) and with input flows q_{ggH}, q_{ggO}. The expression of the subsystem is then

$$\left[k_{pgg}\dot{p}_{gg}\right] = \left[-R_{pgg}\right]\left[pgg\right] + (q_{ggH} + q_{ggO}) - k_{2pgg}(q_{tuH} + q_{tuO}). \tag{3.19}$$

In the case of the turbine pressures, the equations are derived following the same principle as for the main combustion chamber, with the use of the output flow $q_{tuH,out}$ which is computed from the turbine pressure p_{tuH}.

$$\left[k_{ptuH}\dot{p}_{tuH}\right] = \left[-R_{ptuH}\right]\left[ptuH\right] + (q_{tuH}). \tag{3.20}$$

Finally, the different energies of the associated equations are as follows

$$\begin{aligned} \text{kinetic rotational} : e_{cr} &= \frac{1}{2}J\omega^2, \\ \text{kinetic hydraulic} : e_{ch} &= \frac{1}{2\rho}Iq^2, \\ \text{potential pressure} : e_{pp} &= \frac{1}{2}k_p p^2, \end{aligned} \tag{3.21}$$

for a rotational speed ω, a mass flow q and a pressure p.

3.2.2 . Physical domains and interactions of the subsystems

Identification of the different domains and subsystems is a key part of Port-Hamiltonian design for systems. In this subsection, we recall the different domains covered by both state-space models described in (2.31) for the simplified model and (2.35) for the complex model. In particular, the interaction between the system and its environment is described, denoting the passive input and output of both models. Interconnection is then described between the different physical domains. While the hydraulic and chemical domains can be interconnected directly, interactions with the mechanical domain require further computation.

Simplified Model

In the case of the simplified system using moto-pumps 2.2.1, the LPRE system interacts with its environment through three main nodes : the outlet pressure of the supply tanks p_{ep}, the motor torque T_m, the output flow of the main combustion chamber $q_{cc,out}$. The output flow is approximated with the pressure in the modeling, therefore the corresponding term is considered dissipative in the system equations. The interactions through p_{ep} and T_m are energetic inputs of the system and are represented in red in figure 3.3. The exterior interaction effort vector e_p is

$$e_p = \begin{bmatrix} T_m \\ p_{ep} \end{bmatrix}, f_p = \begin{bmatrix} \omega \\ q_{cc} \end{bmatrix} \tag{3.22}$$

with associated flows ω and q_{cc}. The power provided to the system with both interactions is given by the product $e_p^\top f_p = T_m\omega + p_{ep}q_{cc}$. The passive output ($y$ in equation 3.8) represents the rotational speed ω and the mass flow entering the combustion chamber q_{cc}.

Complex model

In this modeling, the turbopump's motor torque evolves following the turbine equation and is not considered an input of the system. The system interacts with its environment with is comprised of two entries, the tank outlet pressures and the valve surfaces. The valve surfaces do not provide energy to

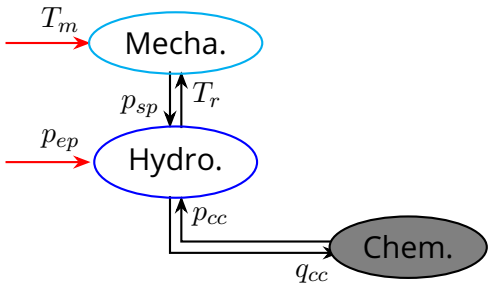

Figure 3.3 – Interconnection of the physical domains and energetic inputs for the simplified model

node	flow	effort	nodes connected	physical domain	equation reference	component
1	$J\dot{\omega}$	ω	2, exterior	mechanical	3.16	motopump
2	$I\dot{q}$	q	1,3, exterior	hydrodynamical	3.15	fuel line
3	$k_{pcc}\dot{p}_{cc}$	p_{cc}	2	chemical	3.18	combustion chamber

Table 3.1 – Interconnections and domains covered by the simplified model

the system and are *workless*. The *workless* control is not considered an exterior interaction of the system in the sense of the couple (e_p, f_p). The exterior interaction effort vector e_p is

$$e_p = \begin{bmatrix} p_{ep} \\ p_{ep} \end{bmatrix}, f_p = \begin{bmatrix} q_{cc} \\ q_{gg} \end{bmatrix} \tag{3.23}$$

The energetic inputs of the complex model are represented in red in figure 3.4. The power provided by the tanks is given by $e_p^\top f_p = p_{ep}q_{cc} + p_{ep}q_{gg}$.

The construction of the Port-Hamiltonian system for the LPRE consists in connecting the individual subsystems using the flow and efforts described. The connections can be made smoothly for the hydrodynamical part, where both efforts and flows equate following mass flows and pressures as illustrated in figure 3.4.

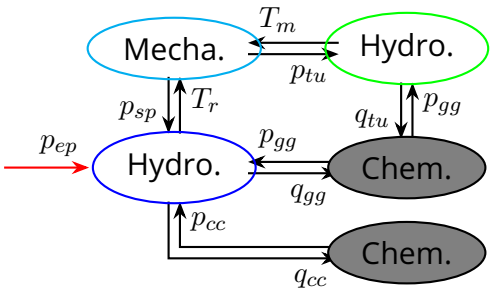

Figure 3.4 – Interconnection of the physical domains covered by the LPRE modeling

node	flow	effort	nodes connected	physical domain	equation reference	component
1	$J\dot{\omega}$	ω	2, 7	mechanical	3.16	turbopump
2	$I_{cc}\dot{q}_{cc}$	q_{cc}	1,5, p_{ep}, A_{vg}	hydrodynamical	3.15	CC fuel line
3	$I_{gg}\dot{q}_{gg}$	q_{gg}	1,6, p_{ep}, A_{vc}	hydrodynamical	3.15	GG fuel line
4	$I_{tu}\dot{q}_{tu}$	q_{tu}	6,7	hydrodynamical	3.15	hot gas line
5	$k_{pcc}\dot{p}_{cc}$	p_{cc}	2	chemical	3.18	combustion chamber
6	$k_{pgg}\dot{p}_{gg}$	p_{gg}	3,4	chemical	3.19	gas generator
7	$k_{ptu}\dot{p}_{tu}$	p_{tu}	4,1	hydrodynamical	3.20	turbine inlet

Table 3.2 – Interactions and domains covered by the complex model

Interconnection of the physical domains

The interconnection of the hydrodynamical part of the system can be driven directly, by corresponding both flow and efforts of the individual subsystems. Indeed the flows and efforts are already part of a shared space of variables (e.g. the mass flows and pressures). Furthermore, the introduction of the energy-conservation equation (3.17) uses the same space of variables as the hydrodynamical equations (3.15). Therefore the chemical domain can be interconnected to the hydrodynamical domain directly, using the space of variables (q, p).

The mechanical system presents a different physical domain and therefore the interfaces at both ends require a shared space of variables. A proposition driven in [78] is to formulate the torque on the mechanical end into an equivalent pressure. This results in equating the output pressure of the pump with the resistive torque equivalent pressure. However, the main hypothesis of the reversible hydropump system in [78] is a linear relation between the mass flow and the rotational speed $q = k_{q\omega}\omega$, and that both the pressure increase p_{ip} and the resistive torque T_r solely depend on respectively q and ω, e.g. $p_{ip} = k_{prp}q^2$, $T_r = k_{Tr}\omega^2 = k_{q\omega}k_{Tr}q^2$. This leads to expressing the resistive torque with only the mass flow involved.

To express the whole system under the same shared space of variables, the mechanical domain is expressed under a hydraulic formulation, meaning that an equivalent mass flow and pressure are derived from the rotational speed ω and the torque s T_r, T_m. Note that the shared space of variables (ω, T) could have been chosen, but requires the reformulation of 6 equations rather than 1 equation for the chosen approach. The turbo pump studied does not present the simplification mentioned in [78]. However, it is possible to identify the driving terms of the polynomial functions to approximate an equivalent pressure. Suppose a lower value for the resistive torque, given with $\frac{a_c}{\rho}q^2$ and an upper value for the pressure increase, given with $b_p q\omega$. Define

$$\alpha_q = \frac{b_p \rho}{a_c}, \tag{3.24}$$

where the coefficients b_p, a_c are taken as in (2.10) and (2.11). With the notations $\overline{p}_{ip} = b_p q\omega$ for the upper value of the pressure increase and $\underline{T}_r = \frac{1}{\alpha_q}b_p q^2$ for the lower value of the resistive torque, the real torque

and pressure increase are rewritten

$$p_{ip} = \overline{p}_{ip} - (\frac{a_p}{\rho}q - c_p\rho\frac{\omega^2}{q})q + p_{ep} \leq \overline{p}_{ip}$$
$$T_r = \underline{T}_r + \alpha_q(b_c q + c_c\omega)\omega \geq \underline{T}_r.$$

Then the equations of ω and a mass flow q through the pump read :

$$\alpha_q J\dot{\omega} = -b_p q^2 - \alpha_q(b_c q + c_c\omega)\omega + \alpha_q T_m$$
$$I\dot{q} = b_p q\omega - (Z_{eq}q - \frac{a_p}{\rho}q - c_p\rho\frac{\omega^2}{q})q + p_{ep},$$

which gives the following dynamical equation :

$$\begin{bmatrix}\alpha_q J\dot{\omega}\\ I\dot{q}\end{bmatrix} = \begin{bmatrix}-R_\omega & -b_p q\\ b_p q & -R_q\end{bmatrix}\begin{bmatrix}\omega\\ q\end{bmatrix} + \begin{bmatrix}\alpha_q T_m\\ p_{ep}\end{bmatrix}, \tag{3.25}$$

where $R_q = Z_{eq}q - \frac{a_p}{\rho}q - c_p\rho\frac{\omega^2}{q}$ and $R_\omega = \alpha_q(b_c q + c_c\omega)$ have to be positive to satisfy the upper and lower value hypothesis. Here two conditions are derived for the validity of the Port-Hamiltonian formulation of the system, which can be used as a validation test for the stability of the system.

For the turbine part, a new shared space of variables is proposed. Let the effort $\alpha_q T_m = \alpha_q ST(\omega)w_{tu}p_{tu}$ (see the motor torque equation in (2.18)). Again, suppose that a minimal bound for the pressure loss in the turbine is $\alpha_q ST(\omega)w_{tu}\omega$. A proposition to close the system in Port-Hamiltonian framework is to re-formulate the p_{tu} term into :

$$k_{2tu}p_{tu} = \alpha_t\omega + \beta_t p_{tu}, \tag{3.26}$$

for the state-space evolution of the turbine pressure p_{tu} (2.27),

$$\dot{p}_{tu} = k_{2tu}\Theta_{gg}q_{tu} - k_{3tu}\sqrt{\Theta_{gg}}p_{tu},$$

where $\alpha_t = \alpha_q ST(\omega)w_{tu}$ and β_t is computed from $k_{2tu}p_{tu} - \alpha_t\omega$. Hence the following interconnection :

$$\begin{bmatrix}\alpha_q J\dot{\omega}\\ k_{ptu}\dot{p}_{tu}\end{bmatrix} = \begin{bmatrix}0 & \alpha_t\\ -\alpha_t & -R_{ptu}\end{bmatrix}\begin{bmatrix}\omega\\ p_{tu}\end{bmatrix}. \tag{3.27}$$

Here $\alpha_t\omega$ is supposedly a lower bound of the term $k_{2tu}p_{tu}$. The term $\beta_t p_{tu}$ has to be positive, with $R_{Ptu} = \beta_t \geq 0$. This leads to a third condition on the system for the Port-Hamiltonian formulation.

3.2.3 . Formulation of the state-space systems under Port-Hamiltonian framework

In this subsection, the formulations for both state-space models of the simplified and complex model of an LPRE are presented. Note that a Port-Hamiltonian formulation of a system is not unique and therefore, the formulation proposed is no unique solution for the modeling. The choices made during the modeling concern the matrix $J(x)$ for both systems. The dynamics written in 3.2.1 regroup the scaling terms with the derivative of the state in the equation, to create a matrix $J(x)$ close to unitary values. This aims to improve the conditioning on the matrices $J(x)$ and $R(x)$.

Port-Hamiltonian formulation of the simplified LPRE model

In this paragraph, the formulation of the simplified rocket engine using an input torque 2.31, is presented. For clarity, only the hydrogen line is written here. Note that to write the system for hydrogen dynamics, the oxygen part is supposed well-regulated, meaning that the mixture ratio in the combustion chamber is constant $MR = 6$. Therefore the increase in energy due to the mass flows entering the chamber is multiplied by $(MR + 1)q_{cc,H}$ which by this hypothesis is equal to $(q_{cc,H} + q_{cc,O})$. First, the geometric structure of Port-Hamiltonian systems yields the following,

$$\begin{bmatrix} \alpha_q J\dot{\omega} \\ I_{cc}\dot{q}_{cc} \\ k_{pcc}\dot{p}_{cc} \end{bmatrix} = \big[J(X) - R(X)\big] \begin{bmatrix} \omega \\ q_{cc} \\ p_{cc} \end{bmatrix} + \begin{bmatrix} T_m \\ p_{ep} \\ 0 \end{bmatrix}, \tag{3.28}$$

where the structure matrix is

$$J(X) = \begin{bmatrix} 0 & -\lambda & 0 \\ \lambda & 0 & -1 \\ 0 & 1 & 0 \end{bmatrix}$$

and the resistive matrix is

$$R(X) = diag(\begin{bmatrix} R_\omega & R_{qcc} & R_{pcc} \end{bmatrix}). \tag{3.29}$$

The different scaling terms are expressed as,

$$\begin{aligned} k_{pcc} &= \frac{MR+1}{(k_{4cc} + k_{5cc} + (k_{2cc} - k_{1cc})\Theta_{cc})} \\ \alpha_q &= \frac{b_p \rho}{a_c} \\ \lambda &= b_p q_{cc}, \end{aligned} \tag{3.30}$$

while the terms of the resistive matrix R follow

$$\begin{aligned} R_\omega &= \alpha_q(b_c q_{cc} - c_c \rho \omega) \\ R_{qcc} &= Z_{eqcc} q_{cc} - \frac{a_p}{\rho} q_{cc} - c_p \rho \frac{\omega^2}{q_{cc}} \\ R_{pcc} &= k_{3cc}\sqrt{\Theta_{cc}} k_{pcc}. \end{aligned} \tag{3.31}$$

Port-Hamiltonian formulation of the complex non-linear LPRE model

The complex Port-Hamiltonian LPRE is expressed in this paragraph for the hydrogen half of the engine. As for the simplified system, the complete model is given in **Appendix A**. The expression of the

states under Port-Hamiltonian form yields the system,

$$\begin{bmatrix} \alpha_q J\dot{\omega} \\ I_{cc}\dot{q}_{cc} \\ I_{gg}\dot{q}_{gg} \\ I_{tu}\kappa_{tu}\dot{q}_{tu} \\ k_{pcc}\dot{p}_{cc} \\ k_{pgg}\dot{p}_{gg} \\ k_{ptu}\dot{p}_{tu} \end{bmatrix} = \big[J(X) - R(X)\big] \begin{bmatrix} \omega \\ q_{cc} \\ q_{gg} \\ q_{tu} \\ p_{cc} \\ p_{gg} \\ p_{tu} \end{bmatrix} + \begin{bmatrix} 0 \\ p_{ep} \\ p_{ep} \\ 0 \\ 0 \\ 0 \\ 0 \end{bmatrix} \tag{3.32}$$

where the structure matrix is

$$J(X) = \begin{bmatrix} 0 & -\lambda & -\lambda & 0 & 0 & 0 & \alpha_t \\ \lambda & 0 & 0 & 0 & -1 & 0 & 0 \\ \lambda & 0 & 0 & 0 & 0 & -1 & 0 \\ 0 & 0 & 0 & 0 & 0 & \kappa_{tu} & -\kappa_{tu} \\ 0 & 1 & 0 & 0 & 0 & 0 & 0 \\ 0 & 0 & 1 & -\kappa_{tu} & 0 & 0 & 0 \\ -\alpha_t & 0 & 0 & \kappa_{tu} & 0 & 0 & 0 \end{bmatrix}, \tag{3.33}$$

and the resistive matrix is

$$R(X) = diag(\begin{bmatrix} R_\omega & R_{qcc} & R_{qgg} & R_{qtu} & R_{pcc} & R_{pgg} & R_{ptu} \end{bmatrix}).$$

The scaling terms read,

$$\begin{aligned} &\lambda = b_p(q_{cc} + q_{gg}) \\ &\kappa_{tu} = k_{3gg}\sqrt{\Theta_{gg}}k_{gg},\ k_{ptu} = \frac{\kappa_{tu}}{k_{2tu}\Theta_{gg}} \\ &k_{pcc} = \frac{MR+1}{(k_{4cc} + k_{5cc} + (k_{2cc} - k_{1cc})\Theta_{cc})},\ k_{pgg} = \frac{1}{(k_{4gg} + k_{5gg} + (k_{2gg} - k_{1gg})\Theta_{gg})} \\ &\alpha_q = \frac{b_p\rho}{a_c},\ \alpha_t = \alpha_q ST(\omega)w_{tu} \end{aligned} \tag{3.34}$$

And the resistive terms composing the matrix R are expressed as

$$\begin{aligned} &R_\omega = \alpha_q(b_c(q_{cc} + q_{gg}) - c_c\rho\omega) \\ &R_{qcc} = Z_{rescc}q_{cc} - \frac{a_p}{\rho}(q_{cc} + q_{gg}) - c_p\rho\frac{\omega^2}{q_{cc}} \\ &R_{qgg} = Z_{resgg}q_{gg} - \frac{a_p}{\rho}(q_{cc} + q_{gg}) - c_p\rho\frac{\omega^2}{q_{gg}} \\ &R_{qtu} = \kappa_{tu}Z_{resqtu}q_{tu},\ R_{pcc} = k_{3cc}\sqrt{\Theta_{cc}}k_{pcc} \\ &R_{pgg} = 0,\ R_{ptu} = \beta_t \end{aligned} \tag{3.35}$$

3.2.4 . Advantages and limitations of the framework

Hypothesis on the dynamic system

It is important to notice that the expression of the hydraulic energy $e_{ch} = \frac{1}{2\rho} I q^2$ requires the knowledge density of the considered fluid ρ. In both the GG and CC feeding lines (q_{cc} and q_{gg}), the densities can be considered constant. However, the density of the fluid in the hot gases line (q_{tu}) can not be set as a constant and requires to be computed if used. To account for this, a modified Hamiltonian is used, which is equivalent to an energy multiplied by a density. This leads to a reformulation of the energy associated to the mechanical subsystem. The term α_q introduced in (3.24) for the expression of the equivalent mass flow is equivalent to a constant density, such that

$$q_\omega = \alpha_q \omega, \tag{3.36}$$

is equivalent to a mass flow. With this associated mass flow, the kinetic rotational energy is expressed under a kinetic hydraulic form :

$$e_{cr} = \frac{1}{2} J \omega^2 \alpha_q. \tag{3.37}$$

Remark 4. The equivalent mass flow related to the rotational speed $q_\omega = \alpha_q \omega$ leads to a simple expression of the total energy of the system, which can be resumed to the kinetic hydraulic and the potential pressure energies. Additionally, the terms $\alpha_q T$ where T is the motor or resistive torque, bear the dimension of a pressure. The interconnection between the mechanical and hydraulic systems mentioned in both the simplified and complex systems can then be reformulated similarly to a simple hydrodynamical system, using only mass flows and pressures, under

$$\begin{bmatrix} \dot{q} \\ \dot{p} \end{bmatrix} = [J(x) - R(x)] \begin{bmatrix} \frac{\partial H}{\partial q} \\ \frac{\partial H}{\partial p} \end{bmatrix} \tag{3.38}$$

Addition of dynamics

In the modeling of the system, the dynamics of the actuators (valves) have been neglected due to their low impact on the uncontrolled system, and their time-response has been supposed instantaneous. In this paragraph, the addition of such dynamics in Port-Hamiltonian framework is discussed. First recall the actuators' dynamics under a second-order form,

$$\ddot{A_v} = -2\xi w_0 \dot{A_v} - w_0^2 A_v + w_0^2 u_A, \tag{3.39}$$

for the valve surface A_v, the pulsation w_0, the damping coefficient ξ and the valve actuator setpoint u_A. Such a system can be easily derived in Port-Hamiltonian framework under the form

$$\begin{bmatrix} \dot{A_v} \\ \frac{1}{w_0^2} \ddot{A_v} \end{bmatrix} = \begin{bmatrix} 0 & 1 \\ -1 & -2\xi \end{bmatrix} \begin{bmatrix} A_v \\ \dot{A_v} \end{bmatrix} + \begin{bmatrix} 0 \\ 1 \end{bmatrix} u_A. \tag{3.40}$$

Although the geometric structure of the Port-Hamiltonian framework is directly retrieved from a second-order system, the choice of using the surface A_v as a state variable leads to the Hamiltonian function

$$H_{valve} = \frac{1}{2} A_v^2 + \frac{1}{2w_0^2} \dot{A_v}^2, \tag{3.41}$$

which is not equivalent to an energy ($[A_v^2] = m^4$). In order to connect this subsystem to the other LPRE components, it is necessary to formulate an energy from the moving surface of the actuator. Several solutions are available for this,

- Using the equivalent inertia of the moving surfaces, it is possible to derive a coefficient that expresses the kinetic energy of the moving surface. Let a kinetic energy to the valve, $\frac{1}{2}m_{eq}\dot{A_v}^2$ where m_{eq} is a unitary linear mass $[m_{eq} = [kq.m^{-1}]$. Then the Hamiltonian expresses kinetic energy and can be added to the original system. This method requires however numerical values for the linear mass, which is not available in the literature.
- In [13], the author describes the actuators with the opening angle of the valve, from which it is possible to retrieve a surface. From this opening angle, it is possible to obtain a mechanical equation under the form 3.16. This solution also suffers from the lack of numerical values available.
- A third solution is to directly add the dynamics in the controller equation, and assert stability for the new controller function,

$$\ddot{u}_{actuator} = -2\xi w_0 \dot{u_{actuator}} - w_0^2 u_{actuator} + w_0^2 u_A. \tag{3.42}$$

  This solution will be used in the chapter 6, to account for the lack of numerical values for the other propositions.

In a first approach, the stability of the engine is considered regarding the value of the actuators (namely the surface value A_{vg}). In this case, the dynamics of the actuator are not considered. The validation of the work on the stability will take into account the actuators in the chapter 6.

3.3 . Fixed-point stability and stability conditions

In this section, the implications of the Port-Hamiltonian formulation regarding the stability of the system are discussed. The Hamiltonian function obtained with the Port-Hamiltonian modeling allows to assert the passivity of the system over a domain of functioning. However, it is necessary to assert the Port-Hamiltonian formulation (namely that $R(x) \geq 0, \forall x$. Verification of the upper and lower bound hypothesis in 3.2.2 yields the conditions for the passivity of the system. Paragraph 3.3.1 details the passivity analysis of the simplified system. In a second time, the complex system is studied and the impact of the valves' values on the stability is investigated in 3.3.2.

3.3.1 . Simplified system analysis

Hamiltonian of the system and passivity The Hamiltonian function of a system is derived from the couples effort/flow used in the subsystem formulation (3.15), (3.16) and (3.17). As the storage elements are defined using $\frac{dH}{dt}(x) = -e_s^\top f_s$, the two vectors,

$$x = \begin{bmatrix} \alpha_q J\omega \\ Iq \\ k_p p \end{bmatrix} \text{ and } \frac{\partial H}{\partial x}(x) = \begin{bmatrix} \omega \\ q \\ p \end{bmatrix}, \tag{3.43}$$

are used to retrieve the formulation of the Hamiltonian. Therefore the Hamiltonian of the simplified system (3.28) reads,

$$H(x) = \frac{1}{2}J\omega^2\alpha_q + \frac{1}{2}I_{cc}q_{cc}^2 + \frac{1}{2}k_{pcc}p_{cc}^2, \tag{3.44}$$

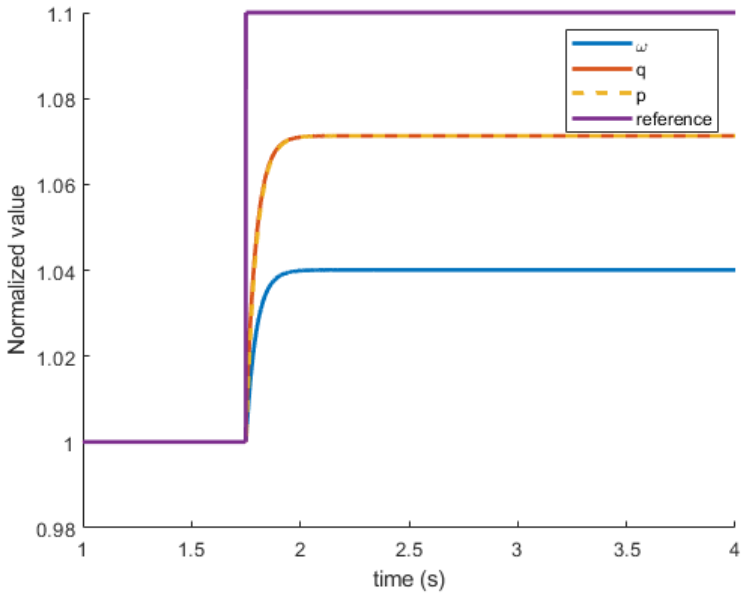

Figure 3.5 – Evolution of the states for a step-response

which was predictible since this is the formulation of the total energy of the system. Using the Dirac structure equation 3.7, the Hamiltonian function respects the following,

$$\frac{dH}{dt}(x) \leq e_p^\top f_p, \tag{3.45}$$

which is the equation of a storage function. The Hamiltonian $H(x)$ is positive due to its quadratic formulation ($\frac{1}{2}\omega^2 \geq 0 \forall x \in \mathbb{R}$). The passivity of the simplified system (3.28) with respect to the energetic input e_p is proved, using the definition of the passivity 6.

in figure 3.6, the resistive terms used in the simplified LPRE are illustrated during the response to a step. The simulations are performed in open-loop with a step function for the motor torque. The data is represented under a normalized form, where the plot displays $\frac{R_\bullet}{|R_{\bullet 0}|}$. As the resistive terms do not become negative during the functioning, the dissipated power $e_r^\top f_r$ is indeed negative, and the Hamiltonian

$$H(x) = \frac{1}{2}J\omega^2\alpha_q + \frac{1}{2}I_{cc}q_{cc}^2 + \frac{1}{2}k_{pcc}p_{cc}^2,$$

is a candidate storage function for the simplified LPRE. Note that the Hamiltonian proves the passivity at an equilibrium defined by the minimal value of the Hamiltonian function, here for all states at 0. This equilibrium is not physically attainable, as it resides outside of the polynomial functions' domain of validity (no guarantee of a solution) and because this would require the tank pressure p_{ep} to be equal to 0. However, the simulation in figure 3.5 illustrates the existence of another equilibrium of the system depending on the values of p_{ep} and the motor torque T_m. Indeed, before the step ($t < 1s$) the system is situated at the equilibrium $x = x_0$. At time $t \geq 1s$, the system converges to a new equilibrium, due to the change in the motor torque.

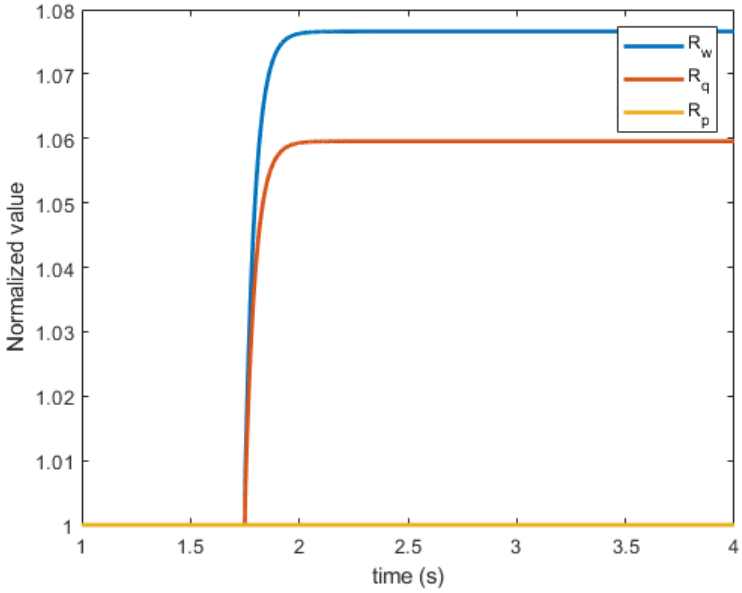

Figure 3.6 – Evolution of the resistive terms for a step-response

Limitation of the passivity domain To analyze the passivity regarding a non-zero equilibrium, it is necessary to reformulate the equations of the system with a change of variables. Let x_0 be the considered equilibrium of the simplified system (3.28) and for a state $x \in \mathbb{R}^n$, define $\hat{x}(t) = x(t) - x_0$. The dynamics of $\hat{x}$ are then expressed,

$$\begin{aligned}
\alpha_q J\dot{\hat{\omega}} &= \left(\frac{a_c}{\rho}(2q_0+\hat{q})\hat{q} + b_c(\hat{q}+q_0)\hat{\omega} + b_c\hat{q}\omega_0 + c_c\rho(2\hat{\omega}+\hat{\omega}^2)\frac{1}{\hat{q}}\right) + \hat{T}_m \\
I\dot{\hat{q}} &= \left(\frac{a_p}{\rho}(2q_0+\hat{q})\hat{q} + b_p(\hat{q}+q_0)\hat{\omega} + b_p\hat{q}\omega_0 + c_p\rho(2\hat{\omega}+\hat{\omega}^2) - Z_{eqcc}(q_0+\hat{q})\hat{q}\right) - \hat{p} \\
k_p\dot{\hat{p}} &= \hat{q} - k_{pcc}\hat{p}
\end{aligned} \tag{3.46}$$

these equations are obtained by development of the reformulation $\hat{x}(t) = x(t) - x_0$, and subtracting the equilibrium terms whose sum is equal to 0. This shift in the equilibrium allows to reformulate the resistive terms inside the equations, to study the passivity toward a new equilibrium. While both R_ω and R_p remain unchanged, the resistive term for the mass flow $\hat{R}_q$ follows,

$$\hat{R}_q = \left(-\frac{a_p}{\rho}(2q_0+\hat{q}) - b_p\omega_0 - c_p\rho(2\hat{\omega}+\hat{\omega}^2)\frac{1}{\hat{q}} + Z_{eqcc}(q_0+\hat{q})\right), \tag{3.47}$$

and the term $-b_p\omega_0$ is new from the formulation of the resistive term,

$$R_q = Z_{eqcc}q - \frac{a_p}{\rho}q - c_p\rho\frac{\omega^2}{q}, \tag{3.48}$$

for a certain value of q, the new resistive matrix $\hat{R}$ is then non positive, when $\hat{R}_q$ becomes negative. This explains an unstable zone of the system for a low value of q, where the passivity of the system is not proven anymore.

3.3.2 . Hamiltonian function and stability of the complex model

For the complex system, the Hamiltonian function is obtained via the system's formulation. As storage ports are defined with $\frac{dH}{dt}(x) = -e_s^\top f_s$, the two vectors x and $\frac{\partial H}{\partial x}(x)$ are used to retrieve the expression of $H(x)$,

$$\begin{aligned} H(x) = \frac{1}{2}J\omega^2\alpha_q + \frac{1}{2}I_{cc}q_{cc}^2 + \frac{1}{2}I_{gg}q_{gg}^2 + \frac{1}{2}I_{tu}q_{tu}^2 \\ + \frac{1}{2}k_{pcc}p_{cc}^2 + \frac{1}{2}k_{pgg}p_{gg}^2 + \frac{1}{2}k_{ptu}p_{tu}^2. \end{aligned} \tag{3.49}$$

It is important to note that the use of the scaling terms $k_{p\bullet}$ and α_q impact the Hamiltonian function of the system by scaling all terms to the order of magnitude of the mass flows. This allows a better scaling of the contributions in the total energy from all the states. Such terms enable to write the total pseudo-energy of the system under a common unit ($J.kg.m^{-3}$) which is equivalent to an energy times a constant density. This Hamiltonian function is positive definite, due to the quadratic formulation. We recall here Dirac structure equation,

$$\begin{aligned} -e_s^\top f_s &\leq e_p^\top f_p, \\ \frac{dH}{dt} &\leq e_p^\top f_p. \end{aligned} \tag{3.50}$$

Then $H(x)$ is a candidate storage function for the passivity of the system. The minimum of the Hamiltonian is located at the origin of the system (for $x = 0$). Therefore, the system is passive with respect to the energetic input. However, it is important to note that the tank pressure p_{ep} is the energetic input of the system. As p_{ep} is fixed over time, the origin ($p_{ep} = 0$) is not physically attainable. As seen in the simulations, the system proves to have an equilibrium for the constant pressure p_{ep} and a valve surface A_{vgg}.

To determine the equilibrium generated by the tank pressure and the valve surface, it is possible to use a different Hamiltonian function, as in (3.46), where the system is shifted to another equilibrium. Since the pressure equations are linear in the states, the mass flow $q_\bullet$, and the rotational speed ω equation have been defined for a different equilibrium than the origin, it is possible to propose a shifted equation for the complex system. This allows to determine the same unstable zone for the mass flow q_{cc}. However, in 3.3.2, it is shown that a resistive term in the equation is not positive, therefore this direct method is not valid.

The shifted Hamiltonian function can also be defined using the shifted passivity conditions defined in [79]. The shifted Hamiltonian function is expressed as,

$$\mathcal{H}(x) := H(x) - (x - x_0)^\top \frac{\partial H}{\partial x}(x_0) - H(x_0), \tag{3.51}$$

if the system verifies two assumptions, namely that the original Hamiltonian H is strictly convex and that the mapping of the storage and dissipative matrices expressed in terms of co-energy variables respects the following

$$\nabla(\mathcal{F}(s)\overline{s}) + \nabla(\mathcal{F}(s)\overline{s})^\top - 2R^* \leq 0, \tag{3.52}$$

where $s := \frac{\partial H}{\partial x}$ and $\mathcal{F}(x) := J(x) - R(x)$. R^* is a constant positive matrix, such that $R(x) \geq R^*$ for all x. As pointed out previously, the obtained formulation of the system leads to the resistive matrix not being

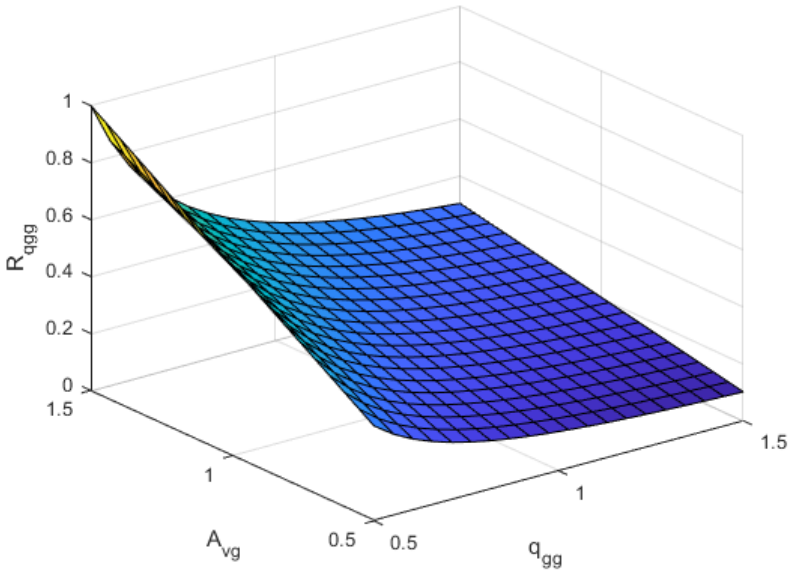

Figure 3.7 – Evolution of the resistive inertia depending on the mass flow and the valve (3.53)

positive definite, therefore no suitable R^* can be found. In order to apply the shifted passivity theorem in [79] it is required to first act on the Port-Hamiltonian structure.

Influence of the valves on the passivity domain

In this paragraph, the stability requirements evolution with the usage of the valves is illustrated.

The passivity domain of the system is also characterized by the resistive terms defined previously in the Port-Hamiltonian formulation of the system in 3.2.3. Mainly, the terms defining the resistive influence of the valves (without considering the valve's inner dynamics) on the system are recalled :

$$\begin{aligned} Z_{resgg} &= Z_{line,gg} q_{gg} + \frac{1}{2\rho A_{vgg}^2} q_{gg}, \\ R_{qgg} &= Z_{resgg} q_{gg} - \frac{a_p}{\rho}(q_{cc} + q_{gg}) - c_p \rho \frac{\omega^2}{q_{gg}}. \end{aligned} \tag{3.53}$$

From the formulation of the resistive inertia Z_{resgg}, the valve surfaces have a direct influence on the value of the resistive terms R_{qgg}. The condition $R_{qgg} \geq 0$ illustrates the need for friction to counteract the residual terms of the polynomial function. in figure 3.7, the evolution of R_{qgg} is plotted depending on both the mass flow q_{gg} and the valve surface A_{vgg}. As the mass flow increases, the valve surface value A_{vgg} required to maintain stability also increases, although the condition $R_{qgg} > 0$ is respected through the span of the considered domain.

As a valve's surface value is bounded by mechanical constraints, the stability of the system is not guaranteed for the whole state-space but only with respect to the valve's surface span.

Stability conditions and resistive terms

As stated in 3.2.2, the formulation under Port-Hamiltonian framework requires a hypothesis on the positivity of the resistive terms $R_{qgg}, R_{qcc}, R_{ptu}, R_{\omega}$. From figure 3.7, illustrates the positivity of the resistive terms R_{qgg}, R_{qcc}. The resistive term R_{ω} is also positive as illustrated in figure 3.9.

Remark 5. The resistive term R_{ptu} is not however positive in figure 3.9. Because of the scaling α_t the motor torque provided exceeds the pressure drop induced by the turbine. Since the hypothesis on the Port-Hamiltonian structure $R \geq 0$ is not respected, this is an obstacle to the proof of passivity of the system. A solution to this is to use a passivity-based controller which is developed in the following chapter 4. Such a controller can be designed to assign a specified resistive term, in this case R_{ptu} to a closed-loop system.

Remark 6. The positivity of the resistive terms relies on the model chosen. In reality, the pressure drop is not directly due to the turbine, but to the exhaust mass flow of the cavity. This same mass flow then provides kinetic energy to the turbine. As this modeling does not consider this mass flow, this shortcut results in a positive R_{ptu}. Port-Hamiltonian formulation provides here a good insight on approximations and stability analysis. As long as the residual terms in approximations can be considered resistive, then the system is stable. However positive residual terms imply to provide additional analysis on the power-balance of the system, provided in the following paragraph.

Although the condition on the resistive terms is not met at all points, it is still possible to assert the passivity of the system if the overflow in the other components exceeds the passivity shortage in the turbine pressure. In other words, if the power dissipated in the other components compensates for the shortage in R_{ptu}, then the power balance equation is verified :

$$-e_s^\top f_s \leq e_p^\top f_p, \text{ if } e_r^\top f_r < 0 \tag{3.54}$$

in figure 3.9, the evolution of the resistive terms for a step scenario is presented. In this scenario, the control input u represents the opening surface of the valve A_{vgg} in open-loop. The total dissipated energy is represented in figure 3.10, although the resistive term R_{ptu} is positive, the hypothesis $e_r^\top f_r < 0$ still holds in the definition of the geometric structure 3.6. As the total dissipated power is negative, equation (3.54) is respected throughout the step scenario and the system is passive around the origin.

3.4 . Summary

In this chapter, a reformulation of the state-space systems presented in 2 under Port-Hamiltonian formulation is conducted. The new formulation adapts to multi-physical systems by defining subsystems that characterize the evolution of each separate domain, and by then performing the interconnection between the different domains. The reformulation yields the Hamiltonian function of the system, a powerful tool for proving the passivity of a system. Provided the system respects the hypothesis on the Hamiltonian structure, a Port-Hamiltonian system is passive with respect to the origin of the system.

The analysis of the different terms in the formulation allowed to prove the passivity of the simplified system, with respect to the origin of the system (zero) and the original equilibrium of the system (non-zero equilibrium). This additionally allowed to prove an unstable behavior in low values of the main

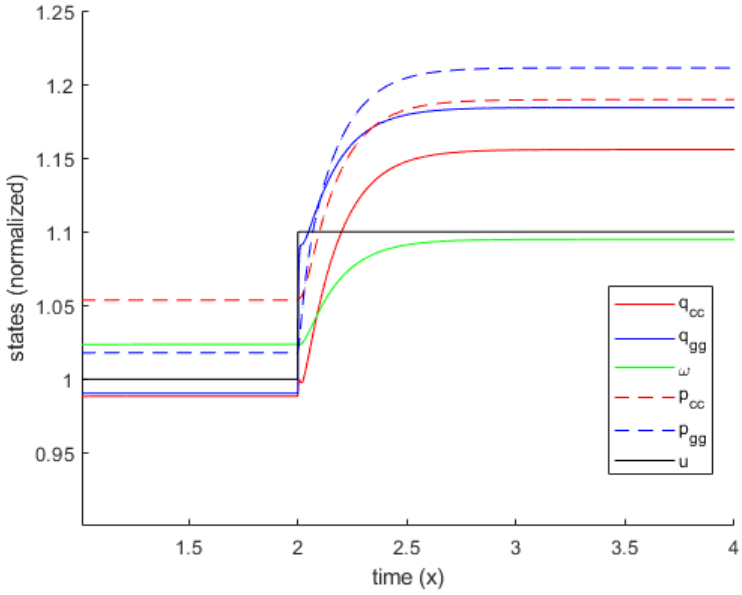

Figure 3.8 – Evolution of the states for a step-response

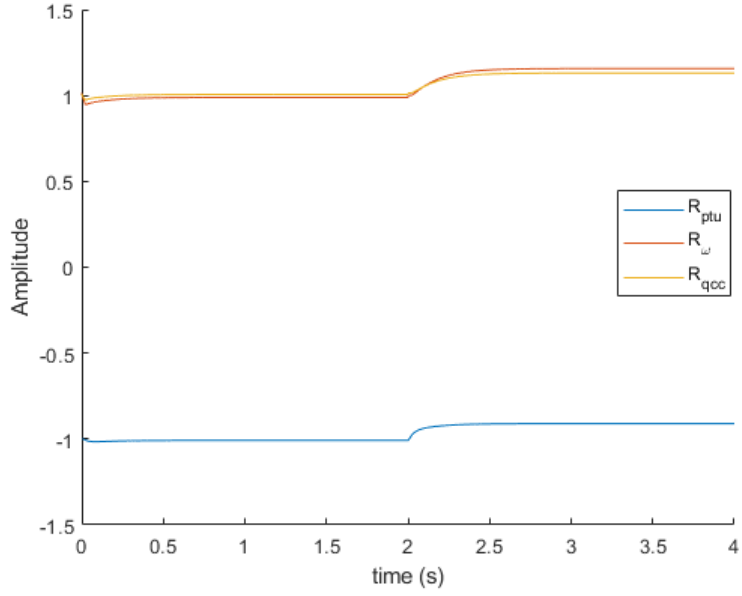

Figure 3.9 – Evolution of the resistive terms for a step-response

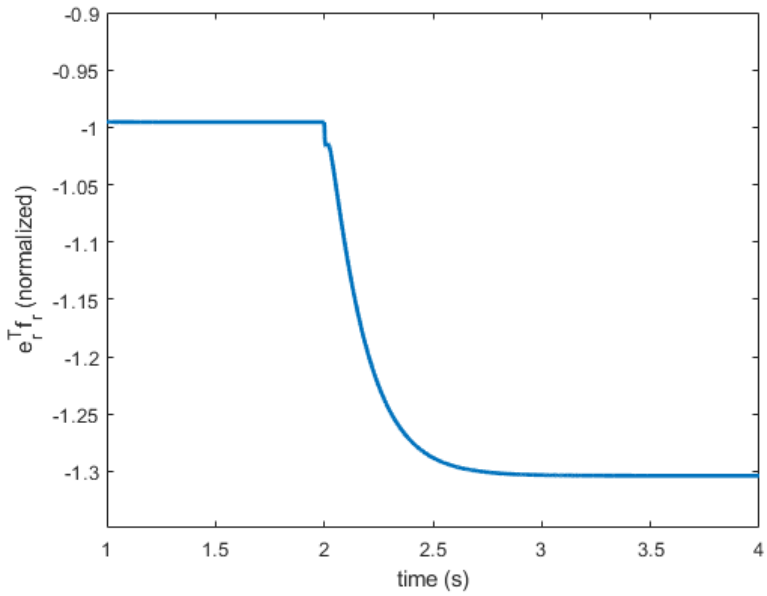

Figure 3.10 – Evolution of the total dissipated power for a step-response

chamber mass flow, where the resistive term R_{qcc} becomes negative and does not respect the Port-Hamiltonian structure ($R > 0$).

The passivity of the complex system can be proved, however, as it does not respect the Port-Hamiltonian structure due to the turbine pressure p_{tu} equation, it is necessary to introduce a controller to render the system passive with respect to a chosen equilibrium.

In this scope, the introduction of a passivity-based controller is proposed in chapter 4.

4 - Passivity-based controller

Using Port-Hamiltonian modeling of a system, it is possible to prove the passivity of a system, and the asymptotic stability around an equilibrium. However, the LPRE complex system presents a positive resistive term R_{ptu} that proves problematic for the passivity analysis. Additionally, while proof of the stability around the origin is possible, demonstration of the stability around a desired equilibrium is lacking. This chapter presents an approach to designing a passivity-based controller for a liquid-propelled rocket, using Port-Hamiltonian representation. This controller aims to make the closed-loop controlled system passive and assign a new chosen equilibrium.

4.1 . Passivity-based control theory

Passivity-based control [74] is a classical control design method in Port-Hamiltonian systems theory. It is briefly recalled here. Note that $R(x)$ and $J(x)$ are noted R and J per abuse of notation, however, the dependency on the state is still considered.

Let a Port-Hamiltonian system of the form

$$\dot{x} = (J - R)\frac{\partial H}{\partial x} + g.u(x,t), \tag{4.1}$$

where $x \in \mathbb{R}^n$, $u \in \mathbb{R}^p$, with the associated desired system behavior given by

$$\dot{x}_d = (J_d - R_d)\frac{\partial H_d}{\partial x}, \tag{4.2}$$

where the matrices $J_d = -J_d^\top, R_d \geq 0$ represent the desired storage and damping matrices, and H_d is the desired resulting Hamiltonian function.

The principle of the design of the controller is to define a new stable equilibrium to the system (4.1). To do so, a new Hamiltonian function $H_d(x)$ is assigned to the system (4.1). This new energy function should be minimal at the desired equilibrium and consequently be a candidate function for the passivity condition of the new closed-loop system. This requires the new Hamiltonian function to respect $H_d(x) \geq 0$ and to conserve the Port-Hamiltonian structure $J_d(x) = -J_d(x)^\top, R_d(x) \geq 0$. While J_d and R_d are defined by the user, the Hamiltonian function H_d is not known a priori.

The developed method consists in searching for a controller u such that the dynamics of the closed-loop system (4.1) converges to the dynamics of (4.2). This translates into

$$\forall x \in \mathbb{R}^\varkappa, (J - R)\frac{\partial H}{\partial x} + gu = (J_d - R_d)\frac{\partial H_d}{\partial x}, \tag{4.3}$$

which is the generation equation for the controller. This equation is used to define both the new Hamiltonian $H_d(x)$ and the controller $u(x)$. Let a full rank left annihilator $g^\perp$ of g. If $p < n$, then the full rank left annihilator $g^\perp \in \mathbb{R}^{n\times(n-p)}$ is defined such that $\forall x \in \mathbb{R}^n, g^\perp(x)g(x) = 0$. Using (4.3), where the control action is nullified, it is possible to obtain the following partial derivative equation, where the control action $u(x)$ is nullified,

$$g^\perp(J_d - R_d)\frac{\partial H_d}{\partial x} = g^\perp(J - R)\frac{\partial H}{\partial x}. \tag{4.4}$$

To find the unknown desired Hamiltonian H_d, from the known matrices R_d, J_d, define the matrices added to the system, and the added Hamiltonian $H_a(x)$,

$$\begin{aligned} R_a(x) = R_d(x) - R(x), R_a(x) \geq 0 \\ J_a(x) = J_d(x) - J(x), J_a(x) = -J_a(x)^\top \\ H_a(x) = H_d(x) - H(x). \end{aligned} \tag{4.5}$$

Assuming we can find $u(x)$,$R_a(x)$,$J_a(x)$ and $\frac{\partial H_a}{\partial x}$, with properties specified in the following, the closed-loop system (4.1) is a Port-Hamiltonian system with dissipation $R_d(x)$ and a stable equilibrium at a specified $x = x_0$ (see [77], Prop. 1.)

While R_a and J_a follow from the knowledge of R_d and J_d, $H_a(x)$ is a Hamiltonian function added to the system and must be determined (note that from the definition of $H_a(x)$, finding H_a is equivalent to finding $H_d(x)$). $H_a(x)$'s hessian is defined by the partial derivative equation (4.4) and must respect the following existence conditions,

- $\frac{\partial H_a}{\partial x}$ is the gradient of a scalar function, and should be integrable, therefore $H_a(x)$ must respect an integrability condition

$$\frac{\partial^2 H_a}{\partial x^2} = \left[\frac{\partial^2 H_a}{\partial x^2}\right]^\top. \tag{4.6}$$

  This condition can be directly injected in (4.4). It is not directly applicable to $H_d(x)$ and therefore justifies the introduction of the intermediary Hamiltonian function $H_a(x)$.
- The equilibrium assignment at $x = x_0$ defines the minimum of $H_d(x)$. In other terms, $min_x(H_d(x)) = H_d(x_0)$. Paired with the passivity conditions ($H_d(x) \geq 0$, see 3.1.2), the minimal value of H_d is set to $H_d(x_0) = 0$. The function $H_a(x)$ is then defined at x_0 by

$$\begin{aligned} H_a(x_0) = -H(x_0) \\ \frac{\partial^2 H_a}{\partial x^2}(x_0) > \frac{\partial^2 H}{\partial x^2}(x_0). \end{aligned} \tag{4.7}$$

Following the definitions of H_a, R_a, J_a, (4.4) can be written

$$g^\perp(J + J_a - R - R_a)\frac{\partial H_a}{\partial x} = -g^\perp(J_a - R_a)\frac{\partial H}{\partial x} \tag{4.8}$$

The partial derivative equation (4.8), paired with the two conditions on H_a (4.6) and (4.7) allows to solve the system and define the added Hamiltonian H_a. with the added Hamiltonian $H_a(x)$, the desired Hamiltonian follows directly using $H_d(x) = H(x) + H_a(x)$, and the controller $u(x)$ is defined directly using

$$u(x) = (g^\top g)^{-1} g^\top \left((J_d - R_d)\frac{\partial H_d}{\partial x} - (J - R)\frac{\partial H}{\partial x} \right) \tag{4.9}$$

where $(g^\top g)^{-1} g^\top$ is a left inverse of the control matrix g.

4.2 . Application to the simplified LPRE model

To illustrate the design of the passivity-based controller, we present it using the simplified model of the LPRE (3.28). We recall here the geometric structure of the model,

$$\begin{bmatrix} J\alpha_q\dot{\omega} \\ I\dot{q} \\ k_p\dot{p} \end{bmatrix} = (J(x) - R(x))\frac{\partial H}{\partial x} + g(x)T_m + \begin{bmatrix} 0 \\ p_{ep} \\ 0 \end{bmatrix}, \tag{4.10}$$

where

$$J(x) = \begin{bmatrix} 0 & -\lambda & 0 \\ \lambda & 0 & -1 \\ 0 & 1 & 0 \end{bmatrix}, R(x) = \begin{bmatrix} -R_\omega & 0 & 0 \\ 0 & -R_q & 0 \\ 0 & 0 & -R_p \end{bmatrix} \tag{4.11}$$

$$\frac{\partial H}{\partial x} = \begin{bmatrix} \omega \\ q \\ p \end{bmatrix} \text{ and } g(x) = \begin{bmatrix} 1 \\ 0 \\ 0 \end{bmatrix}. \tag{4.12}$$

The application of PBC to the simplified LPRE model aims to change the stable equilibrium of the system. Indeed, the simplified system is passive with respect to the origin, and a PBC controller is designed to stabilize the system to an equilibrium that differs from the origin of the system ($x_0 \neq 0$). To do so, a new Hamiltonian function $H_d(x)$ is retrieved for the system.

4.2.1 . Determination of the desired functions

The first step for the design of the PBC controller is to establish the desired effect of the controller on the system. The equilibrium is defined by a known chamber pressure p_0, for which the corresponding ω_0, q_0 can be computed (therefore are supposed known). As the initial Hamiltonian function of an LPRE is quadratic in the states in (3.44), the Hamiltonian H_d is chosen under a quadratic form,

$$H_d(x) = x^\top Q x \tag{4.13}$$

where Q is a positive symmetric square matrix that represents the equivalent inertia of the system. Additionally, let the state vector x_d be of the form,

$$x_d = \begin{bmatrix} J\alpha_q\omega - J\alpha_q\omega_0 \\ Iq - Iq_0 \\ k_p p - k_p p_0 \end{bmatrix}, \tag{4.14}$$

for an equilibrium defined by $x_0 = \begin{bmatrix} J\alpha_q\omega_0 & Iq_0 & k_p p_0 \end{bmatrix}^\top$. The state vector at the equilibrium is then defined by $x_d(x_0) = \begin{bmatrix} 0 & 0 & 0 \end{bmatrix}^\top$. As the LPRE simplified system is expressed under Port-Hamiltonian form, there is no need for a new resistive matrix $R_d(x)$. In this approach, define $J_d = J$ and $R_d = R$, (leading to $J_a = R_a = 0$) as there are no other requirements than equilibrium assignment.

4.2.2 . Choice of the Hamiltonian $H_d(x)$

After having selected the desired matrices $J_d(x), R_d(x)$, the determination of $H_d(x)$ must be performed via the determination of $H_a(x)$. This step makes use of equations (4.6), (4.8) and (4.13) to express the Hamiltonian function.

Let a full rank left annihilator of g be

$$g^{\perp} = \begin{bmatrix} 0 & 1 & 0 \\ 0 & 0 & 1 \end{bmatrix}. \tag{4.15}$$

Equation (4.8) yields

$$\begin{bmatrix} \lambda & -R_q & -1 \\ 0 & 1 & -R_p \end{bmatrix} \frac{\partial H_a}{\partial x} = 0, \tag{4.16}$$

which translates into two equations for the partial derivatives of H_a,

$$\begin{aligned} \frac{\partial H_a}{\partial Iq} &= R_p \frac{\partial H_a}{\partial k_p p} \\ \frac{\partial H_a}{\partial J\alpha_q \omega} &= \frac{(R_q R_p + 1)}{\lambda} \frac{\partial H_a}{\partial k_p p}. \end{aligned} \tag{4.17}$$

The new Hamiltonian H_d is proposed with an quadratic form in (4.13). Additionally, (4.17) implies cross terms within the different components. Then H_d's partial derivatives can be written,

$$\begin{aligned} \frac{\partial H_d}{\partial J\alpha_q \omega} &= Q_\omega(\omega - \omega_0) + k_{\omega q}(q - q_0) + k_{\omega p}(p - p_0), \\ \frac{\partial H_d}{\partial Iq} &= Q_q(Iq - Iq_0) + k_{q\omega}(\omega - \omega_0) + k_{qp}(p - p_0), \\ \frac{\partial H_d}{\partial k_p p} &= Q_p(p - p_0) + k_{p\omega}(\omega - \omega_0) + k_{pq}(q - q_0), \end{aligned} \tag{4.18}$$

where $Q_\bullet$ is the equivalent inertia coefficient for a state and $k_\bullet$ is a cross-term coefficient in the inertia matrix Q. Here the state vector corresponds to x_d defined in (4.14) to ensure the equilibrium assignment. The matrix Q expresses as :

$$Q = \begin{bmatrix} Q_\omega & k_{\omega q} & k_{\omega p} \\ k_{q\omega} & Q_q & k_{qp} \\ k_{p\omega} & k_{pq} & Q_p \end{bmatrix} \tag{4.19}$$

The relation $H_a(x) = H_d(x) - H(x)$ is used to translate (4.18) into

$$\begin{aligned} \frac{\partial H_a}{\partial J\alpha_q \omega} &= (Q_\omega - 1)(\omega - \omega_0) + k_{\omega q}(q - q_0) + k_{\omega p}(p - p_0) + \omega_0, \\ \frac{\partial H_a}{\partial Iq} &= (Q_q - 1)(q - q_0) + k_{q\omega}(\omega - \omega_0) + k_{qp}(p - p_0) + q_0, \\ \frac{\partial H_a}{\partial k_p p} &= (Q_p - 1)(p - p_0) + k_{p\omega}(\omega - \omega_0) + k_{pq}(q - q_0) + p_0, \end{aligned} \tag{4.20}$$

The integrability condition in (4.6) gives

$$\begin{aligned} k_{\omega q} &= k_{q\omega}, \\ k_{\omega p} &= k_{p\omega}, \\ k_{qp} &= k_{pq} \end{aligned} \tag{4.21}$$

From (4.17), (4.20), (4.21) it is possible to express every unknown term in terms of a single one. Q_q is selected as the common parameter. The other parameters are computed with a projection of equation (4.17) on the states. Let for example the first partial derivative equation,

$$\frac{\partial H_a}{\partial Iq} = R_p \frac{\partial H_a}{\partial k_p p} \tag{4.22}$$

projected on the state ($J\alpha\omega$ which is equivalent to a projection on ω as J, α_q are time-invariant),

$$k_{q\omega}(\omega - \omega_0) = R_p.(k_{p\omega}(\omega - \omega_0)). \tag{4.23}$$

The projections for the system lead to the definition of 6 equations, with 1 redundancy, for a total of 5 independent equations. The system is then solvable, and all unknown parameters can be expressed under one common parameter. The other terms of the equation expressed as a function of Q_q read as,

$$\begin{aligned}
Q_\omega &= \frac{(R_q R_p + 1)^2}{\lambda^2 R_p^2}(Q_q - 1) + 1 \\
k_{\omega q} &= \frac{R_q R_p + 1}{\lambda R_p}(Q_q - 1) \\
k_{\omega p} &= \frac{R_q R_p + 1}{\lambda R_p^2}(Q_q - 1) \\
Q_p &= \frac{1}{R_p^2}(Q_q - 1) + 1 \\
k_{qp} &= \frac{1}{R_p}(Q_q - 1)
\end{aligned} \tag{4.24}$$

The equilibrium assignment (4.7) can be easily verified from (4.18).

The controller can finally be expressed using (4.9),

$$u = -R_\omega \frac{\partial H_a}{\partial J \alpha_q \omega} - \lambda \frac{\partial H_a}{\partial Iq}, \tag{4.25}$$

or in a developed form,

$$\begin{aligned}
u(x) = -R_\omega \Bigg[& \frac{(R_p R_q + 1)}{\lambda R_p}(Q_q - 1) \\
& \left(\frac{(R_p R_q + 1)}{\lambda R_p}(\omega - \omega_0) + (q - q_0) + \frac{1}{R_p}(p - p_0) \right) \\
& + \omega_0 \Bigg] - \lambda \Bigg[(Q_q - 1) \Bigg((q - q_0) + \frac{(R_p R_q + 1)}{\lambda R_p}(\omega - \omega_0) \\
& + \frac{1}{R_p}(p - p_0) \Bigg) + q_0 \Bigg].
\end{aligned} \tag{4.26}$$

This controller is then a non-linear state feedback since the non-linear expression of the resistive terms implies the non-linearities in the expression of the controller.

4.2.3 . Controller tuning

The tuning parameter of the controller Q_q is derived from conditions on H_a summarized by (4.7). To ensure a minimum of the Hamiltonian function at the desired equilibrium x_0, the parameter Q_q is set to satisfy

$$\begin{bmatrix} Q_\omega & k_{\omega q} & k_{\omega p} \\ k_{\omega q} & Q_q & k_{qp} \\ k_{\omega p} & k_{qp} & Q_p \end{bmatrix} > 0 \tag{4.27}$$

As the eigenvalues of the matrix Q are

$$\begin{bmatrix} Q_q + \frac{1}{R_p^2 \lambda^2}(Q_q - 1)\left(R_q^2 + 2R_q R_p + \lambda^2 + 1\right) \\ 1 \\ 1 \end{bmatrix}, \tag{4.28}$$

a simple choice is to use $Q_q = 1 + k_u.v(x)$ where $v(x)$ is a positive function $v : \mathbb{R}^n \to \mathbb{R}_+$ and $k_u \in \mathbb{R}_+$.

Additionally, to obtain the desired behavior the function $v(x)$ is tuned to mitigate the highest eigenvalue of the matrix Q, which means that for the highest eigenvalue,

$$Q_q + \frac{1}{R_p^2 \lambda^2}(Q_q - 1)\left(R_q^2 + 2R_q R_p + \lambda^2 + 1\right), \tag{4.29}$$

we want $v(x)$ such that this eigenvalue is close to 1. Note that the hessian of the original Hamiltonian is composed of constant terms, with eigenvalues

$$\begin{bmatrix} \frac{1}{J\alpha_q} \\ \frac{1}{J} \\ \frac{1}{k_p} \end{bmatrix}. \tag{4.30}$$

As the resistive term R_p is small before 1, $R_p << 1$, we define $v(x) = k_u.R_p^2$, and the equivalent inertia of the Hamiltonian is defined as

$$Q_q = 1 + k_u R_p^2 \tag{4.31}$$

where the parameter k_u can vary and influence the speed and precision of the controller. And the max eigenvalue of Q is then,

$$\frac{k_u}{\lambda^2}\left(R_q^2 + 2R_q R_p + \lambda^2 + 1\right). \tag{4.32}$$

The parameter k_u is a tuning parameter of the controller, and impacts the speed and stabilizing properties of the controller. In the controller expression (4.26), $k_u v(x)$ multiplies the error $(x - x_0)$, and has a high impact on the behavior of the controlled system. Therefore the choice of k_u must be justified by the system behavior desired by the user and the actuators' performance. Note that for $v(x) = 1$, the controller is equal to $R_\omega \omega_0 + \lambda q_0$ which corresponds to the value of the desired equilibrium u_0.

The impact of $v(x) = k_u R_p^2$ can be witnessed on the system with simulations for different k_u. Figure 4.1 illustrates the behavior of the pressure p for different tuning parameters k_u in the range $[0.1, 10]$. The controller follows a step from the nominal value $x_0 = 1$ to $x = 1.1x_0$. The figure illustrates the speed increase with a higher parameter k_u, however, an overshoot appears in the highest value of k_u. This behavior was expected as k_u scales the importance of the state difference to the equilibrium $(x - x0)$.

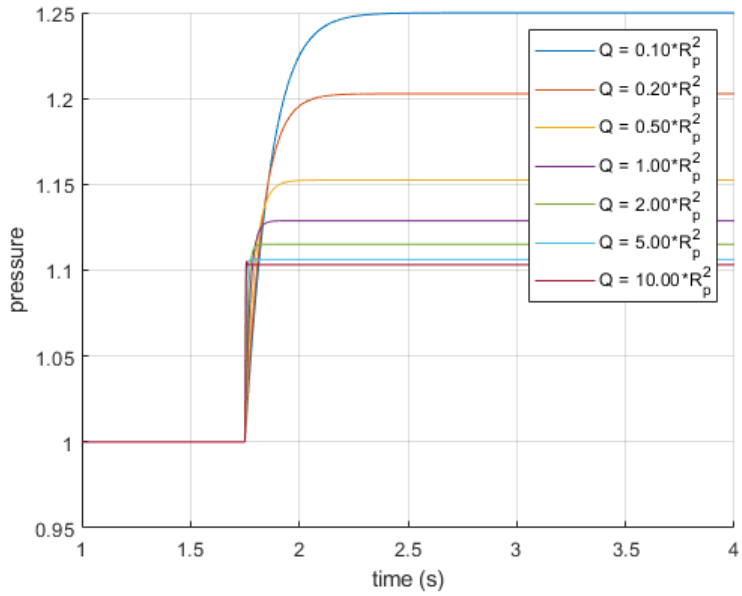

Figure 4.1 – Evolution of the pressure for different tuning parameters Q_q

A small k_u leads to a slow system, with a high static error, while a high k_u leads to a fast system, with an overshoot and a low static error.

In the chapter 6, the open-loop system displays a time-response of $0.74s$, therefore a suitable value is $k_u = 0.1$, as it proves to have a similar time-response ($0.61s$ in figure 4.1).

Note that in this design the controller obtained yields the closed-loop (4.2). The introduction of an integral action in the definition of the equilibrium x_0 in (4.14) suppresses the resulting static error while conserving the Port-Hamiltonian structure.

4.3 . Determination of a controller for the complex system with application to trajectory tracking

In this section, the steps to extend the PBC design method to the complex system in Port-Hamiltonian form (3.32) are depicted. Note that the Port-Hamiltonian form is comprised of the H-half of the LPRE only, and is composed of 7 states. Additionally, the additional elements to perform trajectory tracking with the controller are described. We note R^s a matrix for the simplified system and R^c a matrix for the complex system.

4.3.1 . Controller design for the complex system

In a first time, consider the approach where the matrices $J_a^c(x) = R_a^c(x) = 0$ as for the simplified system in the previous section 4.2. The PDE defined by

$$g^{\perp}(J + J_a - R - R_a)\frac{\partial H_a}{\partial x} = -g^{\perp}(J_a - R_a)\frac{\partial H}{\partial x}$$

yields the following

$$\begin{aligned}
-R_{\omega}\frac{\partial H_a}{\partial(\alpha_q J\omega)} + \alpha_t\frac{\partial H_a}{\partial(k_{ptu}p_{tu})} - \lambda\frac{\partial H_a}{\partial(I_{cc}q_{cc})} - \lambda\frac{\partial H_a}{\partial(I_{gg}q_{gg})} &= 0\\
-R_{qcc}\frac{\partial H_a}{\partial(I_{cc}q_{cc})} + \lambda\frac{\partial H_a}{\partial(\alpha_q J\omega)} - \frac{\partial H_a}{\partial(k_{pcc}p_{cc})} &= 0\\
-R_{qtu}\frac{\partial H_a}{\partial(I_{tu}q_{tu})} + \kappa_{tu}\frac{\partial H_a}{\partial(k_{pgg}p_{gg})} - \kappa_{tu}\frac{\partial H_a}{\partial(k_{ptu}p_{tu})} &= 0\\
-R_{pcc}\frac{\partial H_a}{\partial(k_{pcc}p_{cc})} + \frac{\partial H_a}{\partial(I_{cc}q_{cc})} &= 0\\
-R_{pgg}\frac{\partial H_a}{\partial(k_{pgg}p_{gg})} + \frac{\partial H_a}{\partial(I_{gg}q_{gg})} - \kappa_{tu}\frac{\partial H_a}{\partial(I_{tu}q_{tu})} &= 0\\
-R_{ptu}\frac{\partial H_a}{\partial(k_{ptu}p_{tu})} + \kappa_{tu}\frac{\partial H_a}{\partial(I_{tu}q_{tu})} - \alpha_t\frac{\partial H_a}{\partial(\alpha_q J\omega)} &= 0
\end{aligned} \tag{4.33}$$

Similarly to the simplified system, the desired Hamiltonian function H_d^c for the complete LPRE is computed using the variables separation method as in [80]. In the complex modeling case however, the multiple projections of the partial derivative equation (4.33) lead to an over-defined equation system, which corresponds to the number of unique equations exceeding the number of unknown parameters. In this section, the solution explored consists in changing the desired dissipation matrix $R_d^c(x) \neq R^c(x)$. This new assignment serves two distinct goals, increase the number of unknown parameters to grant the closure of the PDE equations, and assign a new damping to the complex LPRE system, whose resistive matrix contains a negative resistive term $R_{p_{tu}}$ (see 3.3.2).
Let a positive symmetric matrix $Q^c \in \mathbb{R}^{7\times 7}$ such that the desired Hamiltonian $H_d^c(x)$ is under the form

$$H_d(x) = x^\top Q^c x. \tag{4.34}$$

The PDE,

$$\forall x \in \mathbb{R}^{\kappa}, (J^c - R^c)\frac{\partial H^c}{\partial x} + g^c u^c = (J_d^c - R_d^c)\frac{\partial H_d^c}{\partial x},$$

grants 42 equations, and has no solution for $R_a^c = J_a^c = 0$, due to over-definition of the equations (42 equations for only 28 parameters that compose the matrix Q^c). In comparison, the same PDE for the simplified system granted 6 equations with one repetition (5 unique equations), and Q^s is composed of 6 parameters. To find a solution for the PDE, it is then necessary to define a new suitable matrix R_a. Let a diagonal matrix $R_a \neq 0$,

$$\begin{aligned}
R_a^c(x) = diag(&R_{a\omega}, R_{aqcc}, R_{aqgg}, R_{aqtu},\\
&R_{apcc}, R_{apgg}, R_{aptu}).
\end{aligned} \tag{4.35}$$

The introduction of this unknown matrix adds 7 unknown parameters to the equation (4.33). This allows the user to solve the equations (as several equations in the 42 are not unique, resolution has proven that there are only 31 unique equations). In particular, 4 conditions on the added resistive matrix $R_a(x)$ are

derived from solving the equation,

$$\begin{aligned} R_{aq_{cc}} &= R_{qcc} \\ R_{ap_{cc}} &= 0 \\ R_{a\omega} &= R_{\omega} - R_{pcc} \\ R_{ap_{gg}} &= R_{q_{tu}} - R_{aq_{tu}} \end{aligned} \tag{4.36}$$

Using the newly defined matrix $R_a^c(x)$ with conditions stated in (4.36), the equations (4.33) are now solvable, with the separation of the variables method. A more powerful method is presented in [74], to solve partial derivative equations using the method of characteristics. However, in the case of a separation method, a sufficient condition on the rank of the equation matrix (the rank of the equations is $n-1$, leading to no over-definition) is enough to solve the system.

The computation of the controller is determined using the symbolic computing tool *Maple*. The formulation of the controller is given in **Appendix B** as obtained in *Maple*. A simpler expression is given using the co-energy variables under the form,

$$\begin{aligned} u(x) = -\frac{1}{q_{gg}^2}(-R^c_{aq_{gg}}\frac{\partial H_d}{\partial I_{qgg}q_{gg}} - (\lambda\frac{\partial H_d}{\partial \alpha J\omega} - R_{qgg}\frac{\partial H_d}{\partial I_{qgg}q_{gg}} - \frac{\partial H_d}{\partial k_{pgg}p_{gg}}) \\ +\lambda\frac{\partial H}{\partial \alpha J\omega} - R_{qgg}\frac{\partial H}{\partial I_{qgg}q_{gg}} - \frac{\partial H}{\partial k_{pgg}p_{gg}}). \end{aligned} \tag{4.37}$$

Notice that at the equilibrium x_0, which is a minimum of the function H_d, the controller value leads to $I_{qgg}\dot{q}_{gg} = 0$ as the equation can be found back into the controller.

The equations are solved by expressing every parameter depending on the value of Q_{qgg}, which is the equivalent impedance for the state q_{gg} in the desired Hamiltonian $H_d(x) = x^\top Q^c x$. As the controller influences the mass flow q_{gg}, in

$$I_{gg}\dot{q}_{gg} = \alpha_q\omega - p_{gg} - R_{qgg}q_{gg} - Z_{vgg}q_{gg}^2 \tag{4.38}$$

it is of interest to associate the common parameter to Q_{qgg}. Indeed, the computation of the other impedance terms $Q_\omega, ...$ is more complex at each equation. The Q_{qgg} parameter is then a suitable choice since it distributes on all the system. In this case the equilibrium assignment condition (4.7) yields the following parameter Q_{qgg}

$$Q_{qgg} = 1 + v(x,t) \tag{4.39}$$

where $v(x,t)$ remains a positive function.

4.3.2 . Application to trajectory tracking

In this subsection, the controller's performance for trajectory tracking is presented. At this point, the controllers designed for both the simplified system in 4.2 and for the complex system in 4.3 are able to stabilize the system around a desired equilibrium. This subsection discusses the options to generate a reference that is suitable for the tracking of a trajectory and is illustrated by step functions to show the differences between the options.

First introduce the notion of a reference trajectory. A reference trajectory is a vector function of time $x_r(t) : \mathbb{R}_+ \to \mathbb{R}^n$, which defines a known state vector at all times $t > 0$.

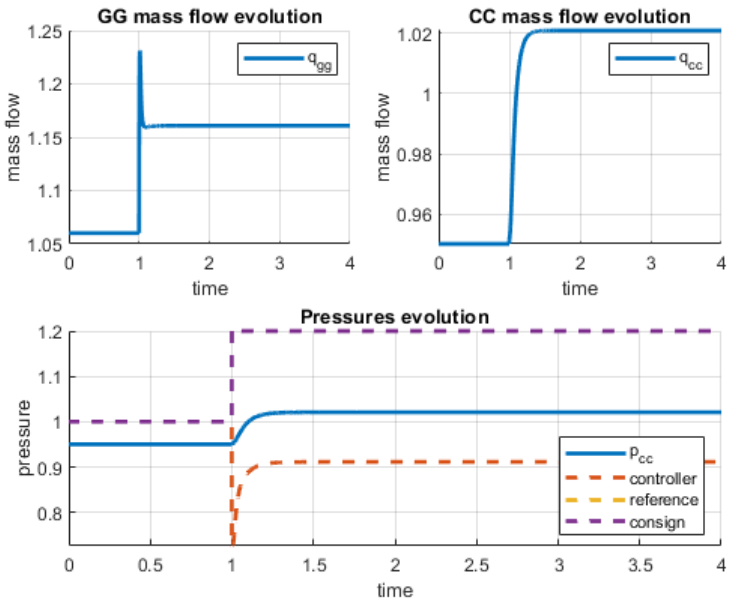

Figure 4.2 – Step response of the controlled system, with no reference generation

A trajectory $x(t)$ of the system is a solution to the equations of the system over time.

Define also the notion of objective function $x_{obj}(t)$ which is the trajectory that the state must follow. The difference between objective and reference is illustrated in the following, with the notion of error with the reference $(x - x_r)$.

To perform a trajectory tracking, the difference between the current trajectory $x(t)$ and the reference at the same time t, $x_r(t)$ is used, $(x(t) - x_r(t))$. The first example of trajectory tracking is provided for the PBC controller with the equilibrium assignment in the term $(x - x_0)$. This consists in a trajectory tracking of a constant reference $x_r(t) = x_0$.

To define a reference x_r from a continuous function, it is necessary to discretize this function into multiple equilibrium assignments. This process is for example realized in simulations, when the discretization is generated by the time-step of the simulation.

In the following paragraphs, solutions are illustrated on a step response in closed-loop control of the complex system with the controller in 4.3. The simulations are computed with the parameter Q_{ggg} such that,

$$Q_{ggg} = 1 + k_u \frac{R_{pc}^2}{R_{qt}}. \tag{4.40}$$

As for the simplified system, the value of Q_{ggg} is selected to minimize the highest eigenvalue in the matrix Q^c

To illustrate the problem of reference generation, let a first reference defined by

$$x_r = (p_{cc,obj} - p_{cc}) \frac{x_0}{p_{cc,0}}. \tag{4.41}$$

where $p_{cc,obj}(t)$ the objective function for the main chamber pressure p_{cc}. This reference aims to perform trajectory tracking of the main chamber pressure, with equilibrium assignment at $(x(t) - x_r(t))$. This

simple reference generation approximates each state using a first-order Taylor expansion of the state $x_r = \frac{x_0}{p_{cc,0}} p_{cc}$. In the simulation using this reference, a static error is expected, due to the error between the state and the reference x_r. The objective function is a step, which translates to

$$p_{cc,obj} = \begin{cases} p_{cc_0} & t < 1 \\ 1.2 p_{cc_0} & t \geq 1 \end{cases} \tag{4.42}$$

in figure 4.2, the controlled system responding to the step is proposed. A static error appears at the start and the end of the step function. This static error originates from the reference generation in the controller. As mentioned in the design of the controller 4.2.1, the new state associated with the desired behavior is $x - x_r$, where x_r is the desired equilibrium of the system. In this work, the states are supposed measurable therefore it is possible to compute the controller for a known equilibrium of the system.

The static error illustrates the requirement for a reference generation method, to define a new function $x_r(t)$ that allows the system to precisely converge to the objective x_{obj}. As shown in figure 4.2, an insufficient design of the reference leads to the loss of precision in the tracking. Two solutions for reference generation are proposed in the following, a simple reference generation and the addition of an integrator.

Addition of a simple reference governor

In this paragraph, the reference x_r used in the system is comprised of two vectors corresponding to the desired equilibria during a step. The first vector is composed of an equilibrium where $p_{cc} = p_{cc0}$ and the second vector of an equilibrium where $p_{cc} = 1.2 p_{cc_0}$. Until the step, the first vector $x_{r,p_{cc_0}}$ is injected in the system, and at the time of the step ($t = 1s$), the second vector $x_{r,1.2p_{cc_0}}$ is used. Note that $x_r \in \mathbb{R}^n$ is a known equilibrium of the system, describing each state with precision. The main difference with the reference defined by (4.41), is that this reference provides a real value for all states, rather than an approximation. Consequently, no static error is expected in the simulation. The closed-loop system equation with this reference is

$$\dot{x} = (J_d - R_d) \frac{\partial H_d}{\partial x}(x, x_r) \tag{4.43}$$

where

$$x_r = \begin{cases} x_{r,p_{cc_0}} & t < 1 \\ x_{r,1.2p_{cc_0}} & t \geq 1 \end{cases} \tag{4.44}$$

The response to this reference is provided in figure 4.3. The figure displays the controller, which is the value of the PBC controller u, the reference, which is the state x_r, and the consign which is the objective function. In this case, the reference and the consign overlap, as they represent the same quantity for the state p_{cc}.

A proper reference allows the system to converge to the desired value $p_{cc} = 1.2 p_{cc0}$, without an added integrator. The term proper designates the fact that the reference requires prevision of the 7 states of the system at the desired p_{cc}. The step response provides a spike in the controller u at time $t = 1s$, which is echoed on the state q_{gg}. Such a spike is not desired in this system, as it is not representative of the capabilities of the real actuators.

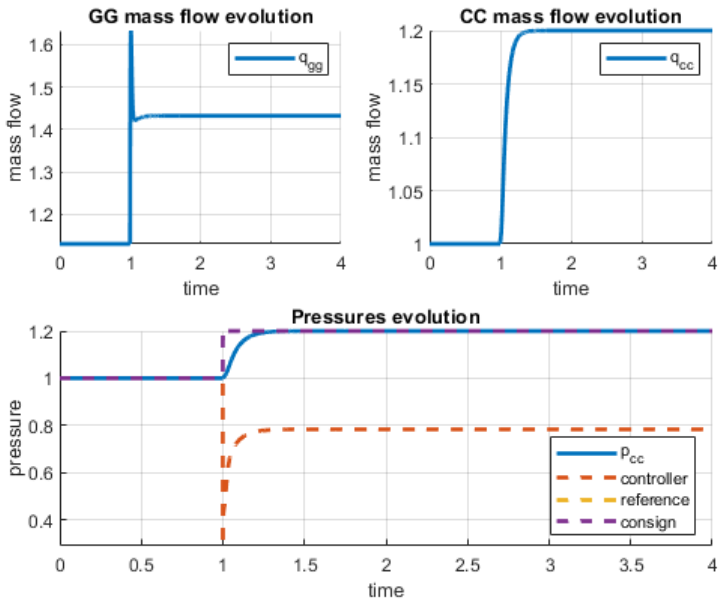

Figure 4.3 – Step response of the controlled system, using a simple reference governor

Additionally, such reference requires a new step in the implementation of the controller. For example, on 4.3, previous simulations allowed to determine all values for the states in the reference before and after the step (at $t = 1s$).

While the stability of the system is guaranteed by the new Hamiltonian function $H_d(x, x_r)$ before the step it is required to verify that the Hamiltonian is valid for both points. Finally, such reference is difficult to retrieve when a smooth reference is required (rather than scattered points), and is sensible to perturbations and measurement errors, see 6.

Addition of an integrator

In this subsection, the addition of an integrator before the controller to generate a reference is proposed. This means that the objective function $p_{cc,obj}$ is compared to the current state p_{cc}, then is processed by the integrator to obtain $x_r(t)$ which is finally injected in the PBC controller. The global equation of the closed-loop system is

$$\dot{x} = (J_d - R_d)\frac{\partial H_d}{\partial x}(x, x_r),$$
$$x_r = \left((p_{cc,obj} - p_{cc}) + k_I \left(\int_0^t (p_{cc,obj} - p_{cc})dt\right)\right)\frac{x_0}{p_{cc,0}} \tag{4.45}$$

for $k_I = 0$, the equation for a simple reference is retrieved. For $k_I > 0$ the system proposes a new reference x_r that allows the suppression of the static error present in figure 4.2. To illustrate this, figure 4.4 reproduces the controller in figure 4.3, where a proportionate-integral (PI) defines the reference with $k_I = 30, k_P = 1$. Define an integrator on the static error between p_{cc} and the reference pressure p_{ccref}.

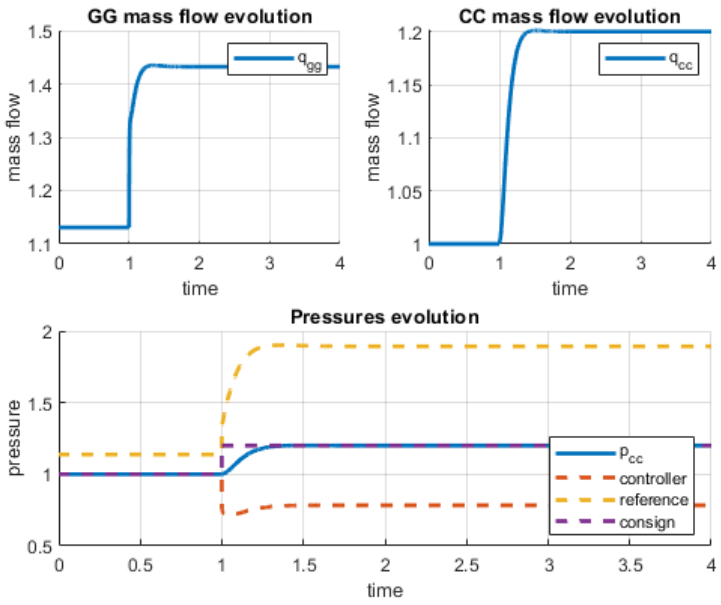

Figure 4.4 – Step response of the controlled system, using an integrator

In this simulation the controller and mass flow q_{gg} present a smooth behavior at $t = 1s$, and a more feasible behavior for the real physical system. Because of the integrator, the step function in the objective is smoothed with the integration process, in

$$x_r = \left((p_{cc,obj} - p_{cc}) + k_I \left(\int_0^t (p_{cc,obj} - p_{cc}) dt \right) \right) \frac{x_0}{p_{cc,0}} \tag{4.46}$$

Additionally, this reference is in practice easier to obtain than a full reference for the states since it only requires the consign value which is p_{cc}. From the value of p_{cc}, it is possible to define a reference that allows precise equilibrium assignment and a slower time-response. The slow time response is of interest in the scope of the addition of actuators dynamics to the system since a non-smooth behavior is unfeasible with a real system.

4.4 . Summary

In this chapter, to answer the equilibrium assignment problem, a controller using passivity-based properties has been designed for both the simplified and complex Port-Hamiltonian models of the LPRE. Additionally, it is shown that the PBC design allows to introduce a new damping matrix, to enforce the Port-Hamiltonian behavior on a system, and cancel a negative term in the resistive matrix $R(x)$ of the original system. This is used on the turbine pressure resistive term R_{ptu} which was shown to be positive in the previous chapter 3. Finally, the controller proves to have tuning capabilities, and a first tuning method is proposed, with a common parameter Q_q for the simplified system.

In a second time, the adaptation of the design to the tackle trajectory tracking scenario is discussed, in particular the reference generation problem, where it is necessary to inject a suitable function in the

controller to perform the equilibrium assignment and the convergence of the system. The controller presented in this chapter is to be compared with other applications of the PBC design in the literature. Notably, in [81] and [82], the authors developed control strategies to adapt the PBC design developed in [77] to trajectory tracking applications.

In [81] the author derives the PBC design to render the tracking error, in this instance corresponding to $x_{obj} - x$, under a Port-Hamiltonian form. The PBC controller is then used to make the tracking error a passive system with equilibrium 0, where the trajectory is correctly followed. In comparison, the trajectory tracking defined in this chapter is only able to render the same properties for a constant trajectory, or an almost constant trajectory (a step between two operating points). Indeed, a constant trajectory only adds an invariant term to the design, and therefore the error system follows the dynamics specified by H_d, R_d, J_d. In the case of a time-varying trajectory, the tracking ability of the design is hindered by the lack of integration of its dynamics into the design.

In [82], the notion of a contracting Port-Hamiltonian system is introduced, and the synthesis of a controller is recalled to be the design of a contracting controller with the PBC tools. This design allows to construct an exponentially stable controller, which is suited to perform trajectory tracking. The author searches for a contraction metric (see chapter 5) using the PBC method to assign the desired matrices J_d, R_d with a structure that enables contraction of the system. To do so, the author supposes that it is possible to find constant matrices in the desired structure (J_d, R_d), which in the case of the LPRE, has proven not to be possible in the computations driven. Indeed, the necessary fixed terms in the new resistive matrix R_d imply that $R_{aqcc} = R_{qcc}$ which is time-dependent. A solution to make the system contractive is presented in the following chapter, using another design method.

For trajectory tracking, PBC however proves to have a complex design in the reference generation, as well as limited stabilizing properties (stability must be proved around each point of the reference). To answer this, contraction theory is introduced in the following chapter, which is a tool that analyses stability with respect to a trajectory.

5 - Contraction theory analysis

Using Port-Hamiltonian systems framework, the analysis of the fixed-point stability of an LPRE model (simplified and complete) has been described using the passivity of the system. Additionally, the controller derived from a PBC approach in chapter 3 has proven suitable to stabilize the system around several operating points, allowing for the tracking of simple setpoint trajectories. However, the passivity-based controller additionally requires precise knowledge of the overall system, as the equations to determine the controller highly depend on the system's structure. PBC ensures the asymptotical stability of the system towards a reference point, which can prove insufficient in high-perturbated scenarios. As shown in 3.3.1, the Port-Hamiltonian modeling passivity is only applicable in a certain domain of stability. In the event of a more complex trajectory, the system can then be imposed *unstable* references, which cross the domain threshold and lead to unstable behavior. In such cases, it seems preferable to propose increased stability guarantees. In the case of a prior analysis of the domain of passivity, and the restriction of the reference to this domain, asymptotic stability with the PBC controller is sufficient. In this chapter a controller that renders the system exponentially stable is proposed, to face the event of an *unstable* trajectory.

The stability guarantees derived from the PBC controller yield convergence of the system to the desired operating point. For two successive points of a trajectory, a controller can be designed to ensure stability in a neighborhood of these points. However, when the neighborhoods are too distant from one another, portions of the transition trajectory may belong to regions where stability is not guaranteed (see figure 5.1). The transition between two stable equilibria in certain scenarios can lead to the loss of stability guarantee in uncertain regions (in blue on figure 5.1). In such a scenario it is interesting to provide analysis of the stability from a trajectory preservation point of view. Contraction theory [83, 45] focuses on the convergence of the different possible trajectories of a system and proves to be a well-suited framework for the analysis of nonlinear systems. The stability of the system is proven when the trajectories with potentially different initial conditions converge to a reference trajectory. Moreover, the stability of the system is guaranteed with respect to the reference trajectory. This means that if a stable trajectory is found for the transition between two operating points, contraction theory implies a stable behavior along the transition.

In this chapter, contraction theory is briefly recalled in 5.1. A contractive controller design is presented

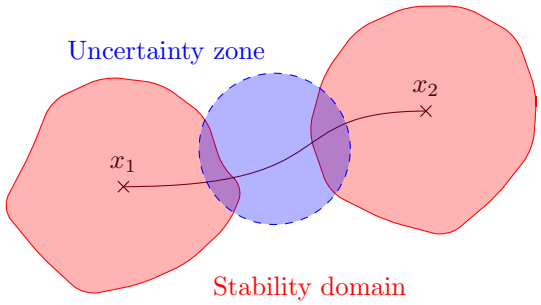

Figure 5.1 – Example of navigation between reference points

in 5.2, and applied to the simplified system. Performance and stability guarantees are shown in section 5.3. Complements to the existing design and the extension of the controller for the complex system are presented in 5.4.

5.1 . Contraction theory, definition and properties

Contraction theory for non-linear systems developed in [83], [45], is a powerful analysis tool for non-linear systems. In particular, contraction theory is used to describe the convergence of different solutions for a system. Typically, for an evolution equation of the form,

$$\dot{x} = f(x,t) + d(t), \tag{5.1}$$

where $d(t)$ is a time-varying perturbation, the solution of the equation depends on the initial condition $x(0)$ and on the perturbation $d(t)$. Contrary to classical analysis which focuses on the convergence of a solution to a point, contraction theory considers the flow of trajectories of a system. Contraction theory has mainly been used for studying the convergence of non-linear systems [84], [85] and controller design in [86], [87], [88].

Consider the following non-autonomous system

$$\dot{x} = f(x,t), \tag{5.2}$$

where x is an n-dimension state vector and f an n-dimension non-linear vector function with Jacobian $\frac{\partial f}{\partial x}$. If f is continuously differentiable, a virtual displacement δx is defined as an infinitesimal displacement at a fixed time. A virtual velocity is derived using the system equation (5.2),

$$\delta\dot{x} = \frac{\partial f}{\partial x}(x,t)\delta x, \tag{5.3}$$

representing differential dynamics of the flow of trajectories. Define a trajectory as a possible solution for the equation (5.2). Define the notion of neighboring trajectories as two trajectories solution to the same equation, with variance in a parameter (for example initial condition or perturbation). Consider now two neighboring trajectories $x_1(t)$, $x_2(t)$ and the virtual displacement between them at time t, $\delta x = x_1(t) - x_2(t)$. From here, define the squared distance between the two trajectories $\delta x^\top \delta x$. The rate of change of this squared distance is deduced from equation (5.2),

$$\frac{d}{dt}(\delta x^\top \delta x) = 2\delta x^\top \frac{\partial f}{\partial x}\delta\dot{x} \leq 2\lambda_{max}\delta x^\top \delta\dot{x}. \tag{5.4}$$

were λ_{max} is the highest possible eigenvalue of $\frac{\partial f}{\partial x}$. Then if there exists ϵ such that $\lambda_{max} \leq \epsilon < 0$, then the trajectories converge to each other, exponentially.

Definition 8. [45] Given the system dynamics equations $\dot{x} = f(x,t)$, a region of the state space is called a contraction region if the Jacobian matrix $\frac{\partial f}{\partial x}$ is uniformly negative definite in that region, which means $\exists \epsilon > 0, \frac{\partial f}{\partial x} + \frac{\partial f}{\partial x}^\top < -\epsilon Id < 0$.

Using this definition, Theorem 2 introduces a first condition for assessing the exponential convergence of a set of trajectories.

Theorem 2. *Lohmiller & al.* Given the system equations $\dot{x} = f(x,t)$, any trajectory, with initial conditions x_0, belonging to a ball of constant radius centered on a given trajectory, and contained at all times within a contraction region, remains in that ball and converges exponentially to this trajectory. Furthermore, global exponential convergence to the given trajectory is guaranteed if the whole state space is a contraction region.

The definition of a contraction region 8 is seldom verified under this formulation. In the literature, the sufficient condition that composes this definition has been extended [45]. Let a coordinate transformation

$$\delta z = \Theta \delta x \tag{5.5}$$

where $\Theta(x,t)$ is a square invertible matrix. Then the squared distance between two neighboring trajectories is expressed

$$\delta z^\top \delta z = \delta x^\top \mathcal{P}(x,t) \delta x \tag{5.6}$$

where $\mathcal{P}(x,t) = \Theta^\top \Theta$ is a symmetric positive matrix and defines a *metric*. The use of a metric allows to apply the sufficient condition for contraction to a wider range of systems. From here, we will consider a symmetric positive $\mathcal{P}$.

Definition 9. Given the system dynamics equation (5.2), a region of the state space is called a contraction region with respect to the metric $\mathcal{P}(x,t)$ if there exists a metric $\mathcal{P}(x,t)$ such that,

$$\partial_f \mathcal{P}(x,t) + \frac{\partial f}{\partial x}^\top \mathcal{P}(x,t) + \mathcal{P}(x,t) \frac{\partial f}{\partial x} \leq -\epsilon \mathcal{P}(x,t) \tag{5.7}$$

where $\partial_f \mathcal{P}(x,t)$ is defined in [89] as the derivative of $\mathcal{P}(x,t)$ along the vector field f. $\mathcal{P}(x,t)$ is said to have a derivative along f if the following limit exists,

$$\partial_f \mathcal{P}(x,t) = \lim_{h \to 0} \frac{\mathcal{P}(\tilde{X}(\tilde{x},h)) - \mathcal{P}\tilde{x}}{h}, \tag{5.8}$$

where $\tilde{X}(\tilde{x}, \bullet)$ is the flow of trajectories generated by the vector field f for initial condition $\tilde{x}$.

Theorem 2 leads to the following metric-oriented theorem.

Theorem 3. *Lohmiller & al.* Given the system dynamics (5.2), any trajectory, with initial conditions x_0, belonging to a ball of constant radius with respect to the metric $\mathcal{P}(x,t)$ (in the coordinate transformation $\Theta \delta x$), contained at all times within a contraction region with respect to the metric $\mathcal{P}(x,t)$, remains in that ball and converges exponentially to that trajectory.

This theorem allows to prove the exponential convergence of a system to a trajectory or a point (a constant trajectory over time). If the controlled LPRE system verifies Theorem 3, then any trajectory, regardless of its initial conditions [90] (to the extent of the contraction region), converges exponentially fast to a reference trajectory. In practice, however, contraction conditions are hard to obtain naturally on a physical system, and the LPRE system studied is no exception.

5.2 . Contraction based control

While simple systems such as a damped oscillator present a contractive behavior. The property of contraction on a complex system is seldom proved, and therefore most of them do not display a contractive behavior. In the literature, contraction-based controllers have been designed using direct methods [88], [86], when a contraction metric can be found. The search for a contraction metric with a direct method can prove difficult, similar to the Lyapunov approach. To perform such task contraction theory has been paired with some reinforcement learning techniques [87], adapted for the search of contraction metrics. A more general approach to providing contractive properties to a system has been studied in [89], leading to the definition of a controller using LMI (Linear Matrix Inequality) tools. In [89], the author considers the definition of a controller for a wide range of non-linearities, provided some sector conditions on the non-linearities are respected. This method is designed to cover a wide range of non-linear systems and results in a simple controller that applies to embedded systems. Due to the nature of the non-linearities of the LPRE (square roots, squared terms) and its limitation to the positive values of the variables, the method in [89] constitutes a suitable design. The study of several solutions of an equation moreover allows to prove the convergence of complex controllers based on machine learning techniques [91], which make use of different trajectories based on neural network computation.

5.2.1 . Contracting controller

We recall here the method derived from [89] for the design of a contraction based controller.

Let a state-space system of the form (5.2), whose non-linear terms are separated from the linear terms in the form,

$$\dot{x} = Ax + M\phi(Lx, t) \tag{5.9}$$

where the matrix A is a square, time-invariant matrix, ϕ is an n-dimensional nonlinear vector function and M, L are two matrices of appropriate dimensions. The dimension of the matrices M, L are defined by the structure of the nonlinear terms in the system. Such reformulation (5.9) isolates the nonlinear terms of the original system in the function ϕ. Definition 9 applied to the state-space reformulation yields the following definition of the contraction region, explicited in [92] :

Definition 10. The system is contracting for an explicit metric $\mathcal{P}(x,t)$, if there exists a C^1 matrix function $\mathcal{P}(x,t) : \mathbb{R}^n \to \mathbb{R}^{n\times n}$ with positive symmetric values such that

$$\exists \epsilon > 0 \, \partial_f \mathcal{P}(x,t) + \mathcal{P}(x,t)\left(A + M\frac{\partial \phi}{\partial Lx}(Lx,t)L\right) + \left(A + M\frac{\partial \phi}{\partial Lx}(Lx,t)L\right)^\top \mathcal{P}(x,t) < -\epsilon Id_n,$$

with

$$\underline{p} Id_n \leq \mathcal{P}(x,t) \leq \overline{p} Id_n, \forall (x,t) \in \mathbb{R}^n \times \mathbb{R}, \tag{5.10}$$

where $\underline{p}, \overline{p}$ are positive real numbers and Id_n is the identity matrix of dimension n.

When a constant matrix $\mathcal{P}$ can be found, then (5.10) translates into :

$$\exists \mathcal{P} \in \mathbb{R}^{n\times n}, \mathcal{P} = \mathcal{P}^\top, \exists \epsilon > 0 \; He(\mathcal{P}(A + M\frac{\partial \phi}{\partial Lx}(Lx,t)L)) \leq -\epsilon Id_n, \tag{5.11}$$

where $He(\bullet) = \bullet + \bullet^\top$.

Assumption 1. ([89]) (Monotonic nonlinearities) The mapping $\phi : \mathbb{R}^m \times \mathbb{R} \to \mathbb{R}^m$ is such that :

$$0 \leq \frac{\partial \phi}{\partial Lx}(Lx,t) + \frac{\partial \phi}{\partial Lx}(Lx,t)^\top, \forall (x,t) \in \mathbb{R}^m \times \mathbb{R}, \tag{5.12}$$

Theorem 4. *Andrieu & al.* Consider a system of the form (5.9). Assume that ϕ satisfies Assumption 1. If there exist a constant symmetric positive definite matrix $\mathcal{P} \in \mathbb{R}^{n \times n}$ and a positive real number ϵ such that :

$$\begin{bmatrix} A^\top \mathcal{P} + \mathcal{P} A + \epsilon Id_n & L^\top + \mathcal{P} M \\ L + M^\top \mathcal{P} & 0 \end{bmatrix} \leq 0, \tag{5.13}$$

then the system (5.9) defines a contraction. This LMI is then split into two constraints : $A^\top \mathcal{P} + \mathcal{P} A + \epsilon Id_n < 0$ and $L^\top = -\mathcal{P} M$ (as the trace of equation (5.13) is equal to the trace of $A^\top \mathcal{P} + \mathcal{P} A + \epsilon Id_n$).

The author in [89] then defines the following theorem for a controller u,

Theorem 5. *Andrieu & al.* The control law u that makes the system

$$\dot{x} = Ax + M\phi(Lx,t) + Bu, \tag{5.14}$$

contracting for a constant metric $\mathcal{P}$ is obtained under the form

$$u = Kx + N\phi(Lx,t), \tag{5.15}$$

where $Z \in \mathbb{R}^{q \times n}$,$N \in \mathbb{R}^{q \times p}$ are obtained with the LMI

$$\begin{aligned} He(AW + BZ)^\top + (AW + BZ) \leq 0, \\ W > 0, WL^\top = -(M + BN), \end{aligned} \tag{5.16}$$

and with $K = ZW^{-1}$ and $W^{-1} = \mathcal{P}$.

Such design for a controller makes use of the assumption that $\mathcal{P}$ is a constant matrix. This implies that the matrices involved in (5.16), namely A, B, L, M, N must be constant. In the next subsection (5.2.2), a controller is developed for the simplified model of the LPRE, where the considered matrices are constant.

In the case of the complex model, the control matrix $B(x)$ of the system is not constant. Indeed, the matrix $B(x)$ denotes the friction induced by the equivalent resistance of the valve,

$$B(x) Z_{valve} = -Z_{valve} q_{gg}^2 \tag{5.17}$$

In this case, the design has to be adapted for a time-varying matrix $B(x)$. This approach is developed in the subsections 5.4.1,5.4.2.

5.2.2 . Application to the motopump system

In this subsection, contraction theory is applied to the motopump model of the LPRE. As the model does not present a contractive behavior in its original form, a contractive controller is designed to regulate the system.

The controller is in a first time designed for the regulation of the hydrogen line of the model. The behavior of the oxygen line of the system is supposed well-regulated and allows for a constant mixture ratio in the combustion chamber MR_{cc}. The input variable in the motopump system is the motor power of the pump P_m (see 2.33), while the regulated output is the chamber pressure p_{cc}. The objective of this controller is to provide a contractive behavior for the closed-loop system with the previously defined input and output.

The design of the controller follows three distinctive steps :

- The linear and non-linear terms are separated into two parts to isolate the non-linearities in a matrix function ϕ.
- The mapping $M\phi$ is then reformulated to respect the sector-bound condition in (5.12), while ensuring a feasible LMI solution.
- Finally, the LMI is solved for the new mapping $M\phi$.

The main part of the system design is eventually to find a suitable reformulation of the system under the form $\dot{x} = Ax + M\phi(Lxs, t) + Bu$. The controller is then directly derived from the solutions W, N, Z of the LMI.

Preliminaries

The formulation of the hydrogen line for the motopump system yields :

$$\begin{aligned}
\dot{\Omega} =& \frac{2}{J}\left(P_m - |\frac{a_c}{\rho}q_{cc}^2\Omega^{\frac{1}{2}} + b_c\Omega q_{cc} + c_c\rho\Omega^{\frac{3}{2}}|\right)\\
\dot{q}_{cc} =& \frac{1}{I_{cc}}\Bigg(p_{ep} - p_{cc} + (\frac{a_p}{\rho} - Z_{res})q_{cc}^2 + b_p\Omega^{\frac{1}{2}}q_{cc}\\
&+ c_p\rho\Omega\Bigg)\\
\dot{p}_{cc} =& k_1\big(1 + MR_{cc}\big)q_{cc} - k_2 p_{cc}.
\end{aligned} \tag{5.18}$$

where for the sake of simplicity $k_1 = (k_{4cc} + k_{5cc} + (k_{2cc} - k_{1cc})\Theta_{cc})$ and $k_2 = \sqrt{\Theta_{cc}}k_{3cc}$ in 2.33. The Jacobian of the system is then,

$$\frac{\partial f}{\partial x} = \begin{pmatrix} \frac{\partial f_1}{\partial \Omega} & \frac{\partial f_1}{\partial q_{cc}} & \frac{\partial f_1}{\partial p_{cc}} \\ \frac{\partial f_2}{\partial \Omega} & \frac{\partial f_2}{\partial q_{cc}} & \frac{\partial f_2}{\partial p_{cc}} \\ \frac{\partial f_3}{\partial \Omega} & \frac{\partial f_3}{\partial q_{cc}} & \frac{\partial f_3}{\partial p_{cc}} \end{pmatrix}, \tag{5.19}$$

where

$$
\begin{aligned}
&\frac{\partial f_1}{\partial \Omega} = -\frac{2}{J_H}(a_{cH}\frac{q_{cc}^2}{2\Omega^{\frac{1}{2}}} + b_{cH}q_{cc} + \frac{3}{2}c_{cH}\rho_H\Omega^{\frac{1}{2}}),\\
&\frac{\partial f_1}{\partial q_{cc}} = -\frac{2}{J_H}(2a_{cH}q_{cc}\Omega^{\frac{1}{2}} + b_{cH}\Omega),\\
&\frac{\partial f_1}{\partial p_{cc}} = 0,\\
&\frac{\partial f_2}{\partial \Omega} = \frac{1}{I_H}(b_{pH}\frac{q_{cc}}{2\Omega^{\frac{1}{2}}} + c_{pH}\rho_H),\\
&\frac{\partial f_2}{\partial q_{cc}} = \frac{1}{I_H}(2\frac{a_{pH}}{\rho_H} - k_{eqH})q_{cc} + b_{pH}\Omega^{\frac{1}{2}},\\
&\frac{\partial f_2}{\partial p_{cc}} = -\frac{1}{I_H},\\
&\frac{\partial f_3}{\partial \Omega} = 0,\\
&\frac{\partial f_3}{\partial q_{cc}} = k_1(1 + MR_{cc}),\\
&\frac{\partial f_3}{\partial p_{cc}} = -k_2,
\end{aligned}
$$

which is not uniformly negative definite. Numerical simulations are used to confirm this claim. To answer this, application of the method from [89] is made to compute a new input signal that will make the system contracting, meaning that the Jacobian of the closed-loop system with the controller respects equation (5.11). Reformulation of the system with (5.14) gives :

$$\dot{x} = Ax + M\phi(Lx, t) + Bu, \tag{5.20}$$

in which the non-linear terms of the simplified model are regrouped into the function ϕ, while the linear terms compose the matrix A.

$$
A = \begin{pmatrix} 0 & 0 & 0 \\ 0 & 0 & -\frac{1}{I_H} \\ 0 & k_1 & -k_2 \end{pmatrix}, Lx = \begin{pmatrix} \Omega \\ q_{cc} \end{pmatrix}, B = \begin{pmatrix} 1 \\ 0 \\ 0 \end{pmatrix}, u = P_m
$$

$$
M = \begin{pmatrix} 1 & 0 \\ 0 & 1 \\ 0 & 0 \end{pmatrix}, L = \begin{pmatrix} 1 & 0 & 0 \\ 0 & 1 & 0 \end{pmatrix},
$$

$$
\phi(y,t) = \begin{bmatrix} \frac{2}{J_H}\left(-\frac{a_{cH}}{\rho_H}q_{cc}^2\Omega^{\frac{1}{2}} - b_{cH}\Omega q_{cc} - c_{cH}\rho_H\Omega^{\frac{3}{2}} \right) \\ \frac{1}{I_H}\left((\frac{a_{pH}}{\rho_H} - k_{eqH})q_{cc}^2 + b_{pH}\Omega^{\frac{1}{2}}q_{cc} + c_{pH}\rho_H\Omega \right) \end{bmatrix}. \tag{5.21}
$$

From the new formulation of the system in (5.20)-(5.21), the design of a contracting controller following the method described in [89] can be driven. From here, the controller design consists in computing the matrices W, Z, N in (5.16). In the following, the reformulation of the system is detailed, to respect the controller design.

Remark 7. The function ϕ is assumed to follow a sector-bound condition. A Lipschitz condition on the non-linearities allows to simplify the design of the contracting controller in [89]. However, analysis of the monotony of the non-linearity as in assumption 1 shows that $\frac{\partial \phi}{\partial Lx}(Lx,t) + \frac{\partial \phi}{\partial Lx}^{\top}(Lx,t)$ is not Lipschitz, as it depends on the states Ω and q_{cc}. Indeed, by taking note that :

$$\frac{\partial \phi}{\partial Lx}(Lx,t) = \begin{pmatrix} \frac{\partial f_1}{\partial \Omega} & \frac{\partial f_1}{\partial q_{cc}} \\ \frac{\partial f_2}{\partial \Omega} & \frac{\partial f_2}{\partial q_{cc}} \end{pmatrix}, \tag{5.22}$$

the non-linearity

$$\frac{\partial f_1}{\partial \Omega} = -\frac{2}{J_H}(a_{cH}\frac{q_{cc}^2}{2\Omega^{\frac{1}{2}}} + b_{cH}q_{cc} + \frac{3}{2}c_{cH}\rho_H\Omega^{\frac{1}{2}})$$

is non-Lipschitz, due to the introduction of squared terms such as q_{cc}^2. The assumption from equation (5.12) is then used to map the non-linearities of the partial derivatives (5.22).

Search of a mapping of the non-linearities $M\phi$ The second step for the design of the controller is to find a mapping of the non-linearities $M\phi$ such that $\frac{\partial \phi}{\partial Lx}(Lx,t) + \frac{\partial \phi}{\partial Lx}^{\top}(Lx,t) \geq 0$, and that the LMI (5.16) has a solution.

$$\frac{\partial \phi}{\partial Lx}(Lx,t) + \frac{\partial \phi}{\partial Lx}(Lx,t)^{\top} \geq 0 \tag{5.23}$$

A first remark on the LMI formulation is that the constraints described in (5.16) impose several terms in the searched matrices W, N, Z. With the expressions of the known matrices described earlier, and for $N = \begin{pmatrix} n_1 & n_2 \end{pmatrix}$,

$$\begin{aligned} WL^{\top} &= -(M + BN), \\ W\begin{pmatrix} 0 & 1 \\ 1 & 0 \\ 0 & 0 \end{pmatrix} &= -\begin{pmatrix} n_1 + 1 & n_2 \\ 0 & 1 \\ 0 & 0 \end{pmatrix}. \end{aligned} \tag{5.24}$$

This constraint fixes six of the terms in W, namely the two left columns of $W = \begin{pmatrix} -n_2 & -n_1 - 1 & \bullet \\ 1 & 0 & \bullet \\ 0 & 0 & \bullet \end{pmatrix}$ which leads to the constraint $(AW + BZ)^{\top} + (AW + BZ) \leq 0$ to have no solutions W, Z. To address this issue, the matrix M is taken as

$$M = \begin{pmatrix} 1 & 0 \\ 0 & -1 \\ 0 & 0 \end{pmatrix}. \tag{5.25}$$

Note that the appropriate sign changes need to be made in the sign of the second row of the $\phi(y,t)$ function.

The new mapping ϕ is expressed :

$$\phi(Lx,t) = \begin{bmatrix} \frac{2}{J_H}\left(-\frac{a_{cH}}{\rho_H} q_{cc}^2 \Omega^{\frac{1}{2}} - b_{cH}\Omega q_{cc} - c_{cH}\rho_H \Omega^{\frac{3}{2}} \right) \\ -\frac{1}{I_H}\left((\frac{a_{pH}}{\rho_H} - k_{eqH}) q_{cc}^2 + b_{pH}\Omega^{\frac{1}{2}} q_{cc} + c_{pH}\rho_H \Omega \right) \end{bmatrix}. \tag{5.26}$$

The mapping ϕ in (5.26) presents negative eigenvalues, so to verify condition (5.12), it is necessary to change the matrices A, ϕ. The addition of a linear term in the expression of $\phi(Lx,t)$ is proposed, under the form $\begin{pmatrix} l_1\Omega & 0 \end{pmatrix}^\top$. The term l_1 is computed from the smallest negative value of $\frac{\partial \phi}{\partial Lx}(Lx,t) + \frac{\partial \phi}{\partial Lx}^\top(Lx,t)$. This term is then subtracted from the matrix A to keep the same equation as in (5.20).

This second reformulation of the system yields,

$$\dot{x} = \left(A - \begin{pmatrix} l_1 \\ 0 \\ 0 \end{pmatrix} \right) x + M\left(\phi(Lx,t) + \begin{pmatrix} l_1 \\ 0 \end{pmatrix} Lx \right) + Bu. \tag{5.27}$$

and respects assumption (5.22). From this reformulation, it is possible to find the matrices W, N, Z to design the contracting controller.

LMI formulation With this formalism, the preliminaries to solve the LMI defined in (5.16) are obtained. The LMI is solved using YALMIP [59], which yields the three constant matrices that enable to build the feedback control for the system : W, N, Z. The control law is then defined by

$$u = Kx + N\phi(Lx,t), K = ZW^{-1}. \tag{5.28}$$

In the sense of [89], the closed-loop system is now contracting as the LMI condition

$$\begin{aligned} He(AW + BZ)^\top + (AW + BZ) \leq 0, \\ W > 0, WL^\top = -(M + BN), \end{aligned}$$

is verified.

Addition of a reference to the controller The closed-loop system with the controller designed previously is contracting to the reference trajectory $x = 0$ per definition. Indeed, as $x = 0$ is the origin of the system, it is the stable trajectory that the system converges to. To regulate the system around a reference trajectory $x_r(t)$, a tracking term is added into the equation (5.27).

This leads to the final controlled system equation,

$$\dot{x} = \left(A - \begin{pmatrix} l_1 \\ 0 \\ 0 \end{pmatrix} \right) x + M\left(\phi(Lx,t) + \begin{pmatrix} l_1 \\ 0 \end{pmatrix} Lx \right) + B\Big(K(x - x_r) + N\phi\big(L(x - x_r), t\big) \Big). \tag{5.29}$$

This tracking term may interfere with the contracting behavior of the system, and therefore the contraction region associated to the controller is detailed in the following section.

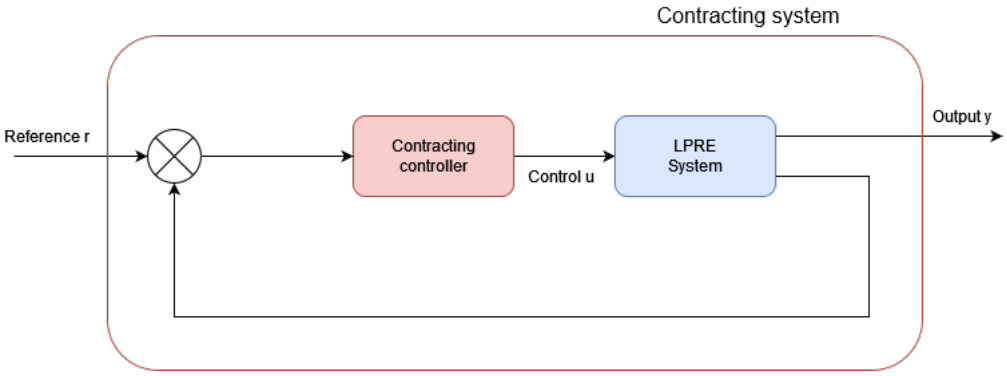

Figure 5.2 – Closed-loop contracting system

5.3 . Analysis and performance of the contracting controller

In this section, the limitations and properties of the contractive controller design are discussed. First, we clarify the notion of contraction region generated by the controller. The stability properties granted by the contraction of the system are then linked to Lyapunov theory. Finally, the controller design requires a reference for the states. The feasibility of this reference on a physical LPRE system is discussed, and alternative solutions to the reference are presented.

The controlled system is represented on figure 5.2, where a reference x_r is injected into the controller. The closed-loop system $\dot{x} = f(x)+u(x-x_r)$ is contracting around the reference x_r provided it is situated in a contraction region. The discussion in this section focuses on the closed-loop system in 5.2.

5.3.1 . Stabilizing property and convergence of the controller

In this subsection, the contracting behavior is illustrated for the controlled simplified system. First consider the exponential convergence of a system. The exponential convergence [33] of a system towards an equilibrium is defined by

$$||x(t) - x_0|| \leq k||x(0) - x_0||e^{-\lambda t}, \forall t > 0 \tag{5.30}$$

with $k \geq 1$, $\lambda > 0$, for all $||x(0)|| < c$. The contracting behavior implies that any couple of trajectories converge [93] exponentially, rather than each trajectory converging to the origin. This leads to the following property of *forgetting initial conditions*, where the system converges to the reference exponentially, independently of the value of the variables at initiation. The distance between a trajectory x and the reference x_r to follow

$$||x(t) - x_r(t)|| \leq k||x(0) - x_r(0)||e^{-\lambda t}, \forall t > 0 \tag{5.31}$$

which is mainly governed by the negative exponential term for $t > 0$. Note that this form of stability is more powerful than exponential stability as it applies to a trajectory rather than the origin of the system [93].

As long as the system is in a contraction region, the initial conditions bear no outcome on the final state of the system. In figure 5.3, the pressure evolution of the controlled closed-loop on figure 5.2 is represented for several initial conditions, and the same reference is injected in the controller. While the

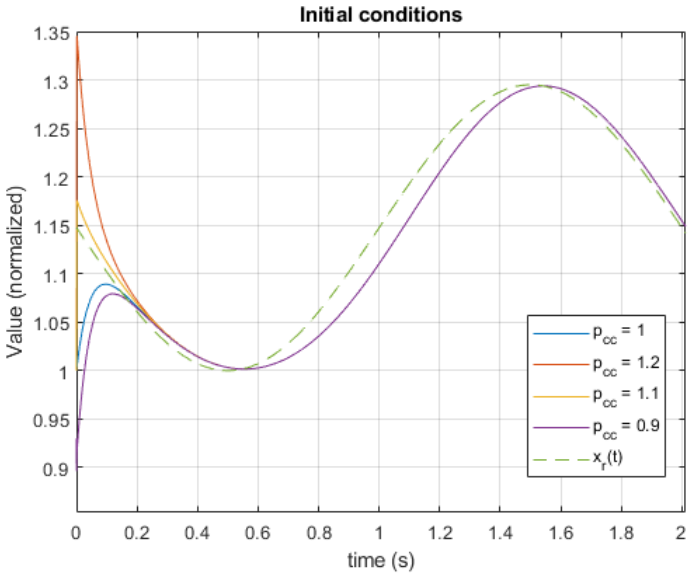

Figure 5.3 – Chamber pressure evolution for different initial conditions

initial conditions imply different evolutions for the first instants of the simulation, the different trajectories converge rapidly to the reference, at a fixed rate. At time $0.2s$, all trajectories merge around the reference for each initial condition.

Additionally the stabilizing properties granted by the controller can be illustrated by the closed-loop motopump system. The polynomial functions for the pressure increase Δp_{ip} and the resistive torque T_r have no solution for low values of mass flows, and therefore the system diverges when crossing a threshold in the mass-flow q_{cc} (this will be further illustrated in chapter 6). On figure 5.4, an unstable scenario is presented for two controllers, a contracting controller following the previous design and a proportional integrate (PI) controller, regulated around the operating point $x_0 = 1$. The figure displays the pressure p_{cc} evolution for both controllers. The unstable scenario is a reference that crosses the threshold $q_{cc,unstable}$ where the system diverges. The PI controller follows the reference as intended and presents the unstable behavior mentioned. On the other hand, the contracting controller does not follow the reference in the unstable region, as the pressure evolution presents an additional inflection point at $t = 2s$, before the reference. This is because the unstable threshold $q_{cc} = q_{cc,unstable}$ is situated outside of the contraction region.

The controller acts then as a barrier function to avoid the system leaving the contraction region. As N is negative, which is expected of a stabilizing controller, when the non-linearities spike to negative values for q_cc, the controller increases at the same time, leading q_{cc} increasing again. As a result, the system avoids the unstable region. Contrary to a classical state feedback, the introduction of the non-linearities in $N\phi(x,t)$ allows for the compensation. This stabilizing behavior from a controller is one of the objectives of this thesis.

5.3.2 . Contraction region

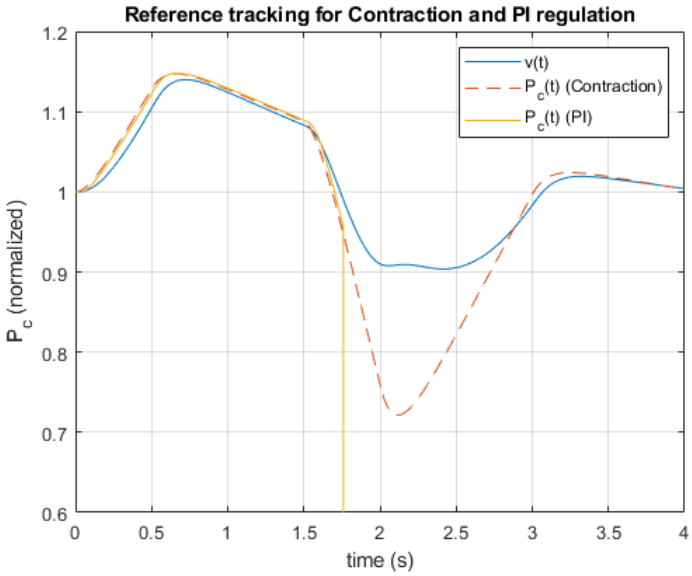

Figure 5.4 – Chamber pressure evolution for an unstable scenario defined by a reference $v(t)$

To illustrate the contraction region, the controlled motopump system is considered. Let the closed-loop system in (5.29),

$$\dot{x} = f_c(x, t) \tag{5.32}$$

where $f_c(x, t)$ represents the controlled closed-loop motopump system for a constant reference $x_r = 1$. The contraction region built with the controller is illustrated with the relation (9) that is recalled here for a constant metric $\mathcal{P}$,

$$\frac{\partial f}{\partial x}^\top \mathcal{P} + \mathcal{P}\frac{\partial f}{\partial x} \leq -\epsilon\mathcal{P}, \tag{5.33}$$

When no reference is defined $x_r = 0$ in the controller equation (5.28), the system defines a contraction around the origin. To define a contraction around the reference $x_r = x_0$, the controller is expressed using $\phi(x - x_0)$. On figure 5.5a, the maximal eigenvalue of the equation,

$$\frac{\partial f}{\partial x}^\top \mathcal{P} + \mathcal{P}\frac{\partial f}{\partial x} \tag{5.34}$$

is represented. To simplify the reading, the positive values have been scaled to 0, and display a plateau. The contraction region of the system is then illustrated by the region where the maximal eigenvalue is negative, and respects (5.33). The range of the states considered is $[70\%, 150\%]$ of the nominal value. In figure 5.5a, the contraction region extends around the nominal value, which is the equilibrium, and is extended for the parameter ω on the right horizontal axis. However, the contraction region stops before $q_{cc} = 0.9q_{cc,0}$ on the left axis, which is on par with the previous simulation in figure 5.4, where the edge of the contraction region was assumed for this value of q_{cc}. For greater values of q_{cc} however, as long as the rotational speed ω is not too far from q_{cc} (for example $\omega = 1\omega_0, q_{cc} = 1.5q_{cc,0}$) the system defines a contraction. The sharpness of the edges of the contraction region corresponds to the increasing value of the controller when the system narrows the unstable region, illustrated in figure 5.4.

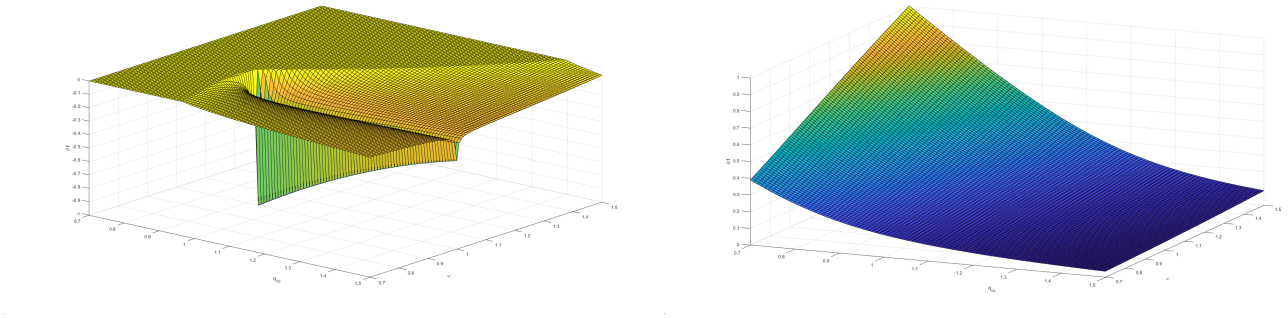

(a) Closed-loop controlled system

(b) Uncontrolled system

Figure 5.5 – Comparison of max eigenvalues for a controlled and uncontrolled system

In comparison, consider the max eigenvalue of the uncontrolled system in figure 5.5b. The eigenvalue is always positive, and then the scaling at 0 is not applied on this figure. Note that the absence of contraction does not imply the absence of stability, as it has been shown that the uncontrolled system is passive in the chapter 3.

As the contraction region covers all the points in the domain $x \in [100\% - 150\%]$ of the nominal value, the controller for the simplified system fulfills its function.

5.3.3 . Reference generation

The contraction-based controller stabilizes a system around a given reference trajectory of the states. This implies providing a trajectory for each considered state in the controller, to generate the reference for the system. However, knowledge of each state in a real application is not achievable, as all states are not physically measurable. Previous simulations allow to obtain a database for the trajectory generation, however, the optimal solution is to make use of a reference governor. In this subsection, we consider a controller, that is placed before the contracting controller and generates the reference x_r, as in figure 5.6. The objective of this paragraph is to illustrate the behavior of the contracting controller when confronted with a high reference. We recall here the equation of the controller with a reference,

$$u = K(x - x_r) + N\phi(L(x - x_r), t). \tag{5.35}$$

Three main solutions are considered for the generation of the reference,

- Simple linear estimation of the state
- Integration and linear estimation of the state
- Prediction of the real reference

A simple linear estimation of the state is a simple tool that provides a good approach for the control. The process is to identify with a linear regression the states from the output p_{cc}. Such identification leads to the definition of $n-1$ parameters (for n states) denoted k_i for $i \in [1, n-1]$ and the remaining states are then evaluated at

$$\hat{x} = k_i p_{cc} \tag{5.36}$$

Typically, the parameter k_i is set to $\frac{x_{i,0}}{p_{cc,0}}$ to respect the initial equilibrium. Results illustrate that a simple reference for the controlled state p_{cc} imposes a static error. Indeed, if x_r is a scalar (rather than a vector

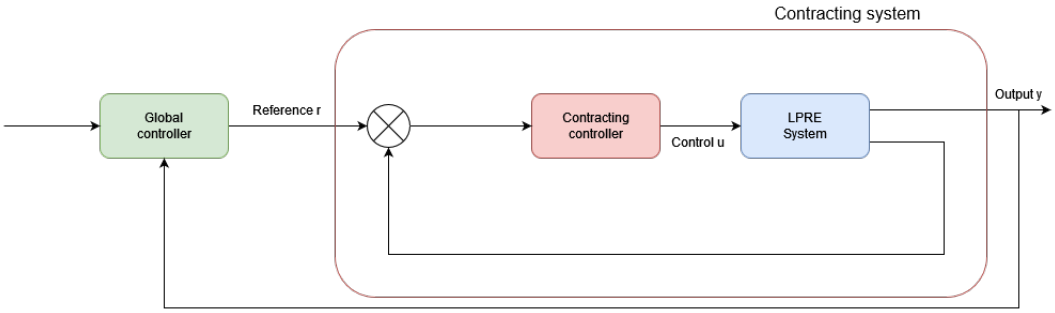

Figure 5.6 – Global controller for the closed-loop contracting system

of dimension equal to the number of states), only one state is appropriately represented, and the other states are assumed to follow a linear relation $x_i = k_i p_{cc}$. This relation leads to a suitable first approach for the system however the linear relation is not representative enough of the behavior of the states, leading to a static error.

To remedy this error, the inclusion of an integrator block before the static error is proposed, leading to a controller of the form

$$u_{ci} = u_c + k_I \int_0^t (p_0 - p_{cc})dt, \tag{5.37}$$

which solves the static error issue. This method has to be applied carefully, however. As the integrator emphasizes the static error to mitigate it, the value of the reference shifts and modifies the contraction region. In figure 5.7, the shifting of the contraction region is illustrated for two constant reference values. In figure 5.7a, the contraction region is represented for a reference $x_r = x_0$, while figure 5.7b represents the contraction region when $x_r = 40x_0$. The shifting is mainly illustrated by the loss of contraction region for low values of the mass flow q_{cc}. For the reference $x_r = 40x_0$, the contraction region only spans to $q_{cc} = q_{cc,0}$, while the original contraction region for $x_r = x_0$ spans to $q_{cc} = 0.9q_{cc,0}$. Due to this shifting, the system can leave the contraction region under the reference's action. A solution to this is to choose the parameter k_I such that the time constant of the integrator is close to that of the system and so that the value of x_r remains low $x_r < 10x_0$.

Finally, the inclusion of a prediction of the states prior to the system is considered. This solution requires being able to compute the real value of the states at all times t, typically by using an estimator before the system as in [13], where a reference governor is used to compute a model predictive controller. This solution applies a high computational cost and is therefore not chosen in the scope of this thesis.

The most suitable solution for a reference generation is therefore the use of an integrator, which will be applied in the chapter 6. Note that while the estimation of the states is not costly for a discrete input, for a continuous reference the computation time can rise significantly. Therefore while the prediction of the reference x_r is a suitable solution for the PBC controller in 3, for the contraction base controller the integrator is preferred. Note that since both controllers are state-feedbacks, the estimation of the states is required to compute the controller.

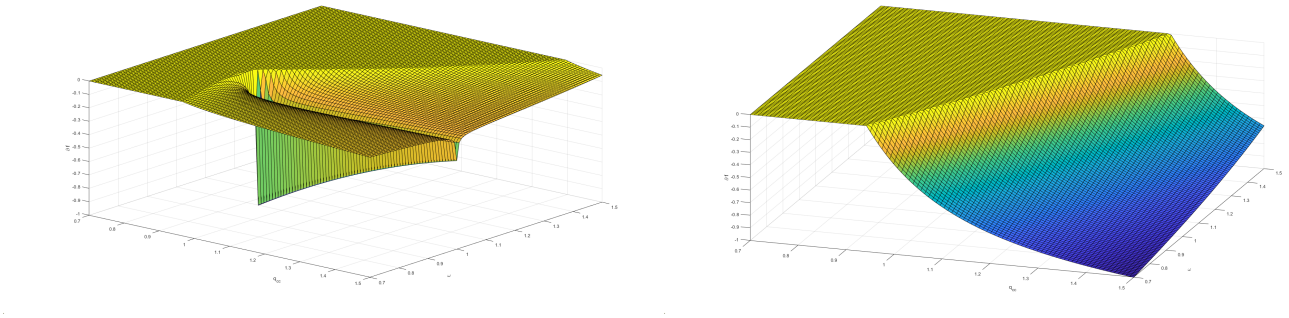

(a) $r = 1$ (b) $r = -40$

Figure 5.7 – Comparison of the maximal eigenvalues for two references

5.3.4 . Contraction metric

Tuning of the controller with the contraction metric

The controller design (5.64) depends on the value of the matrix W. This constitutes a degree of freedom in the system if the LMI (5.57) is solvable for multiple W. If possible, the choice of the metric $W^{-1} = \mathcal{P}$ should be made following a pole placement of the eigenvalues of the resulting closed-loop system. However, due to the tools available for LMI solving, the number of solutions is limited. As an example, the LMI for the simplified system is not solvable for a different W, while the LMI for the complex system is solvable for multiple $W = kW_0$ where k is a positive constant and W_0 is the original solution of the LMI. This is dependent on the formulation of the LMI and the conditioning of the A and B matrices in the LMI (5.57). In figure 5.8, the contraction region is illustrated using the maximal eigenvalue of the equation,

$$\frac{\partial f}{\partial x}^{\top} \mathcal{P} + \mathcal{P} \frac{\partial f}{\partial x}, \tag{5.38}$$

which can be written

$$\frac{\partial f}{\partial x}^{\top} W_0^{-1} + W_0^{-1} \frac{\partial f}{\partial x}. \tag{5.39}$$

The figure 5.8 includes two contraction regions, defined for two different values of W. In 5.8a, the contraction region is extended with the use of a small metric $W = 0.1W_0$, to the point that the state $q_{cc} = 0.80 q_{cc_0}$ is the new limit of the contraction region. Such a metric allows to widen the contraction region, at the cost of a smaller time response and a greater static error (if used with the proportional reference generation method). On 5.8b, the contraction region is shortened with the use of a larger $W = 10W_0$. In this case, only close states to the equilibrium are attainable by the system. This metric allows for faster time-responses, at the cost of the size of the contraction region. Note that in practice, the LMI of the simplified system (5.57) is not solvable for $10W_0$ and this figure is here to illustrate the compression of the contraction region due to the metric.

Lyapunov theory and contraction metric

In this paragraph, we recall the notion of a Lyapunov function for an autonomous system $\dot{x} = f(x)$,

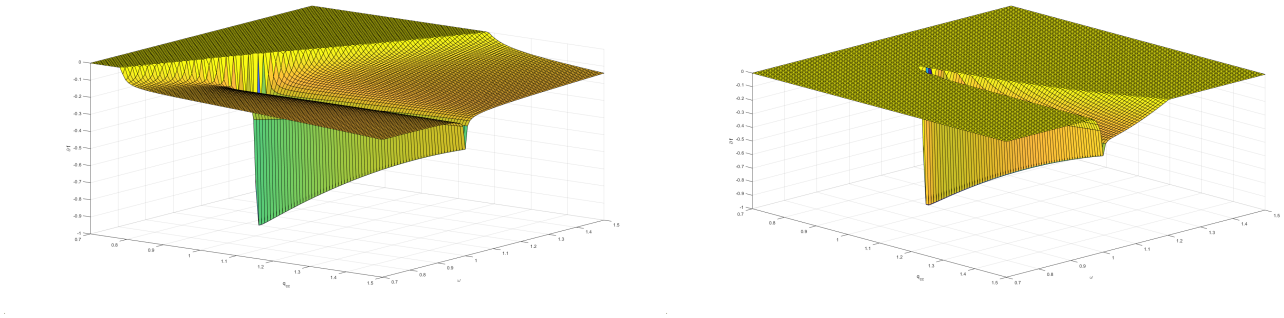

(a) $W = 0.1W_0$ (b) $W = 10W_0$

Figure 5.8 – Comparison of the maximal eigenvalues for two contraction metrics

Theorem 6. *Khalil* If there exists a continuously differentiable positive definite scalar function $V(x)$ such that $\dot{V}(x)$ is negative semidefinite, then the origin of the system is stable. If $\dot{V}(x)$ is negative definite, then the origin is asymptotically stable.

From definition 9, the use of a metric can be linked to Lyapunov theory [83]. Let a globally contracting *autonomous* system , the function

$$V(x,t) = f(x,t)^\top \mathcal{P} f(x,t). \tag{5.40}$$

is a candidate for a Lyapunov function of the system.

$$\dot{V} = f(x,t)^\top (\partial_f \mathcal{P} + \mathcal{P}\frac{\partial f}{\partial x} + \frac{\partial f}{\partial x}^\top \mathcal{P}) f(x,t) \tag{5.41}$$

which per the definition of the contracting region, respects the following

$$\dot{V} \leq -\epsilon V \tag{5.42}$$

therefore V is a Lyapunov function for the closed-loop system. This function is in practice easier to obtain than a direct approach for a Lyapunov function. Moreover, while a regular Lyapunov function verifies

$$\dot{V} \leq 0 \tag{5.43}$$

which proves asymptotic stability, (5.42) proves the exponential convergence of the system.

Note that the Lyapunov function in (5.40) is only valid for the controlled system. For the natural system, no Lyapunov function has been obtained via the contraction theory approach, and one should rely on the Lyapunov function derived from the Port-Hamiltonian approach 3.3.2.

5.4 . Controller design for complex nonlinear systems

In this section, the complex model of the LPRE is considered. While the design of the contractive controller for the simplified model is directly derived from [89], the complex modeling requires additional considerations. The complex model input being the value of the GG valve associated with the line, the

control action is modulated by a time-varying term. In this case, the direct approach is not valid. This section presents the additional considerations brought to the method to compute a controller for the complex system.

The determination of the controller of the form (5.15) based on the LMIs (5.16) relies on the fact that the matrix B in (5.14) is constant. However, for mass flow control systems such as the LPRE, matrix $B(x)$ expresses as :

$$B(x) = \begin{bmatrix} 0 & -q_{gg}^2 & 0 & \dots & 0 \end{bmatrix}^\top, \tag{5.44}$$

and is state-dependent. Therefore the assumption that all the matrices A, B, M, L is not valid since the matrix B is not valid. A direct application of the method described earlier results in a varying $\mathcal{P}(x)$, which does not fulfill the first assumption in [89] summarized in (5.11).

In this section, additional considerations to make the design possible are proposed. In a first time, the notion of virtual contraction [94] of a system is described, which is a useful tool to study the contraction of systems with non-linear control matrices (or highly non-linear dynamics).

5.4.1 . Virtual contractivity

Virtual systems and contracting properties

This problem constitutes a system affine in the control, i.e. the control matrix is dependent on the states. In the literature, an extension of the design of the controller with contraction theory for systems affine in the control has been proposed in [94], using the notion of a virtual system.

Let a system Σ,

$$\Sigma : \dot{x} = f(x) + g(x)u, \tag{5.45}$$

and introduce the associated virtual system Σ_v defined for virtual state x_v, virtual control u_v, where $g(x)$ depends on x and is considered constant with respect to x_v,

$$\Sigma_v : \dot{x}_v = f(x_v) + g(x)u_v. \tag{5.46}$$

The idea behind the use of the virtual system is to separate the variables x and x_v. As $g(x)$ is independent of the variations of x_v, it is possible to study the virtual system for variations of x. In particular, such a method is used in [94] to prove the contraction of a real system from the use of a virtual system.

Theorem 7. *Reyes-Baez & al.* Suppose that $u_v(x, x_v, t)$ is a contracting control for Σ_v. Then, if the system is contracting for every x with respect to x_v, the control action $u_v(x_v, x_v, t)$ is contracting for the system ([94], Theorem 2) :

$$\Sigma_v' : \dot{x}_v = f(x_v) + g(x_v)u_v. \tag{5.47}$$

The result can be extended to the real system Σ by noticing that $\Sigma_v' = \Sigma$ for $x_v = x$. Then a contracting control for the system Σ is $u_v(x, x, t)$.

LMI formulation for virtual systems

The control solution obtained via LMIs from (5.16) depends on $W^{-1} = \mathcal{P}$, which is constant. However, using a virtual system description, the LMIs have to be defined for each potential value of the state x and

it may not be possible to find a solution for each x with a constant $\mathcal{P}$.

To solve this problem, a new formulation of the LMI is proposed (5.16), introducing an additional condition on W (or $\mathcal{P}$).
We recall here the formulation of a real system, expressed under the *Andrieu & al.* form (5.14), with state-dependent matrix $B(x)$,

$$\Sigma : \dot{x} = Ax + M\phi(Lx, t) + B(x)u. \tag{5.48}$$

Suppose the virtual system Σ_v in (5.46) expressed in as (5.14) such that

$$\Sigma_v : \dot{x}_v = Ax_v + M\phi(Lx_v, t) + B(x)u_v. \tag{5.49}$$

Suppose that there exist a vector x_0 and three matrices W_0, Z_0, N_0 such that

$$\begin{aligned} (AW_0 + B(x_0)Z_0)^\top + (AW_0 + B(x_0)Z_0) \leq 0, \\ W_0 > 0, W_0 L^\top = -(M + B(x_0)N_0). \end{aligned} \tag{5.50}$$

According to Theorem 4 *Andrieu & al.*, the control $u_0(x_v) = Z_0\ W_0^{-1}x_v + N_0\phi(Lx_v, t)$ is contracting for the system

$$\Sigma_v : \dot{x}_v = Ax_v + M\phi(Lx_v, t) + B(x_0)u_v.$$

with contraction metric $\mathcal{P}_0 = W_0^{-1}$, as the LMI (5.50) is verified.
Consider now $x \neq x_0$. To obtain a contracting control $u_v(x, x_v)$ with the metric $\mathcal{P}_0$, it is then necessary to find two matrices $N(x)$ and $Z(x)$ such that

$$\begin{aligned} (AW_0 + B(x)Z(x))^\top + (AW_0 + B(x)Z(x)) \leq 0, \\ W_0 L^\top = -(M + B(x)N(x)). \end{aligned} \tag{5.51}$$

Assume that a generalized left inverse of $B(x)$, $\hat{B}(x)$ such that $\hat{B}(x)B(x) = Id$, exists for each x in the state domain of definition. It is then simple to verify that $N(x) = \hat{B}(x)B(x_0)N_0$ and $Z(x) = \hat{B}(x)B(x_0)Z_0$ form a solution of (5.51). Therefore for all x, with respect to the domain of definition of x_v, a control $u_v(x, x_v) = Z(x)W_0^{-1}x_v + N(x)\phi(Lx_v, t)$, is a contracting control with the same metric $\mathcal{P}_0$. Using [94], Theorem 2, the control $u_v(x_v, x_v)$ is then contracting for the system

$$\Sigma'_v : \dot{x}_v = Ax_v + M\phi(Lx_v, t) + B(x_v)u_v. \tag{5.52}$$

With this proposition, it is therefore possible to design a contracting controller for the real system, by solving the LMI for the virtual system (5.49). The LMI yields a new form for the controller, $u_v(x, x_v) = Z(x)W_0^{-1}x_v + N(x)\phi(Lx_v, t)$. This controller is contractive for the virtual system, and its properties are extended to the real system for all x with respect to x_v. With this proposition, the LMI design can be extended to state-dependent control matrices $B(x)$.

Note that this only involves solving the LMI once, at the point x_0. The solution for $x \neq x_0$ is then derived provided a suitable left inverse of $B(x)$ can be found for all x. The matrix W remains at the value W_0 during the process, therefore granting the validity of the hypothesis, $\mathcal{P} = W^{-1}$ is constant.

5.4.2 . Application to the control design for a non-linear control matrix

To illustrate the design method, the controller is explicited for a portion of the system. Consider one of the hydraulic subsystems and let

$$\begin{bmatrix} I_{gg}\dot{q}_{gg} \\ k_{gg}\dot{p}_{gg} \end{bmatrix} = \begin{bmatrix} -R_{qgg} & -1 \\ 1 & -R_{pgg} \end{bmatrix} \begin{bmatrix} q_{gg} \\ p_{gg} \end{bmatrix} + \begin{bmatrix} p_{ep} - uq_{gg}^2 \\ 0 \end{bmatrix} \tag{5.53}$$

where $R_{qgg} = (Z_{resgg} - Z_{vgg})q_{gg} - \frac{a_p}{\rho}(q_{cc} + q_{gg}) - c_p\rho\frac{\omega^2}{q_{gg}} > 0$ and $R_{pgg} = 0$ both represent the friction matrices in PHS framework. $(Z_{resgg} - Z_{vgg})$ corresponds to the friction term in the line, without the valve resistance (as it is represented in the control matrix). The friction induced by the valve is $u\ q_{gg}^2$, where the control corresponds to the resistive coefficient $u = Z_{vgg}$, for the control design. The inertia $I_{gg} = L_{gg}\sqrt{\frac{Z_{VGH}}{2\rho}}$ constitutes a second time dependent term in this setup.

The solution is composed of three steps :

- The expression of a virtual system, in order to separate the control matrix dependency in the state x, and the dependency of the inertia I in the controller u.
- The design of a contracting controller for the virtual system. This step consists in finding a mapping $M\phi$ in the reformulation

  $$\dot{x_v} = Ax_v + M\phi(Lx_v, t) + B(x_0)u,$$

  such that

  $$\frac{\partial\phi}{\partial Lx}(Lx, t) + \frac{\partial\phi}{\partial Lx}(Lx, t)^\top \geq 0$$

  and the LMI, (5.50) is solvable for the mapping $M\phi$. The resolution of the LMI fixes the matrices W_0, Z_0, N_0.
- The validation of the control for the real system, if a solution $(Z(x), N(x)$ is found for the equation (5.51) for all x with respect to x_v, then a controller can be defined for the complete system.

Expression of the virtual system

Let the associated virtual system to (5.53) be

$$\begin{bmatrix} I_{gg}\dot{q}_v \\ k_{gg}\dot{p}_v \end{bmatrix} = \begin{bmatrix} -R_{qv} & -1 \\ 1 & -R_{pv} \end{bmatrix} \begin{bmatrix} q_v \\ p_v \end{bmatrix} + \begin{bmatrix} p_{epv} - u_v q_{gg}^2 \\ 0 \end{bmatrix}, \tag{5.54}$$

where q_v and p_v are the virtual states associated to q_{gg} and p_{gg}, u_v is the virtual control. Here the real inertia I_{gg} and the state q_{gg} are considered constant as they do not depend on the evolution of the virtual state x_v.

Design of a contracting controller for the virtual system

An LMI design for a contracting controller can be found for this system. Let the corresponding reformulation of the system be

$$\begin{aligned}
&\begin{bmatrix} I_{gg0}\dot{q}_v \\ k_{gg}\dot{p}_v \end{bmatrix} = A \begin{bmatrix} q_v \\ p_v \end{bmatrix} + M\phi(q_v, t), \text{ with} \\
&A = \begin{bmatrix} 0 & -1 \\ 1 & -R_p \end{bmatrix}, M = \begin{bmatrix} -1 & 0 \\ 0 & -1 \end{bmatrix}, B = \begin{bmatrix} -q_{gg0}^2 \\ 0 \end{bmatrix}, \\
&\text{and } \phi(q_v, t) = \begin{bmatrix} R_{qv}q_v - p_{epv} \\ 0 \end{bmatrix},
\end{aligned} \tag{5.55}$$

where q_{gg0} and I_{gg0} being the values corresponding to x_0. As mentioned in [46], a change of variables using the appropriate matrix $M = -Id_2$, allows to change $\phi \to -\phi$. Upon verification of the uniform positivity of $\frac{\partial \phi}{\partial q}$ (see (5.12)), the control is then defined by

$$u_{v0}(x_v) = K_0 \begin{bmatrix} q_v & p_v \end{bmatrix}^\top + N_0\phi(q_v, t), \tag{5.56}$$

with

$$\begin{aligned}
(AW_0 + BZ_0)^\top + (AW_0 + BZ_0) \leq 0, \\
W_0 > 0,\ W_0L^\top = -(M + BN_0),\ K_0 = Z_0W_0^{-1},
\end{aligned} \tag{5.57}$$

which is a contracting control for the virtual system (5.54) where $q_{gg} = q_{gg0}$ and $I_{gg} = I_{gg0}$.

Validation of the control for the real system

The definitions of A, M, B, ϕ remain unchanged. A contracting control was designed for the previous virtual system for $q_{gg} = q_{gg0}$ and $I_{gg} = I_{gg0}$. Let first maintain $I_{gg} = I_{gg0}$. As $q_{gg}(x) \neq 0$ on the considered variation domain by hypothesis, a general inverse of B can be defined. Using (5.51), a contracting control is deduced using N_0 and Z_0 for the considered domain. In this case, $N(q_{gg}) = N_0\frac{q_{gg0}^2}{q_{gg}^2}$ and $Z(q_{gg}) = Z_0\frac{q_{gg0}^2}{q_{gg}^2}$.

However, the variations of I_{gg} must be accounted for. We transcribe the new dynamics in (5.58) with a new virtual state x_{v1},

$$\begin{aligned}
\begin{bmatrix} I_{gg} & 0 \\ 0 & 1 \end{bmatrix} \begin{bmatrix} \dot{q}_{v1} \\ k_{gg}\dot{p}_{v1} \end{bmatrix} = \begin{bmatrix} -R_{qv1} & -1 \\ 1 & -R_{pv1} \end{bmatrix} \begin{bmatrix} q_{v1} \\ p_{v1} \end{bmatrix} \\
+ \begin{bmatrix} p_{epv1} - u_{v1}q_{v1}^2 \\ 0 \end{bmatrix}.
\end{aligned} \tag{5.58}$$

As I_{gg} is a strictly positive value that is bounded and varies in an interval $[\underline{I}_{gg}, \overline{I}_{gg}]$, it is possible to transform system (5.58) into

$$\dot{x}_{v1} = c(x)Ax_{v1} + Mc(x)\phi(y_{v1}, t) + c(x)B(q_{v1})u_{v1} \tag{5.59}$$

where $c(x)$ is the following matrix, whose values are computed at state x,

$$c(x) = \begin{bmatrix} \frac{1}{I_{gg}(x)} & 0 \\ 0 & 1 \end{bmatrix}. \tag{5.60}$$

For this system, under the assumption of the uniform positivity of $c(x)\frac{\partial \phi(q_{v1})}{\partial q_{v1}}$ (see (5.12)), $N_1(x, q_{v1})$, $Z_1(x, q_{v1})$, defining the contracting control are solutions of the LMI :

$$\begin{aligned} c(x)He(AW_0 + B(q_{v1})Z_1(x, q_{v1})) \leq 0, \\ W_0 > 0, W_0 L^\top = -(M + c(x)B(q_{v1})N_1(x, q_{v1})), \end{aligned} \tag{5.61}$$

for all x, where $He(\bullet) = \bullet + \bullet^\top$. With the formulation of $c(x)$, let $Z_1(x, q_{v1}) = Z(q_{v1})$, then $c(x)He(AW_0 + B(q_{v1})Z(q_{v1})) \leq 0$ is verified. Define then $N_1(x, q_{v1}) = N(q_{v1})c^{-1}(x)$ which yields

$$\begin{aligned} &c(x)B(q_{v1})N_1(x, q_{v1}) = c(x)B(q_{v1})N(q_{v1})c^{-1}(x), \\ &\text{as } B(q_{v1})N(q_{v1}) \text{ is a square matrix,} \\ &c(x)B(q_{v1})N_1(x, q_{v1}) = B(q_{v1})N(q_{v1}). \end{aligned} \tag{5.62}$$

This choice of $N_1(x, q_{v1}), Z_1(x, q_{v1})$, solutions of (5.61) is valid for all I_{gg} in $[\underline{I}_{gg}, \overline{I}_{gg}]$, and the control associated to $N_1(x, q_{v1}), Z_1(x, q_{v1})$ is contracting for the real system (5.53) with

$$\begin{aligned} u_{v1} &= K(x_{v1})x_{v1} + N_1(x, q_{v1})c(x)\phi(y_v 1, t), \\ \text{or } u_{v1} &= Z(q_{v1})W_0^{-1} + N(q_{v1})\phi(y_v 1, t). \end{aligned} \tag{5.63}$$

The control

$$u(x) = Z_0 \frac{q_{gg0}^2}{q_{gg}^2} W_0^{-1} x + N_0 \frac{q_{gg0}^2}{q_{gg}^2} \phi(y, t) \tag{5.64}$$

is then a contracting control for the real system (5.53), with $q_{gg} > 0$ and $I_{gg} \in [\underline{I}_{gg}, \overline{I}_{gg}]$ with a constant contraction metric $\mathcal{P} = W_0^{-1}$.

Note that the control law developed solely requires solving the LMI in (5.57) for the virtual system. The real system controller is deduced using the derived matrices N_1, Z_1 which verify the LMI (5.57) by construction. The low computational requirements for the practical use of such a control law make it a relevant candidate for an embedded controller.

5.4.3 . Application of the design to a complete complex system

Hydrogen and oxygen lines of the model

Previous section 5.4.2 aims to design a contractive controller for the hydraulic subsystem. The controller is defined for all the problematic non-linearities (time-dependent $B(x)$ and inertia of the line) in (5.53). In the following, the model is defined from the Port-Hamiltonian formulation of the complex model in 3.32. With the better conditioning of the matrix J, the LMI is solvable for the matrix A. Note that with the state-space, the LMI is not solvable due to the poor conditioning of the matrix.

To compute the controller for the full hydrogen half of the system, let the introduction of the new mapping,

$$A = \begin{bmatrix} 0 & 0 & 0 & 0 & 0 & 0 & 0 \\ 0 & 0 & 0 & 0 & -1 & 0 & 0 \\ 0 & 0 & 0 & 0 & 0 & -1 & 0 \\ 0 & 0 & 0 & 0 & 0 & \kappa_{tu,H} & -\kappa_{tu,H} \\ 0 & 1 & 0 & 0 & -R_{pcc} & 0 & 0 \\ 0 & 0 & 1 & -\kappa_{tu,H} & -R_{pgg} & 0 & 0 \\ 0 & 0 & 0 & \kappa_{tu,H} & 0 & 0 & 0 \end{bmatrix}, \; B = \begin{bmatrix} 0 \\ 0 \\ -q_{gg,H}^2 \\ 0 \\ 0 \\ 0 \\ 0 \end{bmatrix} \tag{5.65}$$

$$M = \begin{bmatrix} 1 & 0_{1,8} \\ 0_{8,1} & -I_{d8} \end{bmatrix}, \phi(Lx,t) = \begin{bmatrix} -R_{\omega,H}\omega_H - \lambda_H q_{cc,H} + q_{gg,H} + \alpha_{t,H} p_{tu,H} \\ R_{qgg,H} q_{gg,H} - \lambda_H \omega_H \\ R_{qcc,H} q_{cc,H} - \lambda_H \omega_H \\ R_{qtu,H} q_{tu,H} \\ 0 \\ 0 \\ R_{ptu,H} p_{tu,H} \end{bmatrix} \tag{5.66}$$

And the method described in 5.4.2 is applicable to the complex model. The controller is then denoted

$$u_H = K_H(x)x + N_H(x)\phi(Lx,t). \tag{5.67}$$

Due to the symmetry of the system, the same method is applicable for the design of a controller on the oxygen line. The evolution of the oxygen line follows the same equations, where the numerical values of the terms are changed to represent the differences between the two species. The main change for the system resides in one less resistive term in the main combustion chamber oxygen mass flow $q_{cc,O}$, where there is no resistive term corresponding to the regenerative circuit. Therefore a change is made in the equation of the oxygen controller with the resistive term $R_{qcc,O} = (Z_{valve} + Z_{line} + Z_{inj})q_{cc,O}$.

$$A = \begin{bmatrix} 0 & 0 & 0 & 0 & 0 & 0 & 0 \\ 0 & 0 & 0 & 0 & -1 & 0 & 0 \\ 0 & 0 & 0 & 0 & 0 & -1 & 0 \\ 0 & 0 & 0 & 0 & 0 & \kappa_{tu,O} & -\kappa_{tu,O} \\ 0 & 1 & 0 & 0 & -R_{pcc} & 0 & 0 \\ 0 & 0 & 1 & -\kappa_{tu,O} & -R_{pgg} & 0 & 0 \\ 0 & 0 & 0 & \kappa_{tu,O} & 0 & 0 & 0 \end{bmatrix}, \; B = \begin{bmatrix} 0 \\ 0 \\ -q_{gg,O}^2 \\ 0 \\ 0 \\ 0 \\ 0 \end{bmatrix} \tag{5.68}$$

$$M = \begin{bmatrix} 1 & 0_{1,8} \\ 0_{8,1} & -I_{d8} \end{bmatrix}, \phi(Lx,t) = \begin{bmatrix} -R_{\omega,O}\omega_O - \lambda_H q_{cc,O} + q_{gg,O} + \alpha_{t,O} p_{tu,O} \\ R_{qgg,O} q_{gg,O} - \lambda_O \omega_O \\ R_{qcc,O} q_{cc,O} - \lambda_O \omega_O \\ R_{qtu,O} q_{tu,O} \\ 0 \\ 0 \\ R_{ptu,O} p_{tu,O} \end{bmatrix} \tag{5.69}$$

The controller then reads,

$$u_O = K_O(x)x + N_O(x)\phi(Lx,t). \tag{5.70}$$

Contractivity of the total LPRE system

To assert the contractivity of the interconnection of both systems (hydrogen and oxygen lines), it is necessary to refer to the properties of the interconnection of contracting systems in [83]. Let a feedback combination of the two closed-loop systems, where x_H (resp. x_O) is the vector of the states in the hydrogen line (resp. in the oxygen line).

$$\begin{aligned} \dot{x}_H &= f_H(x_H, x_O, t) \\ \dot{x}_O &= f_O(x_H, x_O, t) \end{aligned} \quad , \tag{5.71}$$

then the feedback combination

$$\begin{bmatrix} \dot{x_H} \\ \dot{x_O} \end{bmatrix} = \begin{bmatrix} F_H & F_f \\ -F_f^\top & F_O \end{bmatrix} \begin{bmatrix} x_H \\ x_O \end{bmatrix} \tag{5.72}$$

is contracting if both systems in 5.71 are contracting using the same metric. The Port-Hamiltonian formulation of the complex system respects the feedback structure in 5.72. Computations show that thanks to the symmetry of the systems, W_0 depicted for the hydrogen line and used in the controller (5.64) is a suitable solution for the contraction metric of the oxygen line. The interconnection is then contractive with contraction metric $\mathcal{P} = W_0^{-1}$.

5.5 . Summary

This chapter introduces a new stability analysis for an LPRE system, contraction theory. The contraction-based analysis of the stability of a system relies on the analysis of the convergence of the possible solutions to the state equations. It is shown that if the system is contractive, the different trajectories generated by the solutions of the state equations converge to a single trajectory named the reference trajectory.

Although the LPRE system is not naturally contracting, a controller that provides such properties is designed for the simplified LPRE model, using the method described in [89]. This method resumes the design of a contracting to solving an LMI equation, providing a powerful design tool for non-linear control. This method is directly applicable to the simplified system, though requires additional considerations to apply to the complex system. The main issue presented occurs when dealing with time-variant control matrices. The complex system being controlled using the friction generated by the valve openings, it presents such an issue. In this chapter, a proposition to generalize the system to non-constant control matrices is proposed, allowing for the design of a controller on the complex model.

In addition to this proposition, this chapter makes use of the reformulation under Port-Hamiltonian form of the system for an easier design, as well as a better conditioning on the LMI matrices.

As presented in 5.3, the contracting behavior of the controller can stabilize the system around the desired equilibrium. The highlighting of the contraction region, the region of the state where the system possesses the contracting properties, allows to show the stabilizing behavior. The different options to use the controller, with tuning of the contraction metric value and choice of reference are also shown to influence on the contracting behavior. Namely, that the choice is to be made between time response and stability of the controller. Finally, the equilibrium defined by the closed loop is considered exponentially stable, which is the stability desired for such a system.

6 - Comparison of performances

The models and methods for control design that have been introduced in the previous chapters need to be evaluated and the resulting performances have to be compared. The evaluations are performed using numerical simulations developed on *Matlab Simulink*.

The objectives of these evaluations are first to determine whether the classical state space model and the Port-Hamiltonian representation of Section 3.2.3 provide similar behaviors, second provide a wider scope of evaluations for the performances of the methods for stability analysis and control designs.

6.1 . Modeling the dynamic behavior

The first mandatory analysis consists at comparing the evolution of the main variables of the LPRE obtained either using the state-space modeling in 2.3.2 and the Port-Hamiltoninan representation in 3.2.3. We first provide a short description of the two model implementations in *Matlab Simulink*.

6.1.1 . Descriptions of the simulations

In this paragraph, the simulations used on *Matlab Simulink* are illustrated and described.

State-space simulation The state-space simulation of the LPRE is composed of one single *Simulink* block, illustrated In figure 6.1. In this figure, the red components represent the states of the LPRE injected in the block on the left side and the derivatives computed by the block on the right. The block contains the evolution equations for the complex system described in (2.35). The green components represent both actuator's values $U_1 = Z_{ggvalve,H}$, $U_2 = Z_{ggvalve,O}$, that are injected in the system. An integrator initialized for the known equilibrium x_0 closes the loop.

This simulation is ran with a time step of $10^{-6}s$, and is unstable for a higher time-step.

Port-Hamiltonian simulation The Port-Hamiltonian simulation of the LPRE is composed of two distinct blocks. In figure 6.2, the left block computes the necessary terms to write the Hamiltonian formulation of equation (3.32). Namely, the resistive terms composing the matrix $R(x)$ are represented in blue, and the light blue terms correspond to the scaling terms $k_{p,\bullet}, \lambda, \alpha_q, \alpha_t, \beta_t, \kappa$ in equation (3.32). The terms computed from the states' values (in red in figure 6.2) are then injected in the system block on the right side of the figure. This block builds the matrices $R(x)$ and $J(x)$ from the terms injected, and proceeds with the equation

$$\dot{x} = (J(x) - R(x))\frac{\partial H}{\partial x} \tag{6.1}$$

An integrator initialized for the known equilibrium x_0 closes the loop.

This simulation is run with a time step of $10^{-5}s$, which is a larger time step than the state-space simulation, due to the better conditioning of the matrices $R(x)$, $J(x)$.

Remark 8. The Port-Hamiltonian modeling has been constructed to respect the equations of the state-space model. This means that in an analytic expression, the equality between the two models is verified.

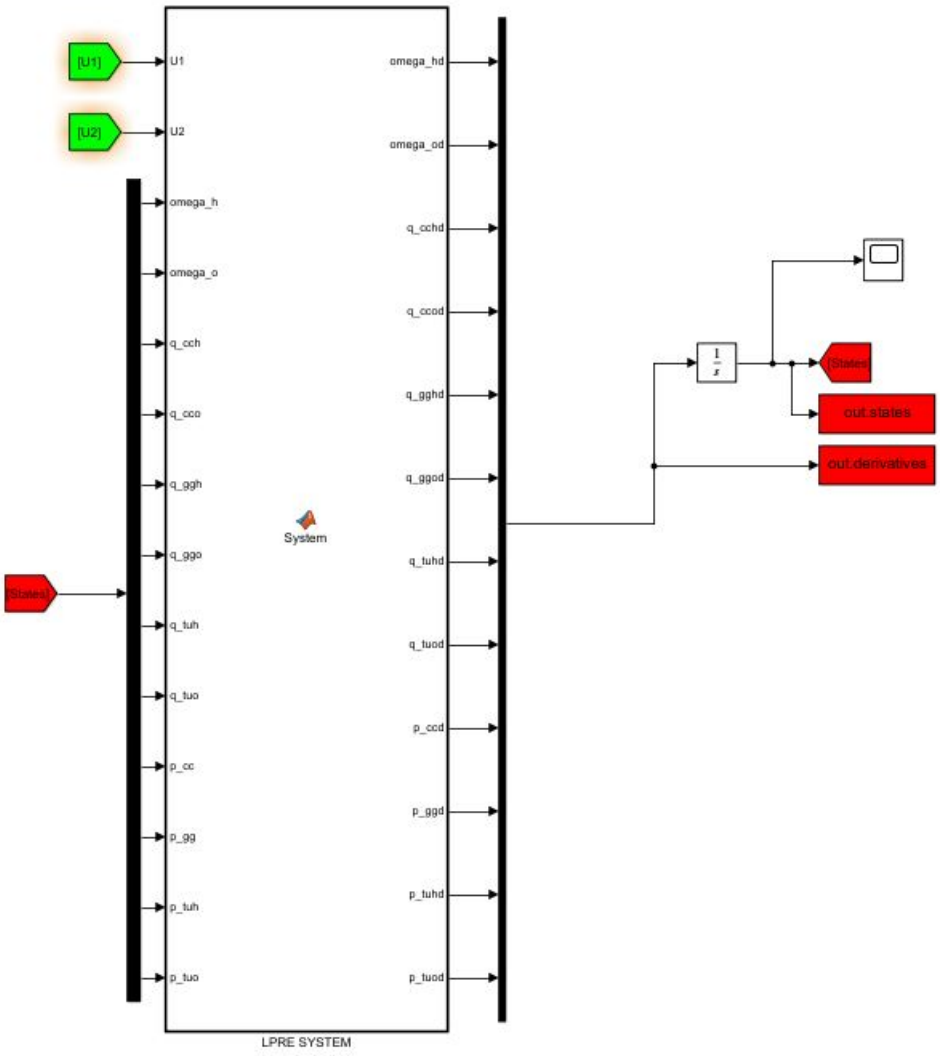

Figure 6.1 – Simulink block for the state-space simulation of an LPRE

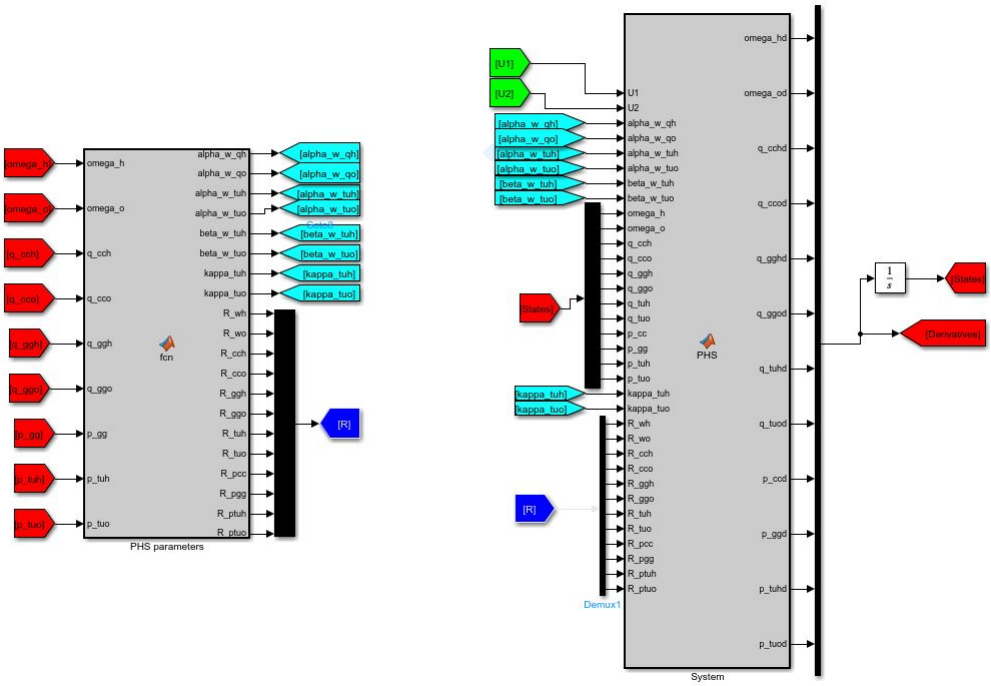

Figure 6.2 – Simulink blocks for the Port-Hamiltonian simulation of an LPRE

For example, both models show derivatives equal to 0 for the equilibrium. In the next subsection, the *simulated* behavior using *Matlab Simulink* is displayed, and differences occur due to the simulator.

Scenarios In this chapter, several scenarios are proposed to illustrate the results.

Short scenarios like step-responses and *unstable* scenarios for the controllers to follow only require short simulations ($4s$) to illustrate the change of operating point or the rapid variations demanded by the simulation. The step response illustrates the behavior of the system during simple transitions from one operating point to another. The objective for this simple transition is to assert performances of the considered controller, for several tuning values.

For realistic scenarios, the time frame of the simulations is extended to $30s$, to illustrate slower variations of the system and cover all the variations during the scenario.

Perturbations in the combustion chamber are illustrated with the addition of noise on the chamber temperature, which will be the noise introduced in further simulations. The choice of temperature as the noised parameter is made to illustrate combustion instabilities and variations in the chamber pressure p_{cc}. Note that such a perturbation is not enough to represent the coupled phenomena that take place in a combustion chamber. In *SIMULINK*, a noise function can be assigned a seed, meaning that every generated noise is not randomized, and the same noise can be added to different simulations using the same seed. The noised used for the temperature Θ_{cc} features the seed 10 and a noise power of 100. With the white noise function, this implies that the temperature varies between $90\% - 110\%$ of the nominal value. Such temperature variations prove to be a suitable modeling of the combustion instabilities discussed

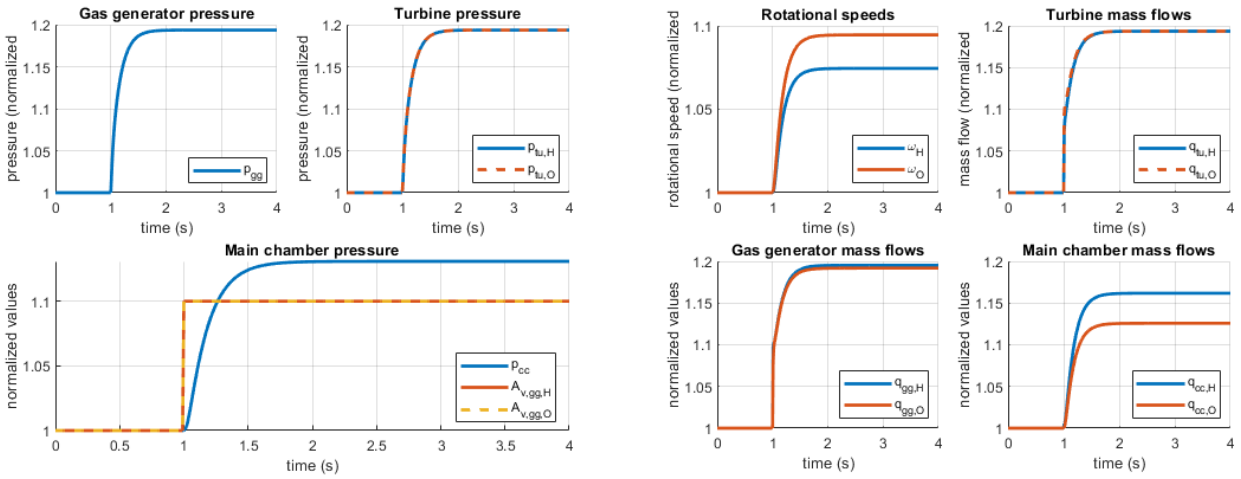

(a) Pressure response

(b) Mass flow response

Figure 6.3 – Open-loop response to a step function

in [42] where the variations in the chamber pressure do not exceed 0.6% of the pressure nominal value for high-frequency pressure variations.

6.1.2 . Comparison of results with actuators inputs

To illustrate the behavior of the LPRE system, figure 6.3a and 6.3b feature the evolution of the states in response to a step in the actuators' value. At time $t = 1s$, the valves' surfaces spike from A_{v0} to $1.1A_{v0}$. The step is illustrated with the evolution of $A_{v,gg,H}, A_{v,gg,O}$ in figure 6.3a. In this comparison, the actuators' dynamics are not modeled, and therefore the step on the actuators is represented by a step on the equivalent resistive inertia Z_{resgg}. The first consequence of this step is observed on the gas-generator mass flows $q_{gg,H}, q_{gg,O}$, which displays a non-smooth behavior due to the step. The mass flows in the gas generator spike at $t = 1s$, following the step in the valve surfaces changing the equivalent resistive coefficient, which is done instantly. The rest of the states follow the evolution smoothly. Note that this behavior is impossible with a real actuator and does not represent a physically realistic valve.

Analysis of dynamic behavior state-space modeling A few remarks can be made from this first step simulation. The system, while being symmetric in the equations, does not behave identically for the oxygen and hydrogen halves. Indeed, an increase of the same percentage 10% in both actuators $A_{vg,H}$ and $A_{vg,O}$ does not lead to the same increase in the states for both species. This illustrates the need to adapt the control methods designed on the hydrogen half in previous chapters when controlling the oxygen half of the system. Most of the methods can be driven directly, by simply changing the numerical values to fit the oxygen equations. Such difference in the main chamber mass flows ($q_{cc,O} = 1.0745$,$q_{cc,H} = 1.0946$), while the gas generator mass flows observe the same increase ($q_{gg,H} = 1.1953, q_{gg,O} = 1.1919$), comes from the fact that the mixture ratio desired in the main combustion chamber is $MR_{cc} = 6$, while $MR_{gg} = 1$.

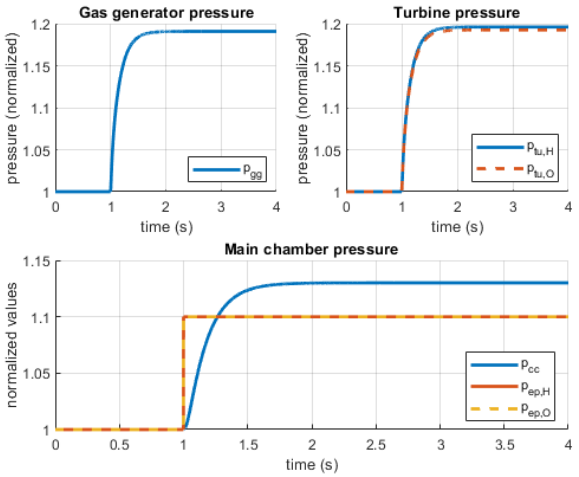

(a) Pressure response

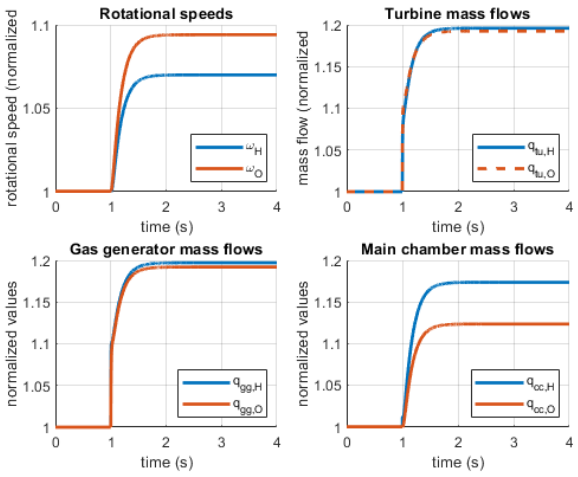

(b) Mass flow response

Figure 6.4 – Open-loop response of the PH model

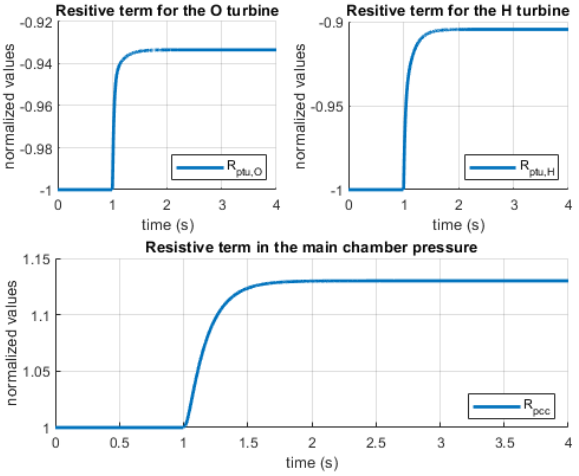

(a) Pressure resistive terms response

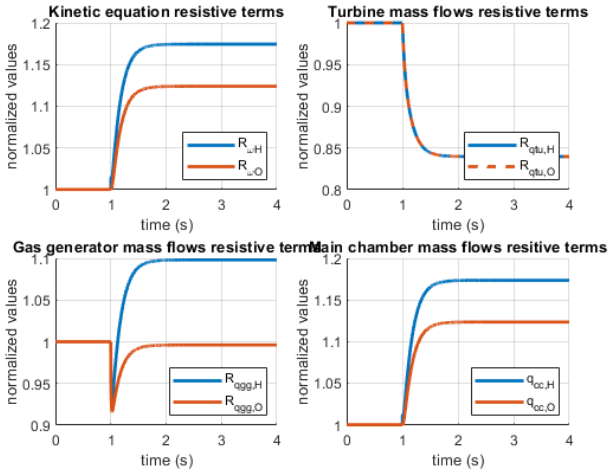

(b) Mass flow resistive terms response

Figure 6.5 – Open-loop response of the resistive terms of the PH model

Observing the final values of the states in response to a step function illustrates the fact that the gas-generator has to be designed for a wider range of variation than the main chamber pressure. In order to generate a high enough pressure at the pump output, the gas generator increases to $p_{gg} = 1.1936$ value while the main chamber pressure reaches $p_{cc} = 1.1308$.

The time response of the system can be considered regarding two different states. The first time response concerns the state $q_{gg,\bullet}$ that responds to the actuators directly and is illustrated by the non-smooth spike at $t = 1s$ in figure 6.3b the total time-response is $t = 0.64s$. This is due to the presence of Z_{resgg} in the GG mass flow equation,

$$\dot{q}_{gg,\bullet} = \frac{1}{I}(p_{ip,\bullet} - p_{gg} - Z_{resgg,\bullet} q_{gg,\bullet}^2). \tag{6.2}$$

The other time constant of the system is denoted by the pressure evolution p_{cc}. This time response is slower than the mass flow response with $0.74s$, and illustrates the evolution of the overall system. To accurately represent an actuator's behavior, it is important to take into account the $q_{gg,\bullet}$ time response, that shows the feasibility of the control law on a real actuator. For example, the non-smooth behavior in figure 6.3b of the gas generator mass flows $q_{gg,\bullet}$ immediately results from a step in the valve surfaces. In the following, the time responses of the system will be expressed in terms of $q_{gg,\bullet}$ to illustrate the feasibility of a controller, and in terms of p_{cc} to illustrate the performance of the controller on the system.

Analysis of dynamic behavior Port-Hamiltonian modeling Figures 6.4a and 6.4b display the evolution of the pressures and the mass flows responding to a step function. The Port Hamiltonian modeling fulfills its purpose of following the same behavior of the original system, apart from the initial conditions ($p_{cc} = 1.3007$ compared to 1.308 with the state-space). This small difference originates from the method used to compute the models in *Matlab Simulink*, where computational artifacts add up and display an error between the two equilibria (for the state-space and the Port-Hamiltonian simulations). In figure 6.5a and 6.5b, the resistive terms composing the matrix R are represented. As discussed in 3, the resistive terms for the turbine pressure $R_{ptu,\bullet}$ are negative, which conflicts with the formulation of the Port-Hamiltonian system. It has been shown however that the passivity of the system can still be proven. This issue is furthermore dealt with using the PBC controller in 6.2.2.

While the evolution of most of the resistive terms follows the state's evolution (figure 6.5a and 6.5b), the turbine mass flows q_{tu} are to consider, as the resistive term R_{qtu} diminishes while the mass flow increases. This originates from the term $\frac{1}{p_{gg}}$, used to express the density of the hot gas (see 2), and will not become negative over time (this would imply the system to cross the origin, which is prevented by the term $\frac{1}{p_{gg}}$).

The Port-Hamiltonian framework also adds new equations to the process, and the computational artifacts induce a different behavior in the start-up of the system. The Port-Hamiltonian system first deviates from the initial equilibrium and then converges normally. This behavior results from the difference in conditioning of the two simulations. The state-space model, with high heterogeneity in the equations, has neglected terms that are taken into account in the Port-Hamiltonian modeling. This difference in the computation comes from the storage of the terms in *Matlab*, which only takes into account a certain To account for this, the simulations are started at a negative time ($-1s$), to obtain the relaxation of the system before starting the simulation.

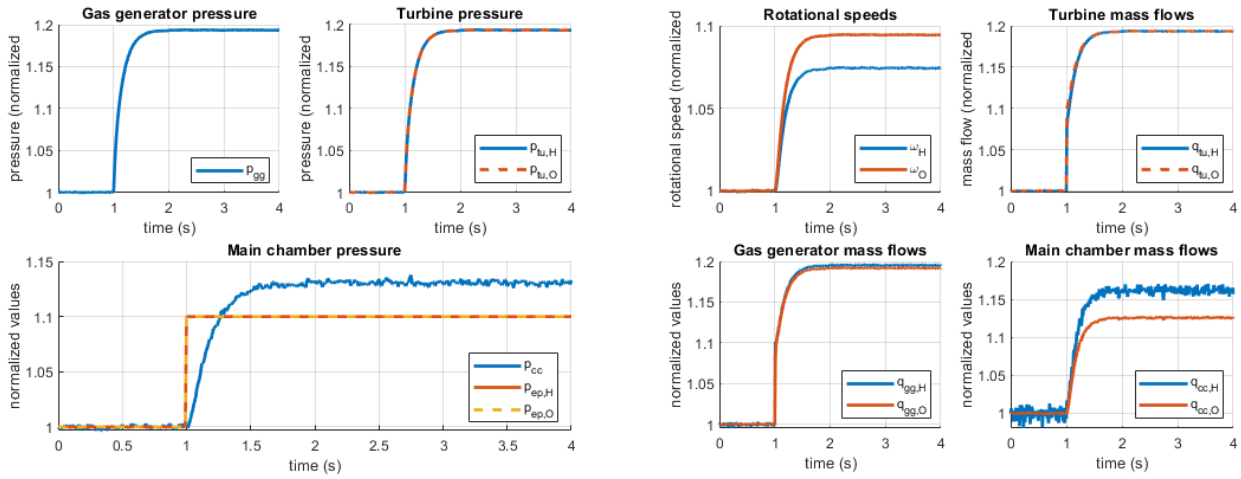

(a) Pressure response

(b) Mass flow response

Figure 6.6 – Open-loop response to a step function with added noise on Θ_{cc}

6.1.3 . Noise influence on the simulations

State-space model and noise Figure 6.6a and 6.6b both illustrate the state's responses to a step with a noise added to the temperature. In figure 6.6a, the simulation illustrates the propagation of the noise on the main chamber pressure p_{cc} (variations that attain 1.1%), while both the gas generator chamber pressure p_{gg} and the turbine pressure p_{tu} are not impacted by the perturbation (less than 0.0022% oscillations). In figure 6.6b, it is shown that the main chamber mass flow q_{cc} is impacted by the perturbation, proving to show higher oscillations than p_{cc} (up to 1.9%). Although the noise can be slightly visible on the rotational speed ω (0.07% variation), its impact is mitigated for the mass flow q_{gg} (0.15% variations) compared to the mass flow q_{cc}. This lower impact is due to the pressure increase of the turbo pump equation p_{ip} that absorbs most of the oscillations.

Port-Hamiltonian and Noise The previous paragraph mentioned that Port-Hamiltonian modeling introduces uncertainty in the simulations due to the use of several *SIMULINK* blocks to represent the model. The addition of noise proves to be tricky as the user must ensure that the noise added is synchronized with the two blocks, i.e. that the same iteration of the noise is injected in both blocks and that no delay in the iterations is created. The addition also creates an unstable behavior if the first iteration lines up with the initial condition shift of the Port Hamiltonian system (typically, if the noise added is sufficient to enter the unstable zone of the system see 6.1.4).

If the simulation is defined properly, meaning that the shift is situated in negative time-values and the noise is synchronized with both blocks of the simulation, the Port-Hamiltonian model follows the same behavior as the original model, as illustrated by the figures 6.7a and 6.7b. Additionally, the noise is carried on to the resistive terms of R as shown in figures 6.8a and 6.8b. For example, R_{pcc} which only depends on the temperature features a 0.6% variation due to the noise. As illustrated figure 6.8b, the noise impact on the resistive terms for $R_{\omega}, 2\%$ and $R_{qgg}, 0.9\%$, far exceeds their state counterparts ω and q_{gg}. This is explained by the dependancy in q_{cc} of the resistive terms, due to the polynomial formulation

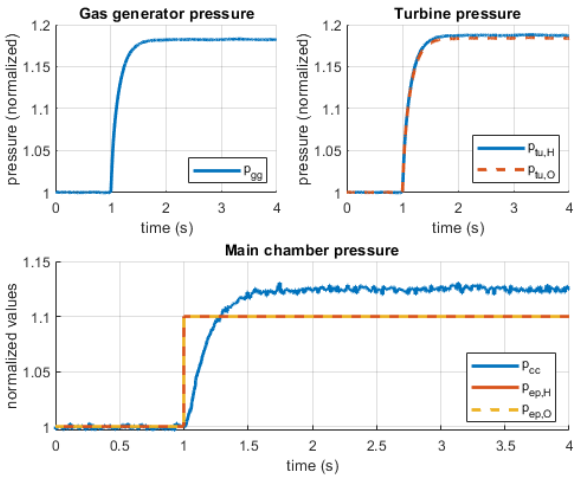

(a) Pressure response

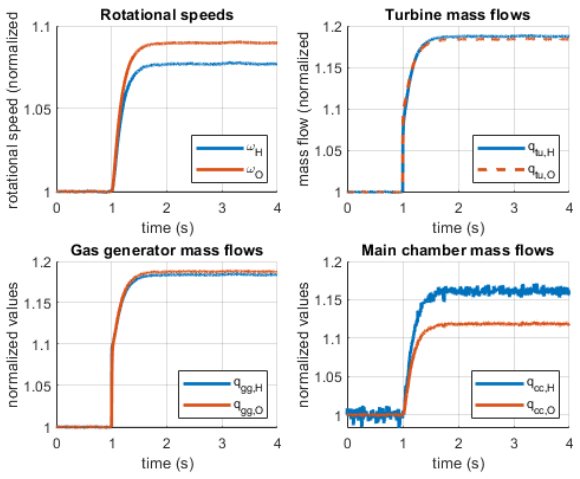

(b) Mass flow response

Figure 6.7 – Open-loop response of the states in the PH model with added noise on Θ_{cc}

of the pressure p_{ip} and resistive torque T_r.

The Port-Hamiltonian model consists of a worse choice for noise modeling. As the startup equilibrium has to be reassigned, it introduces a potential for instability in the system. In fact, the solution of starting the simulation in negative time windows comes from unstable simulations for a start at $t = 0s$ of the noised Port-Hamiltonian model. Considering this with the fact that the two blocks must be well-synchronized, the Port-Hamiltonian model does not constitute a good choice for modeling when dealing with noise.

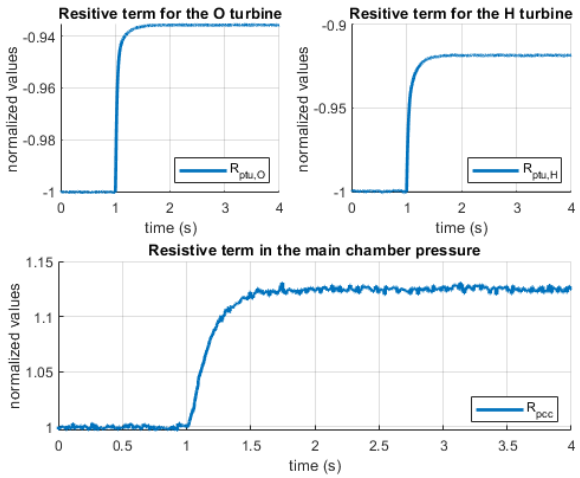

(a) Pressure resistive terms response

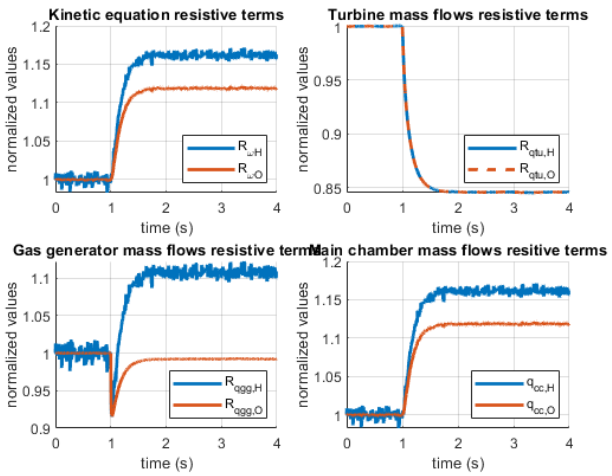

(b) Mass flow resistive terms response

Figure 6.8 – Open-loop response of the resistive terms of the PH model with added noise on Θ_{cc}

6.1.4 . Limitations and unstable zones of the open-loop

In this paragraph, the approach on stability domain analysis with the Port-Hamiltonian system is compared to the state-space simulations.

While the stability domain is difficult to determine for a state-space system, Port-Hamiltonian framework allows for an easier stability analysis. The open-loop system under Port-Hamiltonian form shown in 3, is passive with storage function,

$$H(x) = \frac{1}{2}J\omega^2\alpha_q + \frac{1}{2}I_{cc}q_{cc}^2 + \frac{1}{2}I_{gg}q_{gg}^2 + \frac{1}{2}I_{tu}q_{tu}^2 + \frac{1}{2}k_{pcc}p_{cc}^2 + \frac{1}{2}k_{pgg}p_{gg}^2 + \frac{1}{2}k_{ptu}p_{tu}^2. \tag{6.3}$$

For a shifted equilibrium at x_0, it has been shown in 3.3 that the domain of stability of the Port-Hamiltonian model is characterized by the shifted resistive term

$$\hat{R}_{qcc} = \left(-\frac{a_p}{\rho}(2q_0 + \hat{q}) - b_p\omega_0 - c_p\rho(2\hat{\omega} + \hat{\omega}^2)\frac{1}{\hat{q}} + Z_{eqcc}(q_0 + \hat{q})\right)$$

If this term becomes negative, then the passivity of the system is not proven anymore. Solving this equation gives a minimal limit for the stable domain at $q_{cc,H,lim} = 0.874$. Note that this prediction denotes the domain where the Port-Hamiltonian proof of passivity is not valid anymore. This does not imply that the system is unstable from this limit, but that the method carried to assert stability is not valid anymore. To evaluate the precision of this method, it is then necessary to compare the limit $q_{cc,H,lim}$ obtained with a numerical simulation.

This determination of the equilibrium is to be compared with the result obtained via a state-space simulation. In the following figures 6.9a and 6.9b, the system follows a ramp with a slope of $-0.1A_{vg,H,0} \times t$ for both valve surfaces. Figure 6.9b illustrates that the system equations do not have a solution for a certain surface, and show unstable behavior. At time $t = 1s$, the states display a negative spike that is not compensated, and the simulation is stopped by *Matlab Simulink* due to the apparition of non-finite terms in the derivatives. Taking the last values computed before the simulation stops, the system is stable until $A_{vg,H} = .9A_{vg,H,0}$. The unstable behavior manifests first by an important decrease in the mass flow $q_{cc,H}$ in lower values ($q_{cc,H} = 0.9$). This sudden decrease is then witnessed on the rotational speed ω and the pressure p_{cc}. Finally, the system is unable to recover and the values decrease to $-\infty$. The mass flow equation has no solution for $q_{cc,H} = 0.86$ (no more precise value is available as the threshold is unclear). The Oxygen equation proves to have a solution for lower values of the states, with a different threshold for the loss of stability.

This behavior is difficult to explain with classical automatic methods. However, using a Port-Hamiltonian interpretation, the unstable domain is explained by the lack of natural damping on the system. Indeed, as the damping is insufficient when leaving the neighborhood of the equilibrium, the mass flow $q_{cc,H}$ lacks damping and deviates such that the distance $||q_{cc} - q_{cc,0}||$ increases and becomes unbounded. Therefore, to stabilize the system, it is necessary to increase the damping injected in the mass flow $q_{cc,H}$. A perspective of this work would be to explore the use of the valve $A_{vcc,H}$, supposedly opened at a constant value during the permanent regime, to increase the range of the stable domain. Indeed, by closing the valve, it is possible to increase the resistive term R_{qcc} to a positive value.

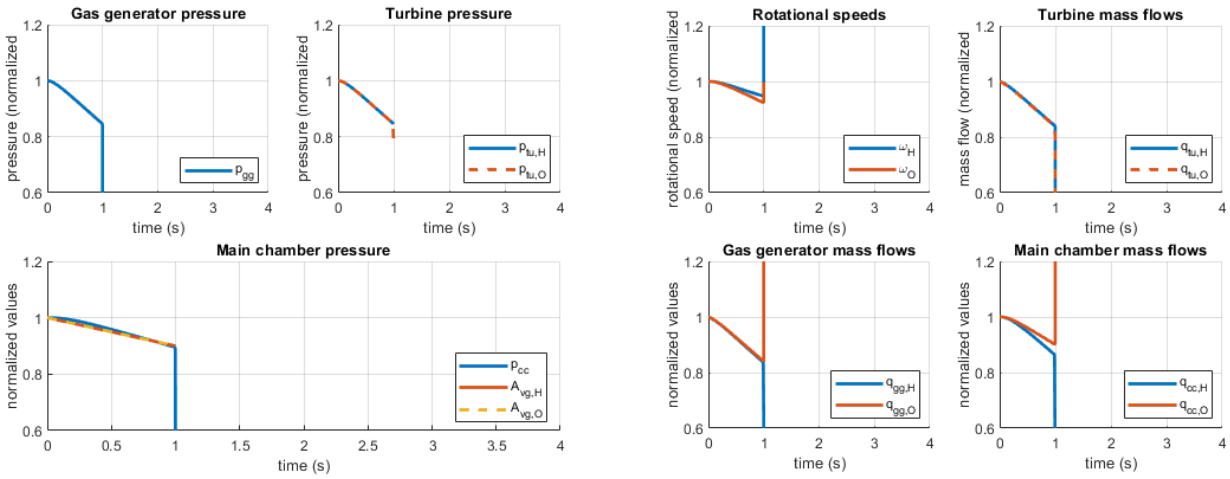

(a) pressure behavior

(b) mass flows behavior

Figure 6.9 – Unstable zone of the LPRE model

6.1.5 . Tank pressure response

During the modeling of the LPRE in section 2, the tank pressure $p_{ep,\bullet}$ for both species has been considered constant. In reality, the tank pressure decreases over time when the amount of fluid in the tanks decreases. A common method to maintain the pressure in the tanks is to use pressurizing gas, which is injected during the emptying of the tanks. This results in a pressure profile over time with slow oscillations around the operating pressure. However, this variation of pressure is negligible as it has close to no impact on the final value of the chamber pressure p_{cc}. In figure 6.10, the state-space system is represented for a step-function on the tank pressures $p_{ep,\bullet}$. This is represented in the simulation with a change of the tank pressure value from $p_{ep,\bullet,0}$, to $1.1p_{ep,\bullet,0}$ at time $t = 1s$. In figure 6.10a the evolution of the pressures in the system is represented. The increase in the main chamber pressure p_{cc} is less than 0.2%, for a 10% increase in the tank pressures $p_{ep,\bullet}$. It is then justified to neglect the pressure variations in the tanks in terms of impact on the final value of the system.

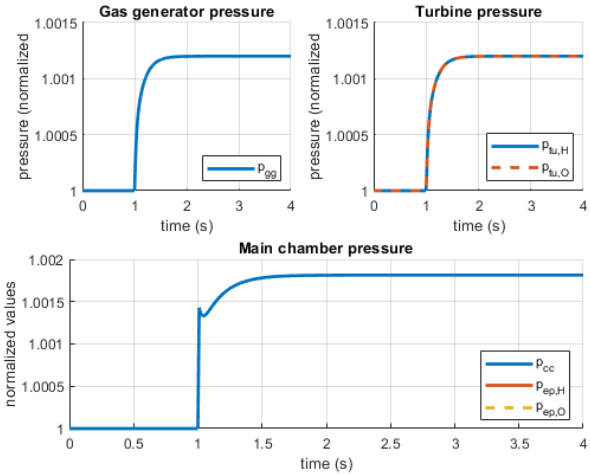

(a) pressure behavior

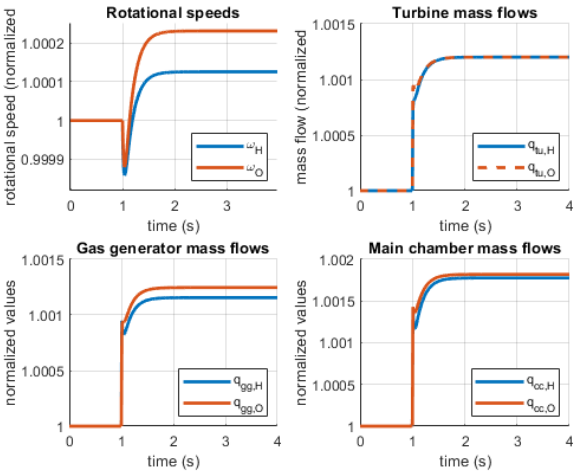

(b) mass flows behavior

Figure 6.10 – State-space open-loop response to a step on the tank pressure

6.2 . Analysis and comparison of performances of the controller designs

The developed approaches in the previous chapters 3 and 5 offer two different improvements to the stable region of the system :

- The PBC controller allows to redefine some of the dynamics of the total closed-loop to extend the stability region.
- The contracting controller provides new guarantees with the notion of contraction region.

In this section, both controllers designed in chapter 3 and 5 are presented. The stabilizing behavior of both controllers is presented, and to this end, a classical PI controller is proposed as a reference. For each controller, a comparison is performed with the PI, on an unstable scenario for the system, e.g. a reference that crosses the unstable threshold q_{cc}. It is important to note that this scenario leaves the practical case of the LPRE, as it is tested for an objective function outside of the validity domain of the model. In a second time, the tunable parameters of the controllers are presented (for example the contraction metric for the contraction-based controller). The impact of these parameters, discussed previously in terms of stability, are recalled here and their performances are illustrated using simple step-responses. Finally, the addition of the dynamics of the actuators is proposed, under the form,

$$\ddot{A_v} = -\xi w_0 \dot{A_v} - w_0^2 A_v + u_A, \tag{6.4}$$

where A_v is the opening surface of the actuator, and u_A is the controller value. The new tuning of the system required to maintain the stabilizing behavior with the addition of the actuators is proposed.

The simulations and considerations are realized on the hydrogen line of the LPRE model, for simplification. As this line presents the unstable behavior, it is chosen to illustrate the stabilizing capabilities of the controllers.

The section is organized around the different controllers used, and after the presentation of the PI controller, the previously mentioned analysis and tuning are performed first for the PBC controller and then for the contraction-based controller. The reference is generated with an integrator for both stabilizing controllers.

Two scenarios are injected to study the stabilizing properties of the controllers. First, an unstable scenario is proposed, where the controllers are compared with the PI reference. This scenario is designed to represent fluctuations around an equilibrium x_0, and cross the limit of the stability domain. A second comparison is made for a transition between two stable points of the system.

6.2.1 . PI controller reference

In the scope of comparing the controllers designed to a more classical solution, a PI controller is defined around the equilibrium point x_0. The PI controller for the feeding valve's surface $A_{vg,H}$ is designed to regulate the chamber pressure p_{cc}, for a fixed mixture ratio $MR_{cc} = 6$ (hydrogen half of the system assumption). The PI controller design follows the control law,

$$u_{PI} = k_P(x_r - p_{cc}) + k_I \int_0^t (x_r - p_{cc})dt \tag{6.5}$$

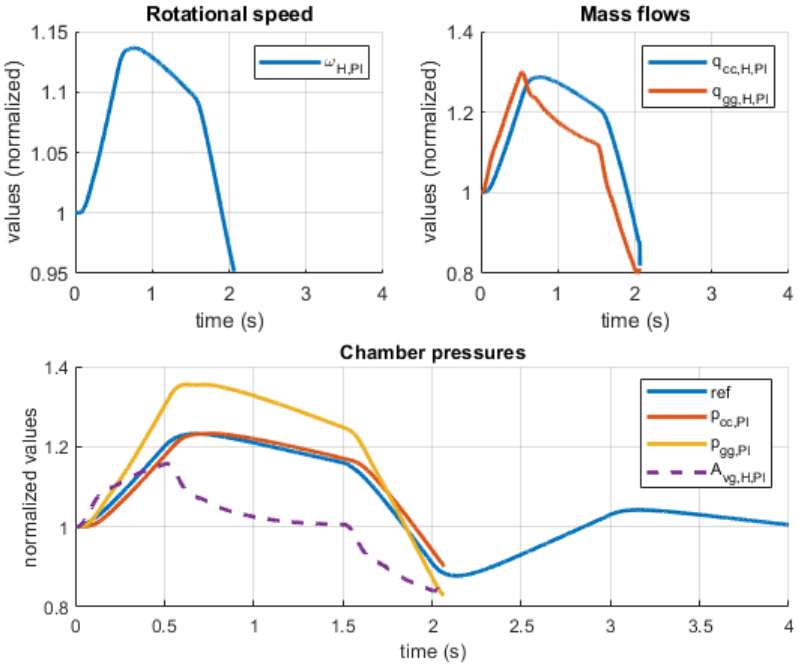

Figure 6.11 – Response to an unstable scenario with a PI controller

where k_P, k_I are the proportionate and integral parameters. Since the chosen equilibrium of the system is different than the origin $x = 0$, a constant term is added to the control law. To assign the equilibrium with the PI controller, define

$$k_A = A_{vg,H,0},\ k_P = 1 \text{ and } k_I = 30 \tag{6.6}$$

where the formulation of the control law is

$$u_{PI} = k_P(x_r - p_{cc}) + k_I \int_0^t (x_r - p_{cc})dt + k_A \tag{6.7}$$

The value of k_I is chosen according to the time response of the open-loop system (see figure 6.13a). The PI controller provides no stability guarantee, it consists in a passive controller, which paired with the Port-Hamiltonian formulation of the systems, makes use of interconnection theorems and the closed-loop system is passive. In the following simulations, this controller is used to show the limitations of classical control when dealing with unstable zones of the system.

In figure 6.11, an unstable scenario is injected as the reference for the controller. This scenario will be referred to as the *unstable scenario* from now on. The unstable section of this scenario is situated at the reference crossing the line $p_{cc} = 0.9p_{cc,0}$ in figure 6.11. As mentioned previously, the PI controller provides no stability guarantees to the system, and as the trajectory of the states enters the unstable zone of the system, the divergence occurs.

The PI controller can nonetheless by a suitable solution for simple operating point transition, provided the trajectory resulting from the transition remains in the stable region of the system. In figure

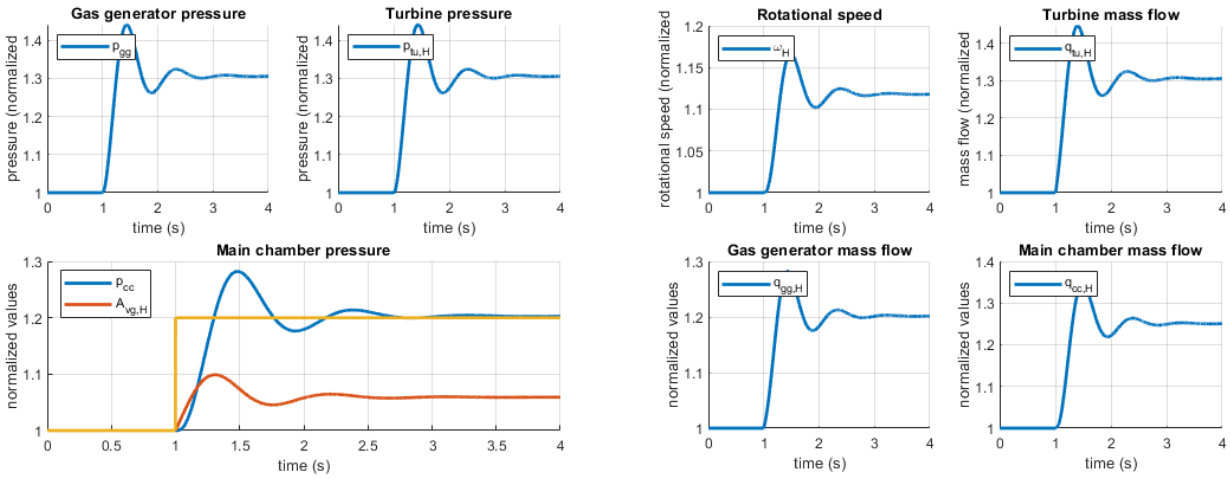

(a) Pressure behavior

(b) mass flows behavior

Figure 6.12 – Step response using the PI controller

6.12a and 6.12b, the PI controller is a sufficient solution for the control of stable trajectories. This is because the system is indeed passive around the equilibrium and above the value x_0. Therefore a negative feedback in the form of a PI controller is a sufficient control to ensure stability in the region where the system is passive. Indeed, given the following lemma [95], if the port-Hamiltonian shifted system in (3.46) is zero-state detectable, then a feedback controller

$$u = -v(x,t)y, v(x,t) \geq \epsilon I_d \geq 0, \tag{6.8}$$

renders the equilibrium $\hat{x}$ for the shifted system in section 3.3 asymptotically stable.

As shown in figure 6.12b, the PI controller presents an asymptotically stable behavior in the stable region of the system. The response to a step is satisfying, for a time response of $0.27s$ of p_{cc}. The time-response of the GG mass flow q_{gg} is identical at $0.276s$. The overshoot due to the PI controller may be reduced, and for this tuning corresponds to 0.276 in p_{cc}.

6.2.2 . Stabilization with PBC controller

This subsection aims to present the use and tuning of the PBC controller, illustrated with numerical simulations of the closed-loop controlled system with the controller.

Tuning of the PBC controller

The objective of the PBC controller is to stabilize the closed-loop system around a desired equilibrium. The stability of the system is proven by the passivity of the closed-loop. For a reachable reference (where the polynomial functions are defined) the system can perform stable transitions between operating points. For an ill-designed reference, the system may cross the unstable zone of the system mentioned in 3.3.1. To improve the stability of the system, a reformulation of the dynamics of the closed-loop 6.10 is performed. As described in 3, the matrix $R_d(x)$ can be tuned to obtain a desired behavior.

A first illustration of the controller design is proposed in figures 6.13a and 6.13b. In this simulation, an integrator has been added to the system as in 4.3.2. Here only the hydrogen half of the system is presented, to study the behavior of the controller towards the unstable zone. As the controller stabilizes the system around a desired equilibrium, it is resilient to uncertainty on the parameters. The parameters used for this simulation are $Q_{qgg} = 1 + \frac{R_{pcc}^2}{R_{qtu}}$. Additionally, the following parameters are fixed for the resistive matrix R_d,

$$\begin{aligned}
R_{dq_{cc}} &= R_{q_{cc}} \\
R_{dp_{cc}} &= R_{p_{cc}} \\
R_{d\omega} &= 2R_{\omega} - R_{p_{cc}} \\
R_{dp_{gg}} &= 2R_{q_{tu}} - R_{aq_{tu}} \\
R_{dq_{tu}} &= 0 \\
R_{dp_{tu}} &= 1 \\
R_{dq_{gg}} &= R_{q_{gg}}.
\end{aligned} \tag{6.9}$$

Most of the conditions are derived from the resolution of the partial derivative equations in 3. The rest of the parameters are fixed for simplification, or to assert the Port-Hamiltonian behavior of the desired system with $R_{dp_{tu}} = 1 > 0$. This choice for R_{ptu} is made to respect the orders of magnitude of the other terms in the matrices $J(x), R(x)$, that are close to a unit. We recall here the equation of the controlled closed-loop system with the PBC design :

$$\dot{x} = (J_d(x) - R_d(x))\frac{\partial H}{\partial x}(x) \tag{6.10}$$

where the matrix $R_d(x)$ is composed of the resistive terms in (6.9), and $J_d(x)$ is the original structure matrix from the model (3.32). The step response with the parameters described in (6.9) is illustrated in figure 6.13. The parameters described allow to obtain a fast time response with minimal overshoot, with stability guarantees of the controller during the step. Note that as the actuator's dynamics are not modeled, the controller presents a spike that is unrealistic (see $A_{vgg,H}$ on orange in figure 6.13a).

In the following tables 6.1 and 6.2, the setup for the system is a simple reference generation, and leads to the function :

$$x_{ref} = (p_{cc,obj} - pcc)\frac{x_0}{p_{cc,0}}, \tag{6.11}$$

$R_{dq_{gg}}$	Minimal q_{cc}	q_{gg} time response	q_{gg} overshoot	p_{cc} time response	p_{cc} overshoot
$0.1R_{q_{gg}}$	0.744	$0.019s$	31%	$0.18s$	None
$0.5R_{q_{gg}}$	0.745	$0.016s$	20%	$0.18s$	None
$R_{q_{gg}}$	0.749	$0.015s$	15%	$0.18s$	None
$2R_{q_{gg}}$	0.748	$0.01s$	8%	$0.18s$	None
$10R_{q_{gg}}$	0.755	$< 0.01s$	2%	$0.18s$	None
$R_{q_{gg},0}$	0.749	$0.015s$	15%	$0.18s$	None

Table 6.1 – Variations of the parameter $R_{dq_{gg}}$

where x_{ref} is the reference injected in the controller and x_{obj} is the objective of the controller (here a step function). Such reference leads to a static error, but better illustrates the step response of the system, and is more suitable to highlight the impact of the different parameters.

The tuning of the controller is due to the choice of the matrices J_d and R_d. From the formulation of the matrix J in (3.32), there is no significant simplification with the matrix J_d. On the other hand, the matrix $R(x)$ contains the unstable polynomial functions and is of interest to tune to obtain a larger stable region. The tuning of $R_d(x)$ consists in finding the best-suited functions for the individual resistive terms, expressed in (6.9). As most of the terms are fixed by the resolution of the PDE equations (see 4.36), three terms remain for tuning : $R_{dq_{tu}}, R_{dp_{tu}}$ and $R_{dq_{gg}}$. The impact on the system behavior of the parameter $R_{dq_{gg}}$ is summed in the following table 6.1. The time response and overshoot are expressed for the state q_{gg} and the state p_{cc}. Indeed, modification of the closed-loop resistive matrix $R_d(x)$ first impacts the state q_{gg}. The response of the main chamber pressure is affected if the state's response is slower than the main chamber pressure. Additionally, an overshoot in the state q_{gg} seldom affects the main chamber pressure, as it occurs for only short time responses, which the main chamber pressure does not react to. As the value of the resistive term decreases, the stable zone is extended, however, such extension is negligible in front of the impact on the step response. The modification of the resistive parameters is not sufficient to obtain the desired time response for the system, which is too fast.

The choice of a tuning parameter Q_{qgg} presents a low impact on the system under a certain threshold. Indeed, in the controller equation the term parameter Q_{qgg} multiplies the difference between the state and the reference, under the form

$$u_{PBC} = u_0 + (Q_{qgg} - 1)(x_{ref} - x) \tag{6.12}$$

see **ANNEX B** for a detailed expression of the controller. For small variations of the operating point (here the new equilibrium is 120%), the time response and the overshoot are not affected until the product (6.12) exceeds the term u_0 in the controller i.e. $k_u = 1000$. In this event the time response of p_{cc} is affected and the resulting spike is not desirable. In the case of trajectory tracking, where no clear u_0 can be found, the parameter Q_{qgg} has a higher impact on the speed of the system. In the following table 6.2 the variations of the performances are depicted following $Q_{qgg} = 1 + k_u \frac{R_{pcc}^2}{R_{qtu}}$. The overshoot and time-response are estimated for the evolution of both q_{gg} and p_{cc}.

Remark 9. From equation (6.12), the controller is subject to a product of two terms, the tuning parameter and the difference between the reference and the state. Depending on the method used to generate the

k_u	Minimal q_{cc}	q_{gg} time response	q_{gg} overshoot	p_{cc} time response	p_{cc} overshoot
0.1	0.748	$0.012s$	14%	$0.18s$	None
1	0.749	$0.015s$	15%	$0.18s$	None
10	0.749	$0.013s$	15%	$0.18s$	None
100	0.748	$0.012s$	16%	$0.18s$	None
1000	0.755	$0.012s$	30%	$0.15s$	1.2%

Table 6.2 – Variations of the parameter k_u

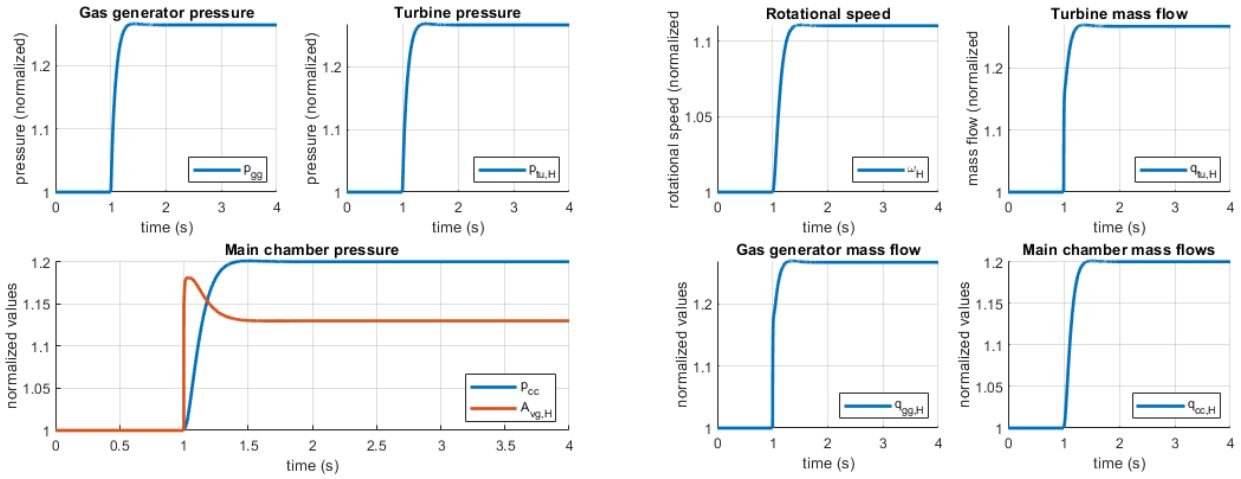

(a) Pressure behavior

(b) mass flows behavior

Figure 6.13 – Step response using the PBC controller

reference, the difference between the reference and the state is subject to high changes in the order of magnitude.

- For a perfect reference generator that provides the exact value for all the states, the user would prefer a high value of k_u ($10^2 - 10^3$) to emphasize a low difference between the reference and the state.
- For an integrator that generates a reference, the difference between the reference and the state grows over time, and the user should prefer a low value for k_u ($.1 - 1$) to minimize the impact of the already high difference.

Since the addition of an integrator is used in this work, the choice for k_u is limited to the range $0.1 - 1$.

Comparison of stabilization with PI design

A comparison is performed with the classical PI controller, to show the extension of the stable zone due to the new dynamics proposed by R_d. in figure 6.14, the results of a simulation for a quick adjustment in the pressure is provided. The scenario used in this simulation corresponds to brief changes in the operating point, to enhance the response performance of the controller. Additionally, the scenario

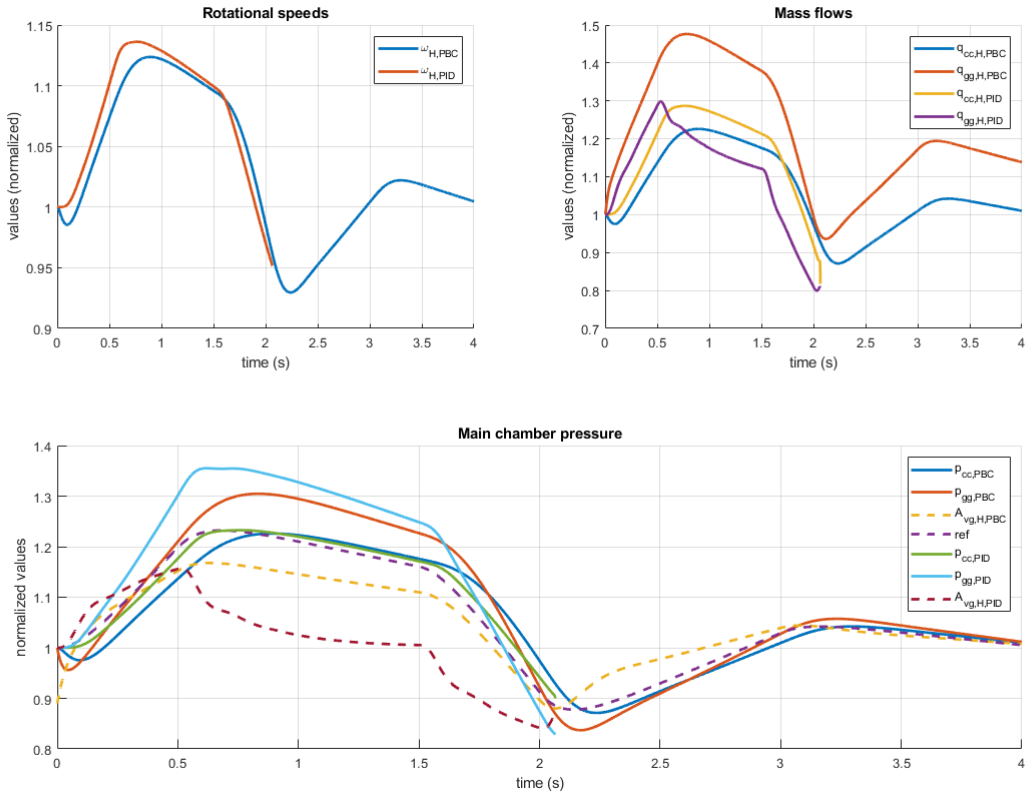

Figure 6.14 – Comparison between PI and PBC responses to an unstable reference

overlaps the unstable zone of the polynomial functions, to illustrate the stabilizing behavior of the PBC controller. On the bottom half, the chamber pressures p_{cc} and p_{gg} are provided along the reference (ref) and the gas generator valve's surface $A_{vg,H}$. On the top half, the evolution of the feeding mass flows $q_{cc,H}, q_{gg,H}$ next to the rotational speed ω_H are figured. Figure 6.14 displays the resulting trajectories of the states for both the PBC and PI controllers. The PBC controller can remain stable for lower values of the states than the PI controller, e.g. $p_{ccmin,PBC} < p_{ccmin,PID}$. Note that although the pressure is lower, $p_{cc,PBC} = 0.8712$, the mass flow q_{cc} does not decrease lower than the threshold value $q_{cc,H} = 0.86$. This is due to the changes applied to the resistive matrices, that influence the system's dynamics.

This is explained by the fact that the PBC controller maintains a higher gas generator mass flow q_{gg} than the PI controller (see the orange and purple evolutions in figure 6.14. This allows to maintain a higher rotational speed ω and higher main chamber pressure p_{cc} with less variations in q_{cc}. The same principle applies for low values, and results in the comparison, where the pressure $p_{cc,PBC} = 0.8712$ attains lower values than the pressure $p_{cc,PID} = 0.8999$.

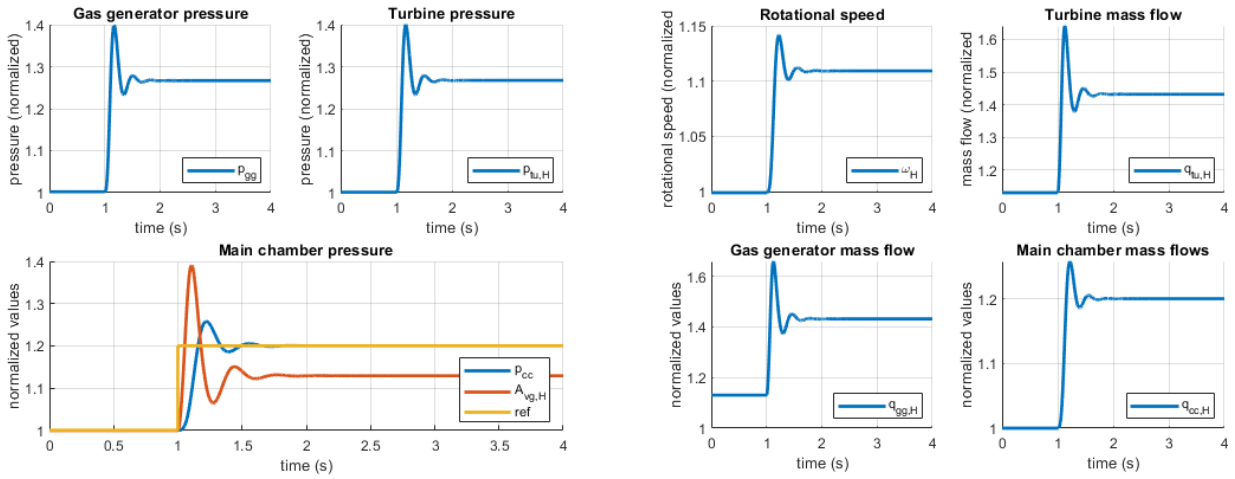

(a) Pressure behavior

(b) Mass flow behavior

Figure 6.15 – Step response using the PBC controller and a second-order actuator

Addition of actuators

The addition of the actuator's dynamics requires tuning the controller to match the time response of the actuators. The parameters selected for the actuators require a time response of $0.3s$ and a low overshoot, as the second-order system already presents an overshoot. Therefore, the parameter k_u is chosen at 1 and $R_{dq_{gg}} = R_{q_{gg},0}$. in figure 6.15, the evolution of both pressures and mass flows in response to a step function with the actuators dynamics are represented. The addition of actuators tends to emphasize the initial overshoot of the system, which is now paired with the overshoot of the second-order function.

The addition of an integrator discussed in 4.3.2 allows to neutralize the static error remaining for under-defined references, and to increase the time response of the system with actuator's dynamics, leading to the reduction of the overshoot.

Conclusion on the PBC tuning

As shown in the tables, the tuning of the resistive parameters of the system can be counter-intuitive, as the increase in a resistive parameter gives a faster time-response to the system in terms of mass-flow q_{gg}, however, decreases the static error of the system. The system furthermore presents low sensitivity to this parameter tuning, as the time-response and overshoot of p_{cc} show very small variations compared to the tuning parameter in table 6.1.

The low impact of the damping parameter on the variations of p_{cc} comes from the fact that without overshoot in the mass flow q_{gg}, the pressure p_cc will follow a pseudo step in the mass-flow, similar to an open-loop control in figure 6.13a, and conserve its slow raising time.

A more impactful parameter resides in the tuning of Q_{qgg} and in particular the parameter k_u, presented in the table 6.2. This parameter influences the rising speed and overshoot of the mass flow q_{gg} with more impact than the damping term. However, the desired effect is only attained at a certain value

k_w	q_{gg} time response	q_{gg} overshoot	p_{cc} time response	p_{cc} overshoot
0.1	$.6s$	None	$0.6s$	None
0.5	$.18s$	0.8%	$0.18s$	$< 0.1\%$
1	$.048s$	8%	$0.18s$	1.7%
2	$.03s$	23%	$0.18s$	3%

Table 6.3 – Variations of the parameter k_w

of $k_u = 1000$. As stated in 4.2.3, the controller presents 2 terms, one devoted to equilibrium assignment, and one multiplying $(x - x_r)$ which is the reference term. For a sufficient k_u, this second term is predominant in the controller's equation and drives the behavior, hence the increase in overshoot. For lower k_u, the equilibrium assignment is predominant.

6.2.3 . Stabilization with contraction design

Contraction controller tuning

In this paragraph, the contracting controller designed in (5.64) is illustrated and compared to the PBC design on the same scenario. Again, the variable to track is the main chamber pressure p_{cc}, and the contracting controller uses as reference generation an integrator, which is slow enough $k_I = 30$ to remain in the contraction region at all times. The contraction metric $P = W^{-1}$ constitutes the tunable parameter for the contraction-based controller. The parameter W will be expressed as a equal to $k_w W_0$, where W_0 is the solution of the LMI,

$$(AW_0 + BZ_0)^\top + (AW_0 + BZ_0) \leq 0, W_0 > 0,\ W_0 L^\top = -(M + BN_0),\ K_0 = Z_0 W_0^{-1},$$

where the matrices A, B, M are computed following the design proposed in subsection 5.4.

In the following table 6.3, the setup for the system is a simple reference generation, and leads to the function :

$$x_r = (p_{cc,obj} - p_{cc})\frac{x_0}{p_{cc,0}}, \tag{6.13}$$

where x_r is the reference injected in the controller and x_{obj} is the objective of the controller (here a step function). Such reference leads to a static error, but better illustrates the step response of the system, and is more suitable to highlight the impact of the different parameters.

As discussed in 5.3.4, the design of the contracting controller allows more than a single solution for the matrix W_0 in the LMI (6.13). The choice of the matrix W_0 has a direct impact on the feasibility of the controller and the performances in closed loop. In table 6.3, the characteristics of the step response are presented for different metrics $k_w W_0$. The performances of the closed-loop system show a high sensibility to the tuning of W_0, and for k_w above 2, there is no solution to the LMI. For a perfect reference, the original metric $W_0, k_w = 1$ is sufficient, with a low overshoot and a quick time response. Following remark 9, in the case of a reference generated with an integrator, a lower metric $k_w \in [0.1, 0.5]$ is chosen, which slows down the system but allows it to remain in the contraction region.

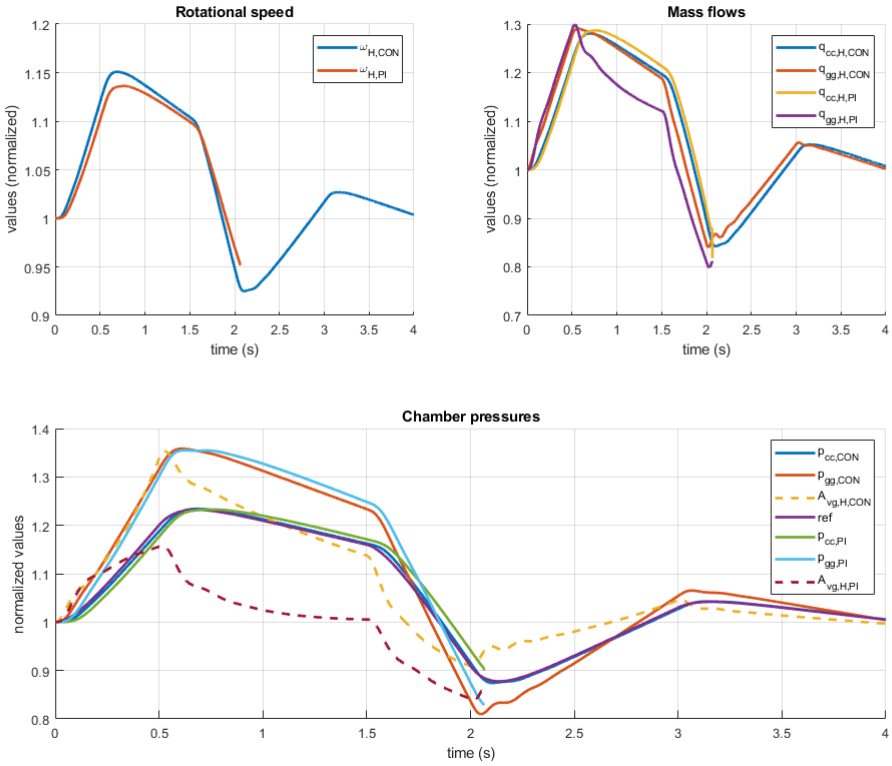

Figure 6.16 – Comparison between Contraction and PI responses to a difficult reference

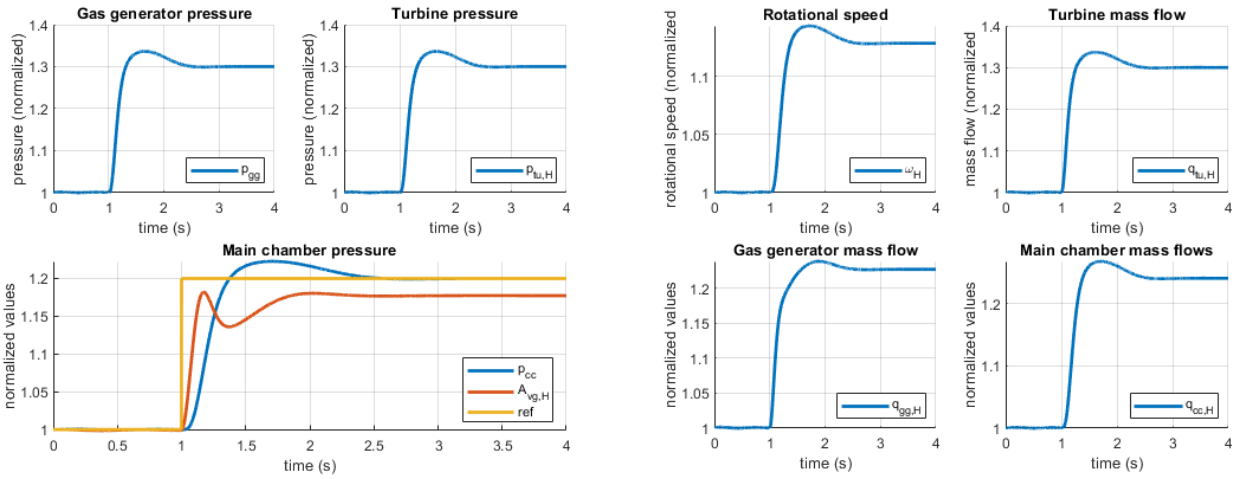

(a) Pressure behavior

(b) Mass flow behavior

Figure 6.17 – Step response using the CON controller and a second-order actuator

Stability via contraction region study

in figure 6.16, the contracting controller is compared to the original PI controller for an unstable reference. The contracting behavior can also be observed as the system remains stable where the PI system diverged. However, contrary to the PBC which extends the stable region, the contracting controller imposes constraints to avoid the borders of the contraction region. This is illustrated by the controller $A_{vg,H,CON}$ in figure 6.16, where at the $2s$ mark, the controller increases before the reference reaches its minimum. This increase is generated by the constraints of the controller, which act like barrier functions at the edges of the contraction region, leading to stabilizing behavior.

Addition of actuators dynamics

The addition of the actuator's dynamics implies a slower dynamic for the controller. The reference is generated using an integrator, with a slow parameter ($k_I = 20$). The choice is oriented towards the metric $0.1 * W_0$, for a match in the time constants of the systems and to limit the impact of the integrator. The step-response of the system with an added actuator is presented in figure 6.17, for both pressures and mass flows. As shown on the figure, if the time-constant differ from one another, it is possible to observe a shift in the curve of the trajectory, at the $1.2s$ mark in the q_{gg} evolution (see 6.17b, in the lower left corner). While admissible for a simple reference as a step, a continuous trajectory would suffer from the error between the time constants. In the following, a parameter $k_w = 0.3$ is chosen to remedy this.

Conclusion on the contraction tuning

The tuning of the contracting controller is revealed to be more intuitive than the PBC controller. Indeed, with only one parameter to act on, the choice of a suitable contraction metric $k_w W_0$ is simplified. However, the system displays a greater sensitivity to this parameter, and it is preferable to remain in low

values of the metric to conserve stability.

6.3 . Realistic scenario for a reusable engine

In this section, a scenario is proposed that approaches the types of trajectories encountered in the landing of a rocket first stage. During the landing maneuver, the first stage detaches from the rocket body, and after performing a U-turn to orient the rocket engine with the velocity, a first burn at maximum thrust is performed to slow down the rocket engine for atmospheric re-entry. In a second time, the engine's thrust is minimized to save fuel, and allow for aerobraking. Once the velocity of the first stage is low enough thanks to friction in the atmosphere, a last burn is performed at maximum thrust to land the engine. Due to the model being designed for $100\% - 150\%$ of the nominal state values, the maximum thrust is set to 140% of the state value and the minimum thrust to 100%. One of the main goals of this thesis is to assert the tracking of the trajectory with the controllers designed and maintain the stability guarantees evoked during the functioning.

To the scenario, a white noise on the temperature Θ_{cc} is added, to represent combustion instabilities and parameter uncertainty on the chemical reaction. The objective of both controllers is to prove a robust design to the noise addition and to the addition of the actuators dynamics. To this end, the parameters used for the controllers are depicted, and chosen to slow the behavior down to match the actuator's time response. To better the comparison, both controllers respond to the same reference, which is represented along the controllers in figures 6.18 and 6.20. The reference is generated using an integrator on the state p_{cc} with the parameter $k_I = 5$.

6.3.1 . PBC controller

This type of scenario implies a continuous objective, that translates into a continuous reference injected in the PBC controller. The discretization of the reference is then performed only by *Matlab Simulink*, and does not present optimal conditions for the PBC controller, which is more adapted to slow transitions. The responses on previous simulations (step responses and unstable reference) show that the requirement for stability implies a low value of k_u ($k_u \leq 100$), and a simple damping term. For a high value of k_u, the table 6.2 shows that the overshoot and time-response are not feasible for the actuators, leading to unstable behavior.

The PBC controller parameter k_u is set to 100, while the remaining resistive terms are taken constant ($R_{dq_{tu}} = 0$,$R_{dp_{tu}} = 1$ and $R_{dq_{gg}} = R_{q_{gg,0}}$). This allows to mitigate eventual oscillations in the design due to the addition of the actuator's dynamics. The main drawback of the slow parameters for the tracking is illustrated in figure 6.18, where the PBC controller imposes a delay on the tracking of the reference. For k_u greater than 100, the controller outpaces the evolution of the actuators, and induces high oscillations on the system, leading to unstable behavior.

The PBC controller shows limited performances towards noise cancellation. In figure 6.18a, it is possible to observe the noise impact on the main chamber pressure p_{cc}, which remains at 1.9% of the normalized value of the state, similar to the open-loop system. Using this controller, the addition of new dynamics is hindered by the high dependency on the original dynamics of the system. This originates from the complex computation of the controller, which fixes a high number of the variables in the desired behavior (4 out of 7 of the terms in the new damping matrix R_d), and is highly sensible to modifications in the system.

To obtain better performances with the PBC controller, it is necessary to increase both the parameter k_u and the integrator k_I. In figure 6.19, the following parameters have been applied : $k_u = 100$, $k_I =$

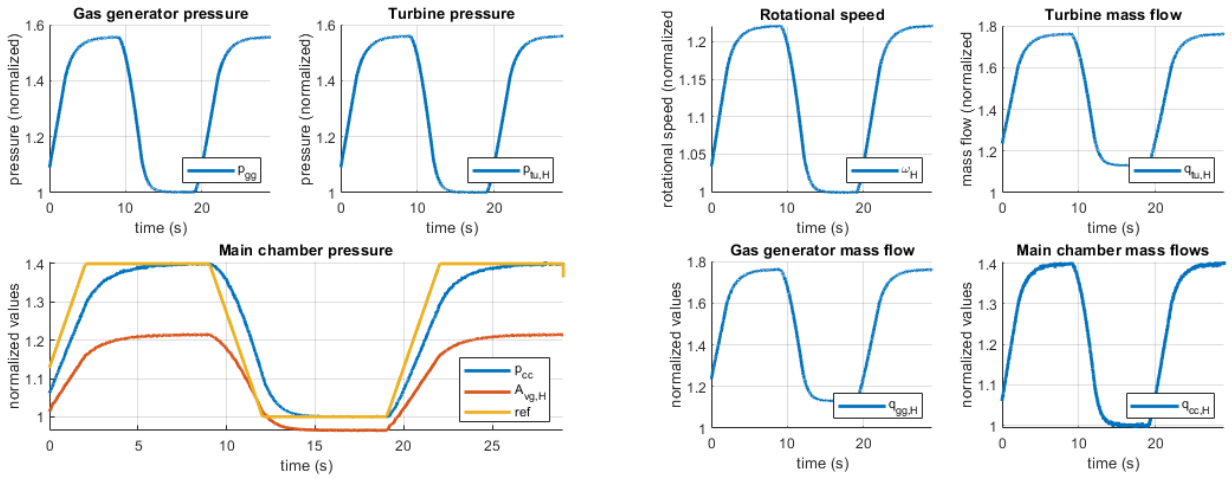

(a) Pressure behavior

(b) Mass flow behavior

Figure 6.18 – Real-life scenario using the PBC controller $k_u = 100$, $k_I = 5$ and a second-order actuator

20. Such an increase allows for closer tracking, in terms of time response and delay. As the system is able to reach the desired value faster, the difference between the objective and the actual pressure p_{cc} decreases. Additionally, a decrease in the noise influence can be noted, as the oscillations in the controller can be dissipated with more efficiency due to the increased time response.

While the PBC controller proves to be a reliable solution for simple transitions between operating points, the performances on trajectory tracking feature a delay that is solved by increasing the added integrator speed. As explained earlier, such tuning implies a loss in the stability domain. While the performances using the newly tuned integrator are satisfying, it is possible to note the apparition of oscillations on the controller value Avg, H in figure 6.19a, due to the increase in speed.

6.3.2 . Contracting controller

The contracting controller is well adapted to trajectory tracking, and the continuous reference generated by the realistic scenario does not pose problems. The simulations presented previously emphasize the need for a low k_w, that stabilizes the system when dealing with high variations of the states' value ($100\% - 140\%$).

The contracting controller parameter k_w mentioned in the table 6.3 is chosen to $k_u = 0.3$. A higher parameter leads to oscillations because it outpaces the actuators, and a lower parameter is unable to follow the reference. The integrator added to suppress the static error of the system is selected with a time constant of 5. This time constant is taken slow before the rest of the dynamics to not interfere with the contracting behavior of the controller (see 5). The results of the simulation are provided in figure 6.20. A closer look to the evolution shows the dissipation of oscillations when tending to low values of the states, where the contracting controller acts as a barrier function. The tracking proves to have a delay illustrated in figure 6.21, however negligible in front of the time-scale of the required variations of the system during the scenario. Similarly, the overshoot and oscillations do not exceed 2% of the amplitude of the scenario and are then satisfying. Contrary to the PBC controller, a contractive controller rejects

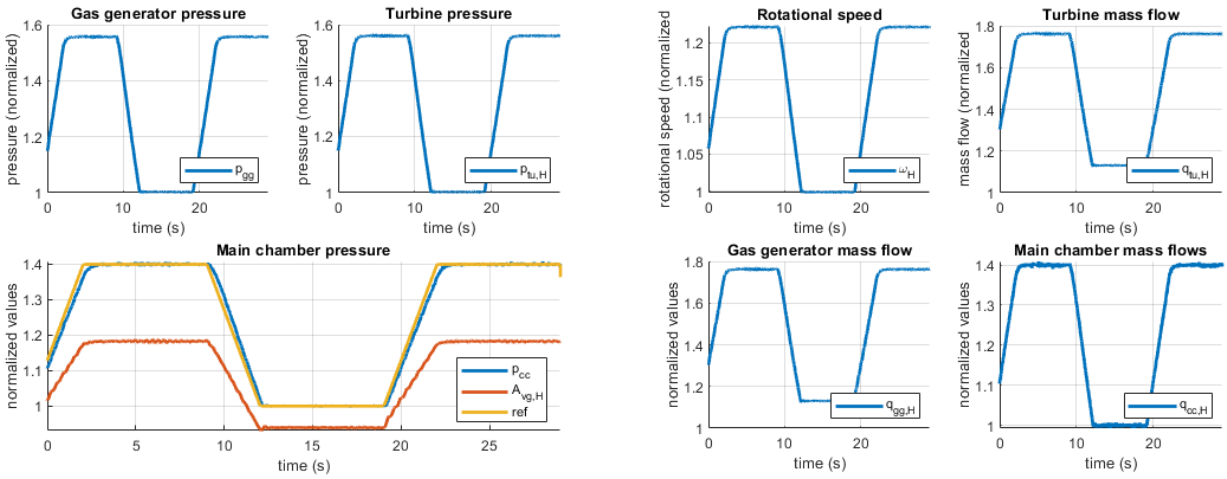

(a) Pressure behavior

(b) Mass flow behavior

Figure 6.19 – Real-life scenario using the PBC controller $k_u = 100$, $k_I = 20$ and a second-order actuator

high frequencies of the system (see [83]), and reduces the impact of the noise injected on the system (average noise amplitude of 1.9% for PBC, compared to 1.2% for the contraction).

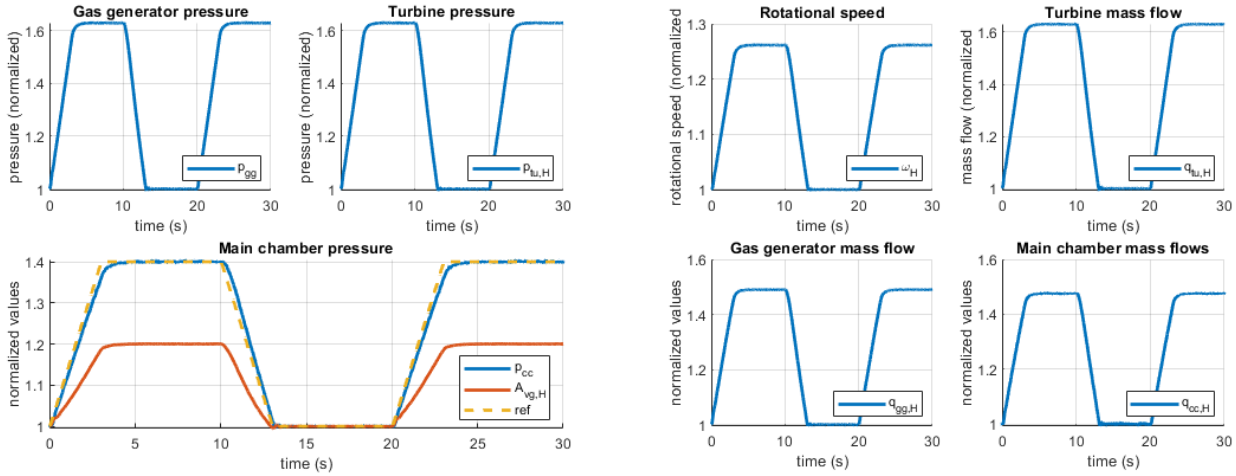

(a) Pressure behavior

(b) Mass flow behavior

Figure 6.20 – Real-life scenario using the contractive controller and a second-order actuator

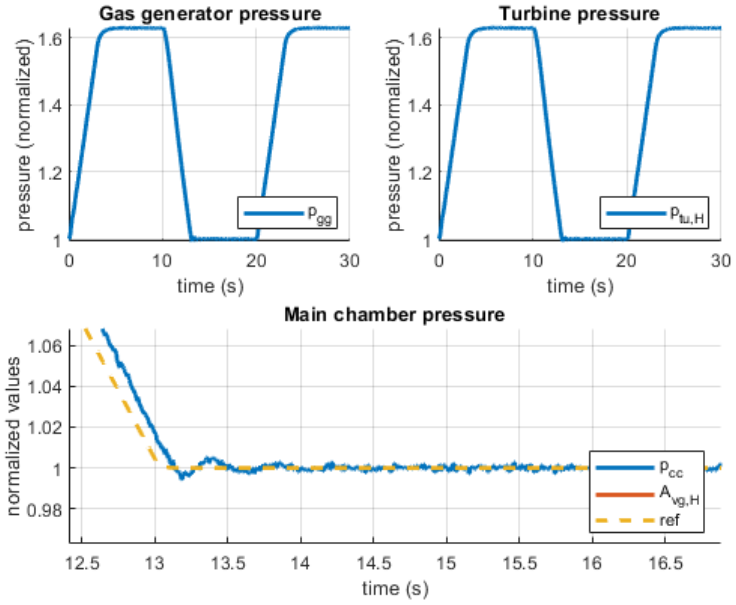

Figure 6.21 – Zoom on oscillations dissipation of the contracting controller

CONTROLLER	Stability	Delay	Oscillations	Noise rejection
PI	None	Low	High	None
PBC	Passive / Extension of the passive domain	High	On the actuator	No noise rejection
CON	Contraction region / Barrier function	Low	For low values	Decrease of 30%

Table 6.4 – Summary of the controllers used

6.4 . Summary

In this chapter, the comparison between the state-space simulations of the system and the Port-Hamiltonian modeling has been presented. The Port-Hamiltonian model allows for an efficient stability analysis, and the prediction for the unstable domain of the system is proven using state-space simulations. The simulations of the Hamiltonian model in permanent regime show a nearly identical behavior to that of the state-space, validating the reformulation of the model. Although some differences can be noticed where the Port-Hamiltonian model takes a longer time to reach the initial equilibrium, due to computation artifacts remaining, the simulation can simply be taken from when the equilibrium has settled.

In a second section, the two controllers proposed are compared with a classical controller (PI), to illustrate the strategies when dealing with unstable references. While the PI controller is unable to maintain stability during the unstable transition, both controllers are able to **remain stable** and end the simulation.

The PBC controller extends the stable region of the system, by design of the new resistive terms in the matrix R_d. Such terms can furthermore be tuned, for improved performances and extend again the stable zone.

The contracting controller acts as a barrier function to reject the unstable domain of the system and remain in the contraction region. It proves to be a powerful tool to stabilize a system, with a low computation time and is very adapted to trajectory tracking, with better performances than the PBC controller.

Finally, both controllers are paired with real actuators dynamics, that add a second-order system to the equations. Such addition requires the proper tuning of the controllers, as the slow response of the actuators has to be taken into account in the design. Simulations of the controllers with realistic state transitions illustrate that both controllers are able to perform with the actuator's dynamics, added noise, and maintain stability. Characteristics of the controllers are briefly recalled in table 6.4.

In summary, the controllers both provide a stable closed-loop in the domain considered. The PBC controller is more adapted to use when dealing with simple transitions between operating points, and delivers a better understanding of the stability conditions provided to the system, namely with a storage function for the passivity of the system. The contracting controller has better performances in trajectory tracking, as it is able to follow more closely a trajectory with a simple reference (whereas to obtain the

same performances, the PBC controller requires a greater integrator).

7 - Conclusion and perspectives

7.1 . Conclusion

This thesis aims to provide tools and methods to assert the stability of a non-linear model of the permanent regime of a reusable LPRE in closed-loop regulation. This objective has been translated into a study of the stability of the system in open-loop to derive stability conditions for a controller design and in a second part, in the design of controllers that provide stability guarantees to the closed-loop system. The state of the art of the stability of LPRE systems has been reviewed in chapter 1. Namely, the field of reusable stages for rockets introduced new requirements, mainly an increase in the range of variation of the thrust produced by the engine. In the literature, closed-loop controllers mainly consist in a regulation designed around a linearized operating point of the system. Robust control also constitutes an important field of the literature, which is aimed at being tolerant of uncertainties and faulty scenarios. An important aspect of reusable technology relies on damage-mitigation control, which consists in the implementation of control policies that minimize the damage caused to the engine during the functioning. However, these approaches seldom account for the stability of the system, and there is a lack of a formal stability analysis of an LPRE in the literature.

In the first place, the state-space modeling of an LPRE is considered. Two distinct models are developed to this end in chapter 2, a simplified model which consists in a moto-pump cycle. This cycle enables to perform stability analysis while considering a reduced number of states, drastically reducing the complexity. A second model, consisting in a gas generator cycle of an LPRE, presents an increase in complexity. The objective of these two models is to demonstrate the versatility of the methods by developing them on both systems. Although convenient for modeling and simulations, a state-space model proves to be a complex approach for stability analysis. The formulation of the states evolution and the poor conditioning of the linearized matrices illustrate the difficulties encountered when trying to derive a Lyapunov function for example. A conclusion to this is the requirement for a reformulation of the state-spaces considered.

The reformulation of the states under a form more adapted to stability analysis is performed, using the Port-Hamiltonian framework. In chapter 3, the formulation of both the simplified and complex systems is carried out. To respect the particular structure of Port-Hamiltonian systems, conditions on the approximations performed in the modeling (chapter 2) can be derived. The first consequences concern the polynomial approximations, where conditions on the construction of such polynomial functions can be stated. Port-Hamiltonian systems enable to prove the passivity of the simplified system, using a storage function. In order to prove the stability of the complex system, further considerations are required. This formal proof of stability and reformulation has been described in [47]. The complex model, however, requires the addition of a controller to respect the Port-Hamiltonian modeling.

To assert the passivity of the complex system around a chosen operating point, a controller is developed. To make use of the passivity properties of the system, a passivity base controller (PBC) is chosen

in chapter 4. The design of the controller is first carried out on the simplified system. In order to compute the controller for the complex system of the LPRE, the notion of damping assignment is introduced, where a new closed-loop behavior of the system is chosen. The PBC controller defines an equilibrium as asymptotically stable and constitutes an important result of the stability in closed-loop control. This type of controller however is more adapted to simple transitions between operating points and decreases in performance when designed for trajectory tracking.

To perform more complex maneuvers, the thrust of the engine is required to follow more complex trajectories. To study the stability with respect to a trajectory rather than an equilibrium, contraction theory is presented in chapter 5. Contraction theory is a powerful tool that is used to prove the exponential stability of a system, which is more powerful than asymptotic stability. This however implies more conditions on the system behavior to fulfill. Similarly to the PBC approach, a contracting controller, a controller that imposes a contracting behavior to the closed-loop system is developed. A first approach is carried out on the simplified system, where it is proven that a simple LMI design is sufficient to design such a controller. This work has been summarized in [46]. To perform the design on a complex model, additional considerations are required and a generalization of the method on more complex non-linear systems has been developed. This application has been published in [49].

A comparison of the different modeling methods is performed in chapter 6. Simulations are performed to compare the behavior of both modelings, Port-Hamiltonian and state-space. Results show that the differences in the numerical values for both modelings (settling time, final value) are negligible, validating the Port-Hamiltonian approach. Simulations however highlight the differences in the implementation under *Matlab Simulink*, of both models. While requiring an additional block to simulate the components required to build the system equations, Port-Hamiltonian modeling proves to have better simulation performances, with the possibility of using reduced time-steps compared to the state-space approach. However, Port-Hamiltonian modeling requires additional considerations when modeling noise on the system, and proves to have a starting dynamic different from the state-space, due to differences in the initialization process.

A comparison of the regulation methods in closed-loop control is proposed, where the stabilizing properties of the controllers is compared with an unstable PI controller. The PBC approach provides a stabilization by extension of the stability domain, where the modification of the closed-loop behavior and in particular the damping allows to extend the domain of validity. On the other hand, the contracting controller proves to act as a barrier function when near the unstable zone and maintains the system in a certain region, designated by the contraction region.

The addition of actuator dynamics defines a second phase of the controller's validation. With second-order dynamics, the actuators add a new constraint of tunability and feasibility to the controller outputs. Previous tests with different parameters allow to determine suitable tuning for both the PBC and contracting controllers.

Finally, the tracking performances on longer scenarios are asserted, with the actuator dynamics and noise perturbation. In this type of simulation, the contracting controller proves to be a more precise and reliable option than the PBC controller.

7.2 . Perspectives

The continuation of this work is possible in the control theory field, with some remarks previously made, that are recalled here. The controllers developed in this thesis share the common structure of a state feedback controller. While being an efficient approach for stability, feedback controllers require the values of the state to be computed. This brings the issue of measurements of the states, for which no solution is provided as of today. Indeed, while states like the rotational speeds of the pumps are well measured during the operation of the engine, the chamber temperatures, pressures, or mixture ratios have no technological solution that allows to measure the state in a real system.

With the objective of conserving the controller structures developed in this thesis, observers can be developed to answer the problem of state measurements. In this case, observers which conserve the contraction properties of a system. Such observers have been recently developed in the literature, with two interesting applications in the scope of this work,

- The use of contraction theory to develop observers, with proof of convergence [96, 97, 98].
- The use of contraction theory on observers, to induce contracting behavior to the loop with observers [99, 100].

Similarly, observer design for Port-Hamiltonian systems has been studied in the literature [101], leading to new possibilities on the observer designs for the LPRE.

In the wake of new technologies for control, and in particular AI-related controllers, the proof of convergence becomes a much-needed requirement for the validation of complex controllers. An extension of the results proposed in this thesis can be studied for these new controllers, and in particular, the notion of contraction when dealing with AI generation mechanisms. Indeed, contraction theory has been considered in the literature to assert the convergence of algorithms and proves to be a powerful tool to qualify AI results [102]. Such a tool can be of great importance to assert the stability of already performing controllers [16]. In this sense, the contraction behavior is used to prove the convergence of the neural networks that generate the controller.

Another aspect of the continuation of this work relies on the Port-Hamiltonian framework used. While the Port-Hamiltonian reformulation has been conducted using the state-space model, several approximations have already been made to fit the state-space. However, these simplifications (namely the turbo pump polynomial functions) lead to more complex interconnections to obtain the formulation. These additional steps allow to formulate qualitative remarks on the approximations. Namely, an approximation can be deemed favorable to stability analysis if all the residual terms are negative, and correspond to energy dissipation. In this sense, a direct formulation of the dynamics under Port-Hamiltonian framework is interesting, as it implies new polynomial approximations more adapted to the study. The framework can also be used to explore other cycles for an LPRE, for example, the expander cycle which requires a more thorough expression of the thermic transfers between the chamber walls and the regenerative circuit.

APPENDIX A : Complete Port-Hamiltonian system

$$\begin{bmatrix} \alpha_{q,H} J_H \dot{\omega}_H \\ \alpha_{q,O} J_O \dot{\omega}_O \\ I_{cc,H} \dot{q}_{cc,H} \\ I_{cc,O} \dot{q}_{cc,O} \\ I_{gg,H} \dot{q}_{gg,H} \\ I_{gg,O} \dot{q}_{gg,O} \\ I_{tu,H} \kappa_{tu} \dot{q}_{tu,H} \\ I_{tu,O} \kappa_{tu} \dot{q}_{tu,O} \\ k_{pcc} \dot{p}_{cc} \\ k_{pgg} \dot{p}_{gg} \\ k_{ptu,H} \dot{p}_{tu,H} \\ k_{ptu,O} \dot{p}_{tu,O} \end{bmatrix} = \big[J(X) - R(X) \big] \begin{bmatrix} \omega_H \\ \omega_O \\ q_{cc,H} \\ q_{cc,O} \\ q_{gg,H} \\ q_{gg,O} \\ q_{tu,H} \\ q_{tu,O} \\ p_{cc} \\ p_{gg} \\ p_{tu,H} \\ p_{tu,O} \end{bmatrix} + \begin{bmatrix} 0 \\ 0 \\ p_{ep,H} \\ p_{ep,O} \\ p_{ep,H} \\ p_{ep,O} \\ 0 \\ 0 \\ 0 \\ 0 \\ 0 \\ 0 \end{bmatrix} \tag{7.1}$$

where the storage matrix is

$$J(X) = \begin{bmatrix} 0 & 0 & -\lambda_H & 0 & -\lambda_H & 0 & 0 & 0 & 0 & 0 & \alpha_{t,H} & 0 \\ 0 & 0 & 0 & -\lambda_O & 0 & -\lambda_O & 0 & 0 & 0 & 0 & 0 & \alpha_{t,O} \\ \lambda_H & 0 & 0 & 0 & 0 & 0 & 0 & 0 & -1 & 0 & 0 & 0 \\ 0 & \lambda_O & 0 & 0 & 0 & 0 & 0 & 0 & -1 & 0 & 0 & 0 \\ \lambda_H & 0 & 0 & 0 & 0 & 0 & 0 & 0 & 0 & -1 & 0 & 0 \\ 0 & \lambda_O & 0 & 0 & 0 & 0 & 0 & 0 & 0 & -1 & 0 & 0 \\ 0 & 0 & 0 & 0 & 0 & 0 & 0 & 0 & 0 & \kappa_{tu} & -\kappa_{tu} & 0 \\ 0 & 0 & 0 & 0 & 0 & 0 & 0 & 0 & 0 & \kappa_{tu} & 0 & -\kappa_{tu} \\ 0 & 0 & 1 & 1 & 0 & 0 & 0 & 0 & 0 & 0 & 0 & 0 \\ 0 & 0 & 0 & 0 & 1 & 1 & -\kappa_{tu} & -\kappa_{tu} & 0 & 0 & 0 & 0 \\ -\alpha_{t,H} & 0 & 0 & 0 & 0 & 0 & \kappa_{tu} & 0 & 0 & 0 & 0 & 0 \\ 0 & -\alpha_{t,O} & 0 & 0 & 0 & 0 & 0 & \kappa_{tu} & 0 & 0 & 0 & 0 \end{bmatrix}, \tag{7.2}$$

and the resistive matrix is

$$R(X) = diag([R_{\omega,H} \quad R_{omega,O} \quad R_{qcc,H} \quad R_{qcc,O} \quad R_{qgg,H} \quad R_{qgg,O} \quad R_{qtu,H} \quad R_{qtu,O} \quad R_{pcc} \quad R_{pgg} \quad R_{ptu,H} \quad R_{ptu,O}]).$$

The terms of the matrix J read

$$
\begin{aligned}
\lambda_H &= b_{p,H}(q_{cc,H} + q_{gg,H}) \\
\lambda_O &= b_{p,O}(q_{cc,O} + q_{gg,O}) \\
\kappa_{tu} &= k_{3gg}\sqrt{\Theta_{gg}}k_{gg} \\
k_{ptu,H} &= \frac{\kappa_{tu}}{k_{2tu,H}\Theta_{gg}} \\
k_{ptu,O} &= \frac{\kappa_{tu}}{k_{2tu,O}\Theta_{gg}} \\
k_{pcc} &= \frac{1}{(k_{4cc} + k_{5cc} + (k_{2cc} - k_{1cc})\Theta_{cc})} \\
k_{pgg} &= \frac{1}{(k_{4gg} + k_{5gg} + (k_{2gg} - k_{1gg})\Theta_{gg})} \\
\alpha_{q,H} &= \frac{b_{p,H}\rho_H}{a_{c,H}} \\
\alpha_{q,O} &= \frac{b_{p,O}\rho_O}{a_{c,O}} \\
\alpha_{t,H} &= \alpha_{q,H}ST_H(\omega_H)w_{tu,H} \\
\alpha_{t,O} &= \alpha_{q,O}ST_O(\omega_O)w_{tu,O}
\end{aligned}
\tag{7.3}
$$

And the resistive terms composing the matrix R are expressed as

$$
\begin{aligned}
R_{\omega,H} &= \alpha_{q,H}(b_{c,H}(q_{cc,H} + q_{gg,H}) - c_{c,H}\rho_H\omega_H) \\
R_{\omega,O} &= \alpha_{q,O}(b_{c,O}(q_{cc,O} + q_{gg,O}) - c_{c,O}\rho_O\omega_O) \\
R_{qcc,H} &= Z_{rescc,H}q_{cc,H} - \frac{a_{p,H}}{\rho_H}(q_{cc,H} + q_{gg,H}) - c_{p,H}\rho_H\frac{\omega_H^2}{q_{cc,H}} \\
R_{qcc,O} &= Z_{rescc,O}q_{cc,O} - \frac{a_{p,O}}{\rho_O}(q_{cc,O} + q_{gg,O}) - c_{p,O}\rho_O\frac{\omega_O^2}{q_{cc,O}} \\
R_{qgg,H} &= Z_{resgg,H}q_{gg,H} - \frac{a_{p,H}}{\rho_H}(q_{cc,H} + q_{gg,H}) - c_{p,H}\rho_H\frac{\omega_H^2}{q_{gg,H}} \\
R_{qgg,O} &= Z_{resgg,O}q_{gg,O} - \frac{a_{p,O}}{\rho_O}(q_{cc,OH} + q_{gg,O}) - c_{p,O}\rho_O\frac{\omega_O^2}{q_{gg,O}} \\
R_{qtu,H} &= \kappa_{tu}Z_{resqtu,H}q_{tu,H} \\
R_{qtu,H} &= \kappa_{tu}Z_{resqtu,O}q_{tu,O} \\
R_{pcc} &= k_{3cc}\sqrt{\Theta_{cc}}k_{pcc} \\
R_{pgg} &= 0 \\
R_{ptu,H} &= \beta_{t,H} \\
R_{ptu,O} &= \beta_{t,O}
\end{aligned}
\tag{7.4}
$$

APPENDIX B : Complex PBC design with $R_a(x) \neq 0$

The complex PDE with a non zero matrix R_a is given by the following :

$$
\begin{aligned}
-R_{\omega}\frac{\partial H_a}{\partial(\alpha_q J\omega)} + \alpha_t\frac{\partial H_a}{\partial(k_{ptu}p_{tu})} - \lambda\frac{\partial H_a}{\partial(I_{cc}q_{cc})} - \lambda\frac{\partial H_a}{\partial(I_{gg}q_{gg})} - R_{a,\omega}(\frac{\partial H_a}{\partial(\alpha_q J\omega)} - \omega) = 0 \\
-R_{qcc}\frac{\partial H_a}{\partial(I_{cc}q_{cc})} + \lambda\frac{\partial H_a}{\partial(\alpha_q J\omega)} - \frac{\partial H_a}{\partial(k_{pcc}p_{cc})} - R_{a,qcc}(\frac{\partial H_a}{\partial(I_{cc}q_{cc})} - q_{cc}) = 0 \\
-R_{qtu}\frac{\partial H_a}{\partial(I_{tu}q_{tu})} + \kappa_{tu}\frac{\partial H_a}{\partial(k_{pgg}p_{gg})} - \kappa_{tu}\frac{\partial H_a}{\partial(k_{ptu}p_{tu})} - R_{a,qtu}(\frac{\partial H_a}{\partial(I_{tu}q_{tu})} - q_{tu}) = 0 \\
-R_{pcc}\frac{\partial H_a}{\partial(k_{pcc}p_{cc})} + \frac{\partial H_a}{\partial(I_{cc}q_{cc})} - R_{a,pcc}(\frac{\partial H_a}{\partial(k_{pcc}p_{cc})} - p_{cc}) = 0 \\
-R_{pgg}\frac{\partial H_a}{\partial(k_{pgg}p_{gg})} + \frac{\partial H_a}{\partial(I_{gg}q_{gg})} - \kappa_{tu}\frac{\partial H_a}{\partial(I_{tu}q_{tu})} - R_{a,pgg}(\frac{\partial H_a}{\partial(k_{pgg}p_{gg})} - p_{gg}) = 0 \\
-R_{ptu}\frac{\partial H_a}{\partial(k_{ptu}p_{tu})} + \kappa_{tu}\frac{\partial H_a}{\partial(I_{tu}q_{tu})} - \alpha_t\frac{\partial H_a}{\partial(\alpha_q J\omega)} - R_{a,ptu}(\frac{\partial H_a}{\partial(k_{ptu}p_{tu})} - p_{tu}) = 0
\end{aligned}
\tag{7.5}
$$

The controller expression as obtained in *Maple* is then given in the following pages, where the simplifications on R_a have been performed.

$$
\begin{aligned}
u = \\
&[-((-R_\omega + R_{pcc})R_{a,qtu} + {\alpha_t}^2 + (R_{qtu} + 1)(R_\omega - R_{pcc}))\, q_{tu,0}\, (-\lambda\, \alpha t - R_{pcc} + R_\omega)\kappa^5 \\
&+ (((Q_{qgg} - 1)(p_{cc,0} - p_{cc})\lambda^4 - (Q_{qgg} - 1)(\omega - \omega_0)\lambda^3 + (R_{pcc}\, (p_{cc,0} - p_{cc}) + ((p_{cc,0} - p_{cc})R_{a,qgg} - q_{gg,0} + q_{gg}) \\
&(Q_{qgg} - 1))(R_\omega - R_{pcc})\lambda^2 + ((p_{gg} - p_{gg,0})\alpha_t - \omega\, R_{pcc} + R_\omega\, \omega_0 - R_{a,qgg}\, (Q_{qgg} - 1)(\omega - \omega_0))(R_\omega - R_{pcc})\lambda - \\
&(R_\omega - R_{pcc})^2(R_{a,qgg}\, (q_{gg,0} - q_{gg})\, Q_{qgg} + R_{qgg}\, q_{gg} + p_{gg}))R_{a,qtu}{}^2 + (-2\, (Q_{qgg} - 1)(R_{qtu} + R_{a,ptu}/2 + 1/2) \\
&(p_{cc,0} - pc)\lambda^4 + 2\, (Q_{qgg} - 1)((p_{cc,0}/2 + p_{gg,0}/2 + p_{tu,0}/2 - p_{cc}/2 - p_{gg}/2 - p_{tu}/2)\alpha_t + (\omega - \omega_0) \\
&(R_{qtu} + R_{a,ptu}/2 + 1/2))\lambda^3 \\
&+ (((p_{cc} - p_{cc,0})R_{pcc} - ((p_{cc,0} - p_{cc})R_{a,qgg} - q_{gg,0} + q_{gg})(Q_{qgg} - 1))\alpha_t{}^2 - (Q_{qgg} - 1)(\omega - \omega_0)\alpha_t - 2 \\
&(((p_{cc,0}/2 - p_{cc}/2)R_{pcc} + 1/2\, ((p_{cc,0} - p_{cc})R_{a,qgg} - q_{gg,0} + q_{gg})(Q_{qgg} - 1))R_{a,ptu} + (R_{pcc}\, (p_{cc,0} - p_{cc}) \\
&+ ((p_{cc,0} - p_{cc})R_{a,qgg} - q_{gg,0} + q_{gg})(Q_{qgg} - 1))R_{qtu} + (p_{cc,0}/2 - p_{cc}/2)R_{pcc} + 1/2\, (Q_{qgg} - 1)((p_{cc,0} - p_{cc}) \\
&R_{a,qgg} + p_{cc,0} - p_{gg,0} - p_{tu,0} - q_{gg,0} \\
&- p_{cc} + p_{gg} + p_{tu} + q_{gg}))(R_\omega - R_{pcc}))\lambda^2 + ((p_{gg,0} - p_{gg})\alpha_t{}^3 + (\omega\, R_{pcc} - R_\omega\, \omega_0 + R_{a,qgg}\, (Q_{qgg} - 1) \\
&(\omega - \omega_0))\alpha_t{}^2 + ((p_{tu,0} - p_{tu})R_{a,ptu} + (2\, p_{gg,0} - 2\, p_{gg})R_{qtu} + (p_{cc} - p_{cc,0})R_{pcc} + R_{a,qgg} \\
&(p_{cc,0} + p_{gg,0} + p_{tu,0} - p_{cc} - p_{gg} - p_{tu})\, Q_{qgg} + (-p_{cc,0} - p_{gg,0} - p_{tu,0} + p_{cc} + p_{gg} + p_{tu}) \\
&R_{a,qgg} + R_{ptu}\, p_{tu} + p_{gg,0} - p_{gg})(R_\omega - R_{pcc})\alpha t - 2 \\
&((-1/2\, \omega\, R_{pcc} + 1/2\, R_\omega\, \omega_0 - 1/2\, R_{a,qgg}\, (Q_{qgg} - 1)(\omega - \omega_0))R_{a,ptu} + (-\omega\, R_{pcc} + R_\omega\, \omega_0 - R_{a,qgg} \\
&(Q_{qgg} - 1)(\omega - \omega_0))R_{qtu} - 1/2\, \omega\, R_{pcc} + 1/2\, R_\omega\, \omega_0 - 1/2\, (Q_{qgg} - 1)(\omega - \omega_0) \\
&(R_{a,qgg} + 1))(R_\omega - R_{pcc}))\lambda - ((-2\, R_{a,qgg}\, (q_{gg,0} - q_{gg})\, Q_{qgg} - 2 \\
&R_{qgg}\, q_{gg} - p_{gg,0} - p_{gg})\alpha_t{}^2 + (-\omega\, R_{pcc} + R_\omega\, \omega_0 + R_{a,qgg} \\
&(Q_{qgg} - 1)(\omega - \omega_0))\alpha_t + (R_\omega - R_{pcc})((-R_{a,qgg}\, (q_{gg,0} - q_{gg})\, Q_{qgg} - R_{qgg}\, q_{gg} \\
&- p_{gg,0} + p_{tu,0} - p_{tu})R_{a,ptu} + (-2\, R_{a,qgg}\, (q_{gg,0} - q_{gg})\, Q_{qgg} - 2\, R_{qgg}\, q_{gg} - 2\, p_{gg})R_{qtu} \\
&+ ((-p_{gg,0} - p_{tu,0} - q_{gg,0} + p_{gg} + p_{tu} + q_{gg})R_{a,qgg} - q_{gg,0} + q_{gg})\, Q_{qgg} \\
&+ (p_{gg,0} + p_{tu,0} - p_{gg} - p_{tu})R_{a,qgg} + (-R_{qgg} - 1)q_{gg} + R_{ptu}\, p_{tu} + q_{gg,0} - p_{gg})) \\
&(R_\omega - R_{pcc}))R_{a,qtu} + (Q_{qgg} - 1)(R_{qtu} + 1)(R_{qtu} + R_{a,ptu})(p_{cc,0} - p_{cc})\lambda^4 - (R_{qtu} + R_{a,ptu}) \\
&(Q_{qgg} - 1)((p_{cc,0} + p_{gg,0} + p_{tu,0} - p_{cc} - p_{gg} - p_{tu})\alpha_t + (\omega - \omega_0)(R_{qtu} + 1))\lambda^3 + \\
&(((R_{pcc}\, (p_{cc,0} - p_{cc}) - (Q_{qgg} - 1)(q_{gg,0} - q_{gg}))R_{a,ptu} + (R_{pcc} \\
&(p_{cc,0} - p_{cc}) + ((p_{cc,0} - p_{cc})R_{a,qgg} - q_{gg,0} + q_{gg})(Q_{qgg} - 1))R_{qtu} + R_{a,qgg}\, (Q_{qgg} - 1) \\
&(p_{cc,0} - p_{cc}))\alpha_t{}^2 + (Q_{qgg} - 1)(\omega - \omega_0)(R_{qtu} + R_{a,ptu})\alpha_t + (((R_{pcc} \\
&(p_{cc,0} - p_{cc}) + ((p_{cc,0} - p_{cc})R_{a,qgg} - q_{gg,0} + q_{gg})(Q_{qgg} - 1))R_{qtu} + R_{pcc}\, (p_{cc,0} - p_{cc}) \\
&+ ((p_{cc,0} - p_{cc})R_{a,qgg} - p_{gg,0} - p_{tu,0} - q_{gg,0} + p_{gg} + p_{tu} + q_{gg})(Q_{qgg} - 1)) \\
&R_{a,ptu} + (R_{pcc}\, (p_{cc,0} - p_{cc}) + ((p_{cc,0} - p_{cc})R_{a,qgg} - q_{gg,0} + q_{gg})(Q_{qgg} - 1))R_{qtu}{}^2 + (R_{pcc}\, (p_{cc,0} - p_{cc}) + (Q_{qgg} \\
&- 1)((p_{cc,0} - p_{cc})R_{a,qgg} + p_{cc,0} - p_{gg,0} - p_{tu,0} - q_{gg,0} - p_{cc} + p_{gg} + p_{tu} + q_{gg}))R_{qtu} + (Q_{qgg} - 1)(p_{cc,0} - p_{cc})) \\
&(R_\omega - R_{pcc}))\lambda^2 + (((p_{tu} - p_{tu,0})R_{a,ptu} + (p_{gg} - p_{gg,0})R_{qtu}
\end{aligned}
$$

$$
+ R_{pcc}\,(p_{cc,0} - p_{cc}) - R_{a,qgg}\,(p_{cc,0} + p_{gg,0} + p_{tu,0} - p_{cc} - p_{gg} - p_{tu})\,Q_{qgg} + R_{a,qgg}
$$
$$
(p_{cc,0} + p_{gg,0} + p_{tu,0} - p_{cc} - p_{gg} - p_{tu}) - R_{ptu}\,p_{tu})\alpha_t{}^3 + ((-\omega\,R_{pcc} + R_\omega\,\omega_0)R_{a,ptu}
$$
$$
+ (-\omega\,R_{pcc} + R_\omega\,\omega 0 - R_{a,qgg}\,(Q_{qgg} - 1)
$$
$$
(\omega - \omega_0))R_{qtu} - R_{a,qgg}\,(Q_{qgg} - 1)(\omega - \omega_0))\alpha_t{}^2 - (((p_{tu,0} - p_{tu})R_{qtu} + R_{a,qgg}\,(p_{cc,0}
$$
$$
+ p_{gg,0} + p_{tu,0} - p_{cc} - p_{gg} - p_{tu})\,Q_{qgg} + (-p_{cc,0} - p_{gg,0} - p_{tu,0} + p_{cc} + p_{gg} + p_{tu})R_{a,qgg} + p_{tu,0} - p_{tu})
$$
$$
R_{a,ptu} + (p_{gg,0} - p_{gg})R_{qtu}{}^2 + ((p_{cc} - p_{cc,0})R_{pcc} + R_{a,qgg}\,(p_{cc,0} + p_{gg,0} + p_{tu,0} - p_{cc} - p_{gg} - p_{tu})
$$
$$
Q_{qgg} + (-p_{cc,0} - p_{gg,0} - p_{tu,0} + p_{cc} + p_{gg} + p_{tu})R_{a,qgg} + R_{ptu}\,p_{tu} + p_{gg,0} - p_{gg})R_{qtu}
$$
$$
+ (p_{cc} - p_{cc,0})R_{pcc} + (p_{cc,0} + p_{gg,0} + p_{tu,0} - p_{cc} - p_{gg} - p_{tu})\,Q_{qgg} + p_{gg} - p_{cc,0} + p_{cc} - p_{gg,0}
$$
$$
+ (R_{ptu} + 1)p_{tu} - p_{tu,0})(R_\omega - R_{pcc})\alpha_t + (R_\omega - R_{pcc})((-\omega\,R_{pcc} + R_\omega\,\omega_0 - R_{a,qgg}
$$
$$
(Q_{qgg} - 1)(\omega - \omega_0))R_{a,ptu} + (-\omega\,R_{pcc} + R_\omega\,\omega_0 - R_{a,qgg}\,(Q_{qgg} - 1)(\omega - \omega_0))R_{qtu} - (Q_{qgg} - 1)(\omega - \omega_0))
$$
$$
(R_{qtu} + 1))\lambda + (-R_{a,qgg}\,(q_{gg,0} - q_{gg})\,Q_{qgg} - R_{qgg}\,q_{gg} - p_{gg,0})\alpha_t{}^4 +
$$
$$
(-\omega\,R_{pcc} + R_\omega\,\omega_0 + R_{a,qgg}\,(Q_{qgg} - 1)(\omega - \omega_0))\alpha_t{}^3 + (R_\omega - R_{pcc})
$$
$$
((-R_{a,qgg}\,(q_{gg,0} - q_{gg})\,Q_{qgg} - R_{qgg}\,q_{gg} - p_{gg,0} + p_{tu,0} - p_{tu})R_{a,ptu}
$$
$$
+ (-2\,R_{a,qgg}\,(q_{gg,0} - q_{gg})\,Q_{qgg} - 2\,R_{qgg}\,q_{gg} - p_{gg,0} - p_{gg})R_{qtu} + ((-p_{gg,0} - p_{tu,0} - q_{gg,0} + p_{gg} + p_{tu} + q_{gg})R_{a,qgg}
$$
$$
- q_{gg,0} + q_{gg})\,Q_{qgg} + (p_{gg,0} + p_{tu,0} - p_{gg} - p_{tu})R_{a,qgg} + (-R_{qgg} - 1)\,q_{gg} + R_{ptu}\,p_{tu} - p_{gg,0} + q_{gg,0})\alpha_t{}^2
$$
$$
+ (R_\omega - R_{pcc})(R_{a,qgg}\,(Q_{qgg} - 1)(\omega - \omega_0)R_{a,ptu} + (-\omega\,R_{pcc} + R_\omega\,\omega_0
$$
$$
+ R_{a,qgg}\,(Q_{qgg} - 1)(\omega - \omega_0))R_{qtu} - \omega\,R_{pcc} + R_\omega\,\omega_0 + (Q_{qgg} - 1)(\omega - \omega_0))\alpha_t +
$$
$$
(R_\omega - R_{pcc})^2(((-R_{a,qgg}\,(q_{gg,0} - q_{gg})\,Q_{qgg} - R_{qgg}\,q_{gg} - p_{gg,0} + p_{tu,0} - p_{tu})R_{qtu}
$$
$$
- R_{a,qgg}\,(p_{gg,0} + p_{tu,0} + q_{gg,0} - p_{gg} - p_{tu} - q_{gg})\,Q_{qgg}
$$
$$
+ (p_{gg,0} + p_{tu,0} - p_{gg} - p_{tu})R_{a,qgg} - R_{qgg}\,q_{gg} - p_{gg,0} + p_{tu,0} - p_{tu})R_{a,ptu} + (-R_{a,qgg}\,(q_{gg,0} - q_{gg})\,Q_{qgg}
$$
$$
- R_{qgg}\,q_{gg} - p_{gg})R_{qtu}{}^2 + (((-p_{gg,0} - p_{tu,0} - q_{gg,0} + p_{gg} + p_{tu} + q_{gg})R_{a,qgg} - q_{gg,0} + q_{gg})\,Q_{qgg}
$$
$$
+ (p_{gg,0} + p_{tu,0} - p_{gg} - p_{tu})R_{a,qgg} + (-R_{qgg} - 1)\,q_{gg} + R_{ptu}\,p_{tu} + q_{gg,0} - p_{gg})R_{qtu}
$$
$$
+ (-p_{gg,0} - p_{tu,0} - q_{gg,0} + p_{gg} + p_{tu} + q_{gg})\,Q_{qgg} - q_{gg} - p_{gg} + q_{gg,0} + p_{gg,0} + (R_{ptu} - 1)p_{tu} + p_{tu,0}))\kappa^4
$$
$$
+ (\lambda\,\alpha_t\,q_{tu}\,(R_\omega - R_{pcc})R_{a,qtu}{}^3 + (\lambda^3(Q_{qgg} - 1)(q_{tu,0} - q_{tu})\alpha t + ((-q_{tu,0} - q_{tu})\alpha_t{}^2 + (R_\omega - R_{pcc})
$$
$$
((q_{tu,0} - 3\,q_{tu})R_{qtu} + R_{a,qgg}\,(q_{tu,0} - q_{tu})\,Q_{qgg} + (q_{tu} - q_{tu,0})R_{a,qgg} - q_{tu,0} - q_{tu}))\alpha_t\,\lambda
$$
$$
+ (R_\omega - R_{pcc})((2\,q_{tu,0} - q_{tu})\alpha_t{}^2 + (R_\omega - R_{pcc})(R_{a,ptu}\,(q_{tu,0} - q_{tu}) + q_{tu,0})))R_{a,qtu}{}^2
$$
$$
+ (-2\,\lambda^3(q_{tu,0} - q_{tu})(Q_{qgg} - 1)(R_{qtu} + R_{a,ptu}/2)\alpha_t + (Q_{qgg} - 1)(q_{tu,0} - q_{tu})(\alpha_t{}^2 - R_{pcc} + R_\omega)\lambda^2
$$
$$
- 2\,\alpha_t\,((-R_{qtu}\,q_{tu} + 1/2\,R_{a,qgg}\,(Q_{qgg} - 1)
$$
$$
(q_{tu,0} - q_{tu}))\alpha_t{}^2 + (1/2\,R_{a,qgg}\,(Q_{qgg} - 1)(q_{tu,0} - q_{tu})R_{a,ptu} + (q_{tu,0} - 3/2\,q_{tu})R_{qtu}{}^2 + (R_{a,qgg}\,(q_{tu,0} - q_{tu})
$$
$$
Q_{qgg} + (q_{tu} - q_{tu,0})R_{a,qgg} - q_{tu})R_{qtu} + 1/2\,(Q_{qgg} - 1)(q_{tu,0} - q_{tu}))(R_\omega - R_{pcc}))\lambda
$$
$$
+ (q_{tu} - q_{tu,0})\alpha_t{}^4 - 3\,((q_{tu,0}/3 - q_{tu}/3)R_{a,ptu} + (q_{tu,0} - 2/3\,q_{tu})R_{qtu}
$$
$$
- 1/3\,(R_{a,qgg}\,Q_{qgg} - R_{a,qgg} - 1)(q_{tu,0} - q_{tu}))
$$
$$
(R_\omega - R_{pcc})\alpha_t{}^2 - 2\,(R_\omega - R_{pcc})^2((R_{qtu} + 1/2)(q_{tu,0} - q_{tu})R_{a,ptu} + 1/2\,R_{qtu}\,q_{tu,0} - 1/2\,R_{a,qgg}
$$
$$
(Q_{qgg} - 1)(q_{tu,0} - q_{tu})))R_{a,qtu} + (R_{qtu}\,\lambda^3(Q_{qgg} - 1)(R_{qtu} + R_{a,ptu})\alpha_t
$$
$$
- (Q_{qgg} - 1)(R_{qtu} + R_{a,ptu})(\alpha_t{}^2 - R_{pcc} + R_\omega)\lambda^2 + R_{qtu}\,((R_{a,qgg}\,Q_{qgg} - R_{a,qgg} + R_{qtu})\alpha_t{}^2
$$
$$
+ (R_{a,qgg}\,(Q_{qgg} - 1)R_{a,ptu}
$$

$$
\begin{aligned}
&+ {R_{qtu}}^2 + (R_{a,qgg}\, Q_{qgg} - R_{a,qgg} + 1)R_{qtu} + Q_{qgg} - 1)(R_\omega - R_{pcc}))\alpha t\, \lambda + (-R_{a,qgg}\, Q_{qgg} + R_{a,qgg} + R_{qtu}){\alpha_t}^4 \\
&+ ((-R_{a,qgg}\, Q_{qgg} + R_{a,qgg} + R_{qtu})R_{a,ptu} + {R_{qtu}}^2 + (-R_{a,qgg}\, Q_{qgg} + R_{a,qgg} + 1)R_{qtu} - (Q_{qgg} - 1)(R_{a,qgg} + 1)) \\
&(R_\omega - R_{pcc}){\alpha_t}^2 + ((R_{qtu}{}^2 + R_{qtu} - R_{a,qgg}\,(Q_{qgg} - 1)) \\
&R_{a,ptu} - (Q_{qgg} - 1)(R_{qtu}\, R_{a,qgg} + 1))(R_\omega - R_{pcc})^2)(q_{tu,0} - q_{tu}))\kappa^3 \\
&+ (((Q_{qgg} - 1)(R_{a,ptu} + 1)(p_{cc,0} - p_{cc})\lambda^4 - (Q_{qgg} - 1)((p_{tu,0} - p_{tu})\alpha_t + (\omega - \omega_0)(R_{a,ptu} + 1))\lambda^3 \\
&+ ({\alpha_t}^2 + (R_{a,ptu} + 1)(R_\omega - R_{pcc}))(R_{pcc}\,(p_{cc,0} - p_{cc}) + ((p_{cc,0} - p_{cc})R_{a,qgg} - q_{gg,0} + q_{gg})(Q_{qgg} - 1))\lambda^2 \\
&+ ((p_{gg} - p_{gg,0}){\alpha_t}^3 + (-\omega\, R_{pcc} + R_\omega\, \omega_0 - R_{a,qgg}\,(Q_{qgg} - 1)(\omega - \omega_0))\alpha_t{}^2 \\
&- (R_\omega - R_{pcc})((p_{tu,0} - p_{tu})R_{a,ptu} + R_{a,qgg}\,(p_{tu,0} - p_{tu})Q_{qgg} + (p_{tu} - p_{tu,0})R_{a,qgg} + R_{ptu}\, p_{tu} + p_{gg,0} - p_{gg})\alpha_t \\
&+ (R_\omega - R_{pcc})(R_{a,ptu} + 1)(-\omega\, R_{pcc} + R_\omega\, \omega_0 - R_{a,qgg}\,(Q_{qgg} - 1)(\omega - \omega_0)))\lambda - (2\,{\alpha_t}^2 \\
&+ (R_{a,ptu} + 1)(R_\omega - R_{pcc}))(R_\omega - R_{pcc})(R_{a,qgg}\,(q_{gg,0} - q_{gg})Q_{qgg} + R_{qgg}\, q_{gg} + p_{gg}))R_{a,qtu}{}^2 \\
&+ (-2\,((R_{qtu} + 1)R_{a,ptu} + R_{qtu})(Q_{qgg} - 1)(p_{cc,0} - p_{cc})\lambda^4 \\
&+ 2\,(((p_{cc,0}/2 + p_{gg,0}/2 + p_{tu,0} - p_{cc}/2 - p_{gg}/2 - p_{tu})R_{a,ptu} + (p_{tu,0} - p_{tu})R_{qtu})\alpha_t \\
&+ ((R_{qtu} + 1)R_{a,ptu} + R_{qtu})(\omega - \omega_0)) \\
&(Q_{qgg} - 1)\lambda^3 + ((((-2\, p_{cc,0} + 2\, p_{cc})R_{pcc} + 2\,(Q_{qgg} - 1)(q_{gg,0} - q_{gg}))R_{a,ptu} \\
&+ ((-2\, p_{cc,0} + 2\, p_{cc})R_{pcc} - 2\,((p_{cc,0} - p_{cc})R_{a,qgg} - q_{gg,0} + q_{gg})(Q_{qgg} - 1))R_{qtu} - 2\,(Q_{qgg} - 1) \\
&((p_{cc,0} - p_{cc})R_{a,qgg} + p_{cc,0}/2 - p_{gg,0}/2 - p_{cc}/2 + p_{gg}/2))\alpha_t{}^2 \\
&- R_{a,ptu}\,(Q_{qgg} - 1)(\omega - \omega_0)\alpha_t - 2\,(R_\omega - R_{pcc})(((R_{pcc}\,(p_{cc,0} - p_{cc}) \\
&+ ((p_{cc,0} - p_{cc})R_{a,qgg} - q_{gg,0} + q_{gg})(Q_{qgg} - 1))R_{qtu} \\
&+ R_{pcc}\,(p_{cc,0} - p_{cc}) + (Q_{qgg} - 1)((p_{cc,0} - p_{cc})R_{a,qgg} \\
&+ p_{cc,0}/2 + p_{gg}/2 - p_{gg,0}/2 + p_{tu}/2 - p_{tu,0}/2 - p_{cc}/2 + q_{gg} - q_{gg,0}))R_{a,ptu} \\
&+ (R_{pcc}\,(p_{cc,0} - p_{cc}) + ((p_{cc,0} - p_{cc})R_{a,qgg} - q_{gg,0} + q_{gg})(Q_{qgg} - 1))R_{qtu} + 1/2\,(Q_{qgg} - 1) \\
&(p_{cc,0} - p_{gg,0} - p_{cc} + p_{gg})))\lambda^2 + (((2\, p_{tu,0} - 2\, p_{tu})R_{a,ptu} + (2\, p_{gg,0} - 2\, p_{gg})R_{qtu} + (p_{cc} - p_{cc,0})R_{pcc} + R_{a,qgg} \\
&(p_{cc,0} + p_{gg,0} + 2\, p_{tu,0} - p_{cc} - p_{gg} - 2\, p_{tu})Q_{qgg} + (-p_{cc,0} - p_{gg,0} - 2\, p_{tu,0} + p_{cc} + p_{gg} + 2\, p_{tu})R_{a,qgg} \\
&+ 2\, R_{ptu}\, p_{tu})\alpha_t{}^3 + ((2\,\omega\, R_{pcc} - 2\, R_\omega\, \omega_0)R_{a,ptu} + (2\,\omega\, R_{pcc} - 2\, R_\omega\, \omega_0 + 2\, R_{a,qgg}\,(Q_{qgg} - 1)(\omega - \omega_0))R_{qtu} \\
&+ 2\,(\omega - \omega_0)(Q_{qgg} - 1)(R_{a,qgg} + 1/2))\alpha_t{}^2 + 2\,(R_\omega - R_{pcc})(((p_{tu,0} - p_{tu}) \\
&R_{qtu} + 1/2\, R_{a,qgg}\,(p_{cc,0} + p_{gg,0} + 2\, p_{tu,0} - p_{cc} - p_{gg} - 2\, p_{tu})Q_{qgg} \\
&+ (p_{cc}/2 - p_{cc,0}/2 + p_{gg}/2 - p_{gg,0}/2 - p_{tu,0} + p_{tu})R_{a,qgg} + p_{tu,0} - p_{tu})R_{a,ptu} \\
&+ (R_{a,qgg}\,(p_{tu,0} - p_{tu})Q_{qgg} + (p_{tu} - p_{tu,0})R_{a,qgg} + R_{ptu}\, p_{tu} + p_{gg,0} - p_{gg})R_{qtu} + (-p_{cc,0}/2 \\
&+ p_{cc}/2)R_{pcc} + (p_{tu,0}/2 - p_{tu}/2)Q_{qgg} + (1/2 + R_{ptu})p_{tu} - p_{tu,0}/2)\alpha_t - 2\,(R_\omega - R_{pcc}) \\
&(((-\omega\, R_{pcc} + R_\omega\, \omega_0 - R_{a,qgg}\,(Q_{qgg} - 1)(\omega - \omega_0))R_{qtu} - \omega\, R_{pcc} \\
&+ R_\omega\, \omega_0 - (\omega - \omega_0)(Q_{qgg} - 1)(R_{a,qgg} + 1/2))R_{a,ptu} + (-\omega\, R_{pcc} + R_\omega\, \omega_0 \\
&- R_{a,qgg}\,(Q_{qgg} - 1)(\omega - \omega_0))R_{qtu} - 1/2\,(Q_{qgg} - 1)(\omega - \omega_0)))\lambda + (2\, R_{a,qgg}\,(q_{gg,0} - q_{gg})Q_{qgg} + 2\, R_{qgg}\, q_{gg} \\
&+ p_{gg,0} + p_{gg})\alpha_t{}^4 + (\omega\, R_{pcc} - R_\omega\, \omega_0 - R_{a,qgg}\,(Q_{qgg} - 1)(\omega - \omega_0))\alpha_t{}^3 \\
&- ((-2\, R_{a,qgg}\,(q_{gg,0} - q_{gg})Q_{qgg} \\
&- 2\, R_{qgg}\, q_{gg} - p_{gg,0} + p_{tu,0} - p_{gg} - p_{tu})R_{a,ptu} \\
&+ (-4\, R_{a,qgg}\,(q_{gg,0} - q_{gg})Q_{qgg} - 4\, R_{qgg}\, q_{gg} - 4\, p_{gg})R_{qtu}
\end{aligned}
$$

$$
\begin{aligned}
&+ ((-2\,p_{gg,0} - p_{tu,0} - 2\,q_{gg,0} + 2\,p_{gg} + p_{tu} + 2\,q_{gg})R_{a,qgg} - 2\,q_{gg,0} + 2\,q_{gg})\,Q_{qgg} \\
&+ (2\,p_{gg,0} + p_{tu,0} - 2\,p_{gg} - p_{tu})R_{a,qgg} + (-2\,R_{qgg} - 2)q_{gg} + R_{ptu}\,p_{tu} - p_{gg,0} + 2\,q_{gg,0} - p_{gg}) \\
&(R_\omega - R_{pcc})\alpha_t{}^2 - (R_{a,qgg}\,(Q_{qgg} - 1)(\omega - \omega_0)R_{a,ptu} + R_\omega\,\omega_0 - \omega\,R_{pcc})(R_\omega - R_{pcc})\alpha_t \\
&- (((-2\,R_{a,qgg}\,(q_{gg,0} - q_{gg})Q_{qgg} - 2\,R_{qgg}\,q_{gg} - 2\,p_{gg})R_{qtu} + ((-p_{gg,0} - p_{tu,0} - 2\,q_{gg,0} \\
&+ p_{gg} + p_{tu} + 2\,q_{gg})R_{a,qgg} - q_{gg,0} + q_{gg})\,Q_{qgg} + (p_{gg,0} + p_{tu,0} - p_{gg} - p_{tu})R_{a,qgg} + (-2\,R_{qgg} - 1)q_{gg} \\
&- p_{gg,0} + p_{tu,0} + q_{gg,0} - p_{gg} - p_{tu})R_{a,ptu} + (-2\,R_{a,qgg}\,(q_{gg,0} - q_{gg})\,Q_{qgg} \\
&- 2\,R_{qgg}\,q_{gg} - 2\,p_{gg})R_{qtu} + ((p_{gg} - p_{gg,0})R_{a,qgg} - q_{gg,0} + q_{gg})\,Q_{qgg} \\
&+ (p_{gg,0} - p_{gg})R_{a,qgg} + R_{ptu}\,p_{tu} + q_{gg,0} - q_{gg})(R_\omega - R_{pcc})^2)R_{a,qtu} + (Q_{qgg} - 1)R_{qtu} \\
&(p_{cc,0} - p_{cc})((R_{qtu} + 2)R_{a,ptu} + R_{qtu})\lambda^4 - (((p_{cc,0} + p_{gg,0} + 2\,p_{tu,0} - p_{cc} - p_{gg} \\
&- 2\,p_{tu})R_{a,ptu} + (p_{tu,0} - p_{tu})R_{qtu})\alpha_t + (\omega - \omega_0)((R_{qtu} + 2)R_{a,ptu} \\
&+ R_{qtu}))(Q_{qgg} - 1)R_{qtu}\,\lambda^3 + (((((2\,p_{cc,0} - 2\,p_{cc})R_{pcc} - 2\,(Q_{qgg} - 1) \\
&(q_{gg,0} - q_{gg}))R_{qtu} - (Q_{qgg} - 1)(p_{gg,0} - p_{gg}))R_{a,ptu} + (R_{pcc}\,(p_{cc,0} - p_{cc}) \\
&+ ((p_{cc,0} - p_{cc})R_{a,qgg} - q_{gg,0} + q_{gg})(Q_{qgg} - 1))R_{qtu}{}^2 + 2\,(Q_{qgg} - 1)((p_{cc,0} - p_{cc})R_{a,qgg} \\
&+ p_{cc,0}/2 - p_{gg,0}/2 - p_{cc}/2 + p_{gg}/2)R_{qtu} + (Q_{qgg} - 1)(p_{cc,0} - p_{cc}))\alpha_t{}^2 \\
&+ R_{qtu}\,R_{a,ptu}\,(Q_{qgg} - 1)(\omega - \omega_0)\alpha_t + (R_\omega - R_{pcc})(((R_{pcc}\,(p_{cc,0} - p_{cc}) \\
&+ ((p_{cc,0} - p_{cc})R_{a,qgg} - q_{gg,0} + q_{gg})(Q_{qgg} - 1))R_{qtu}{}^2 + ((2\,p_{cc,0} - 2\,p_{cc})R_{pcc} \\
&+ 2\,(Q_{qgg} - 1)((p_{cc,0} - p_{cc})R_{a,qgg} + p_{cc,0}/2 + p_{gg}/2 - p_{gg,0}/2 + p_{tu}/2 - p_{tu,0}/2 - p_{cc}/2 + q_{gg} - q_{gg,0}))R_{qtu} \\
&+ (Q_{qgg} - 1)(p_{cc,0} - p_{gg,0} - p_{cc} + p_{gg}))R_{a,ptu} + R_{qtu}\,((R_{pcc}\,(p_{cc,0} - p_{cc}) \\
&+ ((p_{cc,0} - p_{cc})R_{a,qgg} - q_{gg,0} + q_{gg})(Q_{qgg} - 1))R_{qtu} + (Q_{qgg} - 1)(p_{cc,0} - p_{gg,0} - p_{cc} + p_{gg})))\lambda^2 \\
&+ ((-2\,(p_{tu,0} - p_{tu})R_{qtu}\,R_{a,ptu} + (p_{gg} - p_{gg,0})R_{qtu}{}^2 + (R_{pcc}\,(p_{cc,0} - p_{cc}) \\
&- R_{a,qgg}\,(p_{cc,0} + p_{gg,0} + 2\,p_{tu,0} - p_{cc} - p_{gg} - 2\,p_{tu})\,Q_{qgg} + R_{a,qgg}\,(p_{cc,0} + p_{gg,0} + 2\,p_{tu,0} - p_{cc} - p_{gg} - 2\,p_{tu}) \\
&- 2\,R_{ptu}\,p_{tu})R_{qtu} - (Q_{qgg} - 1)(p_{cc,0} + p_{gg,0} + p_{tu,0} - p_{cc} - p_{gg} - p_{tu}))\alpha_t{}^3 + (2\,R_{qtu}\,(-\omega\,R_{pcc} \\
&+ R_\omega\,\omega_0)R_{a,ptu} + (-\omega\,R_{pcc} + R_\omega\,\omega_0 - R_{a,qgg}\,(Q_{qgg} - 1)(\omega - \omega_0))R_{qtu}{}^2 \\
&- 2\,(\omega - \omega_0)(Q_{qgg} - 1)(R_{a,qgg} + 1/2)R_{qtu} - (Q_{qgg} - 1)(\omega - \omega_0))\alpha_t{}^2 \\
&- (((p_{tu,0} - p_{tu})R_{qtu}{}^2 + (R_{a,qgg}\,(p_{cc,0} + p_{gg,0} + 2\,p_{tu,0} - p_{cc} - p_{gg} - 2\,p_{tu})\,Q_{qgg} \\
&+ (-p_{cc,0} - p_{gg,0} - 2\,p_{tu,0} + p_{cc} + p_{gg} + 2\,p_{tu})R_{a,qgg} + 2\,p_{tu,0} - 2\,p_{tu})R_{qtu} \\
&+ (Q_{qgg} - 1)(p_{cc,0} + p_{gg,0} + p_{tu,0} - p_{cc} - p_{gg} - p_{tu}))R_{a,ptu} + R_{qtu}\,((R_{a,qgg}\,(p_{tu,0} - p_{tu})\,Q_{qgg}
\end{aligned}
$$

$$
+ (p_{tu} - p_{tu,0})R_{a,qgg} + R_{ptu}\,p_{tu} + p_{gg,0} - p_{gg})R_{qtu}
+ (p_{cc} - p_{cc,0})R_{pcc} + (p_{tu,0} - p_{tu})\,Q_{qgg} + (2\,R_{ptu} + 1)p_{tu} - p_{tu,0}))
(R_\omega - R_{pcc})\alpha_t + (((-\omega\,R_{pcc} + R_\omega\,\omega_0 - R_{a,qgg}\,(Q_{qgg} - 1)
(\omega - \omega_0))R_{qtu}{}^2 + (-2\,\omega\,R_{pcc} + 2\,R_\omega\,\omega_0 - 2\,(\omega - \omega_0)(Q_{qgg} - 1)(R_{a,qgg} + 1/2))R_{qtu}
- (Q_{qgg} - 1)(\omega - \omega_0))R_{a,ptu} + ((-\omega\,R_{pcc} + R_\omega\,\omega_0 - R_{a,qgg}\,(Q_{qgg} - 1)(\omega - \omega_0))R_{qtu} -
(Q_{qgg} - 1)(\omega - \omega_0))R_{qtu})(R_\omega - R_{pcc}))\lambda + ((-2\,R_{a,qgg}\,(q_{gg,0}
- q_{gg})\,Q_{qgg} - 2\,R_{qgg}\,q_{gg} - p_{gg,0} - p_{gg})R_{qtu} - (Q_{qgg} - 1)
((p_{gg,0} - p_{gg})R_{a,qgg} + q_{gg,0} - q_{gg}))\alpha_t{}^4 + ((-\omega\,R_{pcc} + R_\omega\,\omega_0 + R_{a,qgg}\,(Q_{qgg} - 1)
(\omega - \omega_0))R_{qtu} + (Q_{qgg} - 1)(\omega - \omega_0))\alpha_t{}^3 +
(R_\omega - R_{pcc})(((-2\,R_{a,qgg}\,(q_{gg,0} - q_{gg})\,Q_{qgg} - 2\,R_{qgg}\,q_{gg} - p_{gg,0} + p_{tu,0} - p_{gg} - p_{tu})R_{qtu} - (Q_{qgg} - 1)
((p_{gg,0} - p_{gg})R_{a,qgg} + q_{gg,0} - q_{gg}))R_{a,ptu} + (-2\,R_{a,qgg}\,(q_{gg,0} - q_{gg})\,Q_{qgg} - 2\,R_{qgg}\,q_{gg}
- 2\,p_{gg})R_{qtu}{}^2 + (((-2\,p_{gg,0} - p_{tu,0} - 2\,q_{gg,0} + 2\,p_{gg} + p_{tu} + 2\,q_{gg})R_{a,qgg} - 2\,q_{gg,0} + 2\,q_{gg})\,Q_{qgg} + (2\,p_{gg,0}
+ p_{tu,0} - 2\,p_{gg} - p_{tu})R_{a,qgg} + (-2\,R_{qgg} - 2)q_{gg} + R_{ptu}\,p_{tu} - p_{gg,0} + 2\,q_{gg,0} - p_{gg})R_{qtu} - (Q_{qgg} - 1)
((p_{gg,0} - p_{gg})R_{a,qgg} + 2\,p_{gg,0} + p_{tu,0} + q_{gg,0} - 2\,p_{gg} - p_{tu} - q_{gg}))\alpha_t{}^2 + (R_\omega - R_{pcc})((Q_{qgg} - 1)
(\omega - \omega_0)(R_{qtu}\,R_{a,qgg} + 1)R_{a,ptu} + (-\omega\,R_{pcc} + R_\omega\,\omega_0)R_{qtu})\alpha_t + (R_\omega - R_{pcc})^2
(((-R_{a,qgg}\,(q_{gg,0} - q_{gg})\,Q_{qgg} - R_{qgg}\,q_{gg} - p_{gg})R_{qtu}{}^2 + (((-p_{gg,0} - p_{tu,0} - 2\,q_{gg,0}
+ p_{gg} + p_{tu} + 2\,q_{gg})R_{a,qgg} - q_{gg,0} + q_{gg})\,Q_{qgg} + (p_{gg,0} + p_{tu,0} - p_{gg} - p_{tu})R_{a,qgg}
+ (-2\,R_{qgg} - 1)q_{gg} - p_{gg,0} + p_{tu,0} + q_{gg,0} - p_{gg} - p_{tu})R_{qtu} - ((p_{gg,0} - p_{gg})R_{a,qgg} + p_{gg,0} + p_{tu,0} + q_{gg,0}
- p_{gg} - p_{tu} - q_{gg})(Q_{qgg} - 1))R_{a,ptu} + (-R_{a,qgg}\,(q_{gg,0} - q_{gg})\,Q_{qgg} - R_{qgg}\,q_{gg} - p_{gg})R_{qtu}{}^2
+ (((p_{gg} - p_{gg,0})R_{a,qgg} - q_{gg,0} + q_{gg})\,Q_{qgg} + (p_{gg,0} - p_{gg})R_{a,qgg} + R_{ptu}\,p_{tu} + q_{gg,0} - q_{gg})R_{qtu}
- (Q_{qgg} - 1)(p_{gg,0} - p_{gg})))R_{a,qtu}\,\kappa^2 + (\lambda\,\alpha_t\,q_{tu}\,(\alpha_t{}^2 - R_{pcc} + R_\omega)R_{a,qtu}{}^3
+ (R_{a,ptu}\,\lambda^3(Q_{qgg} - 1)(q_{tu,0} - q_{tu})\alpha_t + (((q_{tu,0} - 3\,q_{tu})R_{qtu} + R_{a,qgg}\,(Q_{qgg} - 1)(q_{tu,0} - q_{tu}))\alpha_t{}^2
+ (R_{a,qgg}\,(Q_{qgg} - 1)(q_{tu,0} - q_{tu})R_{a,ptu} + (q_{tu,0} - 3\,q_{tu})R_{qtu})(R_\omega - R_{pcc}))\alpha_t\,\lambda + (\alpha_t{}^2 - R_{pcc} + R_\omega)(\alpha_t{}^2
+ R_{a,ptu}\,(R_\omega - R_{pcc}))(q_{tu,0} - q_{tu}))R_{a,qtu}{}^2 + (-2\,R_{qtu}\,R_{a,ptu}\,\alpha_t\,(Q_{qgg} - 1)
(q_{tu,0} - q_{tu})\lambda^3 + R_{a,ptu}\,(Q_{qgg} - 1)(q_{tu,0} - q_{tu})(\alpha_t{}^2
- R_{pcc} + R_\omega)\lambda^2 - 2\,(((q_{tu,0} - 3/2\,q_{tu})R_{qtu}{}^2 + R_{a,qgg}\,(Q_{qgg} - 1)
(q_{tu,0} - q_{tu})R_{qtu} + 1/2\,(Q_{qgg} - 1)(q_{tu,0} - q_{tu}))\alpha_t{}^2
+ ((Q_{qgg} - 1)(R_{qtu}\,R_{a,qgg} + 1/2)(q_{tu,0} - q_{tu})R_{a,ptu} + (q_{tu,0} - 3/2\,q_{tu})R_{qtu}{}^2)
(R_\omega - R_{pcc}))\alpha_t\,\lambda - 2\,(\alpha_t{}^2 - R_{pcc} + R_\omega)(\alpha_t{}^2 + R_{a,ptu}\,(R_\omega - R_{pcc}))(q_{tu,0} - q_{tu})
(-1/2\,R_{a,qgg}\,Q_{qgg} + R_{qtu} + R_{a,qgg}/2))R_{a,qtu} + (R_{qtu}{}^2R_{a,ptu}\,\alpha_t\,(Q_{qgg} - 1)\lambda^3 - R_{qtu}\,R_{a,ptu}\,(Q_{qgg} - 1)(\alpha_t{}^2
- R_{pcc} + R_\omega)\lambda^2 + R_{qtu}\,((R_{qtu}{}^2 + R_{a,qgg}\,(Q_{qgg} - 1)R_{qtu}
+ Q_{qgg} - 1)\alpha_t{}^2 + (R_\omega - R_{pcc})((Q_{qgg} - 1)(R_{qtu}\,R_{a,qgg} + 1)R_{a,ptu} + R_{qtu}{}^2))\alpha_t\,\lambda
+ (\alpha_t{}^2 - R_{pcc} + R_\omega)(\alpha_t{}^2 + R_{a,ptu}\,(R_\omega - R_{pcc}))(R_{qtu}{}^2 - R_{a,qgg}\,(Q_{qgg} - 1)R_{qtu} - Q_{qgg} + 1))
(q_{tu,0} - q_{tu}))R_{a,qtu}\,\kappa - ((-R_{a,ptu}\,(Q_{qgg} - 1)(p_{cc,0} - p_{cc})\lambda^4
+ (Q_{qgg} - 1)((p_{tu,0} - p_{tu})\alpha_t + \omega - \omega_0)R_{a,ptu}\,\lambda^3
$$

$$
\begin{aligned}
&+ ((((p_{cc} - p_{cc,0})R_{pcc} + (Q_{qgg} - 1)(q_{gg,0} - q_{gg}))R_{a,ptu} - R_{a,qgg}\,(Q_{qgg} - 1)(p_{cc,0} - p_{cc}))\alpha_t{}^2 \\
&- (R_{pcc}\,(p_{cc,0} - p_{cc}) + ((p_{cc,0} - p_{cc})R_{a,qgg} - q_{gg,0} + q_{gg})(Q_{qgg} - 1))(R_\omega \\
&- R_{pcc})R_{a,ptu})\lambda^2 + (((p_{tu,0} - p_{tu})R_{a,ptu} + R_{a,qgg}\,(p_{tu,0} - p_{tu})Q_{qgg} \\
&+ (p_{tu} - p_{tu,0})R_{a,qgg} + R_{ptu}\,p_{tu})\alpha_t{}^3 + ((\omega\,R_{pcc} - R_\omega\,\omega_0)R_{a,ptu} \\
&+ R_{a,qgg}\,(Q_{qgg} - 1)(\omega - \omega_0))\alpha_t{}^2 + (R_\omega - R_{pcc})((R_{a,qgg}\,Q_{qgg} \\
&- R_{a,qgg} + 1)(p_{tu,0} - p_{tu})R_{a,ptu} + R_{ptu}\,p_{tu})\alpha_t - (R_\omega - R_{pcc})R_{a,ptu}\,(-\omega\,R_{pcc} \\
&+ R_\omega\,\omega_0 - R_{a,qgg}\,(Q_{qgg} - 1)(\omega - \omega_0)))\lambda + (\alpha_t{}^2 - R_{pcc} + R_\omega)(\alpha_t{}^2 + R_{a,ptu}\,(R_\omega \\
&- R_{pcc}))(R_{a,qgg}\,(q_{gg,0} - q_{gg})Q_{qgg} + R_{qgg}\,q_{gg} + p_{gg}))R_{a,qtu}{}^2 + (2\,R_{qtu}\,R_{a,ptu}\,(Q_{qgg} - 1)(p_{cc,0} - p_{cc})\lambda^4 \\
&- 2\,(Q_{qgg} - 1)R_{qtu}\,((p_{tu,0} - p_{tu})\alpha_t + \omega - \omega_0)R_{a,ptu}\,\lambda^3 \\
&+ (((((2\,p_{cc,0} - 2\,p_{cc})R_{pcc} - 2\,(Q_{qgg} - 1)(q_{gg,0} - q_{gg}))R_{qtu} \\
&- (Q_{qgg} - 1)(p_{gg,0} - p_{gg}))R_{a,ptu} + 2\,(Q_{qgg} - 1)(R_{qtu}\,R_{a,qgg} + 1/2)(p_{cc,0} - p_{cc}))\alpha_t{}^2 \\
&+ 2\,((R_{pcc}\,(p_{cc,0} - p_{cc}) + ((p_{cc,0} - p_{cc})R_{a,qgg} - q_{gg,0} + q_{gg})(Q_{qgg} - 1))R_{qtu} \\
&+ 1/2\,(Q_{qgg} - 1)(p_{cc,0} - p_{gg,0} - p_{cc} + p_{gg}))(R_\omega - R_{pcc})R_{a,ptu})\lambda^2 \\
&+ ((-2\,(p_{tu,0} - p_{tu})R_{qtu}\,R_{a,ptu} + (-2\,R_{a,qgg}\,(p_{tu,0} - p_{tu})Q_{qgg} + (2\,p_{tu,0} - 2\,p_{tu})R_{a,qgg} \\
&- 2\,R_{ptu}\,p_{tu})R_{qtu} - (Q_{qgg} - 1)(p_{tu,0} - p_{tu}))\alpha_t{}^3 \\
&+ (2\,R_{qtu}\,(-\omega\,R_{pcc} + R_\omega\,\omega_0)R_{a,ptu} - 2\,(\omega - \omega_0)(Q_{qgg} - 1) \\
&(R_{qtu}\,R_{a,qgg} + 1/2))\alpha_t{}^2 - 2\,(((R_{a,qgg}\,Q_{qgg} - R_{a,qgg} + 1)R_{qtu} \\
&- 1/2 + Q_{qgg}/2)(p_{tu,0} - p_{tu})R_{a,ptu} + R_{qtu}\,R_{ptu}\,p_{tu})(R_\omega - R_{pcc})\alpha_t + 2\,((-\omega\,R_{pcc} \\
&+ R_\omega\,\omega_0 - R_{a,qgg}\,(Q_{qgg} - 1)(\omega - \omega_0))R_{qtu} - 1/2\,(Q_{qgg} - 1)(\omega - \omega_0)) \\
&(R_\omega - R_{pcc})R_{a,ptu})\lambda - 2\,(\alpha_t{}^2 - R_{pcc} + R_\omega)(\alpha_t{}^2 + R_{a,ptu}\,(R_\omega \\
&- R_{pcc}))((R_{a,qgg}\,(q_{gg,0} - q_{gg})Q_{qgg} + R_{qgg}\,q_{gg} + p_{gg})R_{qtu} + 1/2\,(Q_{qgg} - 1)((p_{gg,0} - p_{gg})R_{a,qgg} \\
&+ q_{gg,0} - q_{gg})))R_{a,qtu} - R_{qtu}{}^2R_{a,ptu}\,(Q_{qgg} - 1)(p_{cc,0} - p_{cc})\lambda^4 \\
&+ (Q_{qgg} - 1)R_{qtu}{}^2((p_{tu,0} - p_{tu})\alpha_t + \omega - \omega_0)R_{a,ptu}\,\lambda^3 \\
&- ((((R_{pcc}\,(p_{cc,0} - p_{cc}) - (Q_{qgg} - 1)(q_{gg,0} - q_{gg}))R_{qtu} - (Q_{qgg} - 1)(p_{gg,0} - p_{gg}))R_{a,ptu} \\
&+ (Q_{qgg} - 1)(p_{cc,0} - p_{cc})(R_{qtu}\,R_{a,qgg} + 1))\alpha_t{}^2 + (R_\omega - R_{pcc})R_{a,ptu}\,((R_{pcc}\,(p_{cc,0} - p_{cc}) \\
&+ ((p_{cc,0} - p_{cc})R_{a,qgg} - q_{gg,0} + q_{gg})(Q_{qgg} - 1))R_{qtu} + (Q_{qgg} - 1) \\
&(p_{cc,0} - p_{gg,0} - p_{cc} + p_{gg})))R_{qtu}\,\lambda^2 - R_{qtu}\,((-(p_{tu,0} - p_{tu})R_{qtu}\,R_{a,ptu} \\
&+ (-R_{a,qgg}\,(p_{tu,0} - p_{tu})Q_{qgg} + R_{a,qgg}\,(p_{tu,0} - p_{tu}) - R_{ptu}\,p_{tu})R_{qtu} - (Q_{qgg} - 1)(p_{tu,0} - p_{tu}))\alpha_t{}^3 \\
&+ (R_{qtu}\,(-\omega\,R_{pcc} + R_\omega\,\omega_0)R_{a,ptu} - (Q_{qgg} - 1)(\omega - \omega_0)(R_{qtu}\,R_{a,qgg} + 1))\alpha_t{}^2 \\
&- (R_\omega - R_{pcc})(((R_{a,qgg}\,Q_{qgg} - R_{a,qgg} + 1)R_{qtu} + Q_{qgg} - 1)(p_{tu,0} - pu)R_{a,ptu} + R_{qtu}\,R_{ptu}\,p_{tu})\alpha_t \\
&+ ((-\omega\,R_{pcc} + R_\omega\,\omega_0 - R_{a,qgg}\,(Q_{qgg} - 1)(\omega - \omega_0))R_{qtu} - (Q_{qgg} - 1)(\omega - \omega_0))(R_\omega \\
&- R_{pcc})R_{a,ptu})\lambda + (\alpha_t{}^2 - R_{pcc} + R_\omega)(\alpha_t{}^2 + R_{a,ptu}\,(R_\omega - R_{pcc}))((R_{a,qgg}\,(q_{gg,0} - q_{gg})Q_{qgg} \\
&+ R_{qgg}\,q_{gg} + p_{gg})R_{qtu}{}^2 + (Q_{qgg} - 1)((p_{gg,0} - p_{gg})R_{a,qgg} + q_{gg,0} - q_{gg})R_{qtu} \\
&+ (Q_{qgg} - 1)(p_{gg,0} - p_{gg})))R_{a,qtu}{}^2]
\end{aligned}
$$

$$[Zg\,(((-R_{\omega}+R_{pcc})R_{a,qtu}+{\alpha_t}^2+(R_{qtu}+1)(R_{\omega}\\ -R_{pcc}))\kappa^2+R_{a,qtu}\,(R_{qtu}-R_{a,qtu})({\alpha_t}^2-R_{pcc}+R_{\omega}))(((-R_{\omega}\\ +R_{pcc})R_{a,qtu}+{\alpha_t}^2+(R_{qtu}+R_{a,ptu})(R_{\omega}-R_{pcc}))\kappa^2\\ +R_{a,qtu}\,({\alpha_t}^2+R_{a,ptu}\,(R_{\omega}-R_{pcc}))(R_{qtu}-R_{a,qtu}))]^{-1} \tag{7.6}$$

Bibliographie

[1] S. Le Gonidec, "Automatic & control applications in the european space propulsion domain," *From need expression to preparation for an uncertain future. ACD2016 Airbus Safran Launchers, Lille, France*, 2016.

[2] S. X. Corp., "Merlin engines," 2015.

[3] B. Origin, "Blue origin," *Our approach to technology*, 2016.

[4] M. Soltani, R. Izadi-Zamanabadi, R. Wisniewski, W. Belau, and S. Le Gonidec, "Robust parametric fault estimation in a hopper system," *IFAC Proceedings Volumes*, vol. 45, no. 13, pp. 491–498, 2012.

[5] T. Kai, K. Niu, K. Obase, W. Sakai, Y. Fukuda, T. Hashimoto, M. Sato, S. Takada, T. Kimura, Y. Naruo *et al.*, "Engine control system for the main engine of the reusable sounding rocket," in *Proceedings of the International Astronautical Congress, IAC*, vol. 10. JAXA and MHI Jerusalem, Israel, 2015, pp. 7389–7394.

[6] F. Deneu, M. Malassigne, O. Le-Couls, and P. Baiocco, "Promising solutions for fully reusable two-stage-to-orbit configurations," *Acta Astronautica*, vol. 56, no. 8, pp. 729–736, 2005.

[7] M. J. Casiano, J. R. Hulka, and V. Yang, "Liquid-propellant rocket engine throttling : A comprehensive review," *Journal of propulsion and power*, vol. 26, no. 5, pp. 897–923, 2010.

[8] M. Ragab and F. M. Cheatwood, "Launch vehicle recovery and reuse," in *AIAA SPACE 2015 conference and exposition*, 2015, p. 4490.

[9] P. Baiocco, "Overview of reusable space systems with a look to technology aspects," *Acta Astronautica*, vol. 189, pp. 10–25, 2021.

[10] A. Duyar, T.-H. Guo, and W. C. Merrill, "Space shuttle main engine model identification," *IEEE Control Systems Magazine*, vol. 10, no. 4, pp. 59–65, 1990.

[11] A. Santana, Jr, F. Barbosa, M. Niwa, and L. Goes, "Modeling and robust analysis of a liquid rocket engine," in *36th AIAA/ASME/SAE/ASEE Joint Propulsion Conference and Exhibit*, 2000, p. 3160.

[12] R. BRESHEARS, J. Mccafferty, and C. MCDERMOTT, "Dynamic performance of surveyor throttleable rocket engine operatingon propellants containing dissolved gas," in *3rd Annual Meeting*, 1966, p. 949.

[13] S. Perez Roca, "Model-based robust transient control of reusable liquid-propellant rocket engines," Ph.D. dissertation, Université Paris-Saclay, 2020.

[14] E.-f. Yang, Z.-p. Zhang, and Y.-m. Xu, "Nonlinear dynamic neural network model for rocket propulsion systems," *JOURNAL OF PROPULSION TECHNOLOGY-BEIJING-*, vol. 22, no. 1; ISSU 115, pp. 50–53, 2001.

[15] K. Dresia, "Prediction of heat transfer in methane for liquid rocket engines using artificial neural networks," Ph.D. dissertation, RWTH Aachen Aachen, Germany, 2018.

[16] K. Dresia, E. Kurudzija, J. Deeken, and G. Waxenegger-Wilfing, "Improved wall temperature prediction for the lumen rocket combustion chamber with neural networks," *Aerospace*, vol. 10, no. 5, p. 450, 2023.

[17] E. W. Otto and R. A. Flage, *Control of combustion-chamber pressure and oxidant-fuel ratio for a regeneratively cooled hydrogen-fluorine rocket engine*. National Aeronautics and Space Administration, 1959.

[18] S. Pérez-Roca, J. Marzat, H. Piet-Lahanier, N. Langlois, F. Farago, M. Galeotta, and S. Le Gonidec, "A survey of automatic control methods for liquid-propellant rocket engines," *Prog. in Aerospace Sciences*, vol. 107, pp. 63–84, 2019.

[19] A. Ray, X. Dai, M.-K. Wu, M. Carpino, and C. F. Lorenzo, "Damage-mitigating control of a reusable rocket engine," *Journal of Propulsion and Power*, vol. 10, no. 2, pp. 225–234, 1994.

[20] X. Dai and A. Ray, "Damage-mitigating control of a reusable rocket engine : Part ii—formulation of an optimal policy," 1996.

[21] B. Kiforenko and A. Kharitonov, "Control of thrust of the liquid rocket engines : simulation and optimization," *Journal of Automation and Information Sciences*, vol. 32, no. 8, pp. 47–58, 2000.

[22] J. L. Musgrave, T.-H. Guo, E. Wong, and A. Duyar, "Real-time accommodation of actuator faults on a reusable rocket engine," *IEEE transactions on control systems technology*, vol. 5, no. 1, pp. 100–109, 1997.

[23] E. Nemeth, R. ANDERSON, J. Maram, A. Norman, and W. Merrill, "An advanced intelligent control system framework," in *28th Joint Propulsion Conference and Exhibit*, 1992, p. 3162.

[24] E. Nemeth, R. Anderson, J. Ols, and M. Olsasky, "Reusable rocket engine intelligent control system framework design, phase 2," Tech. Rep., 1991.

[25] C. F. Lorenzo, A. Ray, and M. S. Holmes, "Nonlinear control of a reusable rocket engine for life extension," *Journal of Propulsion and Power*, vol. 17, no. 5, pp. 998–1004, 2001.

[26] C. F. Lorenzo, W. C. Merrill, J. L. Musgrave, and A. Ray, "Controls concepts for next generation reusable rocket engines," in *Proceedings of 1995 American Control Conference-ACC'95*, vol. 6. IEEE, 1995, pp. 3942–3950.

[27] S. Pérez-Roca, J. Marzat, H. Piet-Lahanier, N. Langlois, M. Galeotta, F. Farago, and S. Le Gonidec, "Model-based robust transient control of reusable liquid-propellant rocket engines," *IEEE Transactions on Aerospace and Electronic Systems*, vol. 57, no. 1, pp. 129–144, 2020.

[28] K. Dresia, G. Waxenegger-Wilfing, R. H. Dos Santos Hahn, J. C. Deeken, and M. Oschwald, "Nonlinear control of an expander-bleed rocket engine using reinforcement learning," 2021.

[29] G. Waxenegger-Wilfing, K. Dresia, J. Deeken, and M. Oschwald, "A reinforcement learning approach for transient control of liquid rocket engines," *IEEE Transactions on Aerospace and Electronic Systems*, vol. 57, no. 5, pp. 2938–2952, 2021.

[30] S.-Y. Park and J. Ahn, "Deep neural network approach for fault detection and diagnosis during startup transient of liquid-propellant rocket engine," *Acta Astronautica*, vol. 177, pp. 714–730, 2020.

[31] A. Santana and L. Goes, "Design and dynamic characteristics of a liquid-propellant thrust chamber," in *Proceedings of the National Conference on Mechanical Engineering, Calcutta, India*, 2000, pp. 20–22.

[32] A. S. Junior, "Dynamic modeling and stability analysis of a liquid rocket engine." 1998.

[33] H. Khalil, *Nonlinear Systems*, ser. Pearson Education. Prentice Hall, 2002. [Online]. Available : https://books.google.fr/books?id=t_d1QgAACAAJ

[34] Y.-L. Zhang, "State-space analysis of the dynamic characteristics of a variable thrust liquid propellant rocket engine," *Acta Astronautica*, vol. 11, no. 7-8, pp. 535–541, 1984.

[35] F. Zheng, M. Cheng, and W.-B. Gao, "Variable structure control of time-delay systems with a simulation study on stabilizing combustion in liquid propellant rocket motors," *Automatica*, vol. 31, no. 7, pp. 1031–1037, 1995.

[36] D. K. Huzel, *Modern engineering for design of liquid-propellant rocket engines*. AiAA, 1992, vol. 147.

[37] G. P. Sutton and O. Biblarz, *Rocket propulsion elements*. John Wiley & Sons, 2011.

[38] J. P. García-Sandoval, V. González-Álvarez, and C. Calderón, "Stability analysis and passivity properties for a class of chemical reactors : Internal entropy production approach," *Computers & chemical engineering*, vol. 75, pp. 184–195, 2015.

[39] M. Jankovic and I. Kolmanovsky, "Constructive lyapunov control design for turbocharged diesel engines," *IEEE Transactions on control systems technology*, vol. 8, no. 2, pp. 288–299, 2000.

[40] E. Mooij, "Passivity analysis for a winged re-entry vehicle," in *AIP Conference Proceedings*, vol. 1637, no. 1. American Institute of Physics, 2014, pp. 1362–1376.

[41] A. Ulas, "Passive flow control in liquid-propellant rocket engines with cavitating venturi," *Flow Measurement and Instrumentation*, vol. 17, no. 2, pp. 93–97, 2006.

[42] J. W. Bennewitz and R. A. Frederick, "Overview of combustion instabilities in liquid rocket engines-coupling mechanisms & control techniques," *49th AIAA/ASME/SAE/ASEE Joint PropulsionConference*, p. 4106, 2013.

[43] J. Pieringer, T. Sattelmayer, and F. Fassl, "Simulation of combustion instabilities in liquid rocket engines with acoustic perturbation equations," *Journal of propulsion and power*, vol. 25, no. 5, pp. 1020–1031, 2009.

[44] V. Duindam, A. Macchelli, S. Stramigioli, and H. Bruyninckx, *Modeling and control of complex physical systems : the port-Hamiltonian approach*. Springer Science & Business Media, 2009.

[45] W. Lohmiller and J.-J. E. Slotine, "On contraction analysis for non-linear systems," *Automatica*, vol. 34, no. 6, pp. 683–696, 1998.

[46] J. Gibart, H. Piet-Lahanier, F. Farago, and M. Galeotta, "Regulation of a liquid propelled rocket engine using contraction theory," *IFAC-PapersOnLine*, vol. 56, no. 1, pp. 307–312, 2023.

[47] J. Gibart, H. Piet-Lahanier, and F. Farago, "Port-hamiltonian modelling of complex non-linear systems, application to a liquid propelled rocket engine."

[48] R. Murata, J. Gibart, J. Marzat, H. Piet-Lahanier, S. Boujnah, and F. Farago, "Structural analysis of a rocket's multi-engine propulsion cluster for fault detection and isolation."

[49] J. Gibart, H. Piet-Lahanier, and F. Farago, "Mass flow control design for a reusable liquid propelled rocket engine using contraction theory."

[50] ——, "Stabilizing control design for liquid propelled rocket engines."

[51] S. Durteste, "A transient model of the vinci cryogenic upper stage rocket engine," in *43rd AIAA/ASME/SAE/ASEE Joint Propulsion Conference & Exhibit*, 2007, p. 5531.

[52] A. Iffly and M. Brixhe, "Performance model of the vulcain ariane 5 main engine," in *35th Joint Propulsion Conference and Exhibit*, 1999, p. 2472.

[53] J. Liu, S. Zhang, J. Wei, and O. J. Haidn, "Rans based numerical simulation of a gch4/go2 rocket engine combustion chamber with film cooling and improvement of wall heat flux prediction," *Applied Thermal Engineering*, vol. 219, p. 119544, 2023.

[54] R. Hermsen and B. Zandbergen, "Pressurization system for a cryogenic propellant tank in a pressure-fed high-altitude rocket," in *7th European Conference for Aeronautics And Aerospace Sciences (EUCASS)*, 2017, p. 13.

[55] C. Manfletti, "Transient behaviour modeling of liquid rocket engine components," Ph.D. dissertation, RWTH Aachen, 2010.

[56] J. Lee, T.-S. Roh, H. Huh, and H. J. Lee, "Performance analysis and mass estimation of a small-sized liquid rocket engine with electric-pump cycle," *International Journal of Aeronautical and Space Sciences*, vol. 22, pp. 94–107, 2021.

[57] E. Ruth, H. Ahn, R. Baker, and M. Brosmer, "Advanced liquid rocket engine transient model," in *26th Joint Propulsion Conference*, 1990, p. 2299.

[58] E. Plahte, T. Mestl, and S. W. Omholt, "Feedback loops, stability and multistationarity in dynamical systems," *Journal of Biological Systems*, vol. 3, no. 02, pp. 409–413, 1995.

[59] J. Lofberg, "Yalmip : A toolbox for modeling and optimization in matlab," in *IEEE ICRA*, 2004, pp. 284–289.

[60] J. Moore and B. Anderson, "A generalization of the popov criterion," *Journal of the franklin Institute*, vol. 285, no. 6, pp. 488–492, 1968.

[61] B. M. Maschke and A. J. van der Schaft, "Port-controlled hamiltonian systems : modelling origins and systemtheoretic properties," in *Nonlinear Control Systems Design 1992*. Elsevier, 1993, pp. 359–365.

[62] P. C. Breedveld, "Physical systems theory in terms of bond graphs," *PhD Thesis, Technische Hogeschool Twente*, 1984.

[63] R. Pasumarthy and A. van der Schaft, "A port-hamiltonian approach to modeling and interconnections of canal systems," in *16th International Symposium on Mathematical*, vol. 2, 2006, pp. 1436–1443.

[64] D. Eberard and B. Maschke, "Port hamiltonian systems extended to irreversible systems : the example of the heat conduction," *IFAC Proceedings Volumes*, vol. 37, no. 13, pp. 243–248, 2004.

[65] D. Eberard, B. Maschke, and A. Van Der Schaft, "An extension of hamiltonian systems to the thermodynamic phase space : Towards a geometry of nonreversible processes," *Reports on mathematical physics*, vol. 60, no. 2, pp. 175–198, 2007.

[66] H. Ramirez, B. Maschke, and D. Sbarbaro, "Irreversible port-hamiltonian systems : A general formulation of irreversible processes with application to the cstr," *Chemical Engineering Science*, vol. 89, pp. 223–234, 2013.

[67] J. Cervera, A. J. van der Schaft, and A. Baños, "Interconnection of port-hamiltonian systems and composition of dirac structures," *Automatica*, vol. 43, no. 2, pp. 212–225, 2007.

[68] K. Fujimoto and T. Sugie, "Canonical transformation and stabilization of generalized hamiltonian systems," *Systems & Control Letters*, vol. 42, no. 3, pp. 217–227, 2001.

[69] D. Dirksz and J. M. Scherpen, "Adaptive control of port-hamiltonian systems," in *19th International Symposium on Mathematical Theory of Networks and Systems–MTNS 2010, Budapest, Hungary*. University of Groningen, Research Institute of Technology and Management, 2010, pp. 1503–1508.

[70] Z. Jia, L. Qiao, and W. Zhang, "Adaptive tracking control of unmanned underwater vehicles with compensation for external perturbations and uncertainties using port-hamiltonian theory," *Ocean Engineering*, vol. 209, p. 107402, 2020.

[71] S. P. Nageshrao, G. A. Lopes, D. Jeltsema, and R. Babuška, "Port-hamiltonian systems in adaptive and learning control : A survey," *IEEE Transactions on Automatic Control*, vol. 61, no. 5, pp. 1223–1238, 2015.

[72] P. Borja, R. Cisneros, and R. Ortega, "A constructive procedure for energy shaping of port—hamiltonian systems," *Automatica*, vol. 72, pp. 230–234, 2016.

[73] R. Morselli and R. Zanasi, "Control of port hamiltonian systems by dissipative devices and its application to improve the semi-active suspension behaviour," *Mechatronics*, vol. 18, no. 7, pp. 364–369, 2008.

[74] R. Ortega, A. Van Der Schaft, B. Maschke, and G. Escobar, "Interconnection and damping assignment passivity-based control of port-controlled hamiltonian systems," *Automatica*, vol. 38, no. 4, pp. 585–596, 2002.

[75] R. Rashad, F. Califano, A. J. van der Schaft, and S. Stramigioli, "Twenty years of distributed port-hamiltonian systems : a literature review," *IMA Journal of Mathematical Control and Information*, vol. 37, no. 4, pp. 1400–1422, 2020.

[76] F. M. Márquez, P. J. Zufiria, and L. J. Yebra, "Port-hamiltonian modeling of multiphysics systems and object-oriented implementation with the modelica language," *IEEE Access*, vol. 8, pp. 105 980–105 996, 2020.

[77] R. Ortega, A. Van Der Schaft, F. Castanos, and A. Astolfi, "Control by interconnection and standard passivity-based control of port-hamiltonian systems," *IEEE Transactions on Automatic control*, vol. 53, no. 11, pp. 2527–2542, 2008.

[78] L. M. Esquivel-Sancho, M. Muñoz-Arias, H. Phillips-Brenes, and R. Pereira-Arroyo, "A reversible hydropump–turbine system," *Applied Sciences*, vol. 12, no. 18, p. 9086, 2022.

[79] N. Monshizadeh, P. Monshizadeh, R. Ortega, and A. van Der Schaft, "Conditions on shifted passivity of port-hamiltonian systems," *Systems & Control Letters*, vol. 123, pp. 55–61, 2019.

[80] W. Zhou, Y. Wu, H. Hu, Y. Li, and Y. Wang, "Port-hamiltonian modeling and ida-pbc control of an ipmc-actuated flexible beam," in *Actuators*, vol. 10, no. 9. MDPI, 2021, p. 236.

[81] K. Fujimoto, K. Sakurama, and T. Sugie, "Trajectory tracking control of port-controlled hamiltonian systems via generalized canonical transformations," *Automatica*, vol. 39, no. 12, pp. 2059–2069, 2003.

[82] A. Yaghmaei and M. J. Yazdanpanah, "Trajectory tracking for a class of contractive port hamiltonian systems," *Automatica*, vol. 83, pp. 331–336, 2017.

[83] W. Lohmiller, "Contraction analysis of nonlinear systems," Ph.D. dissertation, MIT, 1999.

[84] A. Davydov, S. Jafarpour, and F. Bullo, "Non-euclidean contraction theory for robust nonlinear stability," *IEEE Transactions on Automatic Control*, vol. 67, no. 12, pp. 6667–6681, 2022.

[85] W. Lohmiller and J.-J. Slotine*, "Contraction analysis of non-linear distributed systems," *International Journal of Control*, vol. 78, no. 9, pp. 678–688, 2005.

[86] S. Thenozhi, A. C. Sánchez, and J. Rodríguez-Reséndiz, "A contraction theory-based tracking control design with friction identification and compensation," *IEEE Transactions on Industrial Electronics*, vol. 69, no. 6, pp. 6111–6120, 2021.

[87] H. Tsukamoto, S.-J. Chung, and J.-J. E. Slotine, "Contraction theory for nonlinear stability analysis and learning-based control : A tutorial overview," *Annual Reviews in Control*, vol. 52, pp. 135–169, 2021.

[88] W. Lohmiller and J.-J. Slotine, "Control system design for mechanical systems using contraction theory," *IEEE Trans.on Autom. Contr.*, vol. 45, no. 5, pp. 984–989, 2000.

[89] V. Andrieu and S. Tarbouriech, "Lmi conditions for contraction and synchronization," *IFAC-PapersOnLine*, vol. 52, no. 16, pp. 616–621, 2019.

[90] A. Pavlov, A. Pogromsky, N. van de Wouw, and H. Nijmeijer, "Convergent dynamics, a tribute to boris pavlovich demidovich," *Systems & Control Letters*, vol. 52, no. 3-4, pp. 257–261, 2004.

[91] H. Tsukamoto, S.-J. Chung, and J.-J. Slotine, "Learning-based adaptive control via contraction theory," in *IEEE CDC*, 2021.

[92] V. Andrieu, B. Jayawardhana, and L. Praly, "Transverse exponential stability and applications," *IEEE Transactions on Automatic Control*, vol. 61, no. 11, pp. 3396–3411, 2016.

[93] J. Jouffroy and J.-J. Slotine, "Methodological remarks on contraction theory," in *Proc. of the 43rd IEEE Conf. on Decision and Control*, vol. 3, 2004, pp. 2537–2543.

[94] R. Reyes-Báez, A. van der Schaft, and B. Jayawardhana, "Virtual contractivity-based control of fully-actuated mechanical systems in the port-hamiltonian framework," *Automatica*, vol. 141, p. 110275, 2022.

[95] D. A. Dirksz and J. M. A. Scherpen, "Adaptive control of port-hamiltonian systems," *19th International Symposium on Mathematical Theory of Networks and Systems*, pp. (pp. 1503–1508).

[96] J. Jouffroy, "A relaxed criterion for contraction theory : Application to an underwater vehicle observer," in *2003 European Control Conference (ECC)*. IEEE, 2003, pp. 2999–3004.

[97] J. Jouffroy and J. Lottin, "On the use of contraction theory for the design of nonlinear observers for ocean vehicles," in *Proceedings of the 2002 American Control Conference (IEEE Cat. No. CH37301)*, vol. 4. IEEE, 2002, pp. 2647–2652.

[98] A. P. Dani, S.-J. Chung, and S. Hutchinson, "Observer design for stochastic nonlinear systems using contraction analysis," in *2012 IEEE 51st IEEE Conference on Decision and Control (CDC)*. IEEE, 2012, pp. 6028–6035.

[99] B. Sharma and I. Kar, "Observer-based synchronization scheme for a class of chaotic systems using contraction theory," *nonlinear dynamics*, vol. 63, pp. 429–445, 2011.

[100] M. Rayguru and I. Kar, "Contraction theory approach to disturbance observer based filtered backstepping design," *Journal of Dynamic Systems, Measurement, and Control*, vol. 141, no. 8, p. 084501, 2019.

[101] A. Venkatraman and A. Van Der Schaft, "Full-order observer design for a class of port-hamiltonian systems," *Automatica*, vol. 46, no. 3, pp. 555–561, 2010.

[102] H. Tsukamoto, *Contraction Theory for Robust Learning-Based Control : Toward Aerospace and Robotic Autonomy*. California Institute of Technology, 2023.